DIELECTRIC AND ULTRASONIC STUDIES OF

MACROMOLECULAR GROWTH DURING POLYMERIZATION

By:

MATTHEW GILES PARTHUN

A Thesis

Submitted to the School of Graduate Studies

in Partial Fulfilment of the Requirements

for the Degree

Doctor of Philosophy.

McMaster University

January 1997

(i)

0-612-30166-4

Canada

ACKNOWLEDGMENTS

"He who has a why to live can deal with any how"

Friedrich Nietzsche

DOCTOR OF PHILOSOPHY (1997)   McMASTER UNIVERSITY

TITLE: Dielectric and Ultrasonic Studies of Macromolecular Growth During

              Polymerization

AUTHOR: Matthew Giles Parthun   B.Sc., M.Sc. (McMaster University)

SUPERVISOR: Professor Gyan Johari

NUMBER OF PAGES: xxiv, 222

ABSTRACT

Measurements by dielectric spectroscopy, ultrasonics and calorimetry of several

low viscosity monomeric liquids undergoing spontaneous chemical reaction, to form

three new, linear chain polymers under isothermal conditions, have been used to

determine how the number of covalent bonds formed during the growth of a linear chain

affects the dielectric and ultrasonic properties, their respective relaxation times, and their

spectral shape. The dielectric properties changed in the following manner. During this

reaction, the static permittivity decreased and the relaxation time increased towards

limiting values. As the number of covalent bonds increased towards the Avogadro

number, the change in the complex permittivity as measured for a fixed frequency was

phenomenologically similar to that observed on varying the frequency, although the exact

formalisms in both cases differed. In both cases the relaxation function could be well

described by a stretched exponential or sum of exponentials, characterized by a

temperature and system dependent exponent that decreased as the state of the system

changed from a monomeric liquid to a fully reacted polymer. At later stages of chemical

reaction a second relaxation process at higher frequencies is revealed. The dielectric

manifestation of the irreversible process of covalent bond formation is remarkably similar

to that observed on supercooling a molecular or polymeric liquid.

Longitudinal velocity and attenuation of ultrasonic waves travelling through the

three molecular liquids at different temperatures have been measured as its molecules

combine irreversibly to form large entities and thereby decrease the diffusivity and

increase the configurational restrictions to their dynamics. From these data, the

longitudinal modulus and compliance are calculated, and the molecular relaxation time and related properties are deduced and interpreted in terms of the number of covalent bonds formed, by a formalism that connects the size of the molecules in the liquid with its elastic behaviour. This relaxation time increases monotonically with increase in the molecule's size, tending to infinity as the number of covalent bonds formed approaches Avogadro's number. The complex plane plots of the modulus and compliance have a shape which is described by a skewed arc function, with a temperature dependent exponent γ, that ranges in values from 0.33- 0.31 for modulus and 0.39-0.45 for compliance. Departure from this shape is shown to be due to contributions from non-zero shear viscosity for relatively small size of molecules, and contributions from a faster, or sub T_g-relaxation process when the molecular size is large, which is similar to the behaviour for the dielectric properties. Simulation of the data suggests that this sub T_g-relaxation process, which is progressively more separated from the main relaxation process as the molecular size increases, contributes significantly to the high frequency elastic properties. The measured longitudinal modulus has been deconvoluted to show that the increase in the bulk modulus, and not the shear modulus, dominates the elastic properties when the molecular size increases. Comparison of the calculated relaxation times for the longitudinal modulus and compliance with the dielectric relaxation time show that the compliance and dielectric data change in a remarkably similar manner with increasing time of chemical reaction, which is unexpected owing to their different mechanisms.

In the last part of this work, the dipolar diffusion in the glassy and supercooled liquid states of 9 additional molecular liquids and of their linear chain or network polymerized states formed by condensation-polymerization at different temperatures and times have been studied by measuring the dielectric properties for a fixed ac frequency of 1 kHz. The study showed that as the extent of polymerization increased with increasing isothermal temperature of polymerization, the sub-T_g relaxation peak due to localized molecular motions in the molecular state became gradually extinct, and a corresponding peak at a higher temperature evolved and reached its maximum height. The temperature of the sub-T_g relaxation peak in the polymerized state differed from that of the α-relaxation peak of the supercooled molecular liquid by as much as 70K, but, in several cases, the two temperatures were similar. Reasons for the latter occurrence are given in phenomenogical terms. It is concluded that the localized relaxation modes of the polar segments of the macromolecule are not related to the modes of molecular diffusion in the monomeric liquid state above its T_g. The localized relaxation characteristic of the glassy molecular state persists in the incompletely polymerized state, where it is seen as a γ-relaxation.

TABLE OF CONTENTS

CHAPTER III: EXPERIMENTAL RESULTS

FIGURE CAPTIONS

Figure 1.1:   Reaction mechanism for the monoamine:epoxide mixtures: (a) reaction of the primary amine with the epoxide to form a secondary amine, (b) reaction of the secondary amine with an epoxide to form a tertiary amine.

Figure 1.2:   Chemical structures of the three monoamines and the epoxide used for the main work in this study. From top to bottom they are: diglycidylether of bisphenol-A (DGEBA), aniline (ANIL), cyclohexylamine (CHMA) and n-hexylamine (HMA).

Figure 1.3:   Chemical structures of the three diamines and one monamine discussed in Chapter VI. From top to bottom they are: ethylene diamine, propylene diamine, hexamethylene diamine and n-octylamine.

Figure 1.4:   Chemical structure of 4-4' diphenylcyanate dimethylmethane (DPDM) as discussed in Chapter VI of this study. The reaction mechanism of DPDM at high temperatures is shown schematically: three $\equiv$CN functional groups combine through a reaction involving a polycylomerization to form a ring. This type of reaction leads to the formation of a three dimensional network structure (Gupta 1991).

Figure 2.1:   Plots of ε', ε'' and tanδ against the logarithm of frequency for a Debye-type relaxation calculated using $\varepsilon_S = 10$, $\varepsilon_\infty = 4$ and $\tau_\varepsilon = 10^{-2}$s.

Figure 2.2:   Cole-Cole plots of ε'' against ε' for (a) a Debye type relaxation, (b) a Davidson-Cole type relaxation and (c) a Cole-Cole type relaxation. The parameters used to calculate the curves were: $\varepsilon_S = 10$, $\varepsilon_\infty = 4$ and $\tau_\varepsilon = \tau_0 = 10^{-2}$s, and $\alpha = \beta_{cd} = 0.5$.

Figure 2.3:   Cole-Cole plots of ε'' against ε' for (a) a Davidson-Cole type relaxation and (b) a stretched exponential relaxation. The parameters used for the calculations were $\varepsilon_S = 10$, $\varepsilon_\infty = 4$, $\tau_0 = 10^{-2}$s and $\beta_{DC} = \beta = 0.5$.

Figure 5.17: The relaxation time <τ> determined from the analysis of both the ultrasonic and dielectric measurements during the isothermal polymerization of the CHMA:DGEBA mixture at 313.4K is plotted against the time of chemical reaction. ε^* refers to the dielectric data, L^* the complex modulus data and C^* the complex compliance data.

Figure 5.18: The relaxation time <τ> determined from the analysis of both the ultrasonic and dielectric measurements during the isothermal polymerization of the HMA:DGEBA mixture at 300.1K is plotted against the time of chemical reaction. ε^* refers to the dielectric data, L^* the complex modulus data and C^* the complex compliance data.

CHAPTER I

INTRODUCTION AND GENERAL BACKGROUND

1.1 Introduction

Polymers can be generally grouped in two categories according to their thermal behaviour. Thermoplastics are polymers which when heated begin to flow and include nylons, polyethylene and polystyrene. Thermosets are polymers which do not flow at elevated temperatures, rather they chemically degrade. Examples of these are bakelite and crosslinked epoxies. Both thermoplastics and thermosets are distinguished by their chemical structures: the former has a linear chain structure and the latter a densely crosslinked structure. Thermoplastics are more widely used than thermosets in structural electronic and medical applications, and they have the attractive feature of possible thermal recyclability.

Polymers can be formed through a wide variety of methods, which can be divided, essentially, into three types of chemical reaction mechanisms: addition, free radical and condensation. In condensation polymerization, chemical reaction occurs between two or more starting materials, termed monomers, with H_2O formed as a reaction product. In free radical polymerization, reaction occurs between a free radical, which acts as the initiator for chemical reaction, and the starting monomers, resulting in the formation of another radical thereby allowing for further reaction. In the third type, step addition polymerization, reaction occurs with equal probability at all reactive groups in the monomers. While the condensation and free radical polymerizations are thought to be well understood, the formation of polymers via a addition type polymerization is still subject to much study (Barton 1985, Johari

1

1994(a)). Their study is complicated because in many step addition systems the initially liquid monomers chemically react under near isothermal conditions to form a vitreous, or glassy, solid. This affects the chemical kinetics in that as reaction occurs, there is an increase in molecular size, and hence a decrease in the diffusivity of the reacting species. As the chains grow, the chemical reaction is slowed by its growth, with the reaction eventually becoming controlled by the diffusivity of the chains themselves. When the polymer reaches a molecular size such that the diffusivity approaches a value essentially near zero, the polymer is said to have vitrified, and the reaction is not observed over a time scale of $\sim 10^3$s (Johari 1994(a)).

While a significant amount of study has been directed at the step-growth of thermosetting polymers (Senturia and Sheppard 1986, Mangion and Johari 1990(a), 1990(b), 1990(c), Johari and Mangion 1991, Parthun and Johari 1992 (a)) little work has focused on thermoplastic addition systems. While the excellent electrical, mechanical and thermal properties of thermosets have made them an increasingly important engineering material (May and Tanaka 1973, Ellis 1993), the advantages in the processing of thermoplastic addition polymers, particularly their reformability, provides a distinct advantage. However, prior to implemention of such materials as end use products, it is crucial to first understand the dynamics of linear chain polymers during their formation. The work in this thesis is aimed at contributing to the knowledge in this area. Specifically, the properties of several new thermoplastic polymers were studied as the structure changed from a molecular liquid mixture to a vitreous or glassy solid. Since the properties change during chemical reaction, it was necessary to use techniques of measurement employing fast times of data acquisition.

For this reason, dielectric spectroscopy and ultrasonics were chosen, since both employ high frequencies, and thus the time periods of measurement were small enough to avoid errors occurring from changes during the measurement. The choice of systems was incidental, rather the physics of the process is applicable to any system in which an initially liquid mixture of monomers reacts by an addition mechanism to form a vitreous solid.

This thesis is divided into seven chapters. This chapter introduces the various definitions and concepts related to the formation of linear-chain polymer by addition reaction. The structures of the starting materials and chemical reaction mechanisms are reviewed, and a brief review of the literature regarding earlier studies is given. The second chapter reviews the phenomenological theories of dielectrics, ultrasonics, and differential scanning calorimetry, and details the experimental apparatus and techniques used for this study.

Chapter III presents the experimental results from measurements of the three polymers used in the study in the molecular liquid state, during the formation of the polymer under isothermal conditions and in the fully reacted state. Here the changes in the dielectric and differential scanning calorimetric properties are shown both as a function of temperature, in the molecular liquid and fully reacted states, and as a function of time, as measured by all three techniques, during polymerization.

The changes in the dielectric properties of the three systems in the molecular liquid and fully reacted states are analyzed in terms of a stretched exponential decay function in Chapter IV. The changes in the dielectric properties during isothermal polymerization are analyzed both as a function of frequency and number of covalent

bonds, n, which was determined from the differential scanning calorimetry data. At higher values of n, both were found to be well described by formalisms based on a stretched exponential decay function, and the theoretical implications are discussed. At low values of n, the changes in the dielectric properties were analyzed in terms of percolation and singularity type equations.

The changes in the ultrasonic velocity and attenuation during chemical reaction are analyzed in terms of the number of covalent bonds formed, n, as determined by differential scanning calorimetry, in Chapter V. Formalisms are developed to account for the observed behaviour, all of which incorporate a distribution of relaxation times functional form. The theoretical implications of the various forms of analysis are compared and contrasted, and the relation between the dielectric and ultrasonic results discussed.

Chapter VI discusses the general findings of both Chapters IV and V where the changing molecular dynamics with increasing number of bonds formed is discussed in light of the experimental data as well as from other experiments and data from the literature. A qualitative description of the overall changes of the localized and long range relaxations with increasing number of chemical bonds formed during reaction is introduced.

The conclusions of this study are given in Chapter VII.

Since this work was initiated, papers on the use of dielectric, ultrasonic and calorimetric techniques for the study of polymerization have appeared in the literature (Lairez et al 1992, Sidebottom 1994). Additionally, several keynote lectures at the 1994 Gordon Research Conferences on Non-destructive Evaluation (June, 1994) and

Dielectrics (July, 1994) have focused specifically on these areas. Therefore it was necessary to submit for publication an account of this study prior to writing this thesis. To that end, several papers outlining both analytic procedures and experimental work have been submitted for publication. Specifically, papers based on some of this work have appeared in the Journal of Noncrystalline Solids (1994, 171, 183), the Journal of the Chemical Society: Faraday Transactions (1995, 91, 329), the Journal of Chemical Physics (1995, 102, 6301; 1995, 103, 440; 1995, 103, 7611) and the Journal of Molecular Liquids (1996, 69, 219; 1996, 69, 283).

1.2   Addition Polymerization

Linear-chain polymers can be formed by addition polymerization through the chemical reaction of two or more low molecular weight liquids. During the reaction, the functional groups of the monomers combine to form junction points, thereby allowing a continuous growth of linear chain molecules. For the systems studied, reaction occurs via two types of chemical reactions, as illustrated in Figure 1.1 for the polymerization of a bi-functional epoxy resin and a monofunctional amine. In the first reaction, a primary amine functional group, $-NH_2$ reacts with the epoxy ring, breaking the ring to form a secondary amine, $-NRH$, and a hydroxyl $(-OH)$group, with the latter then acting as a catalyst for further reaction (Horie et al 1970). In the second reaction, the secondary amine, with its now catalytic pendant hydroxyl group, combines with an epoxy ring from another molecule to form a tertiary amine. Thus the reaction continues to occur with the resulting structure a linear chain. The rates of both the primary and secondary reactions are both temperature dependent and their relative rates
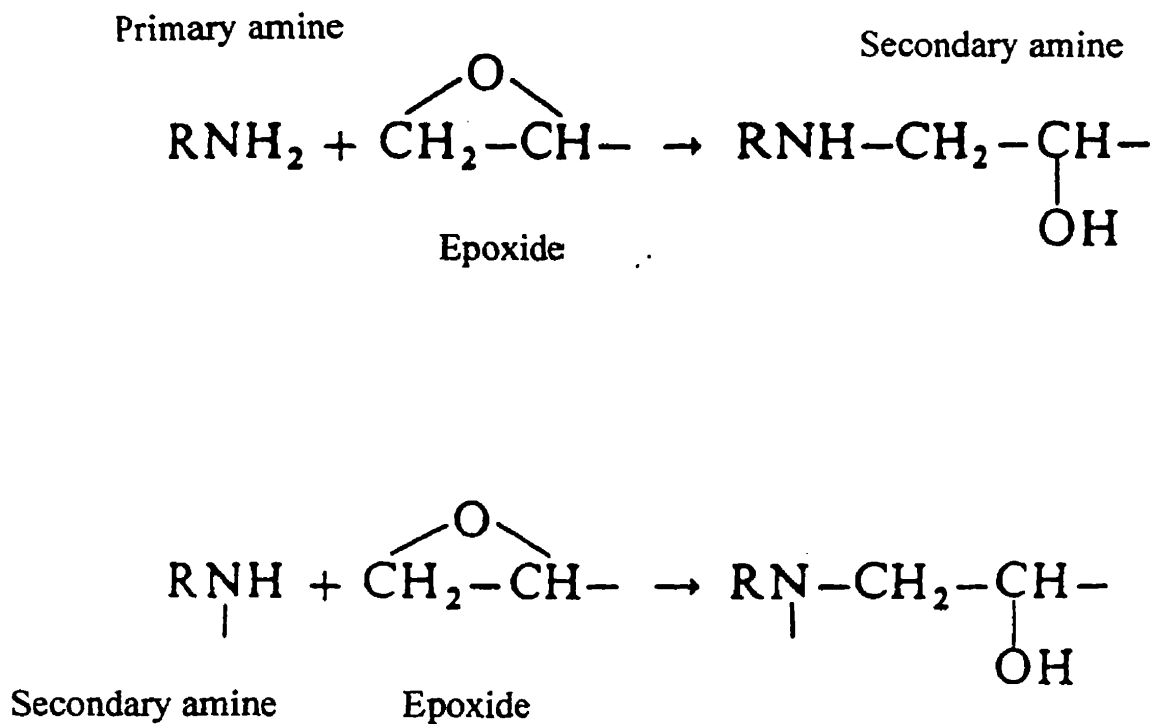
Primary amine

Secondary amine

$$RNH_2 + CH_2{-}CH{-} \rightarrow RNH{-}CH_2{-}CH{-}$$
$$\overset{\diagup O\diagdown}{\phantom{CH_2{-}CH}} \qquad \qquad \overset{|}{OH}$$

Epoxide

$$RNH + CH_2{-}CH{-} \rightarrow RN{-}CH_2{-}CH{-}$$

Secondary amine   Epoxide

Figure 1.1:   Reaction mechanism for the monoamine:epoxide mixtures: (a) reaction of the primary amine with the epoxide to form a secondary amine, (b) reaction of the secondary amine with an epoxide to form a tertiary amine.

determine the ultimate structure of the polymer formed (Barton 1985, Dusek 1986). As the polymer chains grow, the weak van der Waals' interactions are replaced by directional covalent bonds, which in turn increase the viscoelastic relaxation time. Thus the glass transition temperature, T_g , defined as the temperature at which the viscosity, η approaches a value near 10^{13} Poise, continues to increase towards a limiting value as the reaction approaches completion. As vitrification approaches, the reactions become diffusion controlled, though the precise time and viscosity at which diffusion control begins to dominate is still not well understood (Dusek 1986, Chern and Poehlein 1987, Khanna and Chanda 1993).

1.3   The Chemical Structures of the Starting Materials

Aniline (ANIL), cyclohexylamine (CHMA) and n-hexylamine (HMA) of > 99% purity were purchased from Aldrich Chemicals and used as received. Their structures are shown in Figure 1.2 and their properties listed in Table 1.1. A diglycidyl ether of bisphenol-A (DGEBA) tradename EPON 828 was supplied by Shell chemicals, and its structure given in Figure 1.2. These were the materials used for the experiments and analysis in Chapters III-VI. All were liquid at room temperature. These starting materials were chosen for the principle portion of the study because the monoamine:epoxy chemical reaction occurs at near ambient temperatures and the liquids can be readily mixed at room temperature. As well, it is of interest to see the effect of a change in the steric hindrance to both chemical reaction and
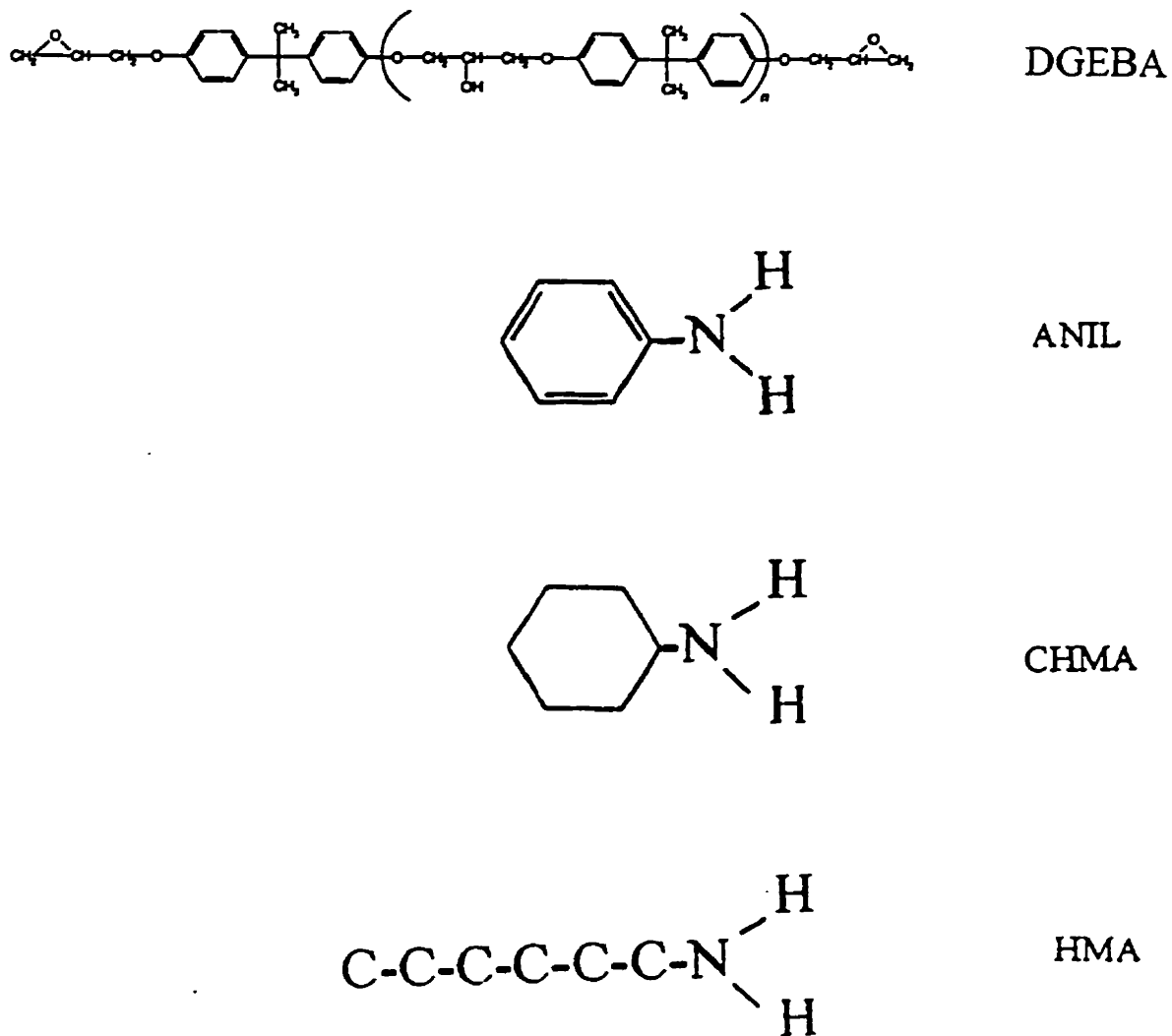
DGEBA

ANIL

CHMA

$$C\text{-}C\text{-}C\text{-}C\text{-}C\text{-}C\text{-}N\begin{smallmatrix}H\\\\H\end{smallmatrix}$$

HMA

Figure 1.2:   Chemical structures of the three monoamines and the epoxide used for the main work in this study. From top to bottom they are: diglycidylether of bisphenol-A (DGEBA), aniline (ANIL), cyclohexylamine (CHMA) and n-hexylamine (HMA).

Table 1.1 Properties of the three monoamines and the bifunctional epoxy used in the studies. All properties are as given from the suppliers. T_{melt} and T_{boil} are the melting and boiling temperatures respectively.

Property	ANIL	CHMA	HMA	DGEBA
mol. wt g/mol	93.13	99.18	101.19	380
density g/cm^3	1.022	0.867	0.919	1.16
T_{melt}/K	267	256	250	Supercools~ 295K
T_{boil}/K	443.4	407	404	decomposes

molecular diffusion when the hydrocarbon group was changed from phenyl to cyclic to linear structure.

For the work described in Chapter VI, several additional systems were studied. Ethylene diamine, propylene diamine, hexamethylene diamine and n-octylamine of >99% purity were purchased from Aldrich Chemicals, and their chemical structures shown in Figure 1.3. 4-4' diphenylcyanate dimethylmethane (DPDM), a difunctional cyanate, was donated by Rhone Poulenc, Kentucky. Its structure is shown in Figure 1.4. The reaction mechanism for the diamine:epoxy systems is identical to that shown for the monoamine:epoxy systems in Figure 1.1, but the resulting structure is a network, since the second amine at the end of the diamine molecule acts as a bridge between linear chains. DPDM requires no additional materials to initiate chemical
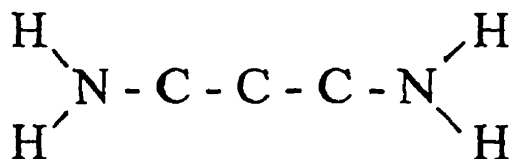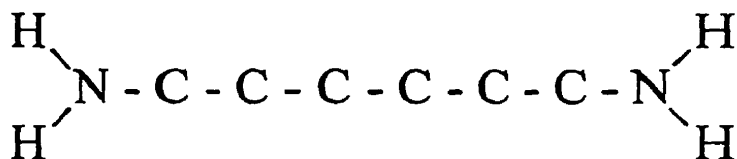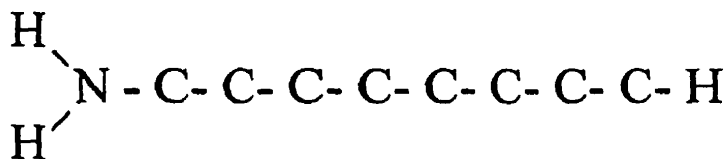
Figure 1.3: Chemical structures of the three diamines and one monamine discussed in Chapter VI. From top to bottom they are: ethylene diamine, propylene diamine, hexamethylene diamine and n-octylamine.

DICYANATE MONOMER

Figure 1.4:   Chemical structure of 4-4' diphenylcyanate dimethylmethane (DPDM) as discussed in Chapter VI of this study. The reaction mechanism of DPDM at high temperatures is shown schematically: three =CN functional groups combine through a reaction involving a polycylomerization to form a ring. This type of reaction leads to the formation of a three dimensional network structure (Gupta 1991).

reaction. The reaction mechanism, as illustrated in Figure 1.4, involves the polycyclotrimerization reaction of three CN functional units of separate molecules to form a network structure. Detailed analysis of the reaction mechanisms in DPDM have been outlined previously (Gupta 1991, Osei-Owusu et al 1992) and may be consulted for further details and discussion.

The structural changes that occur during the growth of the linear chain polymers during isothermal chemical reaction can be described qualitatively as follows. Immediately after mixing, the number of bonds formed, n, is 0 and the structure consists of a mixture of both amine and epoxy monomers. The relaxation time, τ, $\sim$ 100 ps and the shear modulus, G, a measure of the stiffness of the material under a shear stress, $\sim$ 0. As the reaction occurs, progressively longer chains are formed. Eventually, a sufficient number of chains form such that the polymer vitrifies. In the vitreous state, τ>1000s and G$\sim$1-10 GPa. Thus, during the chemical reaction there is an increase of nearly 12 orders of magnitude in τ and 10 orders of magnitude in G. If the polymer is then allowed to fully react, such that n$\rightarrow$n$_{max}$, the ultimate structure formed can be either one continuous chain, or several oligomeric rings. For the former, $\tau \rightarrow \infty$ and G remains near 10 GPa, whereas for the latter, τ approaches a certain finite limiting value and G remains essentially constant. Since both dielectric and ultrasonic techniques allow for the determination of the relaxation time, both can be used to continuously monitor the changes that occur in situ. Calorimetry allows for the determination of the number of chemical bonds formed, so that a combination of the three techniques allows for the study of the changes in both the dielectric and high frequency mechanical behaviour with increasing number of chemical bonds formed. In addition, both dielectric and ultrasonic techniques can be used directly for on-line monitoring during polymer processing.

Prior to this work, there were few dielectric and ultrasonic studies of the formation of linear-chain polymers via addition reactions. However, there has been substantial work on the formation of network, or thermoset polymers that merit some review. As outlined in Section 1.3, the formation of some thermosetting polymers, particularly the diamine:epoxy polymers, also occurs by a two-step process. Chemical reaction leads to the formation of a three dimensional network, or gelled structure, prior to the formation of a vitreous structure. Many of the studies in the literature are concerned with the gelation phenomena (Gillham 1986, Johari and Mangion 1991, Lairez et al 1992, Sidebottom 1994), which is irrelevant to the linear-chain polymers studied here.

1.4   A General Review of the Literature

Since there exist polar groups in all commercial thermosets, dielectric spectroscopy is a useful technique for their study. Senturia and Sheppard (1986) have provided a detailed review with over 100 references describing early work in the field. The results of their work are aimed at providing a relationship between the changes in the measured conductivity and the viscosity of the system, but they do not examine the relaxation behaviour. Subsequent work by their group (Sheppard and Senturia 1986, Bidstrup et al 1989), followed essentially the same lines, but all experimental results were hampered by the experimental technique employing a small, comb circuit sensor that was susceptible to edge effects from stray capacitance.

A study by Kranbuel et al (1989) employing dielectric spectroscopy, differential scanning calorimetry and viscometry was aimed at relating the changing rheological and

dielectric properties. Again the focus was to relate the changing conductivity with the shear viscosity, such that both approach singularities with the onset of gelation.

An alternate method for the analysis was provided by Mangion and Johari (1990(a) 1990(b), 1991(a), 1991(b) and 1991(c)) who thoroughly investigated the isothermal formation of thermosets using dielectric methods. They developed formalisms for relating the changing conductivity with the onset of gelation using a percolation model and for determining the relaxation time changes with increasing time of chemical reaction. These formalisms were tested by Parthun and Johari (1992(a), 1992(b)) who examined the effect of polymerizing temperature on the properties, and showed that the times for gelation were consistent with statistical predictions. Parthun and Johari (1992(c)) developed a formalism, based on the work of Mangion and Johari (1990(a), 1990(b), 1991(a), 1991(b), 1991(c)), to describe the changes observed in the non-isothermal formation of thermosets. The techniques of this group have been successfully used by other workers (Deng and Martin 1994, Alig et al, 1995). The limitations to the work up to this point was that only one frequency was used, and the changes were related to the increasing time of reaction, rather then to the extent of chemical conversion.

Using high frequency (kHz-GHz) dielectric spectroscopy, Tombari and Johari (1992) studied the formation of a thermoset both as a function of frequency and of reaction time. They found that the information obtained on the relaxation time during thermoset curing was the same irrespective of whether measurements were made as a function of increasing time at constant frequency, or as a function of increasing frequency at fixed times. While this study provided extremely useful information, it was hampered by resolution difficulties owing to the effect of high frequency relaxation.

While work is still ongoing in this field (Lairez et al 1992, Mijovic and Belluci, 1996), the emphasis now seems to be on the development of on-line monitoring techniques rather then the development of the physics of the process. To more properly understand the latter a thorough study of the changing dielectric properties with the extent of chemical conversion, and employing multiple frequencies, seems required.

Ultrasonics were introduced as a process control technique for monitoring the formation of thermoset polymers in the by several groups (Sofer et al, 1952; Williamson, 1969), but, following this, there was little subsequent work on this topic until the 1970's. Papidakis (1974) monitored the changing velocity and attenuation of ultrasonic waves during the formation of a thermoset, and attempted to qualitatively discuss the relationship of the observed features, such as peaks in the measured attenuation and step-rises in the velocity, to the gelation and vitrification processes that occur during polymerization. This has led to the rational that the appearance of a peak in the attenuation, when measured during the formation of a thermoset, was indicative of gelation. However, using a different approach, Alig and Johari (1992) related the changes to the increase in the relaxation time during polymerization, that manifests itself as a relaxation feature. Sidebottom (1994) disagreed with this interpretation and provided a percolation theory to explain that the observed feature result from the formation of a gelled structure. To resolve these issues it is useful to examine the polymerization of a system exhibiting no gelation phenomena, such as a linear chain polymer. As well, all studies reported relate the changing properties to the time of chemical reaction, rather then to the extent of chemical reaction. A study focusing on the latter would be useful in relating the changing viscoelastic properties to the structure.

Such relationships between the extent of chemical conversion and the dielectric and mechanical properties have not been made previously. A popular description of the changing properties during the formation of thermosets is the TTT (time-temperature-transformation) diagram proposed by Gillham (1986). This type of diagram qualitatively shows the times at which the gelation and vitrification of the thermoset occur during chemical reaction. However, such diagrams do not discuss the relationship between the time of reaction and the extent of reaction. Further, they minimize the large changes in the properties that occur in the vicinity of the glass transition by representing all regions not vitrified as "sol". It would be useful then to determine a method for characterizing the viscoelastic properties as a function of both increasing chemical reaction and temperature in such a way that the relaxation time could be determined at any time during the reaction at any temperature. This requires a detailed study of the properties of the polymer both as a function of temperature and chemical conversion, and is one of the goals of this work.

It is hoped that this work will serve as a contribution into the general area of polymer science, and that ultimately it will encourage additional work in the field. Specifically, the contributions to a better understanding of the changing dielectric and ultrasonic properties with changing chemical conversion will lead to future work in both reaction rate theory and polymer processing; with the former focusing on the polymer physics and the latter on engineering. For these reasons, I feel that this work is of importance to the scientific community, and that the research contained is valuable.

CHAPTER II

EXPERIMENTAL METHODS

2.1 **Dielectric Measurements**

2.1.1 Phenomenological Aspects of Dielectric Measurements

Dielectric measurements are generally made by placing a sample between two conducting plates of known area and separation distance and applying a fixed or sinusoidal electric field across the dielectric sample, which is distinguished by its lack of electronic conduction. For a fixed electric field, this results in a preferential alignment of electric dipoles in the bulk of the sample which causes an instantaneous and time-dependent charge build-up upon the plates of the capacitor. This build-up of surface charge per unit surface area is referred to as the polarization of a dielectric material.

For a sinusoidal electric field, a phase angle lag, δ, develops between the applied electric field and the resultant electric polarization of the sample, owing to the time associated with dipole reorientation. The phase angle lag varies with the frequency of the applied field. In dielectric measurements using a low frequency, sinusoidal electric field, the magnitude of the applied electric field, $\underline{E}$, and of the resultant charge displacement, $\underline{D}$, are written as time-dependent complex quantities,

$$E^*(t) = E_o \exp(i\omega t),$$ (2.1)

$$D^*(t) = D_o \exp(i\omega t),\qquad\qquad(2.2)$$

where ω is the angular frequency of the measurement, (= $2\pi f$), t is the time of measurement, i = $(-1)^{1/2}$, and E_0 and D_0 are the respective electric field and charge displacement amplitudes. The time-dependent electrical polarization, P(t), of the dielectric sample is then expressed as,

$$P(t) = P_\infty + [1 - \Phi(t)]P_o\qquad\qquad(2.3)$$

where P_∞ refers to the instantaneous polarization, associated with the electronic transitions and atomic vibrations, and P_0, the dipolar polarization which is time dependent through the function $\Phi(t)$. $\Phi(t)$ is the relaxation function which thus describes the time-dependent approach of the polarization from P_∞ towards an equilibrium value, $(P_\infty + P_0)$. The charge displacement, D, resulting from the applied electric field is related to polarization by,

$$D(t) = \varepsilon_o E_o + P(t)\qquad\qquad(2.4)$$

where ε_0 is the permittivity of vacuum (=8.8514 pF/m). Eqn. (2.4) is written as,

$$D(t) = \varepsilon(t)\varepsilon_o E_o\qquad\qquad(2.5)$$

where $\varepsilon(t)$ is the time-dependent permittivity of the dielectric sample subject to the boundary conditions,

$$\begin{aligned}\varepsilon(t \to 0) &= \varepsilon_\infty \quad as \quad \omega \to \infty\\\varepsilon(t \to 0) &= \varepsilon_s \quad as \quad \omega \to 0\end{aligned}\qquad\qquad(2.6)$$

where ε_∞ is the limiting high frequency permittivity and ε_s the static permittivity. The former includes contributions from only electronic and vibrational polarizations while the latter additionally includes dipolar polarization. For a sinusoidal applied field, the displacement is a complex quantity and Eqn. (2.5) may be written as,

$$D^* = \varepsilon^* \varepsilon_o E^* \qquad (2.7)$$

where ε^* is the complex dielectric permittivity. Combining Eqns. (2.7), (2.2) and (2.1) gives,

$$\varepsilon^* = \frac{D^*}{E^* \varepsilon_o} = \frac{D_o}{E_o \varepsilon_o} [\cos(\delta) - i\sin(\delta)] = \varepsilon' - i\varepsilon'' \qquad (2.8)$$

where,

$$|\varepsilon| = \frac{D_o}{E_o \varepsilon_o} \qquad (2.9)$$

$$\varepsilon' = |\varepsilon| \cos(\delta); \quad \varepsilon'' = |\varepsilon| \sin(\delta); \quad \frac{\varepsilon''}{\varepsilon'} = \tan\delta \qquad (2.10)$$

ε', ε'' and $\tan\delta$ are the dielectric permittivity, the dielectric loss and dissipation or loss factor, respectively.

In the theories of dielectric polarization, a linear response of polarization to the electric field is assumed. This assumption allows the use of the Boltzmann superposition principle (McCrum et al. 1967). Accordingly, D(t), at any instant of time, t_i, is the sum of all displacements arising from incremental fields applied at previous times u, where $u \leq t$:

$$\frac{D(t)}{\varepsilon_o} - \varepsilon_\infty E(t) + (\varepsilon_s - \varepsilon_\infty) \int_0^t dE(u)[1 - \Phi(t - u)] \qquad (2.11)$$

Substituting (t-u) by Θ and integrating Eqn. (2.11) by parts gives,

$$\frac{D(t)}{\varepsilon_o} - \varepsilon_\infty E(t) + (\varepsilon_s - \varepsilon_\infty) \int_0^t E(t - \theta) \left[-\frac{\partial \Phi}{\partial \Theta} \right] d\Theta \qquad (2.12)$$

where $(-d\Phi/d\Theta)$ describes the rate at which the permittivity changes from ε_∞ to the equilibrium value ε_s. E(t) is analogous to the instantaneous displacement or response due to electronic and vibrational polarization.

2.1.2 The Single Relaxation Time or Exponential Relaxation.

In a phenomenological model, Debye (1929), assumed that the rate of change of polarization with time is given by,

$$\frac{dP}{dt} - \frac{[P_o - P(t)]}{\tau_\varepsilon} \qquad (2.14)$$

where τ_ε is a constant referred to as the relaxation time, and P_0 and P(t) are as defined earlier. The solution to Eqn. (2.13) is,

$$P(t) - P_o + \Phi_o exp \left[-\frac{t}{\tau_\varepsilon} \right], \qquad (2.14)$$

where $\Phi(t) = \Phi_0 \exp(-t/\tau_\varepsilon)$ is the relaxation function for a single relation time process. Combining Eqns. (2.12), (2.8) and (2.1) yields,

$$\varepsilon^* = \varepsilon_\infty + (\varepsilon_s - \varepsilon_\infty) \int_0^\infty exp(i\omega t) \left[-\frac{\partial \Phi}{\partial t} \right] dt. \tag{2.15}$$

Substituting Eqn. (2.14) into Eqn. (2.15) leads to the Debye equation,

$$\frac{(\varepsilon^* - \varepsilon_\infty)}{(\varepsilon_s - \varepsilon_\infty)} = \frac{1}{(1 + i\omega\tau_\varepsilon)}, \tag{2.16}$$

which is written in terms of its respective real and imaginary components, ε' and ε'', as,

$$\varepsilon' = \varepsilon_\infty + \frac{(\varepsilon_s - \varepsilon_\infty)}{\left(1 + \omega^2 \tau_\varepsilon^2\right)}, \tag{2.17}$$

$$\varepsilon'' = \frac{(\varepsilon_s - \varepsilon_\infty)\omega\tau_\varepsilon}{\left(1 + \omega^2 \tau_\varepsilon^2\right)}, \tag{2.18}$$

and,

$$\tan\delta = \frac{\varepsilon''}{\varepsilon'} = \frac{(\varepsilon_s - \varepsilon_\infty)\omega\tau_\varepsilon}{\left(\varepsilon_s + \varepsilon_\infty \omega^2 \tau_\varepsilon^2\right)}. \tag{2.18}$$

The relaxation time, τ_ε, in Eqn. (2.16) is the time for the decay polarization by a factor e^{-1} after the removal of the electric field. Plots of the characteristic shapes of ε', ε'' and $\tan\delta$ against $\log \omega$ for the Debye model are shown in Figure 2.1.

2.1.3 Distribution of Relaxation Times

It is now recognized that with the exception of certain dilute solution systems of large polar molecules in non-polar solvents at high temperatures (Daniel 1967, Johari and Smyth 1972), Eqn. (2.16) for the single relaxation time model does not satisfactorily describe the observed dielectric behaviour in polymeric solids. Nevertheless, it has been used as a basis for equations that describe the relaxation behaviour of most dielectric materials in terms of a sum of single relaxation functions, such that,

$$\Phi(t) = \int_0^\infty \exp\left[-\frac{t}{\tau}\right] G(\tau)\,d\tau, \tag{2.20}$$

where,

$$\int_0^\infty G(\tau)\,d\tau = 1 \tag{2.21}$$

The term $G(\tau)d\tau$, a distribution function, acts as a weighting term corresponding to the fraction of relaxation processes with a relaxation time between τ and $d\tau$. Applying the superposition principle leads to,
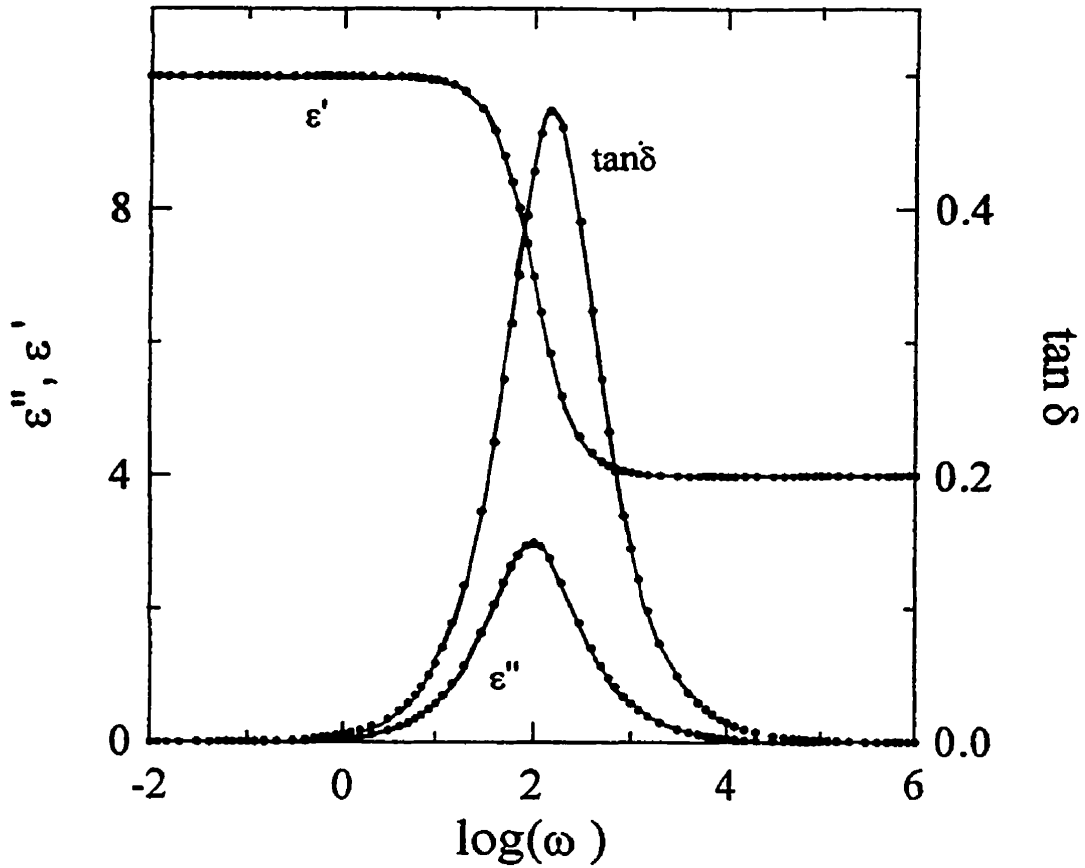
Figure 2.1:   Plots of ε', ε'' and tanδ against the logarithm of frequency for a Debye-type relaxation calculated using $\varepsilon_S = 10$, $\varepsilon_\infty = 4$ and $\tau_\varepsilon = 10^{-2}$s.

$$\varepsilon^*(t) = \varepsilon_\infty + (\varepsilon_s - \varepsilon_\infty) \int_0^\infty \exp(-t/\tau) G(\tau) \, d\tau \qquad (2.22)$$

Several workers in this field (Wagner 1913, Whitehead and Bauer 1932, Yeager 1936), have attempted to evaluate $G(\tau)$ directly; however, all have had limited success in the interpretation of $G(\tau)$.

In an alternative method, empirical equations of the relaxation function, $\Phi(t)$, have been proposed by different groups (Fuoss and Kirkwood 1941, Cole and Cole 1941, Davidson and Cole, 1950 and 1951, Hammon 1951, Havriliak and Negami 1966, Williams and Watts 1970) to describe the relaxation behaviour in a wide range of dielectric materials. This has been done by representing the data as plots of ε'' against ε' in the Argand plane as a function of frequency. Known as Cole-Cole plots (Cole and Cole 1941), they are semicircular in shape for the case of a Debye-type solid according to,

$$\left[\varepsilon' - \frac{\varepsilon_s - \varepsilon_\infty}{2} \right]^2 + \varepsilon''^2 = \left[\frac{\varepsilon_s - \varepsilon_\infty}{2} \right]^2 \qquad (2.23)$$

which follows directly from Eqns. (2.17) and (2.18). A typical shape, shown in Figure 2.2, has a characteristic radius of $(\varepsilon_s - \varepsilon_\infty)/2$, centred at a point $(\varepsilon_s + \varepsilon_\infty)/2$ along the ε' axis from the origin.

For a number of dielectric materials, Cole and Cole (1941) found that an equation of the form,

$$\varepsilon^* = \varepsilon_\infty + \frac{\varepsilon_s - \varepsilon_\infty}{(1 + i\omega\tau_o)^{(1-\alpha)}} \qquad (2.24)$$

more adequately described their data. Separating the real and imaginary components of Eqn. (2.24) gives,

$$\varepsilon' = \varepsilon_\infty + (\varepsilon_s - \varepsilon_\infty)\frac{[1 + (\omega\tau_o)^\alpha \cos(\alpha\pi/2)]}{\left[1 + \dfrac{2(\omega\tau_o)^\alpha \cos(\alpha\pi)}{(2 + \omega\tau_o)^{2\alpha}}\right]} \qquad (2.25)$$

and,

$$\varepsilon'' = (\varepsilon_s - \varepsilon_\infty)\frac{(\omega\tau_o)^\alpha \sin(\alpha\pi)}{1 + 2(\omega\tau_o)^\alpha \cos(\alpha\pi/2) + (\omega\tau_o)^{2\alpha}} \qquad (2.26)$$

According to Eqns. (2.25) and (2.26), a plot of ε'' against ε' would be an arc of a circle centred in the plane below the horizontal, ε', axis. The resultant curve has a radius $[(\varepsilon_s - \varepsilon_\infty)/2]$ cosec $(\alpha\pi/2)$, and, like the Debye curve, is symmetric about the point $(\varepsilon_s + \varepsilon_\infty)/2$. The parameter $0 < \alpha \leq 1$ describes the symmetric broadening of the curve from the semicircular Debye curve, for which $\alpha = 0$. The relaxation time, τ_o, is the average relaxation time. When $\omega\tau_o = 1$, ε'' reaches a maximum, ε' a point of inflection and for both curves a point of symmetry. Figure 2.2 shows characteristic plots for both Debye and Cole-Cole distributions. It should be noted that the parameter, α, can be obtained directly from the plot by measuring the angle, δ, subtending the radius of the circle to the horizontal axis and using the relation $\delta = \alpha\pi/2$.
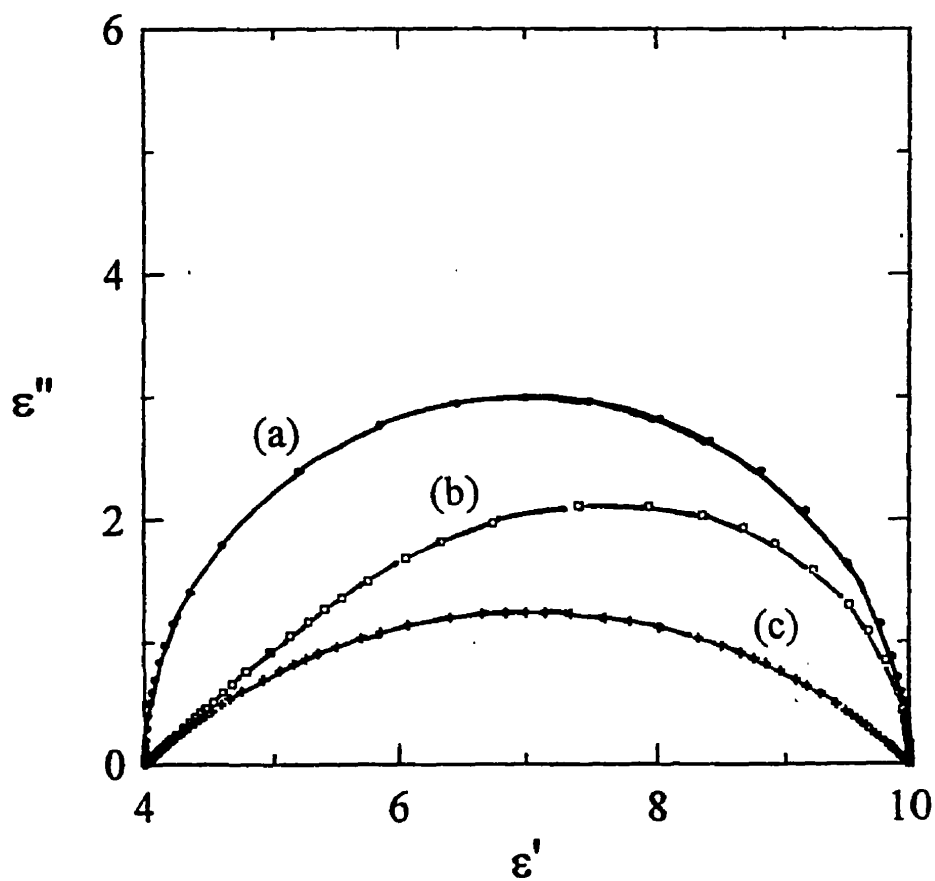
Figure 2.2:   Cole-Cole plots of ε'' against ε' for (a) a Debye type relaxation, (b) a Davidson-Cole type relaxation and (c) a Cole-Cole type relaxation. The parameters used to calculate the curves were: $\varepsilon_S = 10$, $\varepsilon_\infty = 4$ and $\tau_\varepsilon = \tau_o = 10^{-2}$s, and $\alpha = \beta_{cd} = 0.5$.

While the Cole-Cole and Debye empirical equations have been used to describe certain molecular behaviour, it is generally found that the Cole-Cole plots of molecular ratios are not symmetric about $\omega\tau_o = 1$. Rather, the curves are found to deviate or broaden considerably at high frequencies giving the circle the appearance of a skewed arc. An empirical equation for the shape of a skewed arc was first given by Davidson and Cole (1950, 1951) who modified the Debye equation or Eqn. (2.17) to obtain,

$$\frac{\varepsilon^* - \varepsilon_\infty}{\varepsilon_s - \varepsilon_\infty} = \frac{1}{(1 + \omega\tau_o)^{\beta_{cd}}} \tag{2.27}$$

where the real and imaginary components of ε^* are given by,

$$\varepsilon' = \varepsilon_\infty + (\varepsilon_s - \varepsilon_\infty)(\cos\Phi)^{\beta_{cd}} \cos\beta_{cd}\Phi \tag{2.28}$$

$$\varepsilon'' = (\varepsilon_s - \varepsilon_\infty)(\cos\Phi)^{\beta_{cd}} \sin\beta_{cd}\Phi \tag{2.29}$$

and,

$$\tan\Phi = \omega\tau_o \tag{2.30}$$

where Φ is the relaxation function. Clearly for this empirical equation, the maximum loss, ε''_{max}, occurs not at $\omega\tau_o = 1$, but at $\omega\tau_o = \tan[\pi/2(1+\beta_{cd})]$. At limiting high frequencies, the approach of the arc towards the abscissa becomes a straight line, with the angle between the line and the abscissa equal to $\beta_{cd}\pi/2$. The parameter β_{cd} is a measure of the degree of deviation from the Debye equation for which $\beta_{cd} = 1$. In the limiting cases for both Cole-Cole and Cole-Davidson distributions, when $\alpha = 1$ or $\beta_{cd} = 0$ the complex plane plot is a straight line described by $\varepsilon'' = 0$.

Another empirical distribution function, proposed originally by Kohlrausch (1854) for the analysis of creep and popularized by Williams and Watts (1970) to describe the dielectric behaviour of liquids, is given by the stretched exponential function of the form,

$$\Phi(t) = \Phi_o \exp - (t/\tau_o)^\beta \qquad (2.31)$$

where Φ_o is the value of the relaxation function for t $\rightarrow$ 0, τ_o is the characteristic relaxation time, and ß is an empirical parameter whose value is in the range $0 \le \beta \le 1$. While both the Cole-Davidson and stretched exponential distributions are asymmetric, their respective shapes differ substantially. For the Cole-Davidson distribution, the average relaxation time, $\langle\tau\rangle$, is given by:

$$\langle\tau\rangle = \beta_{cd}\tau_o \qquad (2.32)$$

while for the stretched exponential distribution,

$$\langle\tau\rangle = \frac{\tau_o}{\beta}\Gamma\left[\frac{1}{\beta}\right] \qquad (2.33)$$

where $\Gamma(x)$ is the gamma function of x. The shape of the complex plane plot of ε'' vs. ε' for the stretched exponential distribution is shown for typical values in Figure 2.3. It is seen in the plots that the approach towards the Debye-type behaviour in the high frequency domain is much more gradual for the stretched exponential distribution than for the Cole-Davidson. A rigorous mathematical comparison between the Cole-Davidson and stretched exponential forms is given by Lindsey and Patterson (1980),
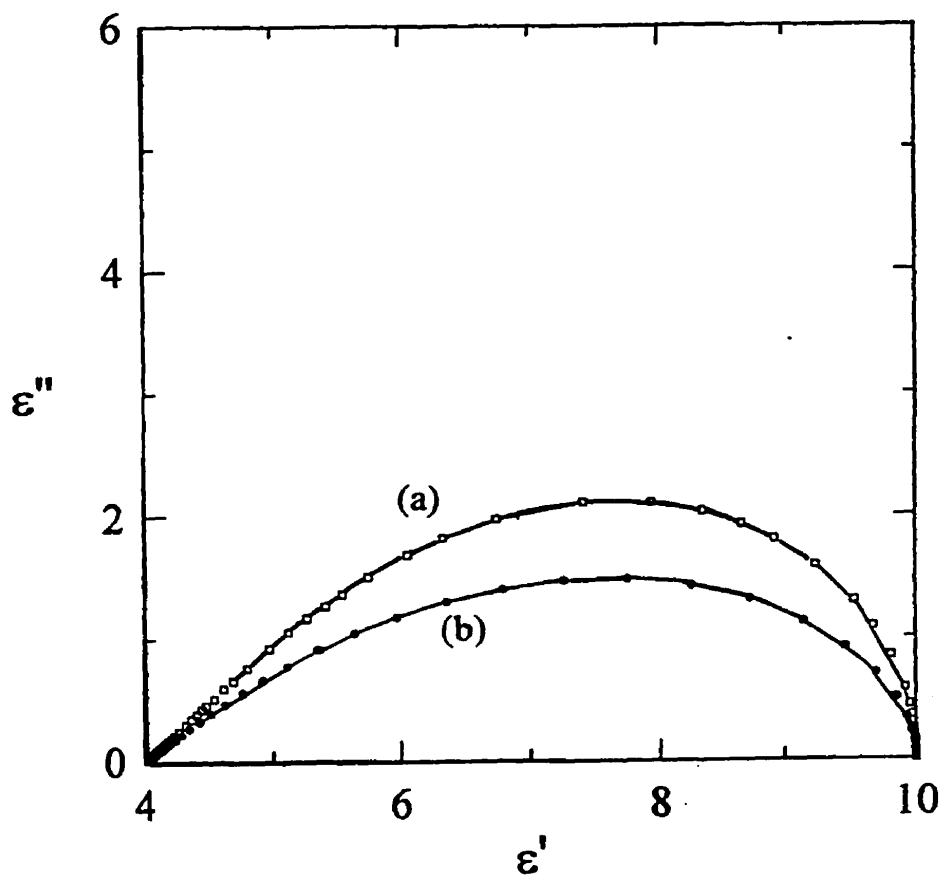
Figure 2.3:   Cole-Cole plots of ε'' against ε' for (a) a Davidson-Cole type relaxation and (b) a stretched exponential relaxation. The parameters used for the calculations were $\varepsilon_S = 10$, $\varepsilon_\infty = 4$, $\tau_0 = 10^{-2}$s and $\beta_{DC} = \beta = 0.5$.

who have shown that within the experimental uncertainty, the two equations are indistinguishable when $\beta \rightarrow 1$.

2.1.4 Conductivity Relaxation

The assumption that a dielectric material has zero conductivity, while facilitating the analysis of the ε'' spectra via the formalisms outlined, is not realistic in that ionic impurities are often present in materials, whose transport contributes to the electrical conductivity. When ions in a material are free to diffuse, a finite current flows through the material whose magnitude is given by,

$$I_\sigma^* - GV^* - GlE^*, \tag{2.34}$$

where V^* and E^* are sinusoidal applied voltage and electric field, G is the d.c. conductance, and l is the thickness of the sample. The current across a dielectric material is written as,

$$I - A\frac{dD^*}{dt}, \tag{2.35}$$

where A is the capacitor plate area and D^* the electrical displacement. The contribution to the electrical displacement from conductivity, D_σ^*, is calculated from Eqns. (2.34) and (2.35) as,

$$D_\sigma^* - \frac{\sigma_o E^*}{i\omega} \tag{2.36}$$

where σ_0 is the d.c. conductivity, and ω is the angular frequency. Thus, in terms of the total complex permittivity,

$$\varepsilon^* = \varepsilon_{dip}^* + \varepsilon_{dc}^* ,$$

(2.37)

or,

$$\varepsilon^* = \varepsilon' - i(\varepsilon''_{dip} + \varepsilon''_{dc})$$

(2.38)

In the absence of a dielectric relaxation due to dipole reorientation, ε^* of the material has a frequency dependence defined as,

$$\varepsilon^* = \varepsilon_\infty - \frac{i\sigma_0}{\varepsilon_0 \omega}$$

(2.39)

The dc conductivity can be written in the form of a relaxation time according to Maxwell's original relation for the relaxation of an RC circuit. This has been extended by Macedo, Moynihan and Bose (1972) to define a conductivity relaxation time, τ_σ, as,

$$\tau_\sigma = \frac{\varepsilon_0 \varepsilon_\infty}{\sigma_0}$$

(2.40)

which gives the relation,

$$\varepsilon^* = \varepsilon_\infty - \frac{i\varepsilon_\infty}{\omega \tau_\sigma}$$

(2.41)

Thus, both the dc conduction and dipolar re-orientation, which contribute to ε^*, can be taken into account.

2.2 Principles of Dielectric Spectroscopy

For the frequency range used in dielectric measurements, it is useful to consider that for fixed values of ω, the dielectric response is equivalent to the response of a capacitance, Cp, in parallel with a resistance, Rp. For a parallel plate capacitor, with plate area A and separation l, the capacitance in vacuum is given by,

$$C_o = \frac{A\,\varepsilon_o}{l} \qquad (2.42)$$

where ε_o = 8.8514 pF/m. If a dielectric sample is placed between the plates the new capacitance is,

$$C = \varepsilon\,C_o \qquad (2.43)$$

where ε is the dielectric permittivity defined earlier. When a sinusoidal voltage of the form,

$$V^* = V_o \exp(i\omega t) \qquad (2.44)$$

is applied across the filled capacitor, the capacitance becomes complex, such that $C^* = \varepsilon^* C_o$, and the resulting current, according to Eqn. (2.35) is,

$$I^* = A\frac{dD^*}{dt} = \frac{d(C^*V^*)}{dt} \tag{2.45}$$

Combining Eqns. (2.44) and (2.45) gives,

$$I^* = \omega C_o V^* (i\varepsilon' + \varepsilon'') \tag{2.46}$$

For a resistor, Rp in parallel with a capacitance, Cp, the electrical admittance, Y^*, is given as,

$$Y^* = \frac{1}{Rp} + i\omega Cp \tag{2.47}$$

Since the admittance is the ratio of current to the voltage applied,

$$I^* = Y^* V^*, \tag{2.48}$$

which, from Eqns. (2.47) and (2.48), implies that,

$$\varepsilon' = \frac{Cp}{C_o}, \tag{2.49}$$

and,

$$\tan \delta = \frac{1}{Rp\,\omega\,Cp} \tag{2.51}$$

If the circuit is instead considered to be a capacitance, Cs, in series with a resistance, Rs, the electrical impedance, Z^* $(= 1/Y^*)$, becomes,

$$Z^* = Rs + \frac{1}{i\omega Cs},$$

(2.52)

Since the impedance is given as the ratio of voltage to current, from Eqns. (2.47) and (2.48),

$$\varepsilon' = \frac{Cs}{C_o(1 + \tan^2\delta)},$$

(2.53)

$$\varepsilon'' = \frac{Rs\,Cs^2\,\omega}{C_o(1 + \tan^2\delta)},$$

(2.54)

$$\tan\delta = Rs\,Cs\,\omega.$$

(2.55)

Equations (2.53) to (2.55) constitute a set of equations that are generally used in the measurement of dielectric properties of a material.

2.2.1 The Equipment and Associated Assembly

All dielectric measurements were made with a microprocessor-controlled, automatic RLC meter model GR 1689 Digibridge manufactured by the General Radio Company. The bridge calculates the desired parameters from a series of 6 or 8 voltage measurements, which include both quadrature $(\pi/2)$ and inverse (π) vector components of the voltages across the device under test, Z_x, and across a standard resistor R_s carrying the same current as Z_x. Each set of voltage measurements is made in rapid

sequence with the same phase-sensitive detector, which, for properly chosen differences between the measurements, allows the fixed offset error to be removed, while the ratios of the voltage measurements eliminates the remaining current and scale factor effects. A schematic diagram for the operations of GR 1689 Digibridge is given in Figure 2.4, where I_x is the current provided by the sine-wave generator. The unknown Z_x and known internal resistance standard, R_s, are both supplied with a test signal at a frequency f from a sine-wave generator. Two differential amplifiers with the same gain, K, then produce voltages e_1 and e_2 according to:

$$e_1 - KZ_xI_x$$
$$e_2 - KR_xI_x, \qquad (2.57)$$

Since K is constant, Eqn. (2.57) gives the following expression for the unknown impedance:

$$Z_x^* - R_s \frac{e_1^*}{e_2^*}. \qquad (2.58)$$

The ratio in Eqn. (2.58) is a complex quantity so that the values of capacitance, C, and loss factor, D, or equivalently tanδ, can be calculated from Eqn. (2.58). Since the effects of the common current and the scale factor are eliminated from the measurement, the calculated values of C and D are accurate to within ≤ 0.5% and ± 0.5%, respectively. The Genrad 1689 was interfaced with an IBM portable computer by means of an IEEE interface card, which allowed the parameters of the bridge to be modified and stored. Additional algorithms were written which allowed the input of
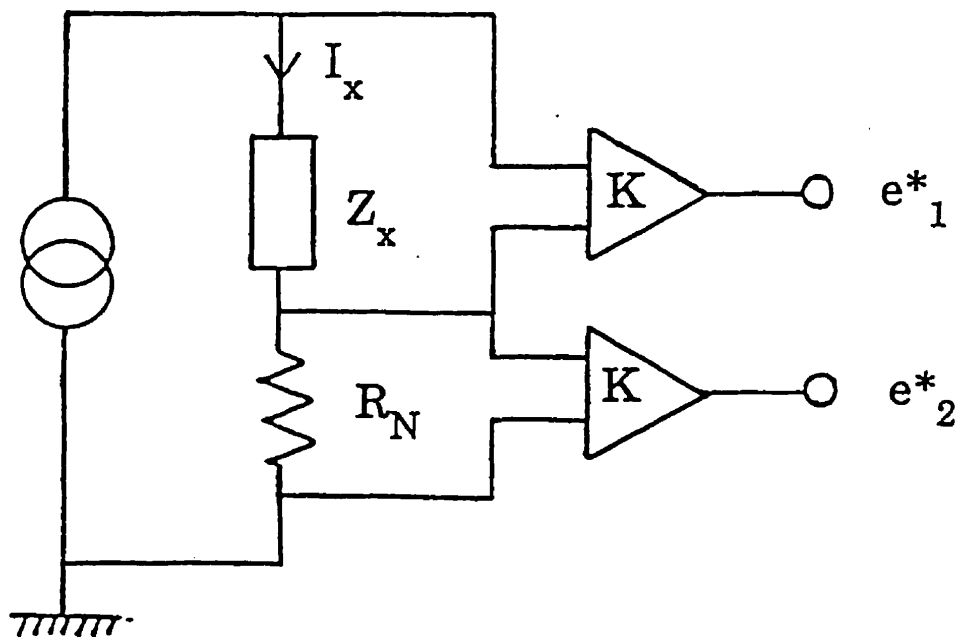
Figure 2.4: Schematic diagram for the operations of the GenRad 1689 digibridge. The parameters e^{*}_1, e^{*}_2, Z_x, I_x and R_N are as discussed in the text and used in Eqns. 2.57 and 2.58.

the parameters necessary for measurements to be carried out in both isothermal kinetic and fixed frequency modes.

An aluminum block 16 cm long, 6 cm in diameter with a concentric 0.5 cm diameter, 5 cm deep bore was used as the thermostat. The block was coated with insulating Al_2O_3 ceramic and was then wound with high resistance nichrome wire, which acted as the heater, to provide a 600 W heating unit. The unit was then coated with additional Al_2O_3 insulating ceramic, and was concentrically placed into a 13 cm diameter, 17 cm long aluminum can. The entire assembly was placed inside an insulated metal dewar containing liquid nitrogen. The temperature of the block was controlled by two thermal temperature control units. For isothermal experiments, the temperature of the block was controlled by a Eurotherm 808 temperature controller manufactured by the Eurotherm Company. For the temperature scans, a model PC6010S, 120 V unit, manufactured by the Valley-Forge Instrument Company was used to regulate the power supply. Since the size of the block used was large, it effectively acted as a heat sink, such that the accuracy of temperature, as limited by the temperature control units could be controlled to better than $\pm$ 0.2K for a period of several days, and $\pm$ 0.1 K for several hours, provided that no strong exotherms resulted from chemical reactions in the samples.

Since the thermocouple used in the measurement of the block's temperature was embedded 3 cm from the centre, a thermal gradient was sustained radially in the aluminum block. Therefore, it was necessary to measure the temperature of the thermoset sample by means of a copper-constantan thermocouple whose one junction

was placed in the thermoset itself and the other in an ice bath maintained at 273.16K. The temperature was measured by means of a Hewlett Packard HP 3478A multimeter, which had been interfaced with the automatic data acquisition system of the General Radio 1689 Digibridge. The temperature was calculated by converting the emf measured by means of a sixth degree polynomial equation between the emf and the temperature. This conversion was accurate to $\pm$ 0.1K.

2.2.2 Dielectric Cells

Owing to the strongly adhesive nature of the polymers formed, one dielectric cell could not be reused for additional experiments. Therefore, a disposable, dielectric cell was required. A small dielectric cell was used with dimensions as shown in Figure 2.5. It consisted of a variable capacitor made with 18 rigid parallel plates. The capacitance could be varied by sliding one set of 9 plates with respect to the others, whose position was fixed, by means of a screw. The capacitors were manufactured by Johnson Trimmer Capacitors and were referred to as model 0109 variable PC mount capacitors. Their capacitance in air was nominally 16.5 pF. Measurements of the empty capacitance at different temperatures showed that its value, or C_o, changed by less than 0.2% over the temperature range 77K to 400K, while its value of loss factor, $\tan\delta$, was less than 10^{-5}. The capacitor was then carefully immersed in the glass vial containing the liquid mixture in such a way that the formation of air bubbles between the plates was avoided. The observation that the values of permittivity, ε', for fully polymerized samples of the same system were nearly constant and well within the
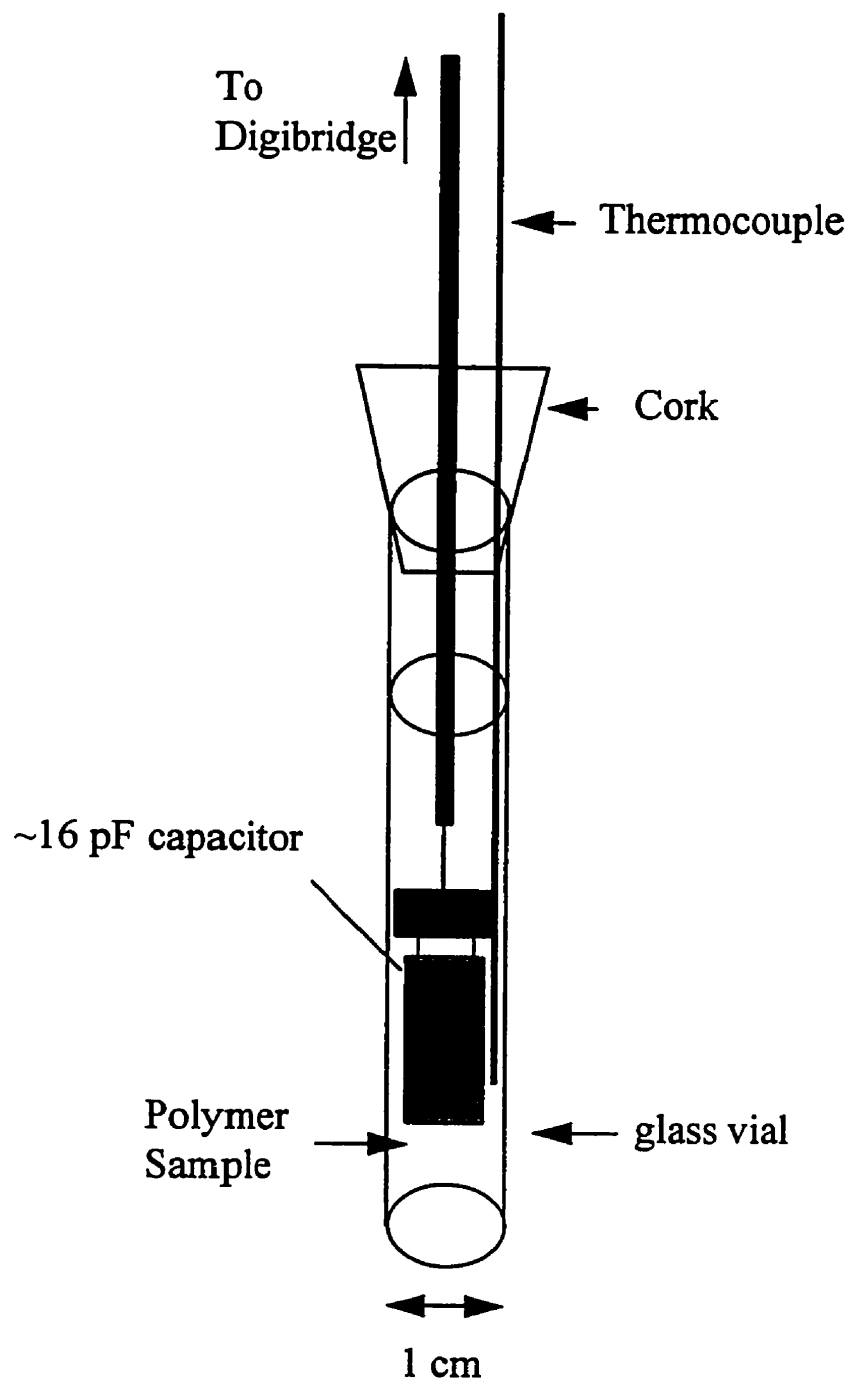
Figure 2.5:   Schematic diagram showing the dielectric cell used for these studies.

uncertainty of the measurements, confirmed that if any air bubbles formed between the plates of the capacitor, they had an insignificant effect on our measurements. A further advantage to this type of cell was that since it was immersed in the liquid, the 5-10% shrinkage occurred from the top of the liquid during the course of its solidification, and thus did not affect the geometry of the capacitor.

It was necessary to devise a method by which the capacitor could be maintained at the required level and position in the liquid mixture. This was done by mounting the rigid connecting wire into a cork snugly fitted to the vial's mouth. This procedure was particularly important, since the capacitor had a tendency to move during the experiment. Prior to insertion of the cell into the heating block or thermostat, the outside of the vial was wrapped in several layers of aluminum foil which improved the thermal contact with the metal heating block, and eliminated the possibility of adhesion on accidental spillage of the mixture from the lip of the vial.

The electrical connections of the cell to the measurement assembly were done in the following manner. The connections of the leads of the capacitor were soldered to a 2.5 mm diameter, shielded co-axial cable, which extended through the cork stopper. This cable was then spliced and soldered to a larger shielded co-axial cable, the connection was insulated with Teflon tape, and covered with aluminum foil to provide a common ground to the shield. The cell itself was electrically grounded by connecting the aluminum foil cover of the vial to the measurement assembly. A schematic drawing of the experimental set-up is given in Figure 2.6.

1. Thermostat Block
2. Dewar Flask
3. Thermocouple
4. Dielectric Cell
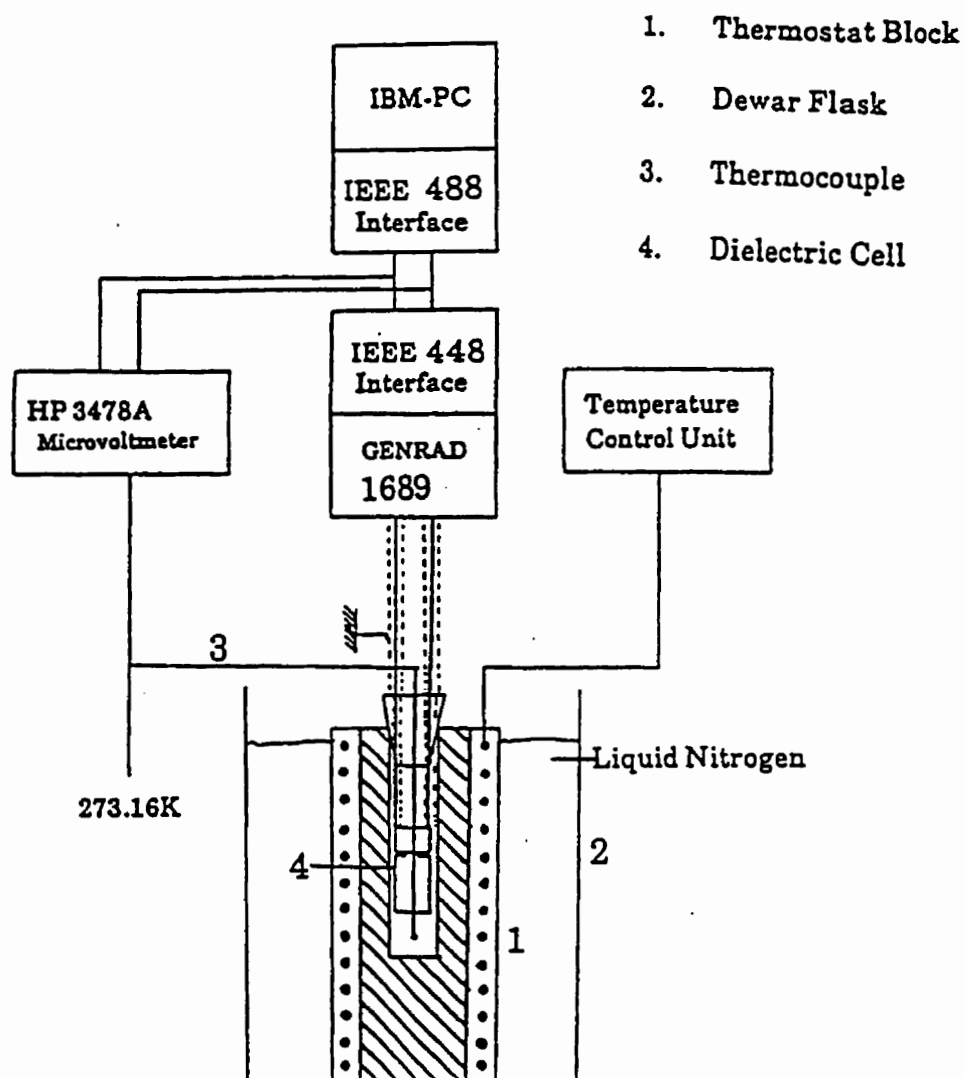
Figure 2.6: Schematic diagram of the experimental setup for the dielectric measurements in these studies.

2.2.3 Dielectric Experimental Method

Three dielectric experiments were carried out. In the first, a sample was mixed at 298K, immediately poured into the shielded dielectric cell and transferred to the thermostat block. The block was quenched in nitrogen to 80K and the dielectric permittivity, ε' and loss ε'' measured at 60s intervals as the sample was heated at 1K/min to 300K. This allowed us to determine the temperatures of the unreacted liquid at which the relaxations could be conveniently studied. It was suspected that chemical reaction had occurred significantly in the later stages of the experiment, so another sample was prepared and cooled to 200K. Its ε' and ε'' were measured over four decades of frequency from 15 Hz to 100 kHz at several temperatures, isothermally. The temperature of the sample was maintained to within ±0.1K.

In the second experiment, a new sample was mixed at the desired isothermal polymerization temperature for two minutes, poured into the dielectric cell and transferred to the preheated thermostat. Measurements were made at 24 frequencies from 15 Hz to 100 kHz during the chemical reaction of the polymer. The measured ε' and ε'' data for the range of frequencies from 15 Hz to 100 kHz is referred to here as a set. At each decade of frequency within a given set, the bridge was zeroed (calibrated automatically), and the time at which ε' and ε'' were measured recorded automatically to 1/10th of a second. As ten measurements were averaged for a single measurement frequency to obtain ε' and ε'' values, and the period for each measurement for the lowest frequency < 0.1s, the total time to measure each data was < 1.0s, over which time we justifiably assume that the physical state of the liquid remained unchanged. (It should be noted that this assumption is not valid for lower

frequencies, since for measurements made at f < .01 Hz, the time for measurement would be ~200 s, over which time the assumption that limited reaction occurs is not valid. Hence the recent work of several groups employing low frequency measurements (Lairez et al, 1992; Deng and Martin 1994), should be approached with caution.) The total period for measuring a complete set was 18 min. 40 such sets of data were measured during the course of one experiment. In this measurement procedure, frequency was increased in a step-wise manner, so that ε' and ε'' data in each set began with the lowest frequency, with data at subsequent higher frequencies measured at longer reaction times. The temperature varied by less than $\pm0.2K$ over the course of the measurements.

In the third experiment, the sample obtained after completion of the isothermal experiment was held at the isothermal polymerization temperature for an additional 24 hrs. The sample was then cooled to 80K and ε' and ε'' were measured at 60s intervals as the temperature of the sample was increased in a controlled manner at 1K/min from 80 to a temperature above the main relaxation. To investigate whether further chemical reaction had occurred, the sample was again cooled to 80K and ε' and ε' measured in the same manner as above. Since the curves were identical for all systems, it was deduced that no further chemical reaction had occurred and that the sample was fully polymerized. The sample was then cooled into the temperature range of the main relaxation and isothermal measurements were made at 24 frequencies from 15 Hz to 100 kHz. The temperature of the sample was maintained to within $\pm0.1K$ during these measurements.

2.3   Differential Scanning Calorimetry (DSC)

2.3.1   Phenomenological Aspects of DSC

In all thermal analysis techniques, the difference between the temperature of a sample and that of some inert, reference material is measured when both are heated at the same rate (Perkin Elmer, 1970). In a differential thermal analysis, or DTA, the sample and reference are placed in pans and are heated at a constant linear rate, with their temperatures measured by separate embedded thermocouples. As the temperature increases, the relative change or difference between the temperatures of the sample and reference, ΔT, is measured. The variation of ΔT with time should then be proportional to the enthalpy change due to chemical reaction or phase transformation, the heat capacity, and the resistance to heat flow R.

The difficulty with the DTA method is that the value of the resistance to heat flow, R, depends upon the packing of the sample into the holder, the subsequent thermal contact area between the sample and the holder, and thus the physical nature of the holder. Because of this, the data obtained cannot easily be related to the energy lost during chemical reaction or phase transformation, and thus the method is not suitable for many calorimetric measurements.

For the calorimetric analysis in this work, differential scanning calorimetry, DSC, was instead used. Unlike the DTA, the DSC method requires that both the sample and reference be heated by their own individual, identical heaters. The sample and reference holders are low thermal mass aluminum pans with no reference material required. In the DSC measurements, the temperature difference, resulting from

chemical reaction or phase transformation, is removed by adding heat to either of the two pans by means of a computer-assisted feedback. The amount of heat is recorded on a data disc. Since the thermal mass of the sample and reference holders are small, and the thermal resistances are then kept to a minimum, the assumption that each remain at an average temperature is valid. Additionally, the small size of the sample ensures that any thermal resistances between the sample and the pan, and the pan and its holder are minimal.

2.3.1 The Calorimeter and the Associated Assembly

A schematic illustration of the DSC4, manufactured by the Perkin Elmer Corporation, is given in Figure 2.7. The heating cell/temperature monitoring head here is connected to the Thermal Data Acquisition Station, or TADS, which allows the data to be analyzed directly via a software supplied by Perkin Elmer.

Two modes of operation were employed in the calorimetric study. For the polymerization process, the sample was heated from room temperature at a rate of 80K/min to the desired temperature of polymerization to minimize the chemical reaction that may occur during the temperature increase. The sample was then isothermally held at the desired polymerization temperature until the signal became linear, indicating that chemical reaction had ceased. This was confirmed by a subsequent DSC scan of the sample, heated at the same rate, which showed no exothermic features that could be attributed to the occurrence of further chemical reactions. This scan was useful as a baseline in order to take into account the thermal
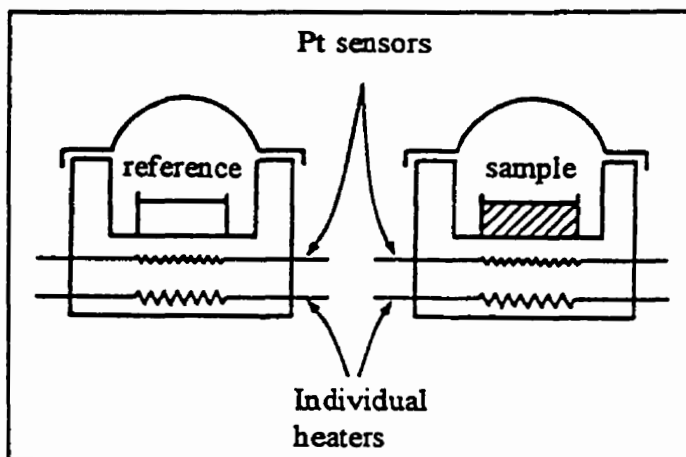
Figure 2.7:   Schematic diagram of the Perkin Elmer DSC-4 used for the thermal
               measurements in these studies. Both sample and reference are heated by
               individual heaters and the heat measured by individual Pt sensors. Note that
               the reference consists of an empty sample pan.

effects that occurred during the initial temperature increase towards the prerequisite polymerization temperature.

In the second mode of measurement, the DSC scan of a sample was obtained as a function of temperature by heating at a rate of 10K/min. For this, the Scanning Auto Zero (SAZ) function of the TADS was employed which allowed the data stored previously in a file made from a scan on empty sample holders, to be automatically subtracted as a baseline. To ensure that the DSC was consistent in calibration, indium was used as a calibration standard, and the calibration done frequently. The stated reproducibility was 2 mcal/sec for the scans with a maximum full scale range of 10 mcal/sec , while the reported baseline accuracy was given as 5%.

2.4   Ultrasonic Attenuation and Velocity Measurements.

2.4.1   Attenuation and Velocity Definitions

Ultrasonic measurements are made by passing high frequency (100 kHz-1 GHz) sound pressure wave pulses through a sample, and measuring the time for traversing the sample and the change in the amplitude of the wave-pulse during transit.

The time of transit of the pulse across the sample, Δt, is related to the velocity of the sound wave, v, according to,

$$v = \frac{\Delta t}{\Delta x},$$
(2.59)

where Δx is the thickness of the sample. If the velocity of sound in the sample is known, it is possible to determine the distance travelled by the sound wave. This technique is of course widely used in commercial applications such as SONAR, where the distance to a submerged object in water is determined by ultrasound, and in other geological applications.

The attenuation of the sound wave pulse refers to the total reduction of the intensity of the pulse as it travels across a sample of width Δx. This attenuation results from two effects, namely the absorption of energy by the medium, and the deflection of energy from the path of the pulse by reflection, refraction, diffraction and scattering. The first effect is characteristic of the physical structure of the medium, while the second set of effects are related to both the geometry and interface properties, and the physical structure of the medium in the case of scattering effects (Cracknell, 1980). For a pulse of intensity, I, the change in intensity, δI, is proportional to the attenuation, α, according to,

$$\delta I = -\alpha I \delta x, \tag{2.60}$$

where δx is the distance travelled by the sound wave pulse. Integration of Eqn.(2.60) gives,

$$I = I_o \exp(-\alpha x), \tag{2.61}$$

where I_0 is the initial intensity of the pulse at $x = 0$. The attenuation can then be written as,

$$\alpha = \frac{1}{x}\ln\left[\frac{I_o}{I}\right],$$

(2.62)

where the units are Nep/m.

2.5 Phenomenological Aspects of Ultrasonic Measurements

2.5.1 Absorption in Liquids.

The total absorption of ultrasound in a liquid may be written as,

$$\alpha = \alpha_{vis} + \alpha_{th} + \alpha_{relax} + \alpha_{struct},$$

(2.63)

where α_{vis} is the contribution from viscosity effects, α_{th} is the contribution from thermal conduction, α_{relax} is the contribution from thermal relaxation and α_{struct} is the contribution from structural relaxation.

The first two contributions have been described in the context of classical physics by Rayleigh (1887) as resultant from the conversion of regular molecular motions into random thermal motions that remove energy, in the form of heat dissipation, from the original ultrasonic wave. The form of these contributions are given by,

$$\alpha_{vis} = \frac{8\pi^3}{3}\left(\frac{\eta}{\rho v^3}\right)f^2,$$

(2.64)

$$\alpha_{th} - \left(\frac{2\pi^2 K}{\rho v^3 C_v}\right)\frac{(\gamma - 1)}{\gamma} f^2, \qquad (2.65)$$

where f is the frequency of measurement, and the remaining symbols are given as follows: ρ is the density of the medium, η the coefficient of viscosity, v the speed of the sound pulse, K the coefficient of thermal expansion, C_v the specific heat capacity at constant volume and the parameter $\gamma = (C_p/C_v)$ where C_p=specific heat capacity at constant pressure. The contributions to α given by Eqns(2.64) and (2.65) are generally referred to as the classical contributions.

It is useful to consider the relation between α and the viscosity. The relation is (Litovitz, 1960),

$$\alpha - \frac{2\pi^2 f^2}{\rho v^3}\left(\frac{4}{3}\eta_s + \eta_v\right), \qquad (2.66)$$

where η_s and η_v are the shear and volume viscosities and the remaining terms are as defined earlier. Since typical shear viscometers measure only the contributions from shear viscosity, ultrasonic techniques provide a unique method for determining the magnitude of the volume viscosity.

2.5.2 Single Relaxation Time Shear and Compressional Moduli

The derivation of the structural relaxation contributions to the absorption has been given in detail by Litovitz and Davis (1965). For a compressional wave propagating through a liquid medium, the compressional pressure stress P and strain S are related according to,

$$P = -KS, \qquad (2.67)$$

where K is the compressional modulus. For a time-varying stress, the general thermodynamic theory of relaxation in liquids gives (Miexner, 1934, 1952, 1953, 1954),

$$p + a\frac{\partial p}{\partial t} = -\left(bs + c\frac{\partial s}{\partial t}\right), \qquad (2.68)$$

where b is the low frequency limiting compressional modulus, K_o, and the ratio c/a is the high frequency compressional modulus, K_∞. The solution of Eqn(2.68) for a step change in volume gives,

$$p - p_o = (p_1 - p_o) + (p_i - p_1)e^{-\frac{t}{a}}, \qquad (2.69)$$

where p is the pressure at any time t, p_o the initial pressure, p_1 the final pressure, p_i the instantaneous pressure occurring immediately after the change in volume and a = τ_v the relaxation time at constant volume. The solution of Eqn(2.68) for a step change in pressure is,

$$s = s_1 - (s_1 - s_i)e^{-\frac{t}{c/b}}, \qquad (2.70)$$

where $s_1 = \Delta p/K_o$ is the fractional volume change at t = ∞, s_i the instantaneous fractional volume change after application of pressure ($\Delta p/K_\infty$) and c/b = τ_p, the relaxation time at constant pressure. τ_p and τ_v are related to the low and high frequency moduli, K_o and K_∞, according to,

$$\tau_p = \frac{K_\infty}{K_o}\tau_v . \tag{2.71}$$

Combining Eqn(2.68) and (2.71) gives,

$$p + \tau_v \frac{\partial p}{\partial t} = -K_o\left(s + \tau_p \frac{\partial s}{\partial t}\right). \tag{2.72}$$

When a sinusoidal stress is applied across the sample, the resulting response

becomes complex, and the resulting complex modulus of compression, K^*, is,

$$K^* = -\frac{P}{s} = K_o + \frac{K_r \omega^2 \tau_v^2}{1 + \omega^2 \tau_v^2} + i\frac{K_r \omega \tau_v}{1 + \omega^2 \tau_v^2} \; ; \; = K' + iK'' , \tag{2.73}$$

where ω is the angular frequency and $K_r = K_\infty - K_o$ is the compressional modulus

dispersion. Eqn. (2.73) describes a relaxation process with a single relaxation time,

and is analogous in form to that seen in the Debye theory for dielectric relaxation.

Eqn. (2.73) can be rewritten to give,

$$P^* = K^*(-s^*) = [ReK + i\omega\,\eta_v(\omega)](-s^*) , \tag{2.74}$$

where ReK is the real component of the complex modulus, and $\eta_v = K_r\tau_v/(1+\omega^2\tau_v^2)$.

Thus $\eta_v(\omega)$, the volume viscosity, is proportional to the energy loss per unit cycle in a

sinusoidal compression of the sample, and at low frequencies $= K_r\tau_v$.

Equations for the shear stress, T, strain, s, and modulus, G, are identical to

Eqns. (2.68)-(2.74), with the resulting relation of the complex shear modulus, G^*, for a

sinusoidal shear stress given by,

$$G^* = \frac{G_\infty \omega^2 \tau_s^2}{1 + \omega^2 \tau_s^2} + i \frac{G_\infty \omega \tau_s}{1 + \omega^2 \tau_s^2} = G' + iG = G' + i\omega \eta_s(\omega), \quad (2.75)$$

where τ_s is the shear relaxation time, G_∞ is the high frequency shear modulus and $\eta_s(\omega)$ is the frequency dependent shear viscosity, which approaches $G_\infty \tau_s$ at low frequencies.

2.5.3 Single Relaxation Time For Longitudinal Modulus

When a longitudinal pulse travels through a medium, both compressional and shear effects contribute to the overall response. The differential equation governing the propagation of a longitudinal wave is given by,

$$\rho \frac{\partial^2 X_1}{\partial t^2} = [K + \frac{4}{3} G] \frac{\partial^2 X_1}{\partial x_1^2}, \quad (2.76)$$

where X_1 is the displacement in the medium and other terms are as defined earlier. Since the displacement at any time is given by,

$$X_1(x,t) \propto \exp\left[i\left(\omega t - \frac{2\pi}{\lambda} x\right)\right], \quad (2.77)$$

where λ is the wavelength of the sound wave, the velocity from Eqns. (2.76) and (2.77) is,

$$v^2 = \frac{K + 4/3G}{\rho}.$$
(2.78)

The complex longitudinal modulus, L^*, is defined as,

$$L^* = L' + iL'' = K^* + \frac{4}{3}G^*.$$
(2.79)

The relation between the L^*, v and α is obtained by assuming that for a sinusoidal longitudinal wave, that X_1 is proportional to exp[$i\omega\tau$-$(\alpha+i\omega/v)x$], which leads to,

$$L^* = \frac{\rho v^2}{\left(1 - i\frac{\alpha v}{\omega}\right)^2}.$$
(2.80)

The real and imaginary components are then given by,

$$L' = \rho v^2\left(\frac{1 - [\alpha v/\omega]^2}{[1 + (\alpha v/\omega)^2]^2}\right) \quad ; \quad L'' = \frac{2\rho v^2(\alpha v/\omega)}{[1 + (\alpha v/\omega)^2]^2}$$
(2.81)

For high frequency measurements, the value of (αv/ω) is generally $\ll$ 1, so that,

$$L' = \rho v^2 \quad ; \quad L'' = \frac{2\rho v^3 \alpha}{\omega}.$$
(2.82)

Combining Eqns(2.73), (2.75), (2.79) and (2.82) gives the absorption per wavelength as,

$$\alpha \lambda = \pi \left[\frac{\dfrac{K_r \omega \tau_v}{1 + \omega^2 \tau_v^2} + \dfrac{4}{3} \dfrac{G_\infty \omega \tau_s}{1 + \omega^2 \tau_s^2}}{K_o + \dfrac{K_r \omega^2 \tau_v^2}{1 + \omega^2 \tau_v^2} + \dfrac{4}{3} \dfrac{G_\infty \omega^2 \tau_s^2}{1 + \omega^2 \tau_s^2}} \right] \tag{2.83}$$

Similarly, the velocity may be written as,

$$v^2 = \frac{1}{\rho} \left(K_o + \frac{K_r \omega^2 \tau_v^2}{1 + \omega^2 \tau_v^2} + \frac{4}{3} \frac{G_\infty \omega^2 \tau_s^2}{1 + \omega^2 \tau_s^2} \right) \tag{2.84}$$

The low and high frequency limits of the velocity are,

$$v^2 = \frac{K_o}{\rho} \quad as \ \omega \to 0 \quad ; \quad v^2 = \frac{1}{\rho} \left(K_o + K_r + \frac{4}{3} G_\infty \right) \quad as \ \omega \to \infty \tag{2.85}$$

The corresponding low and high frequency limits for the absorption per unit wavelength are,

$$\alpha \lambda = \frac{\pi \omega}{K_o} \left(K_r \tau_v + \frac{4}{3} G_\infty \tau_s \right) = \frac{\pi \omega}{K_o} \left(\eta_v + \frac{4}{3} \eta_s \right) \quad as \ \omega \to 0 , \tag{2.86}$$

where $\alpha \lambda \to 0$ as $\omega \to \infty$. Thus the low frequency limit is equivalent to the contributions from classical theory, as given by Eqn(2.66). Similar limits are also seen as the relaxation times, τ_i approach 0 and ∞. It is important to realize that the information obtained from longitudinal wave ultrasound propagation contain both compressional and shear contributions, and that in the event of a structural relaxation, the measured parameters become strongly dependant upon both the frequency of measurement, and the physical state of the material, as characterized by its relaxation time.

2.5.4 Distribution of Relaxation Times

Typically, the structural relaxation of the longitudinal modulus in organic liquids and polymeric materials does not show a single relaxation time behaviour, rather it shows a relaxation with a distribution of times (Litovitz et al., 1954; Meistner et. al, 1960; Taskoprulu et al, 1961; Barlow and Erginsav, 1972; Pethrick, 1973; Barlow and Erginsav, 1975; Meier et al, 1987; Alig et al, 1988; Alig et al, 1992; Alig et al, 1994;, Parthun and Johari, 1995(b)). By analogy with dielectric spectroscopy, the longitudinal modulus is given as,

$$L^*(\omega\tau) = L_o + \Delta L \int_0^\infty e^{-i\omega t}\left(-\frac{\partial\phi(t)}{\partial t}\right)dt , \qquad (2.87)$$

where L_o and ΔL ($= L_\infty - L_0$) are as defined earlier. A variety of relaxation functions such as the Cole-Davidson (Litovitz 1960) and stretched exponential (Alig et al, 1992, Parthun and Johari, 1995(c)) have been used successfully to describe the observed behaviour.

2.5.5 Ultrasonic Equipment and Associated Assembly

Ultrasonic measurements were made by using a computer controlled ultrasonic test system, model MBS-8000 manufactured by Matec Instruments. The system employs a quadrature phase detection method for determining the velocity and attenuation and has been reviewed by Papadakis(1976).

The features of the system are shown schematically in Figure 2.8. Communication between computer and monitoring equipment are made using a IEEE 488 bus interfaced with a National System interface card. The accompanying software allows for measurements using either a single or double transducer assembly, with the former employing the transducer as both transmitter and receiver. All measurements in this study employed a two transducer assembly, where one transducer acted as the transmitter and the second as the receiver.

The measurements of v and α were done in the following way. First the absolute values of the velocity and attenuation were determined. Figure 2.9 shows schematically the measurement method. A transmitted longitudinal pulse is sent from the transmitter and the resulting signals received by the receiver. A gate is placed over one or more of the received pulses. This gate defines the signal over which the calculations are made. A 0° phase detector is selected for the pulse. This represents the amplitude of the received signal multiplied by the cosine of the phase angle between the reference and the signal to be measured. The computer then applies a 90° phase detector to the sample to determine the amplitude of the signal multiplied by the sin of the phase angle. Using this information, the computer then calculates both the amplitude, A, and phase angle Φ of the signal, according to,

$$\Phi = \tan^{-1}\left(\frac{A\sin\Phi}{A\cos\Phi}\right), \tag{2.88}$$
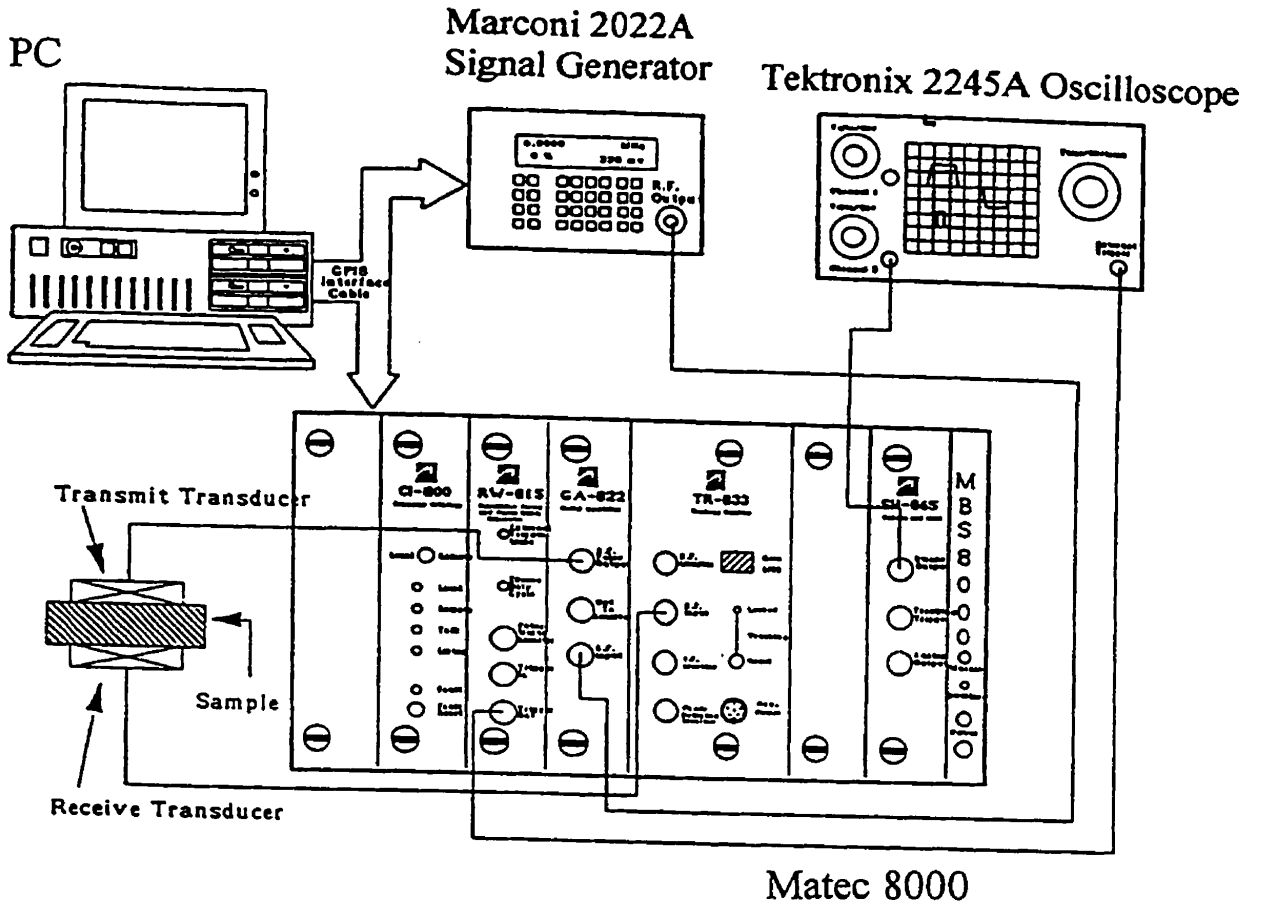
Figure 2.8: Schematic diagram of the experimental setup used for the ultrasonic
measurements in these studies. The diagram shows a typical configuration
employing two transducers.
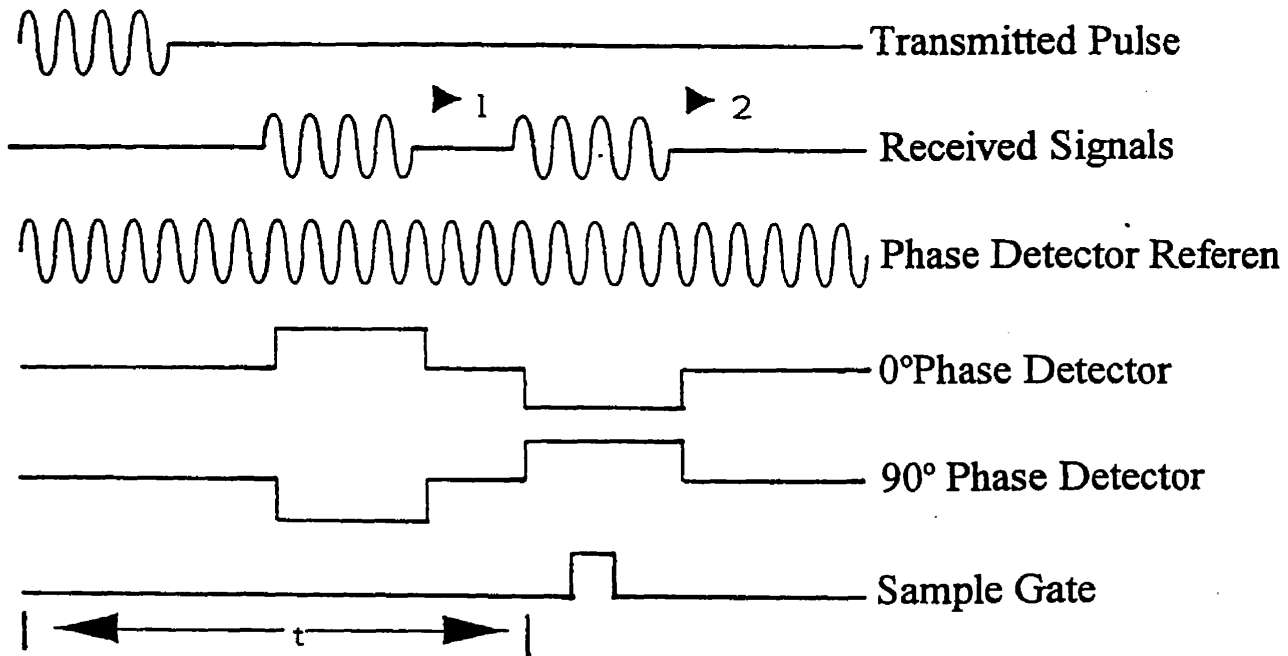
Figure 2.9:   The measurement method for the ultrasonic assembly. The method is as discussed in the text.

$$A = \left(A^2\sin^2\Phi + A^2\cos^2\Phi\right)^{\frac{1}{2}} \qquad \text{(2.89)}$$

The total transit time between the transmitted and received signals is then,

$$t = \frac{\Phi}{2\pi f}, \qquad \text{(2.90)}$$

where f is the measurement frequency. Since it is not possible to quantitatively measure Φ, it is useful to consider the change $\Delta\Phi$ and rewrite Eqn(2.90) as,

$$\Delta t = \frac{\Delta\Phi}{2\pi\Delta f} \qquad \text{(2.91)}$$

where Δt now is the time change for the transmitted pulse for different frequencies to the transmitter to the phase detector, and not the absolute time transit time between the signals at a fixed frequency. To determine Δt, the frequency is increased in small steps until the phase angle of each echo is increased by an approximately integer value of π. The transit time is then determined from,

$$\frac{\Delta\Phi}{2\pi\Delta f} = N\Delta t - (N-1)\frac{\gamma}{2\pi f}, \qquad \text{(2.92)}$$

where N is the echo number and γ is a term representing the errors associated with phase angle shifts at the transducer interface. Typically, γ is small for assemblies employing a buffer rod configuration. Hence Δt is determined by the computer from the slope of the plot of $\Delta\Phi/\pi\Delta f$ against N via a linear least squares algorithm. If the sample thickness, x, is known, then the velocity can be calculated according to $v=x/\Delta t$.

The attenuation is determined as follows. Since the attenuation is more sensitive to small errors in the phase detector, such errors must be included in the measurement. The amplitude is calculated as,

$$A_1^2 = \kappa^2 A^2 \sin^2(\Phi + e_\Phi) + A^2 \cos^2 \Phi, \qquad (2.93)$$

where $\kappa \sim 1$ is a multiplicative factor and e_Φ is the phase angle deviation, which is 0 when no phase detector errors occur. As with the Δt measurements, Φ is then increased by $\pi/2$ radians and the amplitude of the second measurement is,

$$A_2^2 = \kappa^2 A^2 \cos^2(\Phi + e_\Phi) + A^2 \sin^2 \Phi. \qquad (2.94)$$

The average value from Eqns (2.93) and (2.94) is then,

$$A_{avg}^2 = A^2 \kappa^2 \qquad (2.95)$$

The attenuation is then determined from the amplitudes of two echoes, as outlined in Section 2.5.1.

While the determination of absolute v and α is necessary, for the measurements made during polymerization it is more convenient to determine the changes in v and α. Such measurements provide a higher degree of accuracy than the absolute measurements. The procedure for determining Δt and $\Delta \alpha$ is similar to that used for determining the absolute magnitudes, with the exception that the frequencies are fixed at the beginning of the measurement. Δt is determined by monitoring the change in the phase angle with the frequency held constant. Similarly, the changes in the amplitude of the pulse are determined, and the change in attenuation determined. The

errors associated with the measurements are ±5% and ±10% for the absolute v and α measurements, and ±.1% and 1% for the relative v and α measurements.

2.5.7 Ultrasonic Cell and Experimental Apparatus

To monitor the changing ultrasonic properties during polymerization, it was necessary to devise a sample cell. The cell had to be leak-proof, dimensionally stable, non-reactive with the polymers, smooth and reusable. The cell designed for this purpose is shown schematically in Figure 2.10 (top). Two aluminum buffer rods were fitted like pistons into a ring that had a bore drilled into one face, leaving a gap where the sample was kept. The bore allowed the fully assembled cell to be filled with the liquid mixture. Teflon tape was wrapped around the inside surface of the ring prior to inserting the buffer rods to ensure that the cell remained leak proof. The 2.25 MHz transducers, purchased from Harisonics, were coupled to the buffer rods by silicone grease, and were held in tight contact by means of mechanical clamps. To assure that losses arising from the scattering at the polymer/buffer rod interface were minimal, the ends of the aluminum buffer rods were polished to a smooth face using a 0.1μ alumina polisher.

Since the polymerization reactions are highly exothermic, a thermostat with a large thermal mass was required to absorb the heat of reaction with minimal change in the temperature. The thermostat consisted of a 5 litre vessel filled with vegetable oil. It was heated using a 300W wound resistance coil, immersed nearly in the centre of the oil bath. The temperature was controlled with a Eurotherm 808 controller, and the
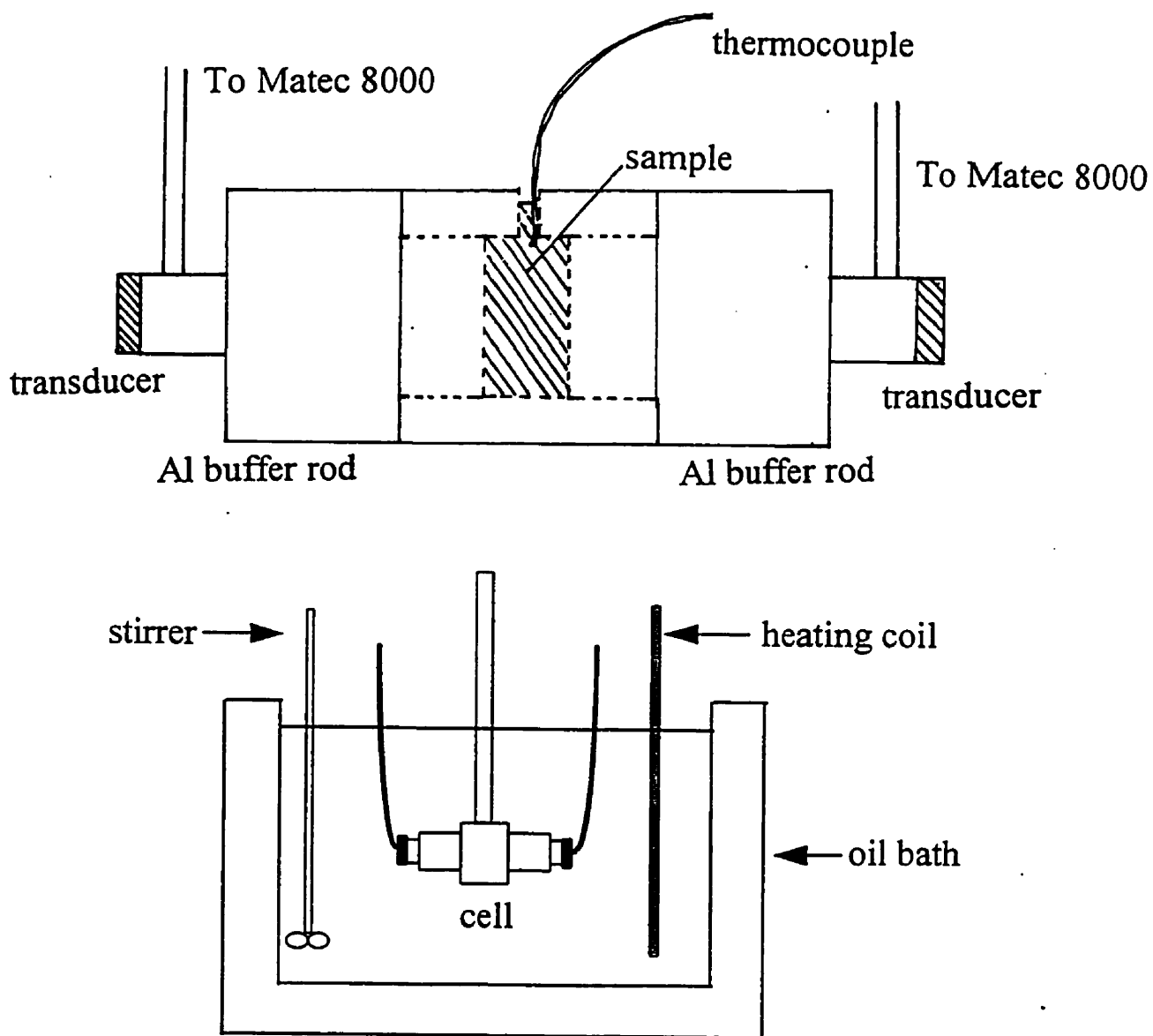
Figure 2.10: Schematic diagram of the ultrasonic cell (top) and the oil bath thermostat and associated assembly (bottom) used for the ultrasonic studies.

bath temperature measured with a copper-constantan thermocouple. A mechanical stirrer was placed in the bath to maintain circulation of the oil around the heater. The experimental configuration for these measurements is shown schematically in Figure 2.10(bottom).

The cell was wrapped in a polyethylene bag to shield the sample and transducers from the oil. After it was lowered into the centre of the oil bath, the cell was secured in position by a clamp.

2.5.8 Experimental Procedure

Approximately 10g of the stoichiometric mixture of the DGEBA and amine were stirred for two minutes in a 20 ml glass vial. Since the DGEBA was more viscous, the amine was pipetted into a pre-weighed sample of the DGEBA. The zero time of reaction was taken as the time at which mixing of the sample was complete. The sample was then carefully pipetted into the partly submerged cell, which was preheated in the thermostat for 1 hr prior to the experiment. After the cell was filled, it was carefully lowered into the oil bath and the temperature allowed to equilibrate. The measurements were initiated by setting the receiver gate of the MBS 8000 on the first transmitted pulse, and measuring the absolute time for transit and attenuation. Following this measurement, the relative velocity and attenuation were measured at 200-300s intervals during the chemical reaction. The total time from the end of mixing until the beginning of the relative measurements during polymerization was

between 8 and 10 minutes. The temperature was held to within ±0.2K over the course of the measurement.

CHAPTER III EXPERIMENTAL RESULTS

3.1   Dielectric Studies

3.1.1 Dielectric Studies of the Unreacted Monomeric State.

The dielectric permittivity, ε', and loss, ε'', of the ANIL:DGEBA mixture in the unreacted, or molecular liquid state were measured at 1kHz as the sample was heated at 1K/min from 80K to 300K. The results are shown as plots of ε' and $\log(\varepsilon'')$ against temperature, T, in Figures 3.1 and 3.2, respectively. In Figure 3.1, ε' initially increases gradually with temperature at low temperatures towards a near plateau value. This plateau is interrupted by a sharp step increase at ~250K. Following the increase, ε' decreases with increasing temperature. In Figure 3.2, $\log(\varepsilon'')$ increases through a broad peak at ~135K with increasing temperature. Following this peak, it decreases to a minimum at approximately 200K then increases gradually until ~225K, when the increase is interrupted by the appearance of a sharp increase through a peak.

Following this peak, $\log(\varepsilon'')$ increases in a nearly linear manner with increasing temperature. ε' and $\log(\varepsilon'')$ for the CHMA:DGEBA and HMA:DGEBA mixtures (the data for the HMA:DGEBA mixture is taken from Johari and Pascheto, 1995) in the molecular liquid state are also plotted in Figures 3.1 and 3.2, and their behaviour is seen to be qualitatively similar to that of the ANIL:DGEBA mixture. The HMA:DGEBA liquid differs slightly in that it shows an additional peak prior to the larger peak at ~220K. This has been attributed to partial crystallization of the sample (Johari and Pascheto, 1995; see also the discussion in Chapter VI).
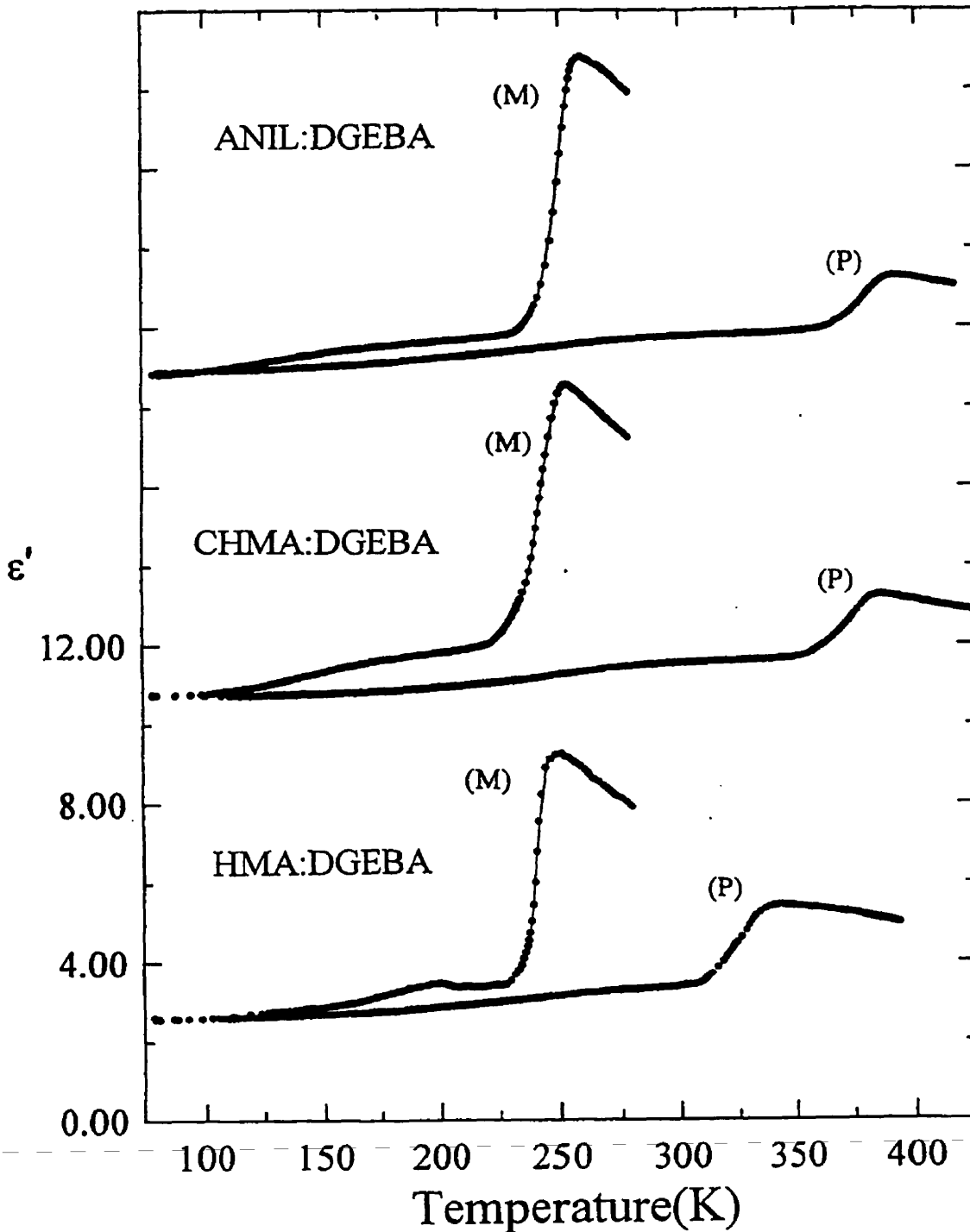
Figure 3.1: ε', measured at a frequency of 1kHz, during heating at a constant rate of 1K/min, is plotted against the temperature for the ANIL:DGEBA, CHMA:DGEBA, and HMA:DGEBA mixtures in the molecular liquid (M) and fully polymerized (P) states. The curves for the ANIL:DGEBA and CHMA:DGEBA mixtures have been shifted vertically 16 and 8 units, respectively.
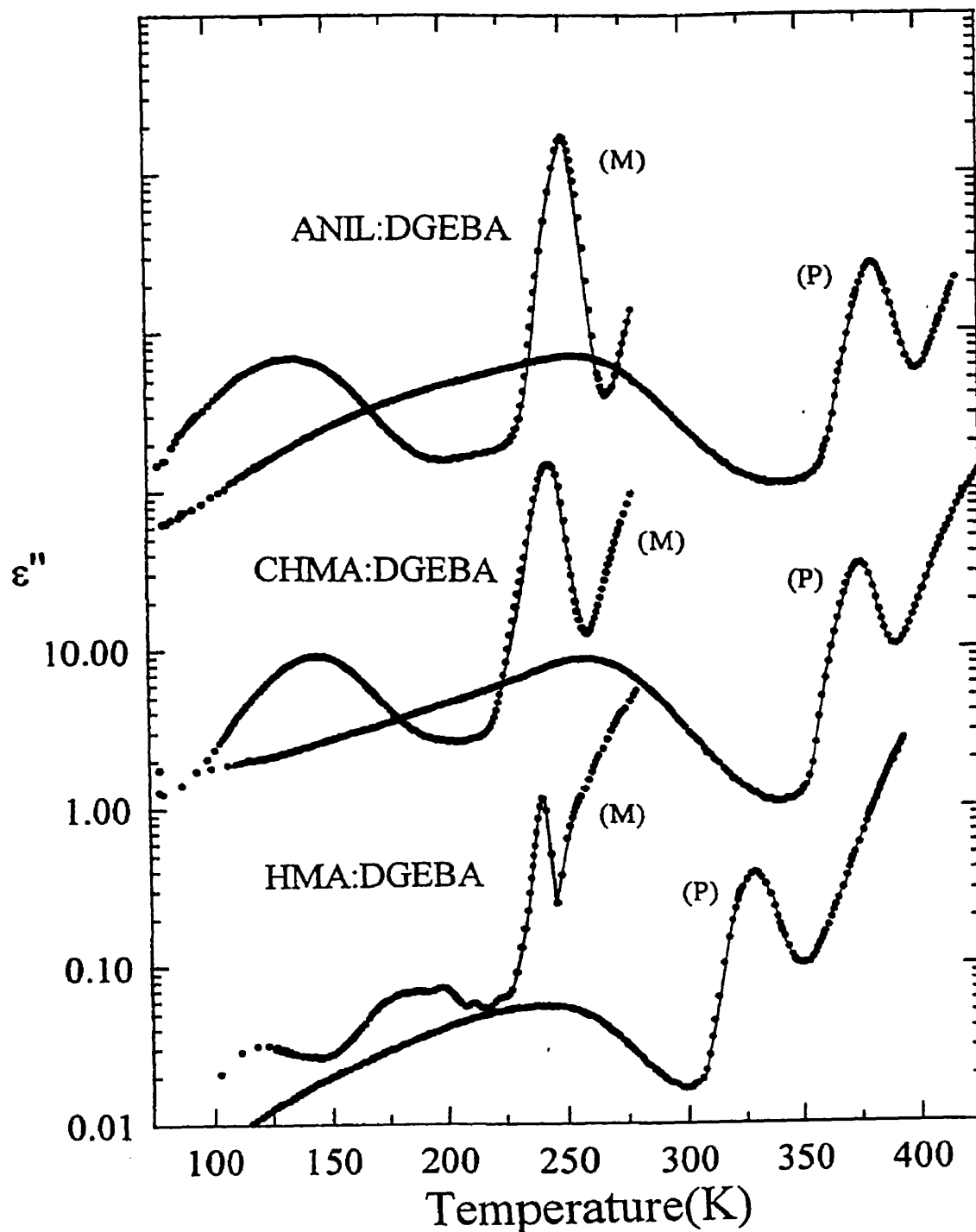
Figure 3.2: ε'', measured at a frequency of 1kHz, during heating at a constant rate of 1K/min, is plotted against the temperature for the ANIL:DGEBA, CHMA:DGEBA, and HMA:DGEBA mixtures in the molecular liquid (M) and fully polymerized (P) states. The baselines for the ANIL:DGEBA and CHMA:DGEBA mixtures have been shifted vertically 4 and 2 decades, respectively.

When a mechanical stress or an electric field is applied to an amorphous solid, it undergoes recoverable deformations, or electrical polarizations, of two types: the first is due to localized atomic diffusion within the otherwise rigid disordered structure, and the second is due to long-range atomic diffusion; the latter leads to a macroscopic deformation or viscous flow when the mechanical stress is sustained for an overly long duration (Cavaille et al, 1989). The kinetics of both types of diffusion are time-, and temperature-dependent. In the mechanical and dielectric spectrometry, the two effects are revealed as separate peaks in the energy absorption or relaxation spectrum, at a high frequency for the first and a low frequency for the second (Johari, 1973; Johari, 1975)

The first, or faster process has been called the β-relaxation.(It is now often referred to as the Johari-Goldstein relaxation, as for example several papers, the most recent of which is a review by Angell (1995), so that it can be distinguished from other relaxation processes deduced from neutron scattering measurements (Frick and Richter 1995).) The second, or slower process is the so-called α-relaxation. In dielectric measurements of polymers or monomeric liquids made for a fixed sinusoidal frequency at different temperatures, their relaxation peaks are observed usually at a temperature below the calorimetric glass transition temperature, T_g, for localized atomic diffusion, and above T_g for the long-range atomic diffusion. In their absorption or loss spectrum, the two peaks are separated in the frequency plane, but this separation is lessened as the temperature is increased (Johari, 1973). In several cases (Johari, 1973), the two peaks remain distinctly resolved even when the temperature is

several degrees above T_g. A similar terminology is used for dielectric relaxations in orientationally disordered crystals (Johari 1976), in which molecules confined to lattice sites do not diffuse in a manner similar to that in liquids.

The two relaxations are observed generally when a liquid or orientationally disordered crystal is cooled, and, as observed for glycerol (Johari and Whalley 1972), when a liquid is compressed at a fixed temperature. Both cooling and compression cause a decrease in the configurational contributions to the volume, enthalpy and entropy, when the radial distribution function of the liquid, a measure of the packing density of atoms, reversibly changes.

The behaviour of these mixtures is typical for amorphous, polymeric systems (McCrum et al, 1967). Generally the low temperature peak is designated the sub T_g-relaxation process, where T_g is the glass transition temperature, while the larger high temperature peak is denoted as the main, or α-relaxation process. The magnitudes of the low and high temperature peaks, as well as their temperatures at which the maximum occurs, are listed for the three mixtures in Table 3.1.

In order to study the frequency dependence of the α-relaxation process, new samples of each of the three mixtures were prepared and cooled to 200K, as discussed in Section 2.3.3. The results are shown as plots of ε' and ε'' against the logarithm of frequency in Figures 3.3, 3.4 and 3.5 for the ANIL:DGEBA, CHMA:DGEBA and HMA:DGEBA mixtures, respectively.

Table 3.1 The magnitudes, $\varepsilon''_{max,Sub\ Tg}$ and $\varepsilon''_{max,\ \alpha}$, and positions, $T_{sub\ Tg}$ and T_α, of the low and high temperature relaxations for the ANIL:DGEBA, CHMA:DGEBA and HMA:DGEBA mixtures in the molecular liquid state.

Mixtures	$\varepsilon''_{max,\alpha}$	$\varepsilon''_{max,sub\ Tg}$	$T_{max,\ \alpha}/K$	$T_{max,\ sub\ Tg}/K$
ANIL:DGEBA	1.72	0.070	250	134
CHMA:DGEBA	1.48	0.092	246	145
HMA:DGEBA(a)	1.16	0.031	240	120

(a)   Johari and Pascheto 1995.

All three mixtures show similar dielectric behaviour. ε' begins at a nearly plateau value at low frequencies, then decreases in a step-wise fashion as the frequency is increased. The step shifts towards lower frequencies and the magnitude of the plateau increases as the temperature is lowered. ε'' shows a peak at frequencies coinciding with the step-decrease in ε', with the magnitude of the peak increasing with decreasing temperature for the ANIL:DGEBA and CHMA:DGEBA mixtures, and decreasing with decreasing temperature for the HMA:DGEBA mixture.

3.1.2   Dielectric Studies During the Formation of the Polymer

Dielectric spectroscopy has proven to be a useful method for following the changing molecular dynamics during the formation of polymers (Mangion and Johari 1991, 1992, Parthun and Johari 1992(a), 1992(b), Johari and Pascheto 1995), with the measurements made at a single frequency, and the resulting data analyzed. In the
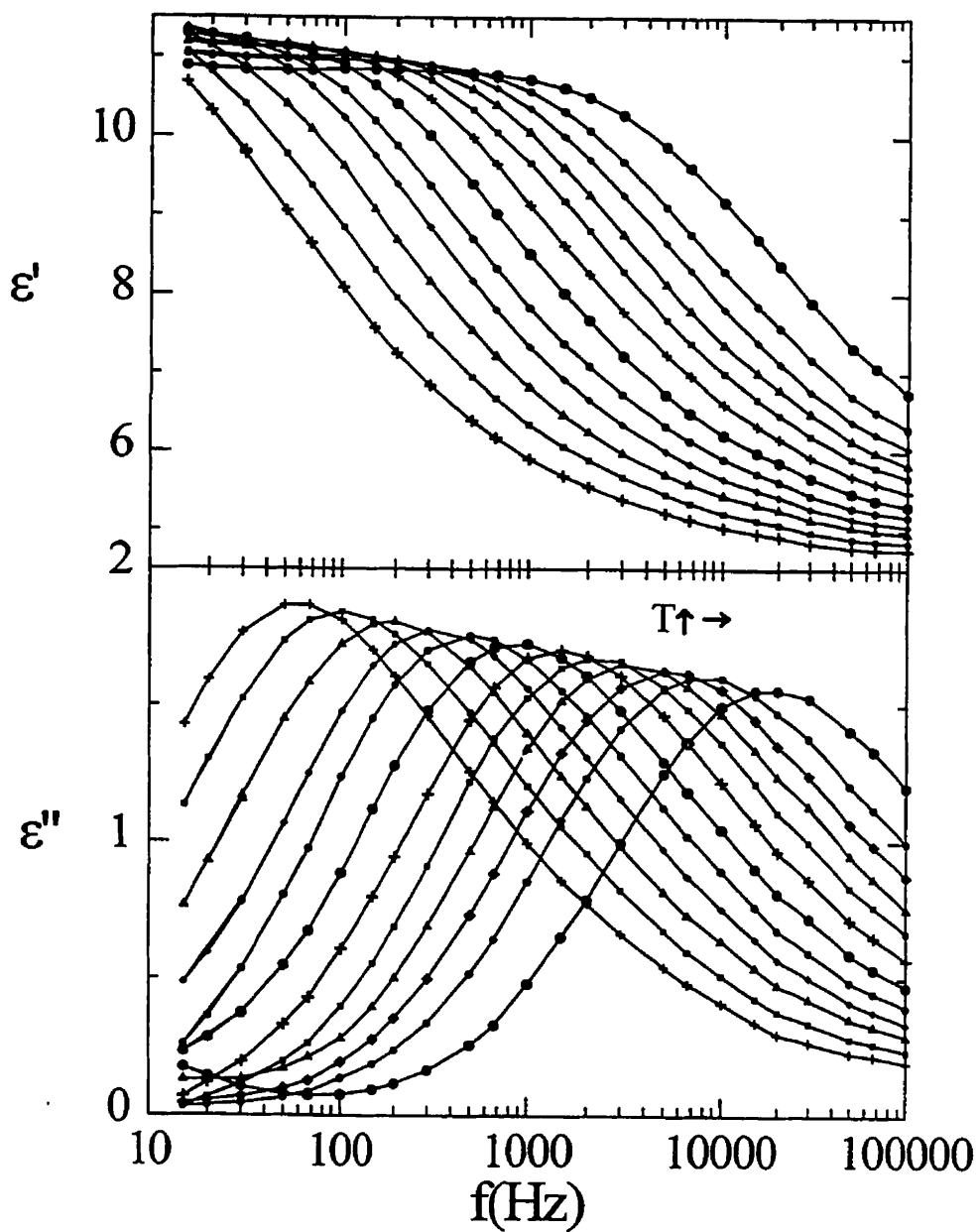
Figure 3.3: ε' and ε'' of the ANIL:DGEBA mixture in the molecular liquid state is plotted against the frequency for isothermal measurements made at 247.0, 247.9, 248.9, 249.9, 250.7, 251.7, 252.7, 253.7, 254.6, 255.6, 256.6 and 258.5K. The curves shift sequentially from high frequency to low frequencies as the temperature is lowered.
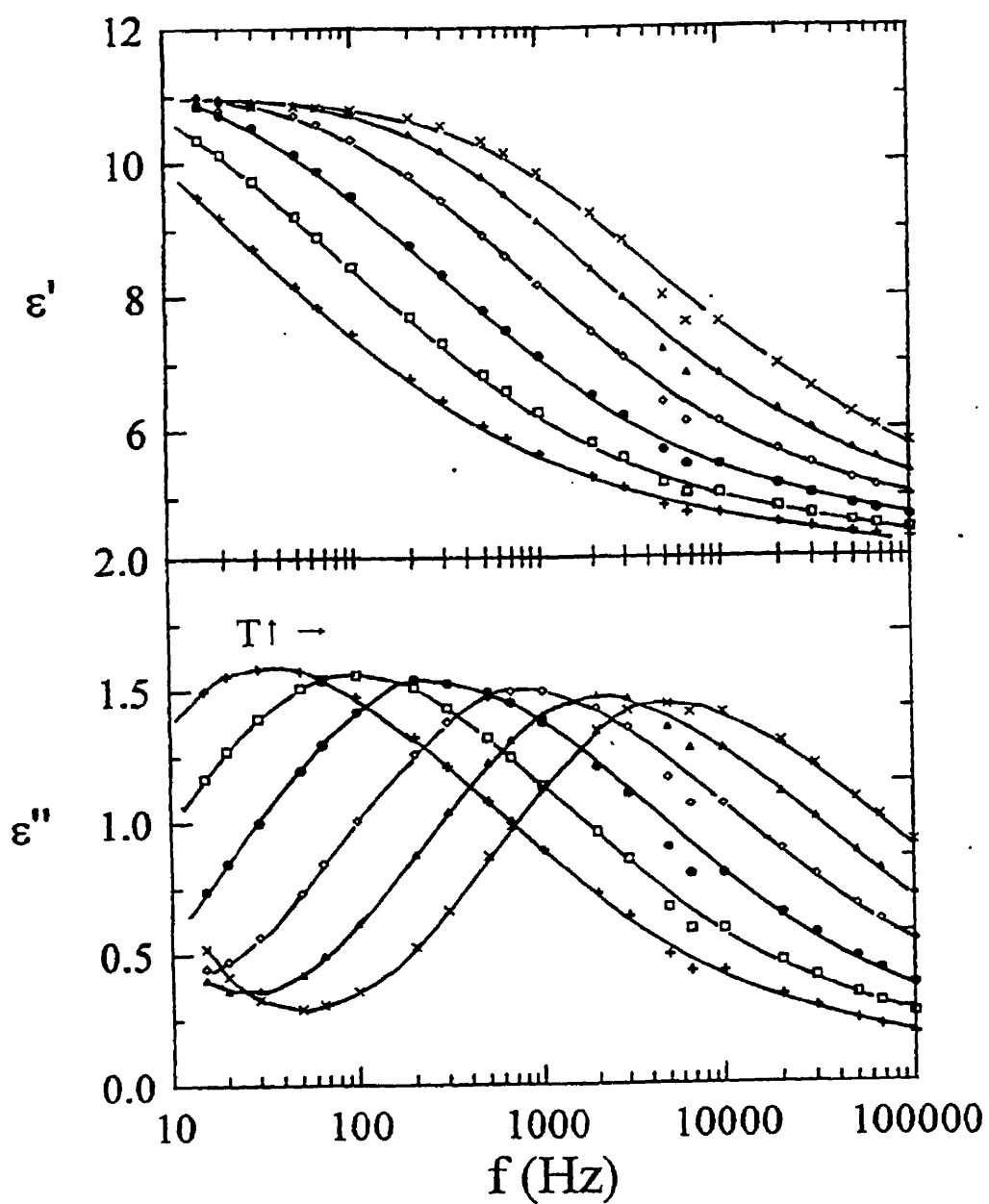
Figure 3.4: ε' and ε'' of the CHMA:DGEBA mixture in the molecular liquid state is plotted against the frequency for isothermal measurements made at 238.1, 240.0, 242.0, 244.0, 246.1 and 247.9K. The curves shift sequentially from high frequency to low frequencies as the temperature is lowered.
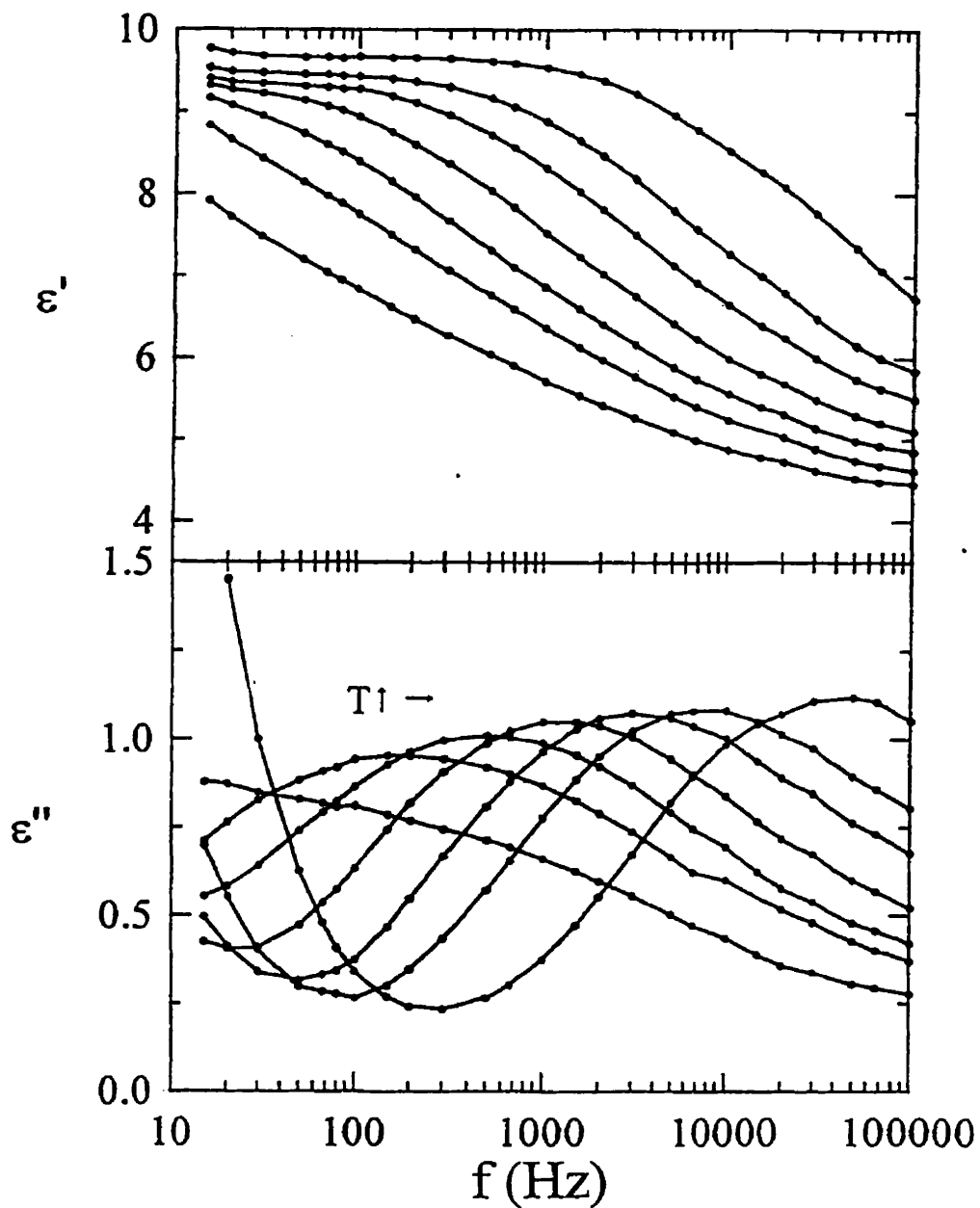
Figure 3.5: ε' and ε'' of the HMA:DGEBA mixture in the molecular liquid state is plotted against the frequency for isothermal measurements made at 238.4, 239.6, 240.2, 241.2, 241.9 and 243.3K. The curves shift sequentially from high frequency to low frequencies as the temperature is lowered.

present study, 24 frequencies: 0.012, 0.015, 0.02, 0.03, 0.05, 0.067, 0.1, 0.2, 0.3, 0.5, 0.67, 1, 2, 3, 5, 6, 7, 10, 20, 30, 50, 66.7, and 100kHz, were used so that both the time- and frequency-dependent changes could be studied.

The method for measurement was outlined in Section 2.3.3. The results for the ANIL:DGEBA mixture isothermally held at 343.4K and 333.4K are shown as plots of ε' and $\log(\varepsilon'')$ against time in Figures 3.6 and 3.7, for eight frequencies of measurement, 0.03, 0.1, 0.3, 1, 3, 10, 30 and 100kHz. Other frequencies have been omitted for clarity. The behaviour at both temperatures is qualitatively similar. ε' decreases slowly at short times of measurement for frequencies > 100 Hz. For lower frequencies, there is a sharp decrease towards this region at short times, the magnitude of the initial value increasing with decreasing frequency. Following this slow decrease, ε' decreases sharply in a step-wise fashion, with the position of the step appearing at shorter times for higher frequencies. Following the step, ε' approaches a nearly constant value for all frequencies.

$\log(\varepsilon'')$ decreases in a progressively more rapid manner with increasing time, at short times of reaction. The initial value is seen to decrease with increasing frequency of measurement. This decrease is interrupted by a peak, that shifts to shorter times and increases in magnitude with increasing frequency. Following this peak, $\log(\varepsilon'')$ decreases to a near plateau value, with the magnitude of the plateau decreasing with increasing frequency up to ~10 kHz, and thereafter increases with increasing frequency.

Since the ANIL:DGEBA mixture reacted much more slowly than the CHMA:DGEBA and HMA:DGEBA mixtures, it was not feasible under the restrictions
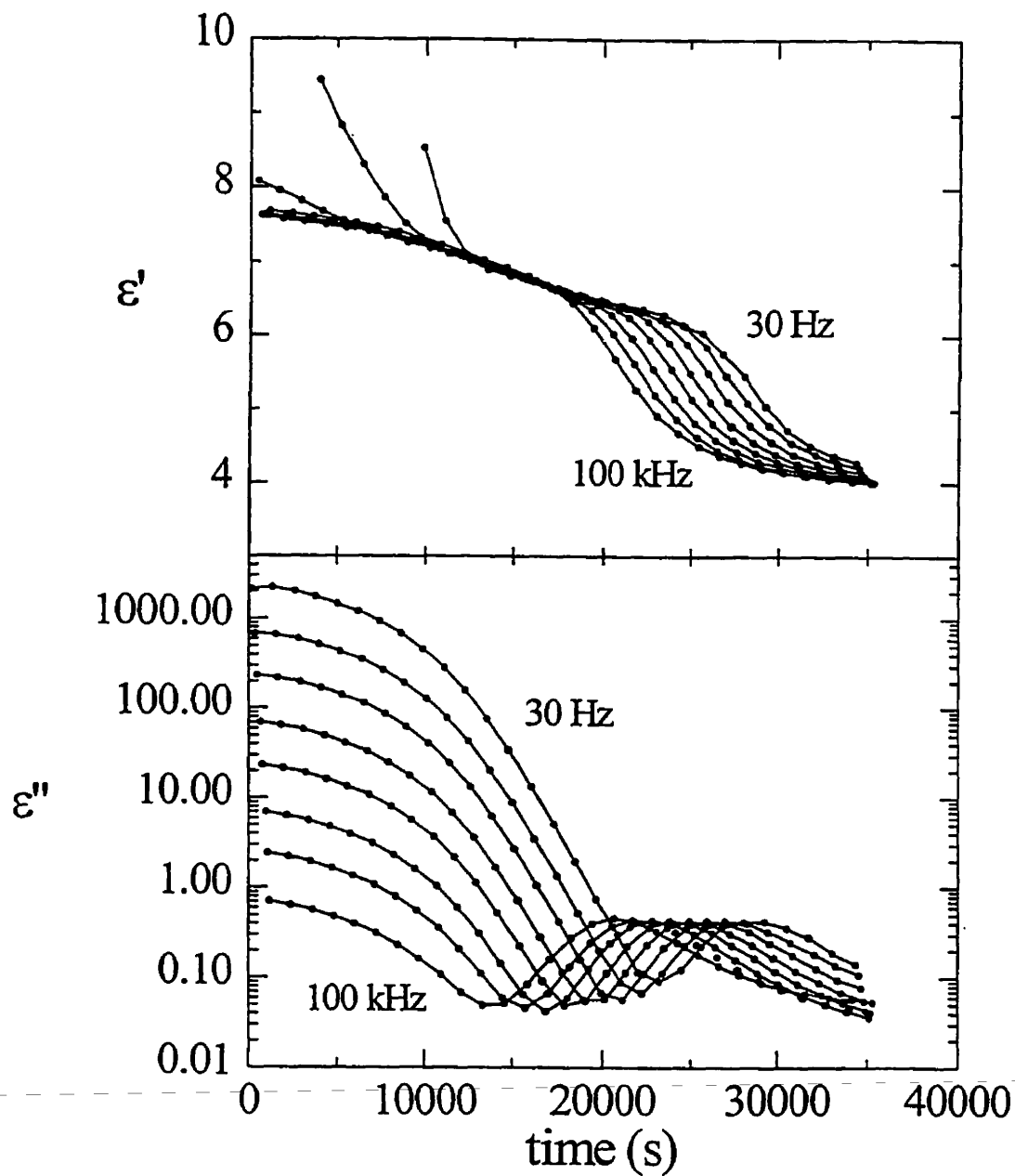
Figure 3.6: ε' and ε'' measured at 8 frequencies during the isothermal chemical reaction of the ANIL:DGEBA mixture at 333.4K are plotted against reaction time. The peaks in the curves of ε'' and the step in ε' shift to successively shorter times as the frequency is increased.
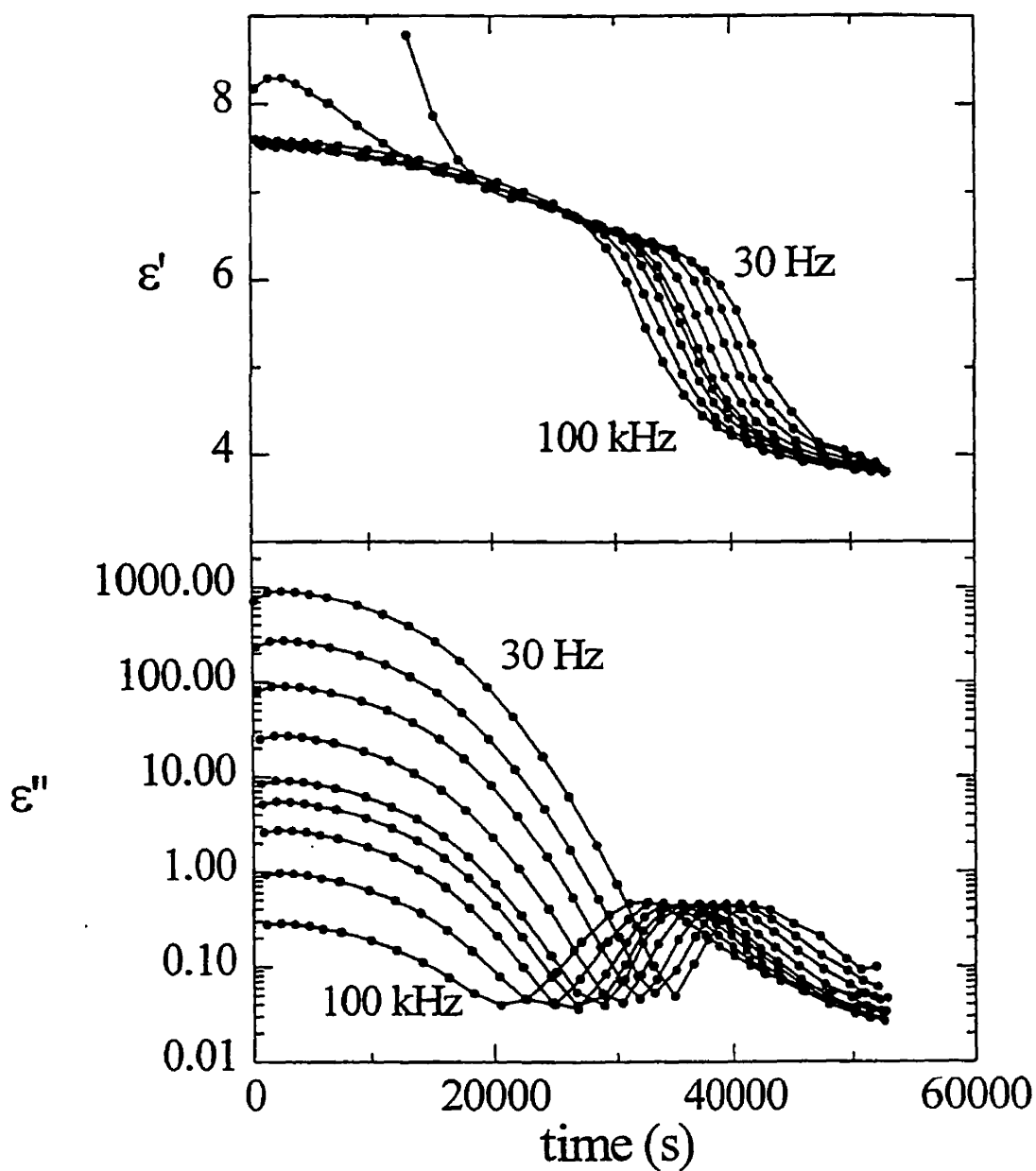
Figure 3.7: ε' and ε'' measured at 8 frequencies during the isothermal chemical reaction of the ANIL:DGEBA mixture at 343.4K are plotted against reaction time. The peaks in the curves of ε'' and the step in ε' shift to successively shorter times as the frequency is increased.

of the experimental set-up to compare the dielectric behaviour of all mixtures at a single temperature, since long times of reaction could call for manual measurements over a period greater than 24 hrs, and short times of reaction would not allow for sufficient data to be taken over the frequency range employed. Hence, the temperatures of measurement for the CHMA:DGEBA and HMA:DGEBA mixtures were chosen as 313.4 and 300.1K respectively.

The changes in the dielectric properties during the polymerization of the CHMA:DGEBA mixture at 313.4 K and the HMA:DGEBA mixture at 300.1K are shown as plots of ε' and $\log(\varepsilon'')$ against time in Figures 3.8 and 3.9. The results are qualitatively similar to those of the ANIL:DGEBA mixture in terms of appearance, though the magnitudes differ.

The change in the conductivity σ (= $\varepsilon''\omega\varepsilon_o$) is shown as plots of $\log(\sigma)$ against time in Figure 3.10 for the ANIL:DGEBA mixture at 333.4 and 343.4K, and in Figure 3.11 for the CHMA:DGEBA mixture at 313.4K and the HMA:DGEBA mixture at 300.1K. The shapes of all plots are qualitatively similar, with the curves for all frequencies nearly superposing at short times of reaction. At longer times, a peak appears, with the magnitude increasing and the position shifting to shorter times as the frequency increases. These results will be discussed in Chapter IV.

3.1.3 Dielectric Studies of the Fully Reacted Polymers

The dielectric properties of the fully reacted polymer were measured according to the method outlined in Section 2.3.3. The results are shown as plots of ε'
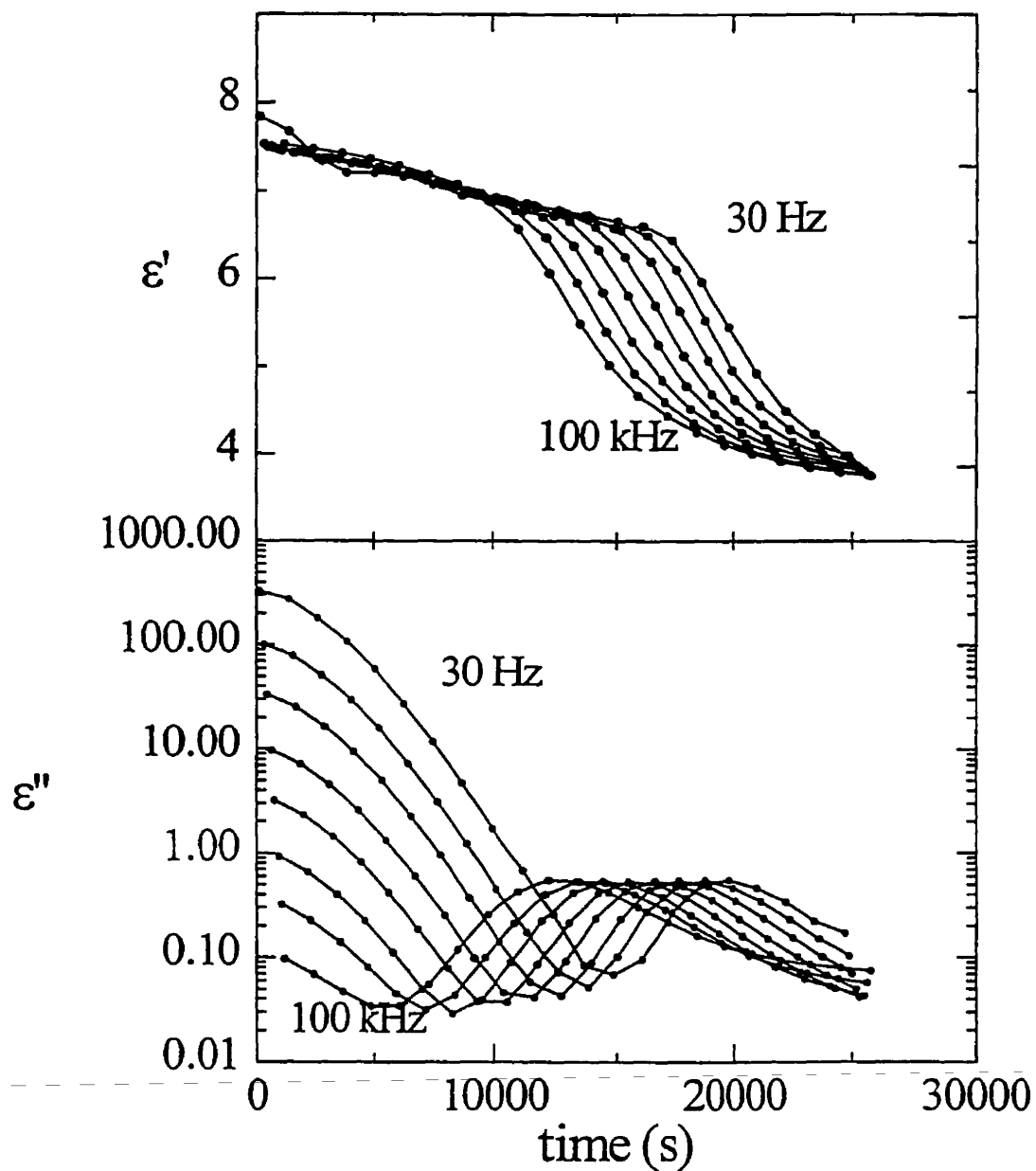
Figure 3.8: ε' and ε'' measured at 8 frequencies during the isothermal chemical reaction of the CHMA:DGEBA mixture at 313.4K are plotted against reaction time. The peaks in the curves of ε'' and the step in ε' shift to successively shorter times as the frequency is increased.
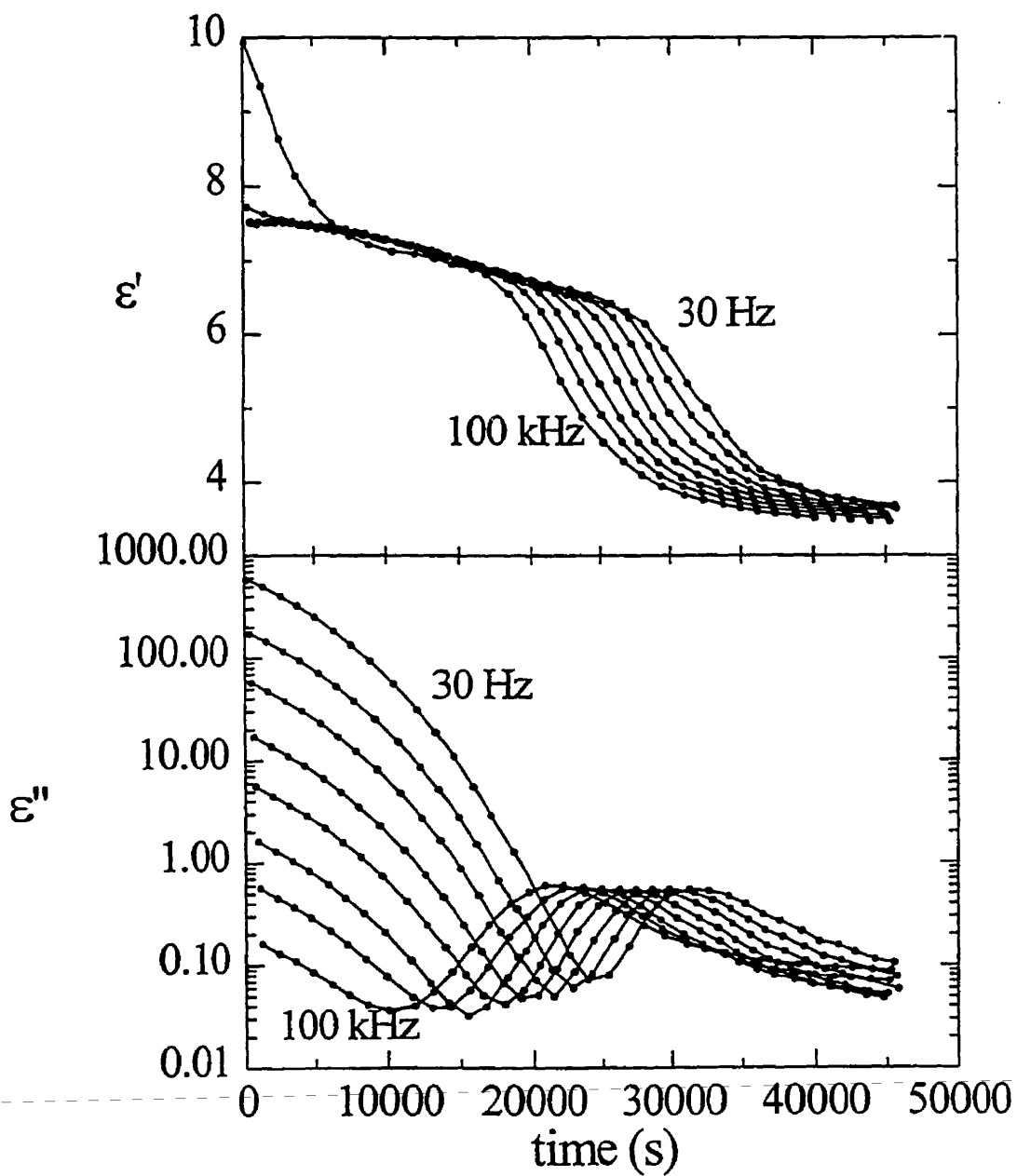
Figure 3.9: ε' and ε'' measured at 8 frequencies during the isothermal chemical reaction of the HMA:DGEBA mixture at 300.1K are plotted against reaction time. The peaks in the curves in ε'' and the step in ε' shift to successively shorter times as the frequency is increased.

Figure 3.10: The conductivity, σ, measured at 8 frequencies during the isothermal polymerization of the ANIL:DGEBA mixture at (a) 343.4 and (b) 333.4K are plotted against the time of chemical reaction. The peaks observed in the curves shift to successively shorter times as the frequency is increased.
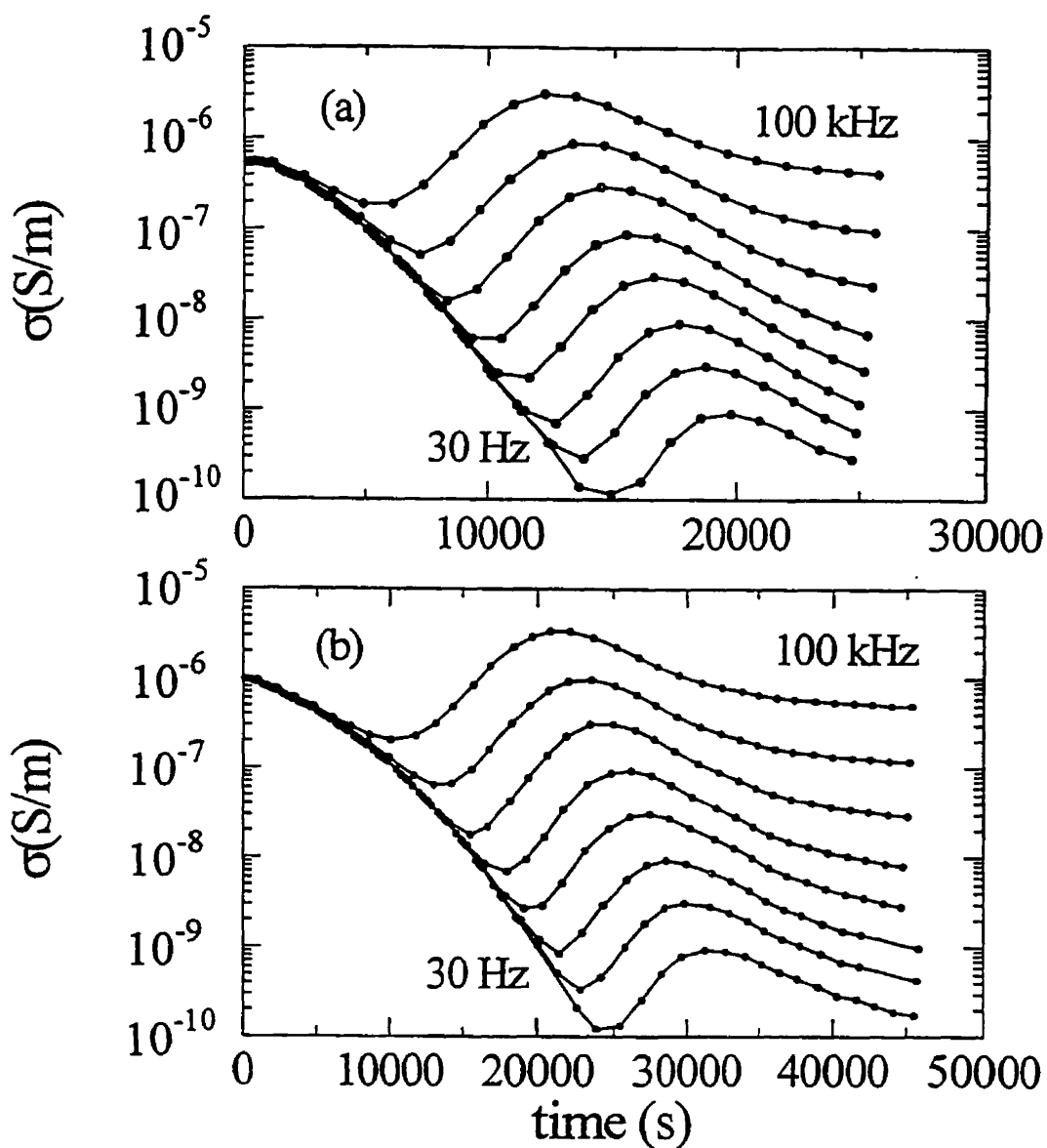
Figure 3.11: The conductivity, σ, measured at 8 frequencies during the Isothermal polymerization of the (a)CHMA:DGEBA mixture at (a) 313.4K and (b) the HMA:DGEBA mixture at 300.1K are plotted against the time of chemical reaction. The peaks observed in the curves shift to successively shorter times as the frequency is increased.

and $\log(\varepsilon'')$ against temperature in Figures 3.1 and 3.2 for all three mixtures. The results for all mixtures were qualitatively similar. Two distinct relaxation processes, indicated by the peak in ε'', are seen; one at lower temperature and the second at higher temperature. Again the low temperature relaxation is referred to as the -sub T_g relaxation, and the high temperature the α-relaxation. The magnitude of the peaks in ε'', $\varepsilon''_{sub\ Tg,max}$ and $\varepsilon''_{\alpha.max}$, and the temperatures at which they appear, $T_{sub\ Tg,max}$ and $T_{\alpha,max}$, are summarized for the three mixtures in Table 3.2.

Table 3.2 Magnitude and temperature of the peak maximum for the relaxation peaks in the fully polymerized states of the ANIL:DGEBA, CHMA:DGEBA and HMA:DGEBA mixtures.

Mixture	$\varepsilon''_{sub\ Tg,max}$	$\varepsilon''_{\alpha,max}$	$T_{sub\ Tg,max}$	$T_{\alpha,max}$
ANIL:DGEBA	0.075	0.267	250	381
CHMA:DGEBA	0.088	0.341	257	376
HMA:DGEBA[a]	0.056	0.388	248	329

(a)   Johari and Pascheto 1995.

Comparison with the behaviour of the mixtures in the molecular liquid state, also shown in Figure 3.1 shows that the lowest temperature, or sub T_g-relaxation, seen in the molecular liquid state, disappears with the formation of the fully reacted
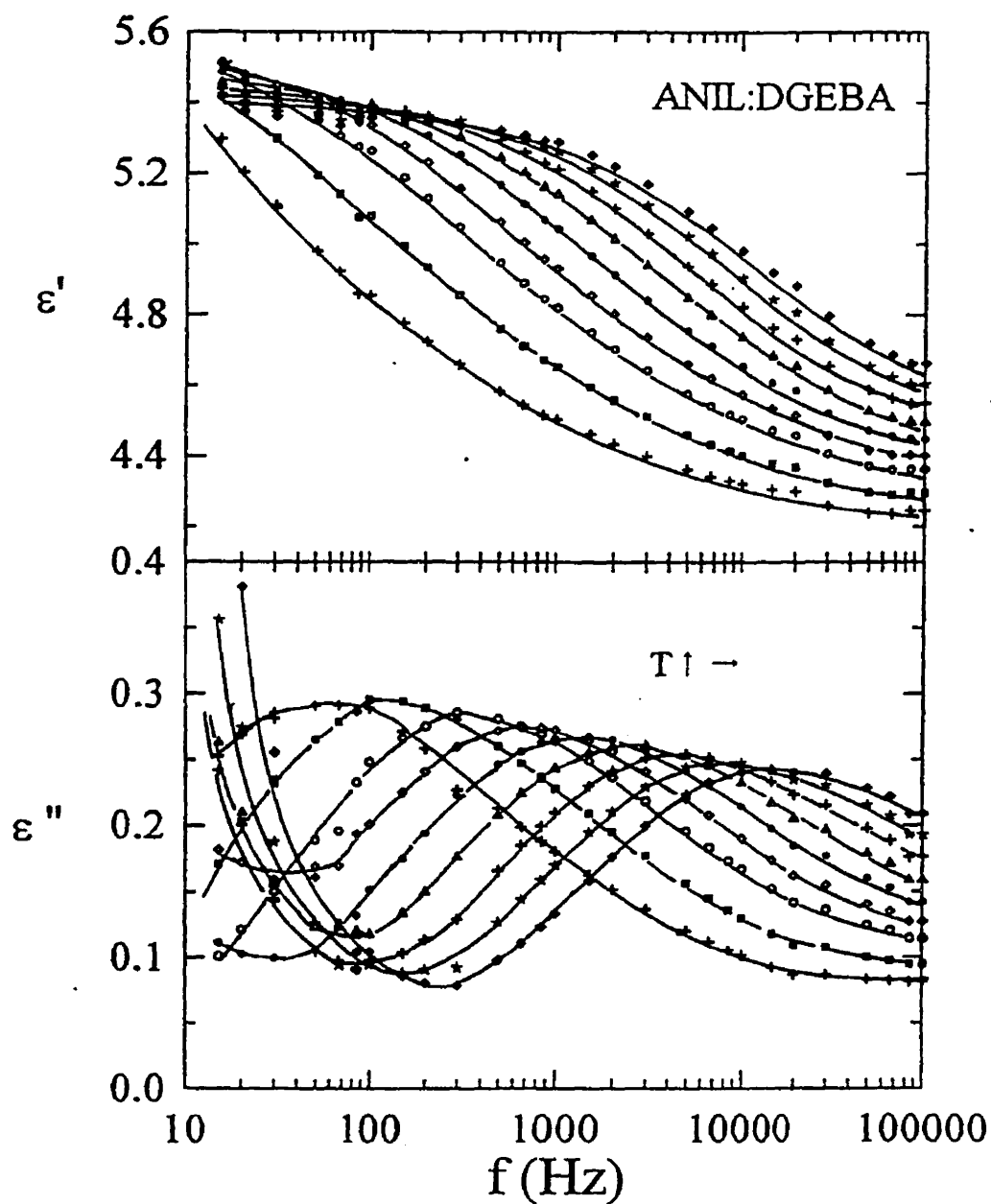
Figure 3.12: ε' and ε'' of the ANIL:DGEBA mixture in the fully polymerized state is plotted against the frequency for isothermal measurements made at 372.5, 375.3, 378.1, 380.2, 382.1, 383.9, 385.8, 387.7, and 389.5K. The curves shift sequentially from higher frequency to low frequencies as the temperature is lowered.
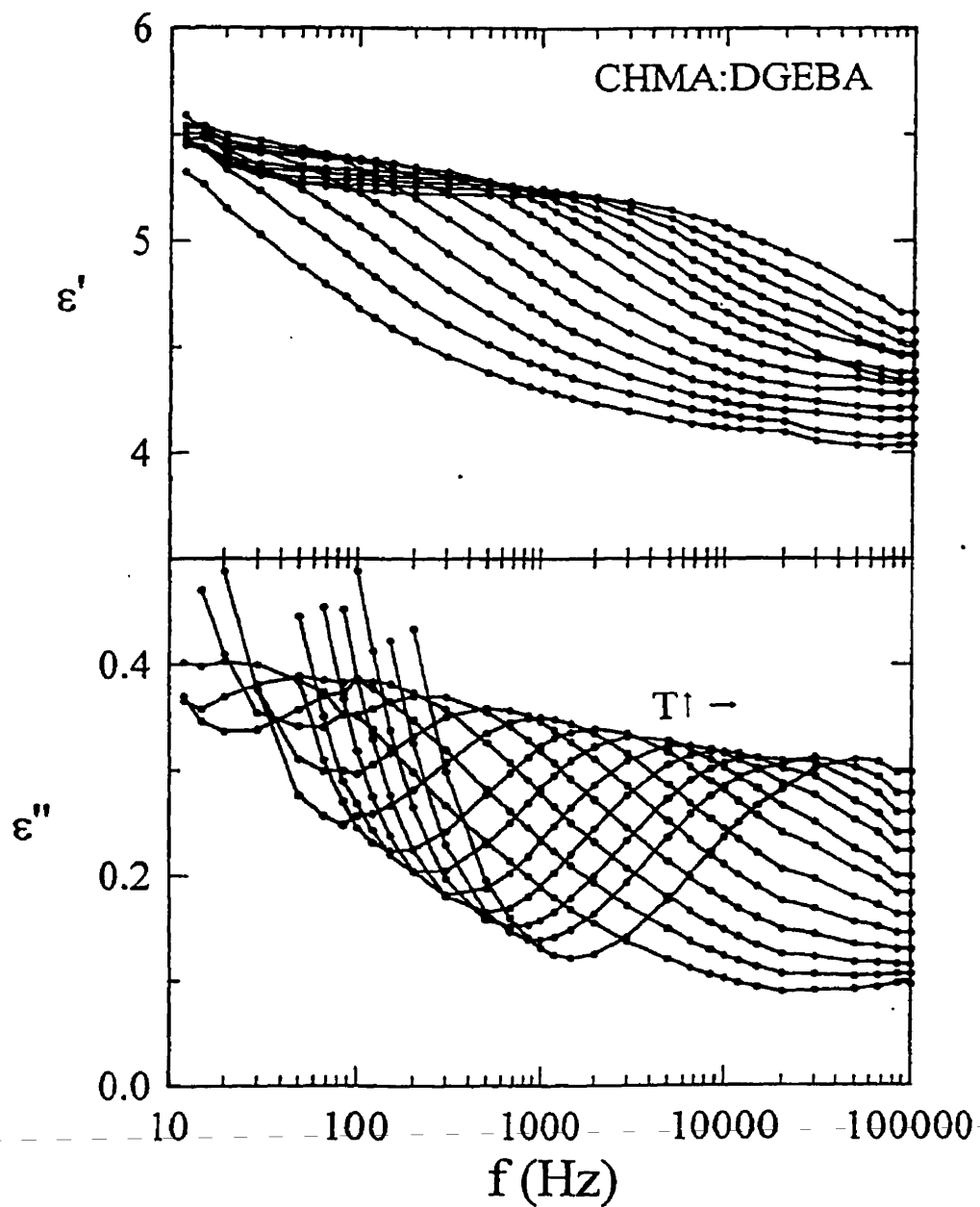
Figure 3.13: ε' and ε'' of the CHMA:DGEBA mixture in the fully polymerized state is plotted against the frequency for isothermal measurements made at 366.8, 368.0, 370.0, 371.8, 373.9, 375.7, 378.1, 379.9, 381.9, 383.7, 385.8, 387.6 and 390.4K. The curves shift sequentially from higher frequency to low frequencies as the temperature is lowered.
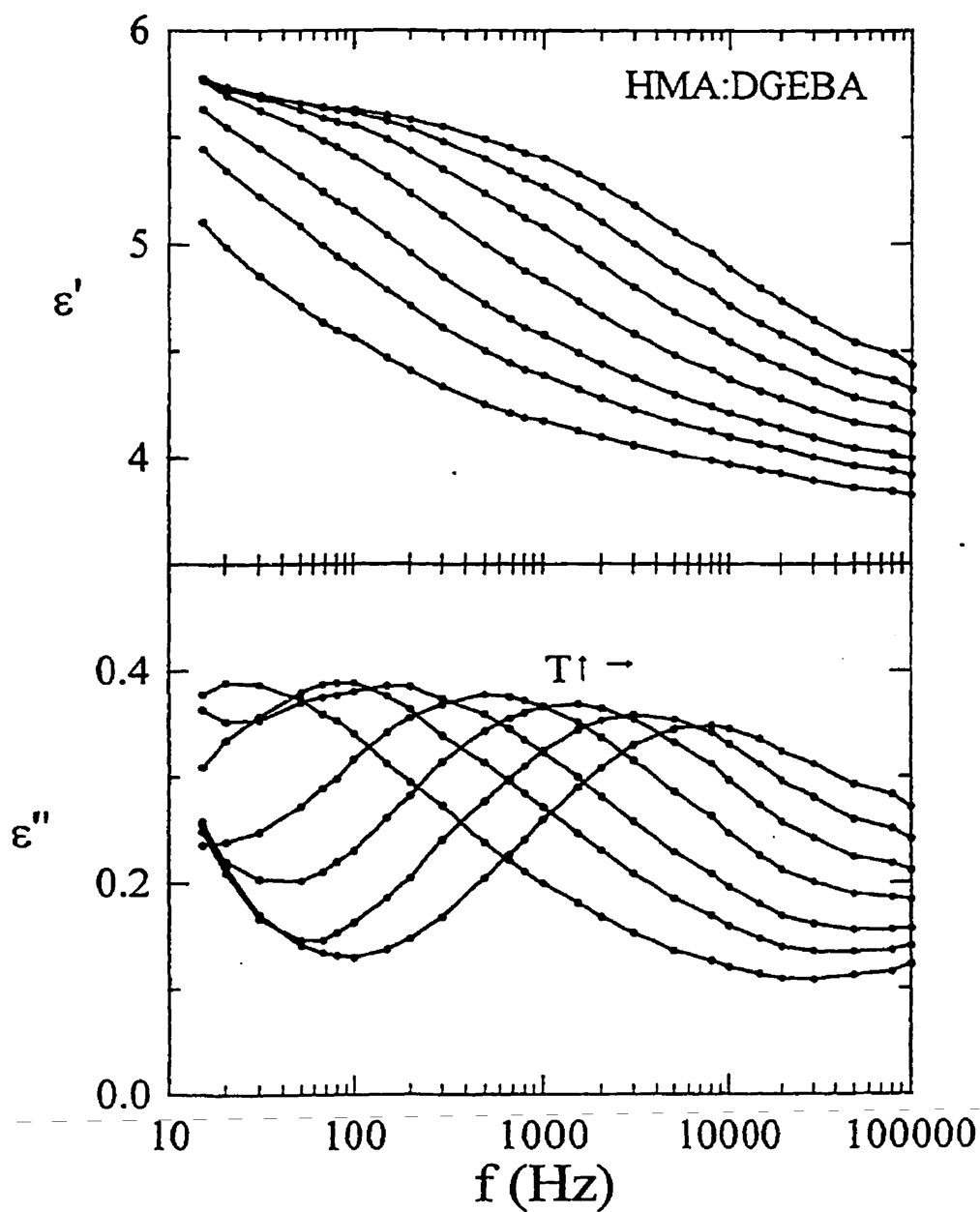
Figure 3.14: ε' and ε'' of the HMA:DGEBA mixture in the fully polymerized state is plotted against the frequency for isothermal measurements made at 323.0, 325.9, 328.2, 331.2, 334.1, 337.1, and 340.0K. The curves shift sequentially from high frequency to low frequencies as the temperature is lowered.

polymer. Concomitantly, there is the appearance of the a new sub T_g-relaxation process, and a shifting of the α-relaxation towards higher temperatures. The plots of ε' show that the magnitude of the step associated with the α-relaxation decreases with increasing polymerization. Such behaviour is not unique, as it has been noted previously for several network polymeric mixtures (Mangion and Johari 1990(a), 1990(b), Sidebottom and Johari 1990), and will be discussed in detail in Chapter VI.

Following the second temperature scans, the mixtures were cooled to temperatures in the range of the α-relaxation. Isothermal frequency spectra were measured in the same manner as outlined in Section 2.3.3, and the results are shown as plots of ε' and ε'' against the logarithm of frequency in Figures 3.12, 3.13 and 3.14, for the ANIL:DGEBA, CHMA:DGEBA and HMA:DGEBA mixtures respectively.

3.2   Ultrasonic Studies During Polymerization

The ultrasonic attenuation, α, and velocity, v, were measured at 2.25 MHz during the polymerization at fixed temperatures. This frequency was chosen for convenience of operation in terms of the sample size. The results are shown as plots of v and α against the logarithm of time in Figure 3.15 for the CHMA:DGEBA mixture at four temperatures, 298, 305, 313 and 323K. v increases very slowly at short times. This increase is interrupted by a sharp step-increase towards a near plateau value. The initial value decreases and the position of the step shifts to shorter times as the temperature is increased. The curve for the lowest temperature did not reach a plateau owing to the slowness of the reaction. The ultimate value at long times increased as the polymerization temperature was increased.
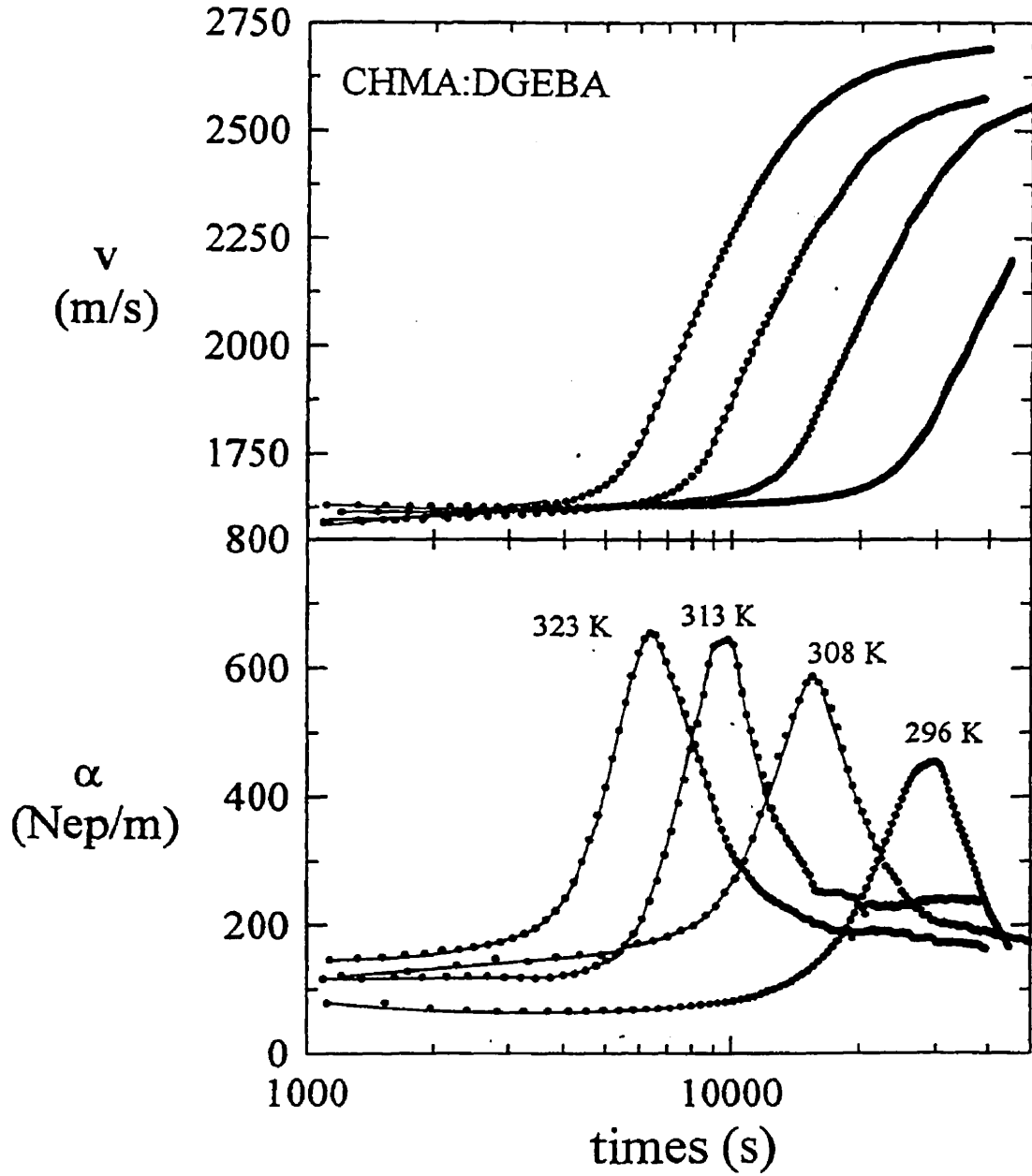
Figure 3.15: The ultrasonic velocity, v, and attenuation, α, measured at 2.25 MHz during the isothermal polymerization of the CHMA:DGEBA mixture at the temperatures as indicated, are plotted against the time of chemical reaction.

The attenuation, α, started at a near plateau value at short times of reaction. As time increased, a peak appeared whose magnitude increased, and whose position shifted to shorter times as the polymerization temperature was increased. Following the peak, α tended towards a plateau value, higher in magnitude than the initial short time value.

Corresponding plots of the HMA:DGEBA mixture measured for 2.25 MHz, at 300, 304, 312 and 320K are shown in Figure 3.16. In contrast to the CHMA:DGEBA mixture, the ultimate value of v did not increase with increasing temperature, rather it decreased with increasing temperature for the two highest temperatures. α showed qualitatively similar behaviour to that of the CHMA:DGEBA mixture, though the magnitudes differ.

It was not possible to make multiple temperature measurements on the ANIL:DGEBA mixture for two reasons: the transducers were limited to operation below 343K, and the slowness of the chemical reaction prohibited performing measurements below 333K. As a result, only one experiment for this mixture was carried out at 333.4K, and these results are included in Figure 3.16. Again the plots are qualitatively similar to those of the CHMA:DGEBA and HMA:DGEBA mixtures.

3.3   Differential Scanning Calorimetric (DSC) Studies

3.3.1   DSC Studies of the Unreacted Molecular Liquid State

The thermal properties of the unreacted, molecular liquid state of the three mixtures was measured as follows. Samples were mixed for two minutes at room
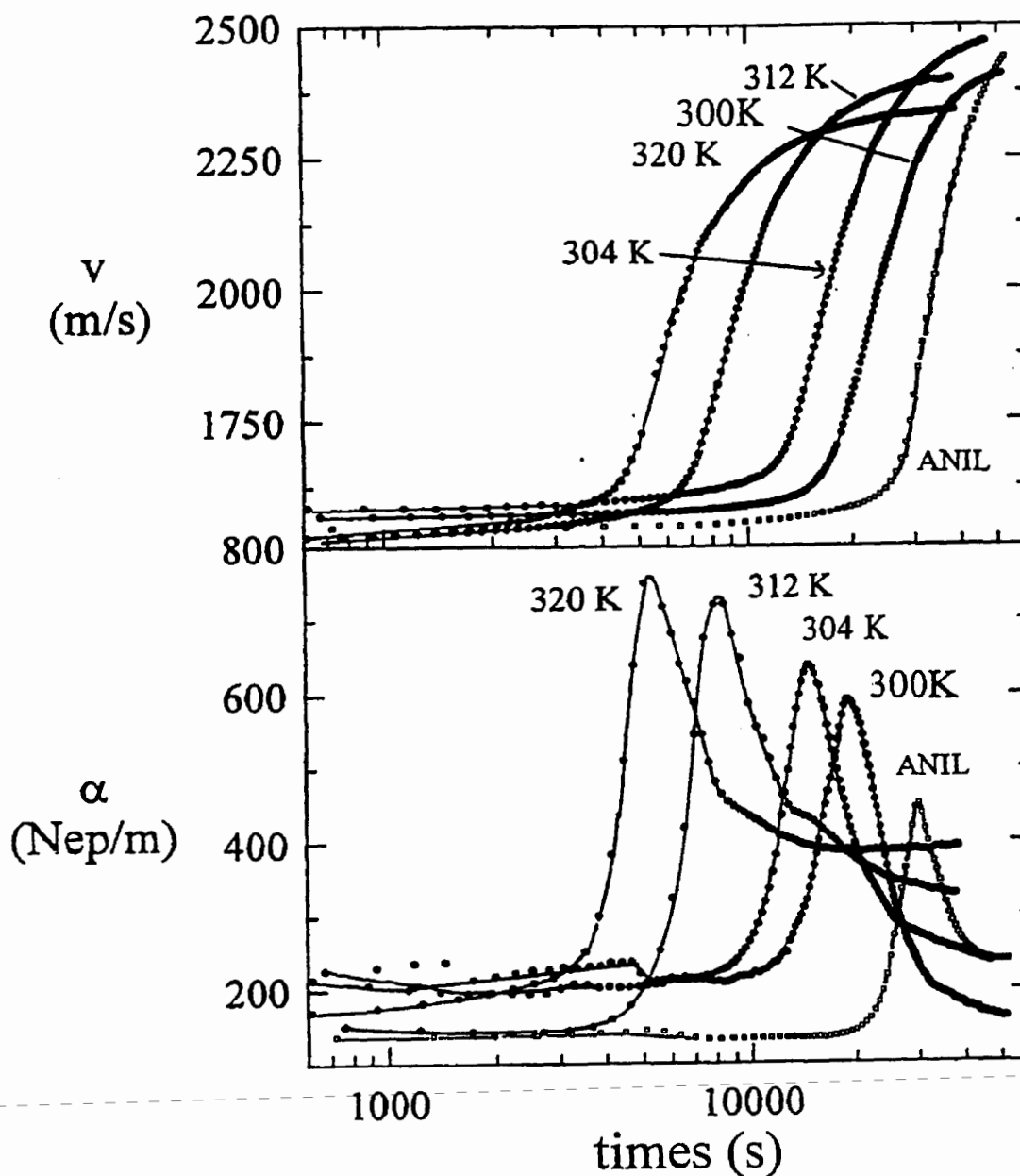
Figure 3.16: The ultrasonic velocity, v, and attenuation, α, measured at 2.25 MHz during the isothermal polymerization of the ANIL:DGEBA mixture at 333.4K and the HMA:DGEBA mixture at the temperatures as indicated, are plotted against the time of chemical reaction.

temperature, poured into the aluminum DSC sample pans, and then cooled at 10K/min to 200K. The rate of heat evolved, dH/dt, was then measured as the samples were heated at 10K/min to 300K. The results are shown as plots of dH/dt against temperature for the ANIL:DGEBA and CHMA:DGEBA mixtures in Figure 3.17. On the plots, an endothermic change is positive on the y-axis. Both show a nearly linear increase at low temperatures, followed by an endothermic step in the curves, the onset of this peak occurring at 235K for the CHMA:DGEBA mixture and at 245K for the ANIL:DGEBA mixture. After this step, dH/dt increased in a linear manner up to 300K. For comparison purposes, a sample of pure DGEBA was also studied and the results shown in Figure 3.17. The onset of the endotherm for the DGEBA occurred at 265K, thus the effect of adding amine to the DGEBA is to shift the endothermic step towards lower temperatures. Typically, this endothermic step is a manifestation of the glass transition, suggesting that all three samples were vitreous.

The results for the HMA:DGEBA mixture are shown in Figure 3.18. They differ from the ANIL:DGEBA and CHMA:DGEBA mixtures in that two features, namely an exothermic peak followed by an endothermic peak, appear rather than a small endothermic step. This suggests that the HMA:DGEBA sample is either partly, or entirely crystalline. An attempt was made to rapidly cool the sample at 40K/min from room temperature to 200K. The subsequent reheating at 40K/min is also shown in Figure 3.18. Again no endothermic step was observed, and the features seen in the 10K/min heating are shifted towards higher temperatures. Since the exotherm occurs at a temperature close to that of the endothermic step in the plots for the
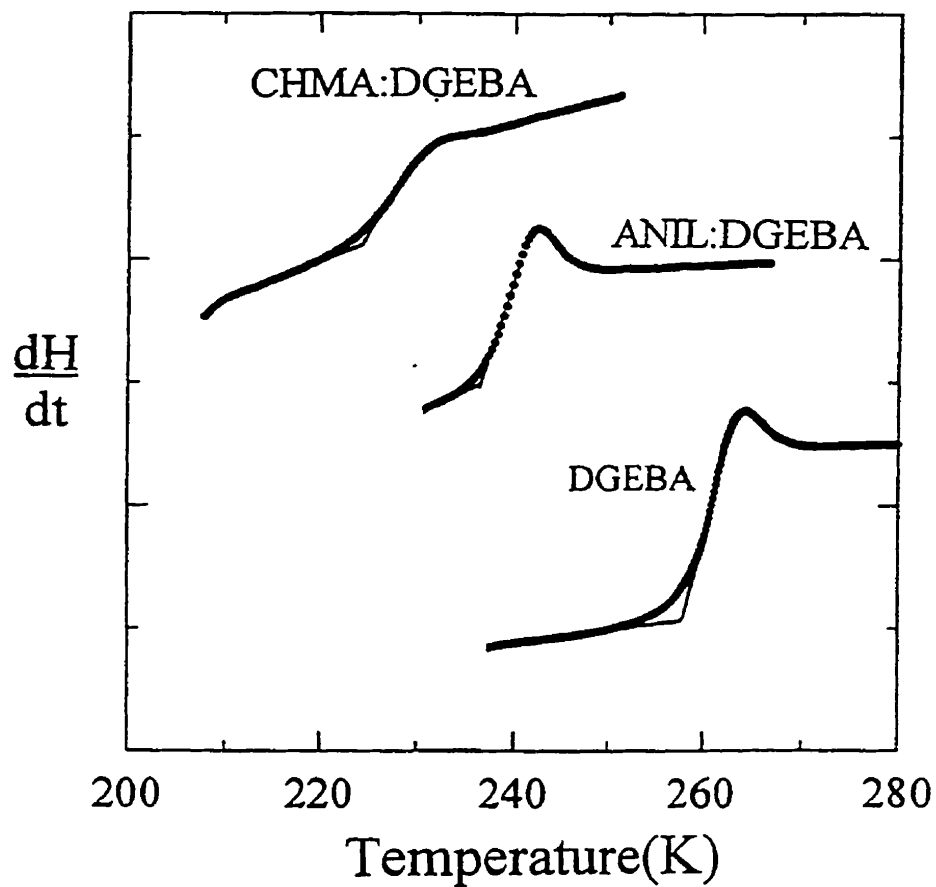
Figure 3.17:   The rate of heat released, dH/dt, for the ANIL:DGEBA and CHMA:DGEBA mixtures in their molecular liquid states, during heating at a constant rate of 10K/min, is plotted against temperature. The plots are endothermic in the positive y-axis direction, and the scale as indicated.
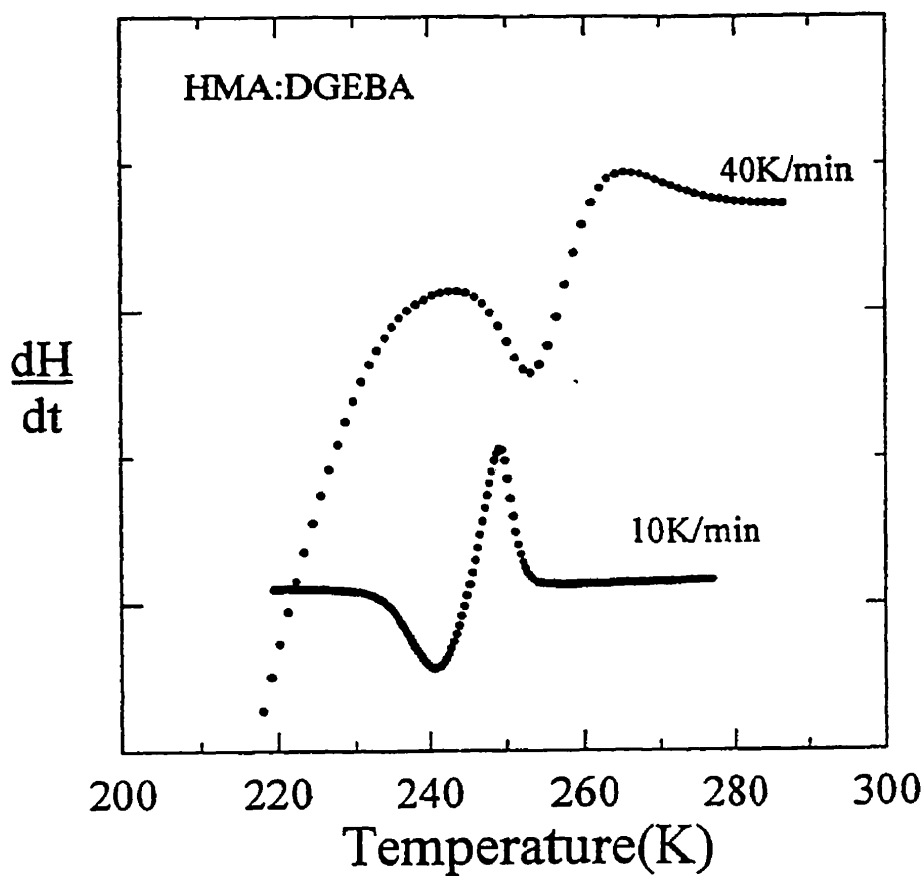
Figure 3.18: The rate of heat released, dH/dt, for the HMA:DGEBA mixture in their molecular liquid states, during heating at constant rates of 10K/min and 40K/min, is plotted against temperature. The plots are endothermic in the positive y-axis direction, and the scale as indicated.

CHMA:DGEBA and ANIL:DGEBA mixtures showed in Figure 3.17, it is surmised that the exotherm could have overlapped the endothermic step, rendering it irresolvable.

3.3.2 DSC Studies During Polymerization

Since it is of use to compare thermal properties with the dielectric and ultrasonic properties, listed in Sections 3.1.2 and 3.2, dH/dt was measured during chemical reaction at temperatures coinciding with those used for the previous isothermal studies. Typical results are shown for the temperatures corresponding to those used in the dielectric studies as plots dH/dt of sample against time for the CHMA:DGEBA mixture at 313 K, the ANIL:DGEBA mixture at 333.4K and 343.4K and the HMA:DGEBA mixture at 300K in Figure 3.19. For all mixtures the reaction is strongly exothermic.

Following the isothermal reaction, the samples from the isothermal experiments were cooled to room temperature, and subsequently reheated at 10K/min. The resulting normalized dH/dt corresponding to the isothermal experiments shown in Figure 3.19 are plotted against temperature in Figures 3.20. All curves show qualitatively similar features. Initially at low temperatures, a sharp endothermic peak appears. Immediately following this peak, there appears a broad exothermic peak, which is due to further chemical reaction that occurs as the sample is heated above its glass transition temperature.
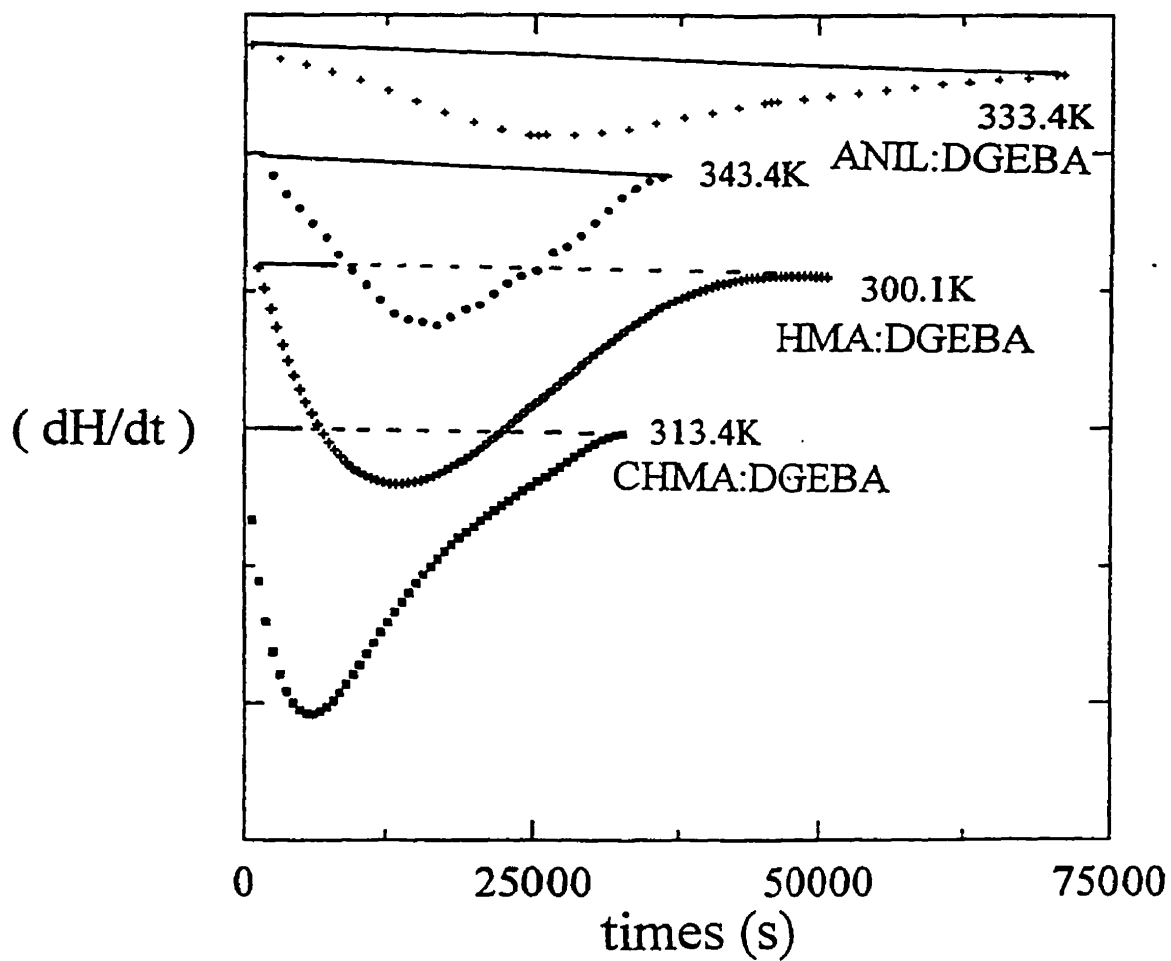
Figure 3.19: The rate of heat released, dH/dt, during the isothermal polymerization of the ANIL:DGEBA mixture at 333.4 and 343.4K, the CHMA:DGEBA mixture at 313.4K and the HMA:DGEBA mixture at 300.1K are plotted against the time of chemical reaction. The plots are endothermic in the positive y-axis direction. Baselines are drawn to show the area integrated to determine the extent of chemical reaction.
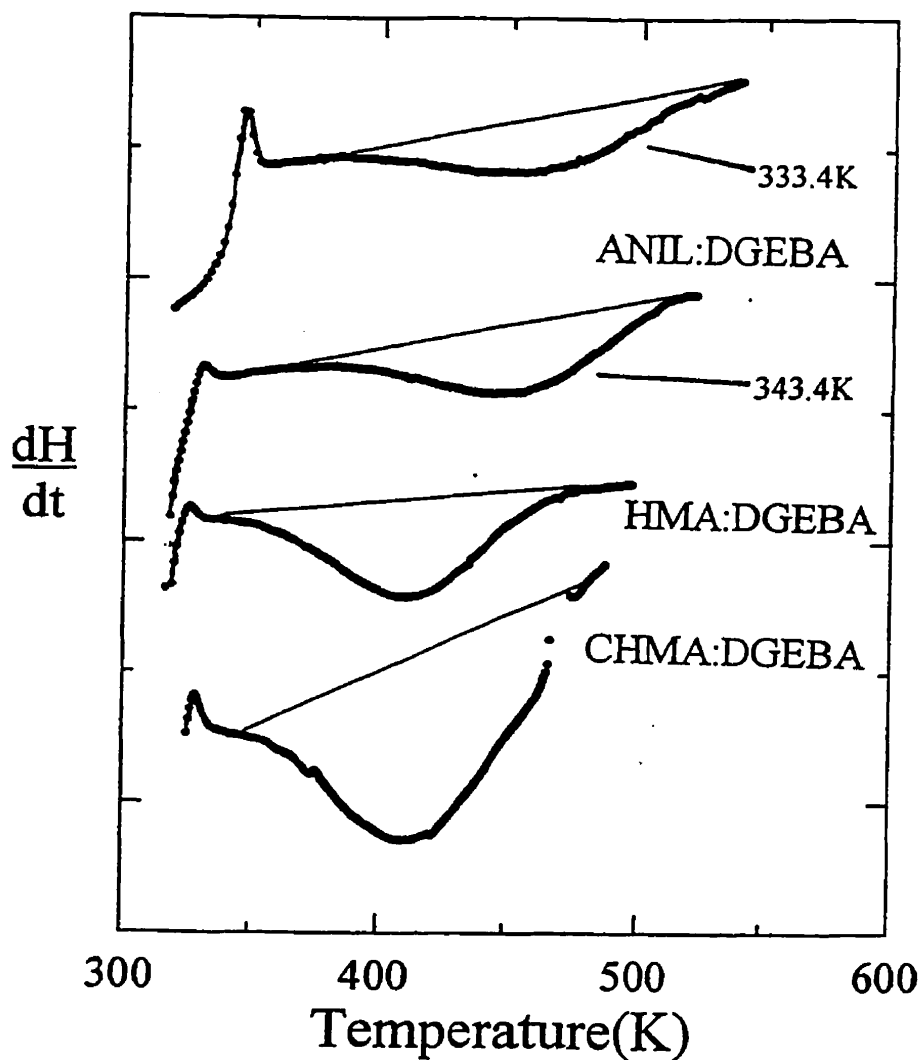
Figure 3.20: The rate of heat released, dH/dt, for the three mixtures following the isothermal reactions shown in Figure 3.19, during their heating at a constant rate of 10K/min, is plotted against temperature. The plots are endothermic in the positive y-axis direction. Baselines are drawn to show the area integrated to determine the extent of chemical reaction.

CHAPTER IV: DISCUSSION OF DIELECTRIC RESULTS

4.1 Molecular Dynamics in the Unreacted Molecular Liquid

4.1.1 Dielectric Relaxations in the Unreacted Molecular Liquid

The relaxation behaviour of the unreacted molecular liquids used in the study provide information on their molecular dynamics. In order to begin the analysis it is necessary to consider the contributions to dielectric response, as outlined in Chapter II.

ε' and ε'' contain contributions from three mechanisms, namely, (i) the dipolar reorientation of molecular dipoles inherent in the material, (ii) the transport of ionic charge resulting from the motion of mobile ions or via proton transfer along an existent hydrogen bonded network, and (iii) the build-up of charge on the electrode interface that forms a layer with a resistance and capacitance, hereto referred as the electrode polarization. The first two effects are intrinsic to the material while the third is an extrinsic effect dependent on the nature of the electrode/material interface. The effects may be summarized simply as,

$$\varepsilon' = \varepsilon'_{dip} + \varepsilon'_{el}, \tag{4.1}$$

$$\varepsilon'' = \varepsilon''_{dc} + \varepsilon''_{dip} + \varepsilon''_{el}, \tag{4.2}$$

where the subscripts dip, dc and el denote the contributions from the dipolar reorientation, ionic conduction and electrode polarization, respectively.

For analysis of the data, it is useful to adapt the procedure given by Cole and coworkers (Johnson and Cole 1951; Tombari and Cole 1991). The complex electrode

impedance is given by (MacDonald 1987), $Z^*_{el} = Z_0(i\omega)^{-k}$, where the temperature independent Z_0 is characteristic of the dielectric interface, ω is the angular frequency (=$2\pi f$) and k is a parameter whose value was chosen by several authors (Johnson and Cole 1951; Tombari and Cole 1991; Johari et al. 1994, Parthun and Johari, 1995(a)) as 0.5. When used as a constant phase element in series with the bulk properties of the sample, it contributes to the measured conductance, G_{meas}, and ε'_{meas} (=C_{meas}/C_0) according to,

$$\frac{G_{meas}}{C_o} - i\omega\varepsilon'_{meas} - \frac{(G_{bulk}/C_o) + i\omega\varepsilon'_{bulk}}{1 + Z^*_{el}\left[(G_{bulk}/C_o) + i\omega\varepsilon'_{bulk}\right]}, \qquad (4.3)$$

where G_{bulk} and ε'_{bulk} are the corresponding values for the sample's bulk or overall conductivity and dipolar relaxation. For frequencies where $G_{bulk} >> \omega\varepsilon'_{bulk}C_0$ and $|Z^*_{el}| = Z_0 G_{bulk}\omega^{-k} << 1$, Eqn. (4.3) can be expanded as a Taylor series, and written, after truncating beyond the first order term, as,

$$\frac{G_{meas}}{C_o} - \frac{G}{C_o} - \left[Z_o\cos\left(\frac{k\pi}{2}\right)\frac{G^2}{C_o}\right]\omega^{-k}. \qquad (4.4)$$

Cole and coworkers (Davidson and Cole 1951, Tombari and Cole 1991) combined Eqns. 4.1-4.4 to give,

$$\varepsilon' - \varepsilon'_{dip} + \left[\left(Z_o\sin\left(\frac{k\pi}{2}\right)\right)\frac{(\sigma_o + \sigma_{dip})^2 C_o}{\varepsilon_o^2}\right]\omega^{-(k+1)}, \qquad (4.5)$$

$$\varepsilon'' = \varepsilon''_{dc} + \varepsilon''_{dip} = \left[\left[Z_o \cos \left[\frac{k\pi}{2} \right] \right] \frac{(\sigma_{dc} + \sigma_{dip}) C_o}{\varepsilon_o^2} \right] \omega^{-(k+1)} \qquad (4.6)$$

where $\sigma_o + \sigma_{dip} = \varepsilon_o G_{bulk}/C_o$, ε_o (=8.8514 pF/m) is the permittivity of vacuum and σ_o and σ_{dip} (in S/m) are the contributions to conductivity from (frequency-independent) direct current and (frequency-dependent) dipolar relaxation in the material. The term containing Z_o represents the contribution from the interfacial impedance at the electrode interface. This contribution increases with increasing magnitudes of Z_o, σ_o and σ_{dip}, and with decreasing frequency. Thus, for materials with identical electrode interface properties, the contribution from electrode polarization becomes significant at low frequencies, and when the total conductivity is high. Eqns. (4.5) and (4.6) can then be used to deconvolute the three contributions to the dielectric spectra, and different techniques for such analysis have been given by several groups (Johnson and Cole 1951; Tombari and Cole 1991; Johari et al 1994, Parthun and Johari 1995(a)).

For the three mixtures studied, the ionic conductivity is low. Hence, from Eqns. 4.5 and 4.6, the contributions from electrode polarization to ε' and ε'' is not significant. However, it is important that these contributions not be neglected at higher temperatures, when the ionic conductivity is high and electrode polarization effects become dominant (Parthun and Johari, 1995(a)). It was also necessary to use this type of analysis to subtract the effects of σ_o to resolve the dipolar relaxation process for the fully polymerized CHMA:DGEBA mixture.

During the growth of a macromolecule from its molecular liquid state to its fully reacted polymeric state, the dielectric properties change continuously. In terms

of chemistry, this is manifested by a decreased in the number of monomers, an increase in the number of oligomers, hence a change in the molecular dipole moment. In terms of physics, the replacement of the van der Waal and H-bonding interactions by strong, directional covalent bonds, changes the diffusivity, density, optical refractive index, viscosity, velocity of sound and the intramolecular vibration frequencies (Johari, 1994(a). Further effects include changes in the nature of the distribution of relaxation times, the development of further relaxation processes and a change in the refractive index. These effects, and their phenomenological description have been discussed in two review articles (Johari, 1994(a); Johari, 1995). In this discussion, it is useful to consider the changes in the specific relaxation processes which occur during the change in molecular structure.

4.2   Evolution of the α-Relaxation Process

4.2.1 α-Relaxation in the Molecular Liquid State

Figures 3.1-3.5 show the dielectric behaviour of the three mixtures in the molecular liquid state. The spectra at different temperatures show the step in ε' and concomitant peak in ε'' that are indicative of a relaxation process, as discussed in Chapter II. For a single relaxation time, the complex plane plots of ε'' against ε' yield a semi-circular arc, as outlined for a single Debye relaxation process as described in Chapter II. The spectra measured at different temperatures, as shown in Figures 3.3-3.5, are replotted in the complex plane in Figures 4.1-4.3 for the ANIL:DGEBA, CHMA:DGEBA and HMA:DGEBA mixtures, respectively. The plots are not semi-
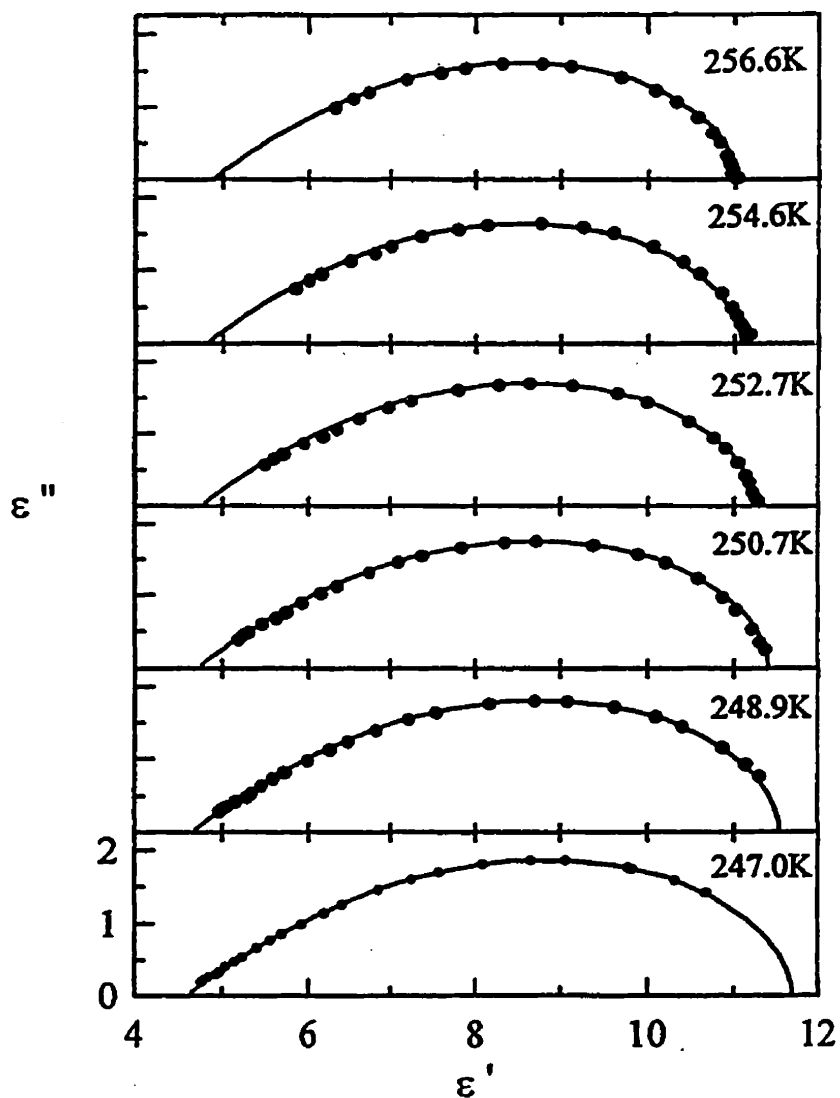
Figure 4.1:   Complex plane plots of ε'' against ε' for the ANIL:DGEBA mixture in the molecular liquid state for isothermal measurements made at 247.0, 248.9, 250.7, 252.7, 254.6, and 256.6K as indicated. The best-fit curves according to the stretched exponential relaxation function, shown as full lines, were calculated from the parameters in Table 4.1. Baselines drawn to the curves indicate $\varepsilon'' = 0$.
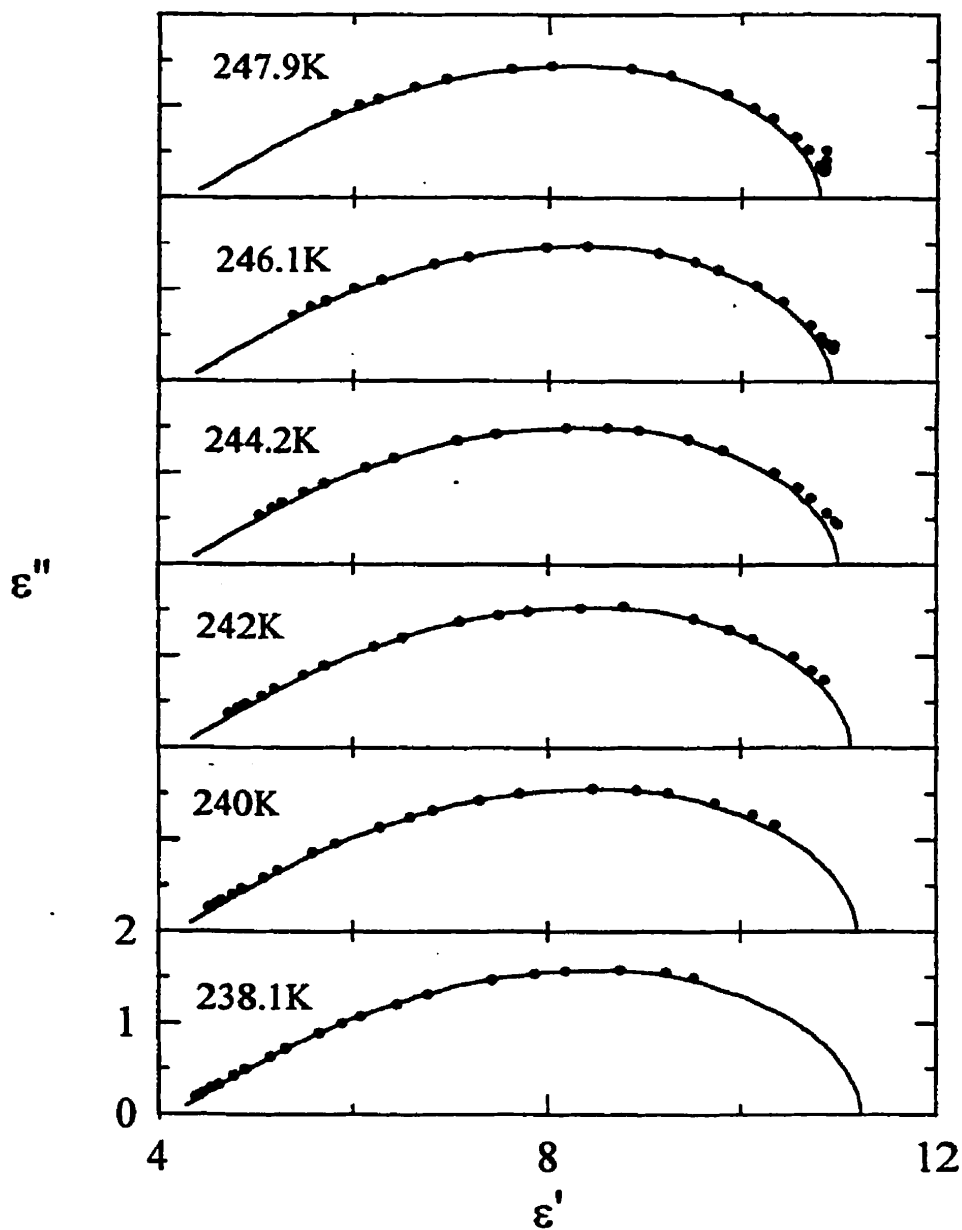
Figure 4.2:   Complex plane plots of ε'' against ε' for the CHMA:DGEBA mixture in the molecular liquid state for isothermal measurements made at 238.1, 240.0, 242.0, 244.0, 246.1 and 247.9K as indicated. The best-fit curves according to the stretched exponential relaxation function, shown as full lines, were calculated from the parameters in Table 4.2.
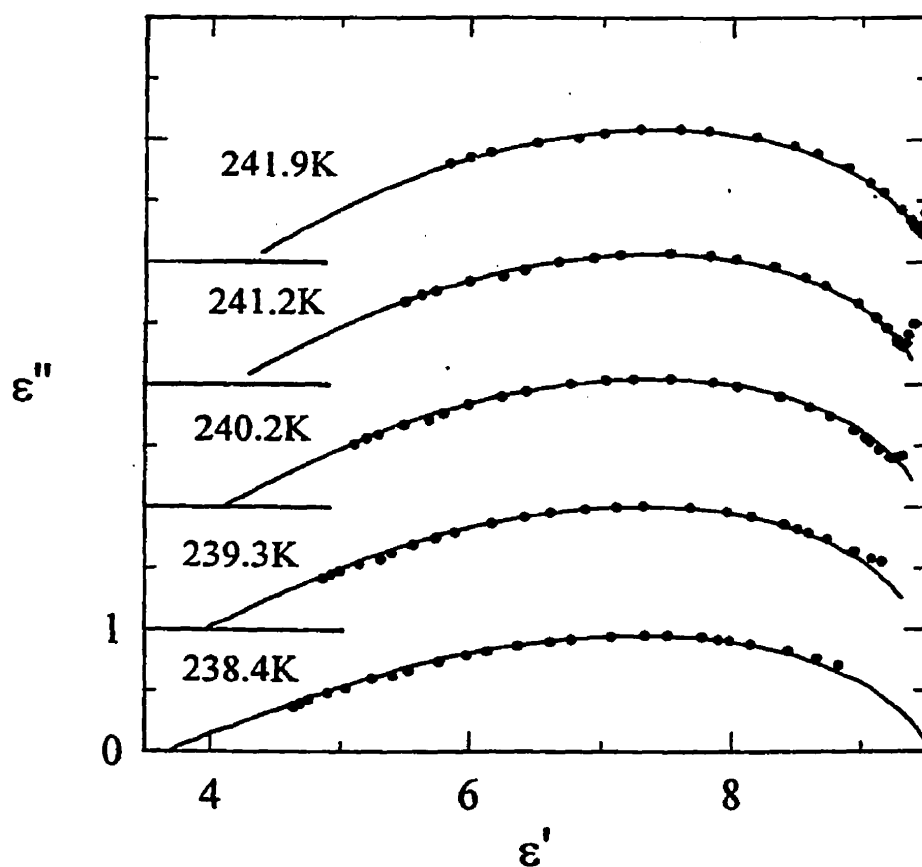
Figure 4.3: Complex plane plots of ε'' against ε' for the HMA:DGEBA mixture in the molecular liquid state for isothermal measurements made at 238.4, 239.6, 240.2, 241.2 and 241.9K as indicated. The best-fit curves according to the stretched exponential relaxation function, shown as full lines, were calculated from the parameters in Table 4.3. Baselines drawn to the curves indicate $\varepsilon'' = 0$.

circular in shape, rather their shape is that of a skewed arc at high frequencies. Several different empirical forms of relaxation functions have been suggested to account for such behaviour (Cole and Cole 1941, Fröhlich 1949, Davidson and Cole 1951, Havriliak and Negami 1968, Watts and Williams 1972), all of which suggest a distribution of relaxation times. It has been found that the empirical stretched exponential form, $\Phi = \exp(-[t/\tau_o]^\beta)]$, of the relaxation function provides a good description of such observed dielectric behaviour (Parthun and Johari 1995(c), Johari and Pascheto 1995).

The complex dielectric permittivity, ε^*, is written as,

$$\varepsilon^* = \varepsilon' - i\varepsilon'' = \varepsilon_\infty + (\varepsilon_o - \varepsilon_\infty) N^*(\omega\tau_o), \qquad (4.7)$$

where N^* is the normalized complex relaxation function given by,

$$N^*(\omega\tau_o) = N'(\omega\tau_o) - iN''(\omega\tau_o) = \int_0^\infty e^{-i\omega t}\left[-\frac{\partial\Phi}{\partial t}\right] dt, \qquad (4.8)$$

The integral on the right hand side is by definition the LaPlace transform, $\mathcal{L}(-\partial\Phi/\partial t)$, and it is this quantity that must be determined in order to proceed with the analysis in terms of Eqn(4.8).

Substitution of the stretched exponential form of the relaxation function into Eqn. (4.8) gives the normalized relaxation from which the complex permittivity can be calculated. The evaluation of Eqn(4.8) has been carried out analytically by several groups (Moynihan et al. 1973, Lindsey and Patterson 1980, Weiss et al, 1985, Dishon et al. 1987). For this work, we used the values calculated by Dishon et al. (1987),

based on the evaluation of the integral in Eqn. (4.8) via a trigonometric substitution and Simpson's rule. These values have been tabulated in the literature for values of β from 0.1 to 2. To check that the tabulated values were accurate, an algorithm was written to calculate the values according to the method outlined by Dishon et al (1987). Since the program required a large amount of computer memory, it was not possible to generate full data table in a feasible amount of time. Nevertheless, several values were calculated, and they were in agreement to those in the published tables of Dishon et al (1987). Thus, Dishon et al's (1987) tabulated values were deemed accurate, and were used for the remainder of the analyses.

To fit the experimental curves, an algorithm was written , that allowed for graphs of the experimental curves to be compared with the fit, according to the choice of parameters, ε_s, ε_∞, β and τ_0. The best-fit curves are shown as full lines in Figures 4.1 - 4.3, for the three mixtures. In all cases, the agreement is good, and the parameters used for the fits are listed in Tables 4.1, 4.2 and 4.3.

It is instructive to study the temperature dependence of the parameters ε_s, ε_∞, β and τ_0 for the three mixtures. The first three are plotted against the reciprocal of temperature in Figure. 4.4, with the curves distinguished according to the scheme outlined in the figure caption. The behaviour of each mixture varies markedly. ε_s decreases with increasing temperature for the CHMA:DGEBA and ANIL:DGEBA mixtures, while β remains constant and ε_∞ increases. For the HMA:DGEBA mixture, ε_s remains essentially constant, and both β and ε_∞ increase with increasing temperature. The dispersion $\Delta\varepsilon$ (= ε_s - ε_∞) is also plotted against $1/T$ in Figure 4.4.
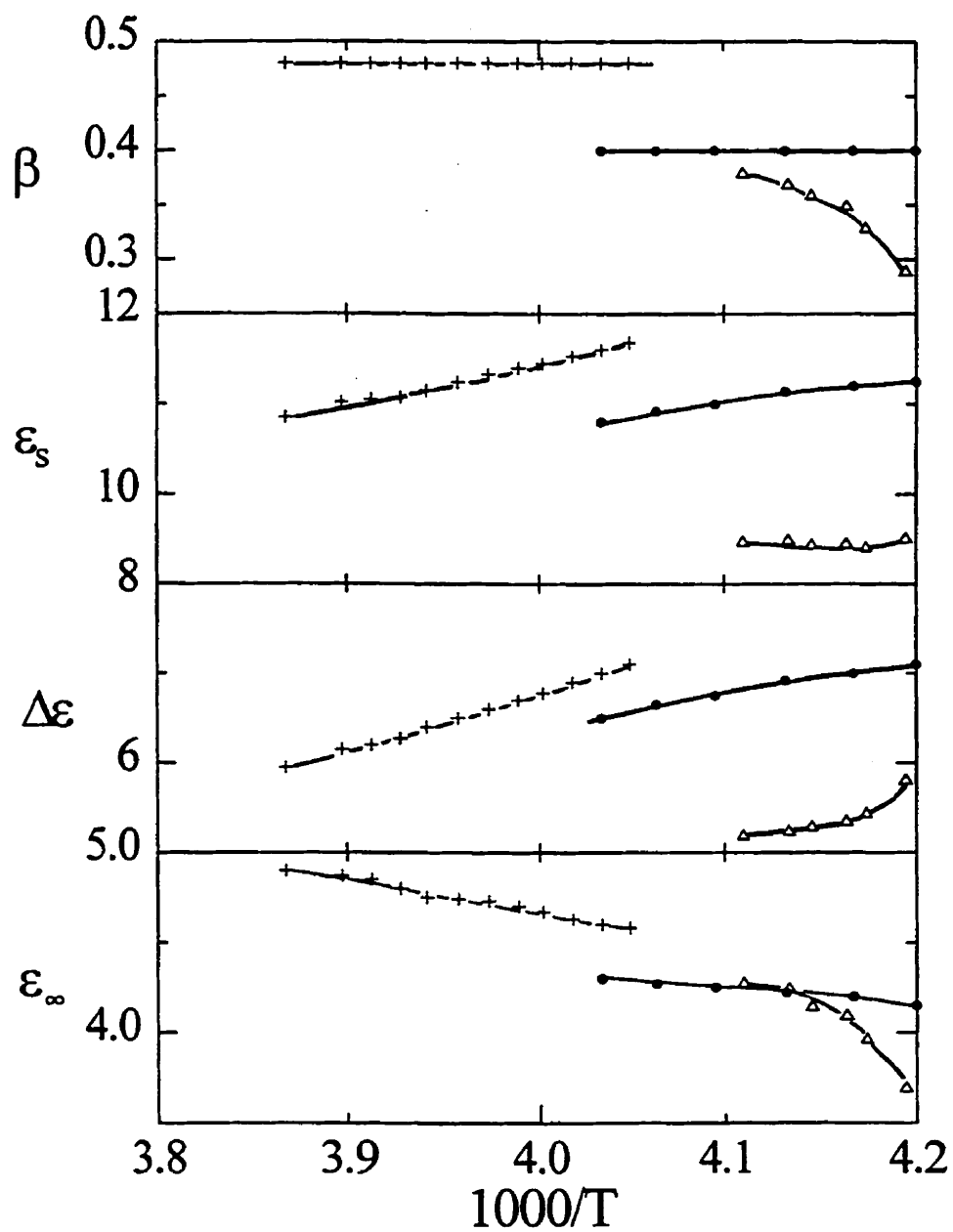
Figure 4.4: The parameters ε_s, ε_∞, β and $\Delta\varepsilon$ determined from the stretched exponential fits to the spectra of the three mixtures in the molecular liquid state, are plotted against the reciprocal of temperature. Notations are: ANIL:DGEBA (+), CHMA:DGEBA (•) and HMA:DGEBA (Δ).

For all three mixtures it decreases with increasing temperature, at temperatures above the glass transition temperature.

Table 4.1: Parameters used from the fits of the stretched exponential relaxation function to the dielectric spectra of the unreacted ANIL:DGEBA mixture at different temperatures.

T/K	β	ε_s	ε_∞	τ_o /μs
247.0	0.48	11.68	4.58	2000
247.9	0.48	11.60	4.60	1150
248.9	0.48	11.53	4.63	630
249.9	0.48	11.45	4.67	350
250.7	0.48	11.4	4.70	225
251.7	0.48	11.33	4.73	140
252.7	0.48	11.24	4.74	80
253.7	0.48	11.15	4.75	50
254.6	0.48	11.07	4.80	33
255.6	0.48	11.05	4.85	22
256.6	0.48	11.02	4.87	14
258.5	0.48	10.85	4.90	6.1

Table 4.2: Parameters used from the fits of the stretched exponential relaxation function to the dielectric spectra of the unreacted CHMA:DGEBA mixture at different temperatures.

T/K	β	ε_s	ε_∞	$\tau_o/\mu s$
238.1	0.40	11.25	4.15	3200
240.0	0.40	11.20	4.20	1200
242.0	0.40	11.14	4.22	400
244.2	0.40	11.00	4.25	140
246.1	0.40	10.92	4.27	50
247.9	0.40	10.80	4.3	20

Table 4.3   Parameters used for the stretched exponential fit to the dielectric spectra

of the unreacted HMA:DGEBA mixture at temperatures as indicated

(Johari and Pascheto 1995). (It should be noted that the plots given by

Johari and Pascheto (1995) differ from those given here owing to a

transcription error in the manuscript.)

T/K	β	ε_s	ε_∞	$\tau_0\ \mu/s$
238.4	0.29	9.52	3.70	570
239.6	0.33	9.42	3.97	210
240.2	0.35	9.46	4.10	88
241.2	0.36	9.45	4.15	31
241.9	0.37	9.50	4.25	14
243.3	0.38	9.48	4.28	2.5

The relaxation time, τ_0 , is plotted on a logarithmic scale against 1/T in Figure

4.5. The curves are not linear, rather there is curvature, suggesting that the behaviour

cannot be described by an Arrhenius form $\tau_0 = \tau_\infty exp(E_a/RT)$, where E_a is the

activation energy and τ_∞ is the limiting value of τ_0 as T $\rightarrow$ ∞. The temperature for a

given relaxation time is lowest for the HMA:DGEBA mixture and highest for the

ANIL:DGEBA mixture.
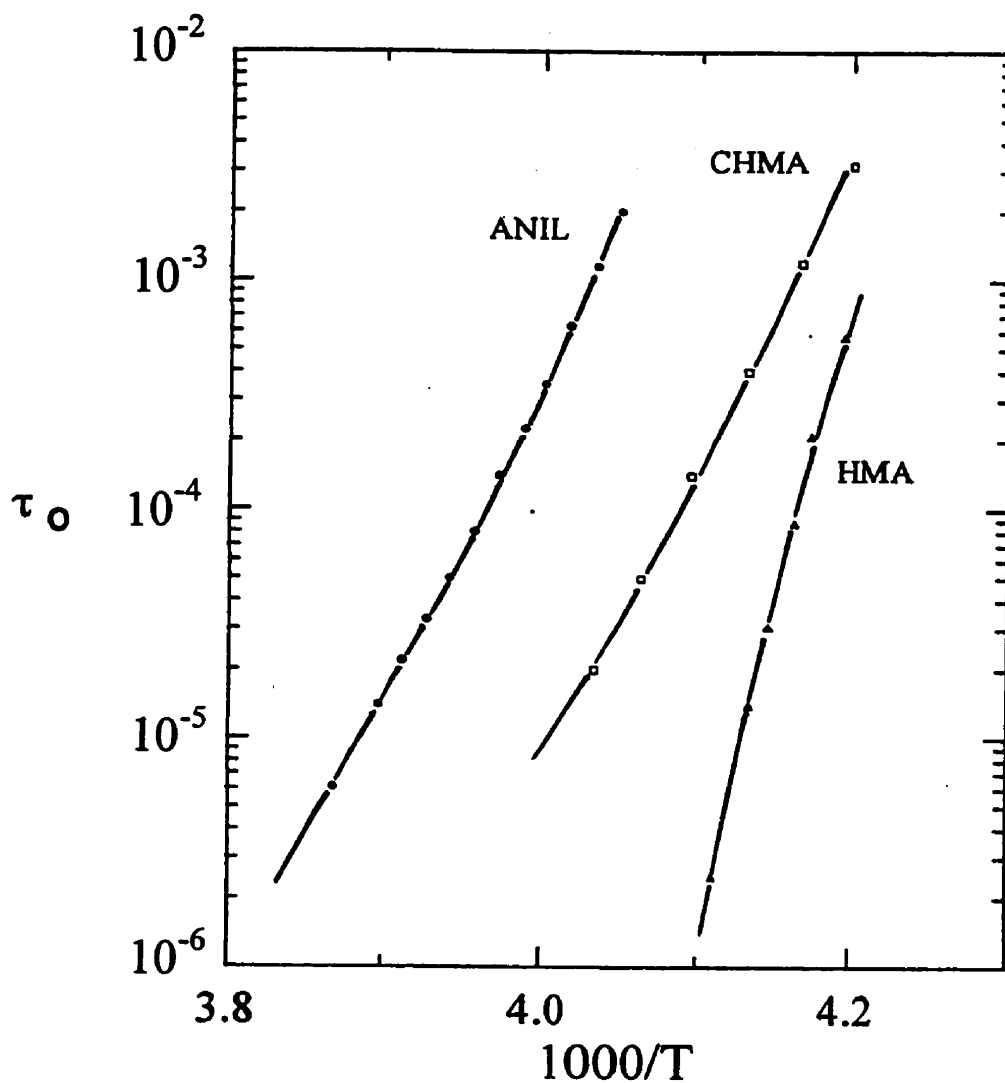
Figure 4.5: The relaxation time, τ_0, determined from the stretched exponential fits to the spectra of the three mixtures, as indicated, in the molecular liquid state, is plotted against the reciprocal of temperature.

4.3   Dielectric and Calorimetric Properties During Polymer Formation

4.3.1   Calculation of the Number of Bonds Formed

In the studies of the unreacted molecular liquids, the mixture's properties at n =

0, where n is the number of chemical bonds formed, was determined. As

polymerization occurs, the chains grow such that for each reaction of the epoxy with

the amine, one new covalent bond is formed. Since equimolar mixtures of the amine

and epoxy were used, the mixture was fully reacted when the total number of chemical

bonds formed is N_A, the Avogadro number. The number of chemical bonds formed at

any time during the reaction, n(t), is given by,

$$n(t) = \frac{N_A \Delta H^o(t)}{\Delta H^o(t \to \infty)} = \frac{N_A \int_0^t \left[\frac{\partial H}{\partial t} \right] dt}{\Delta H^o(t \to \infty)}, \tag{4.9}$$

where $\Delta H^o(t \to \infty)$ is the total heat of reaction, given by,

$$\Delta H^o(t \to \infty) = \int_0^t \left[\frac{\partial H}{\partial t} \right] dt + \frac{1}{q} \int_{T_1}^{T_2} \left[\frac{\partial H}{\partial t} \right] dT, \tag{4.10}$$

where q (= dT/dt) is the heating rate, which was 10K/min. n(t) was calculated from

the DSC curves for the 333.4 and 343.4K reactions of the ANIL:DGEBA mixture, the

313.3K reaction of the CHMA:DGEBA mixture and the 300.1K reaction of the

HMA:DGEBA mixture, as shown in Figures 3.18 and 3.19. The results are shown as

plots of n against time in Figure 4.6, and the values of $\Delta H^o(t \to \infty)$ are listed in Table

4.4. Typically, the curves are sigmoidal with the ultimate value of n following the
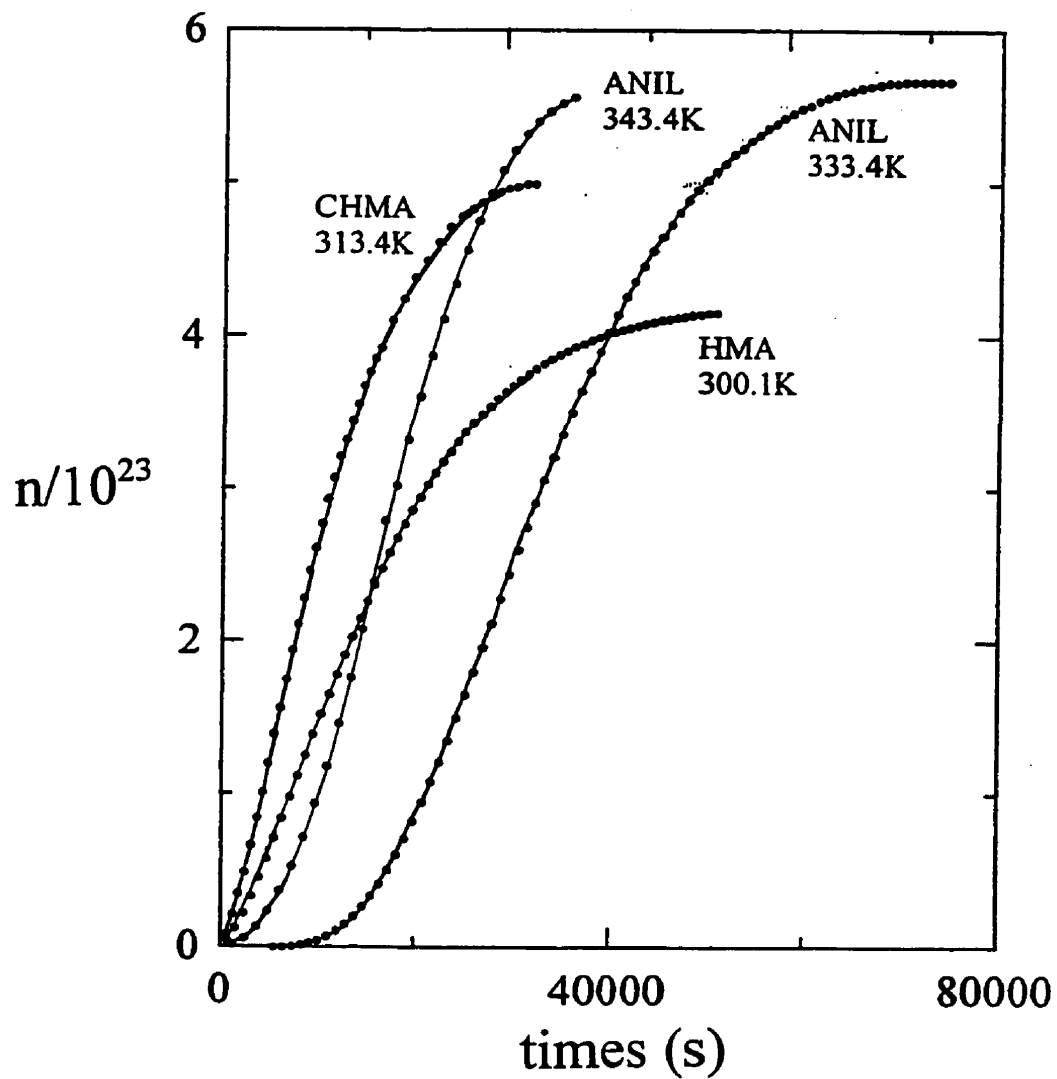
Figure 4.6:   The number of chemical bonds formed, n, during the isothermal polymerization
of the ANIL:DGEBA mixture at 333.4 and 343.4K, and the CHMA:DGEBA
and HMA:DGEBA mixtures at 313.4 and 300.1K respectively, are plotted
against the time of chemical reaction. Curves for the different mixtures are as
indicated on the plot.

isothermal reaction being less than N_A. Since the value of n at any time t during the reaction is known, it is then possible to calculate the change in ε' and ε'', as measured with the time of reaction, in terms of the number of chemical bonds formed. This was done by fitting the data for n against t to a 8th order polynomial, which described the data with a correlation factor $R^2 > 0.999$, and thereafter interpolating the values for the desired time of reaction. Since n is physically more meaningful than the time of reaction, as it dictates the physical state of the mixture, all subsequent analysis will be carried out in terms of n.

Table 4.4   The heat released during the isothermal reaction of the ANIL:DGEBA, CHMA:DGEBA and HMA:DGEBA mixtures at the temperatures as listed.

Mixture	Temp/K	$\Delta H^o(t \rightarrow \infty)$ (kJ/mol amine)
ANIL:DGEBA	333.4	137
	343.4	149.5
CHMA:DGEBA	313.4	109
HMA:DGEBA	300.1	102

The changes in ε' and ε'' with increasing n are shown as plots of ε' and ε'' against n in Figures 4.7, 4.8, 4.9 and 4.10, for the ANIL:DGEBA mixture at 333.4 and 343.4K, the CHMA:DGEBA mixture at 313.4K and the HMA:DGEBA mixture at

Figure 4.7: ε' and ε'' measured at 8 frequencies during the isothermal chemical reaction of the ANIL:DGEBA mixture at 333.4K are plotted against the number of chemical bonds formed, n. The peaks in the curves of ε'' and the step in ε' shift to successively smaller values of n as the frequency is increased.

Figure 4.8: ε' and ε'' measured at 8 frequencies during the isothermal chemical reaction of the ANIL:DGEBA mixture at 343.4K are plotted against the number of chemical bonds formed, n. The peaks in the curves of ε'' and the step in ε' shift to successively smaller values of n as the frequency is increased.

Figure 4.9: ε' and ε'' measured at 8 frequencies during the isothermal chemical reaction of the CHMA:DGEBA mixture at 313.4K are plotted against the number of chemical bonds formed, n.   The peaks in the curves of ε'' and the step in ε' shift to successively smaller values of n as the frequency is increased.

Figure 4.10: ε' and ε'' measured at 8 frequencies during isothermal chemical reaction of the HMA:DGEBA mixture at 300.1K are plotted against the number of chemical bonds formed, n. The peaks in the curves of ε'' and the step in ε' shift to successively smaller values of n as the frequency is increased.

300.1, respectively. These plots correspond to Figures 3.6-3.9, for the isothermal studies at 24 frequencies.

At early stages of conversion, the changes occur gradually over a large change in n. However, at higher values of n, the properties change sharply, with the step in ε' decreasing over a narrow range of n values.

The analysis of this data was done in two ways: first at constant n as a function of frequency, and second at constant frequency as a function of increasing n.

4.3.2   Changes in the Dielectric Properties at Constant n.

In order to determine the changes in the dielectric properties at constant values of conversion, horizontal cuts were made in Figures 4.7, 4.8, 4.9 and 4.10, and the data linearly interpolated towards the value at the cut. The errors involved in this interpolation were estimated to be less than 5% owing to the large number of data collected, and the close separation of the data points. Since the cuts provide values of ε' and ε'' at different frequencies, the spectra could be obtained from these plots. ε' and ε'' against the logarithm of frequency are shown in Figures 4.11, 4.12, 4.13 and 4.14, for the data corresponding to those in Figures 4.7, 4.8, 4.9 and 4.10. All curves show qualitatively the same behaviour. At low values of n, the characteristic step in ε' and the peak in ε'' appear at high frequencies. As n increased, the step and peak move towards lower frequencies, and finally to frequencies below the experimental range. The magnitude of both the peak in ε'' and the step in ε' decreased as n increased. Complex plane plots of ε'' against ε' corresponding to the data in Figures
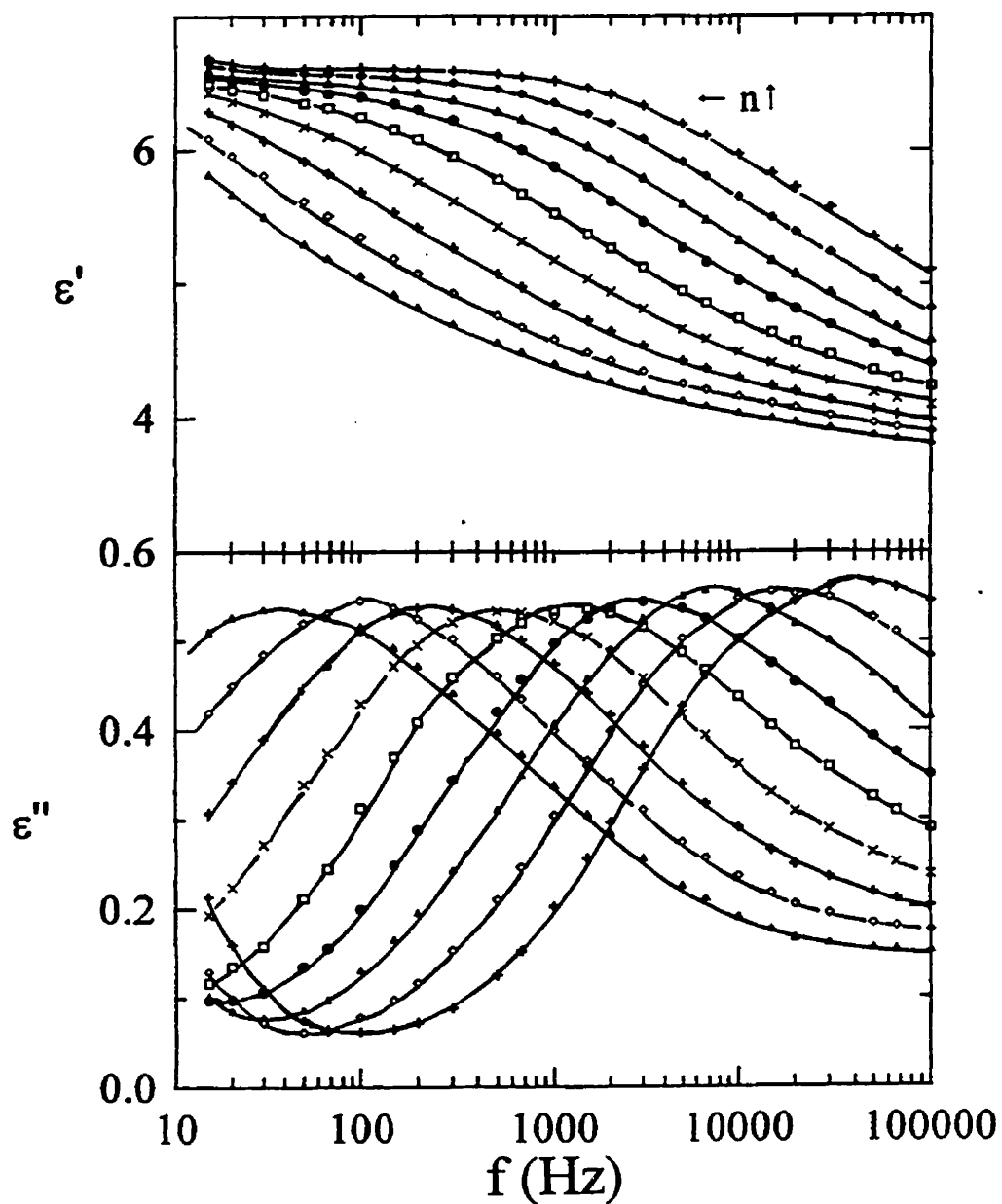
Figure 4.11: ε' and ε'', determined from Fig. 4.7 at fixed values of n is plotted against the frequency for the ANIL:DGEBA mixture isothermally polymerized at 333.4K. Curves from right to left correspond to the following values of $n/10^{23}$: 2.92, 3.16, 3.46, 3.71, 3.89, 4.06 and 4.25.
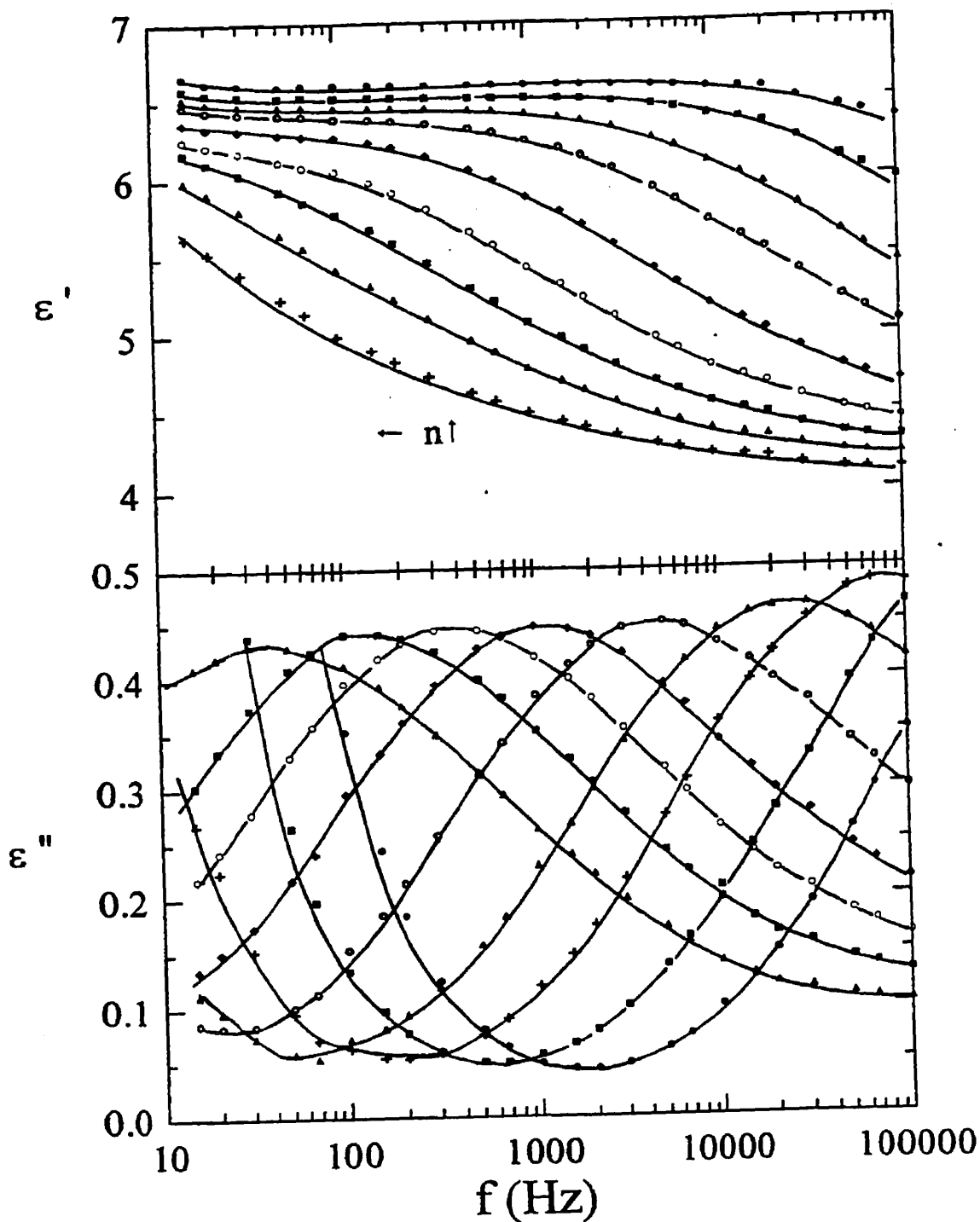
Figure 4.12: ε' and ε'', determined from Fig. 4.8 at fixed values of n is plotted against the frequency for the ANIL:DGEBA mixture isothermally polymerized at 343.4K. Curves from right to left correspond to the following values of $n/10^{23}$: 3.94, 4.19, 4.42, 4.62, 4.82 and 4.99.
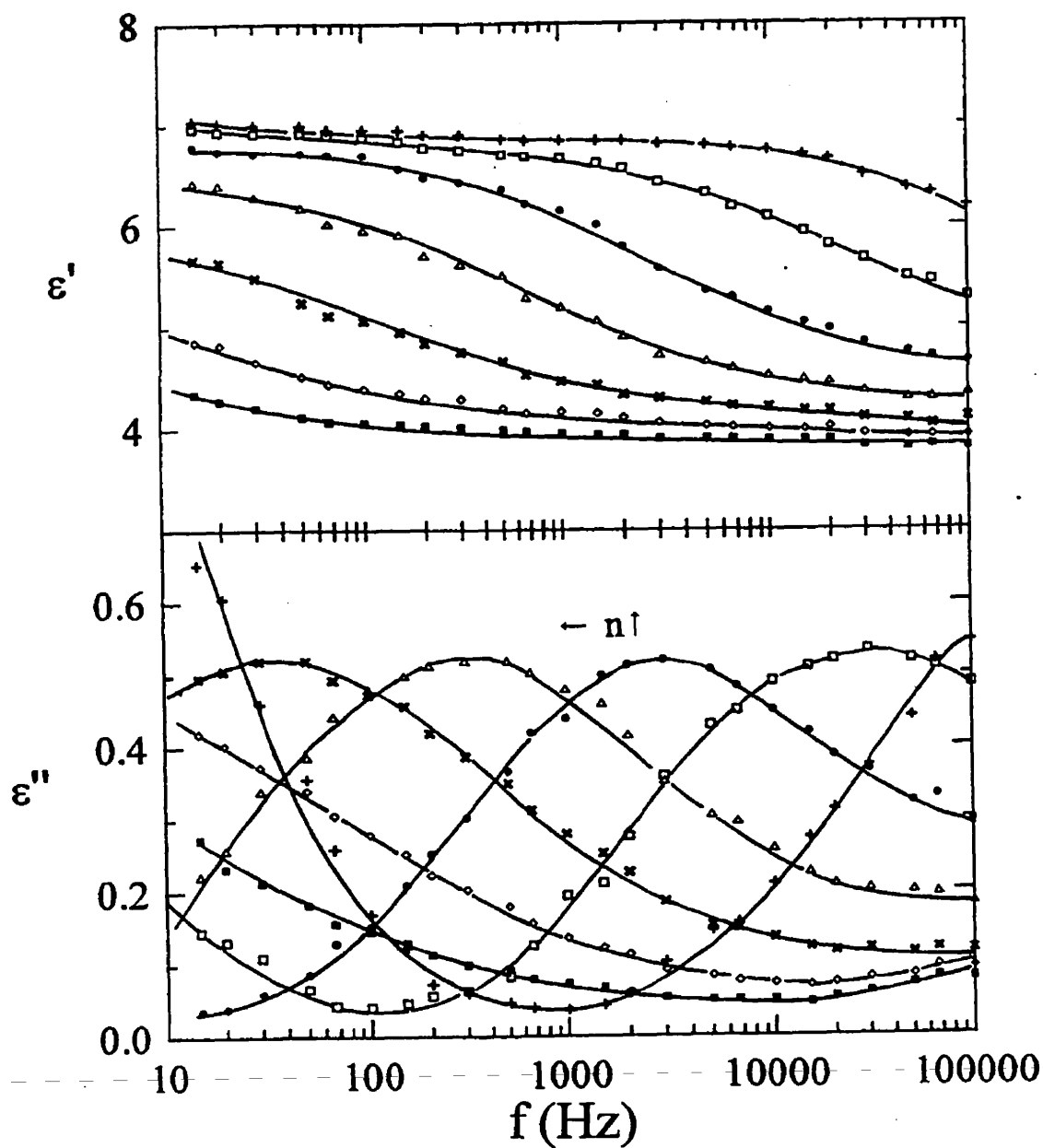
Figure 4.13: ε' and ε'', determined from Fig. 4.9 at fixed values of n is plotted against the frequency for the CHMA:DGEBA mixture isothermally polymerized at 313.4K. Curves from right to left correspond to the following values of $n/10^{23}$: 3.2, 3.6, 3.9, 4.2, 4.4 and 4.6.
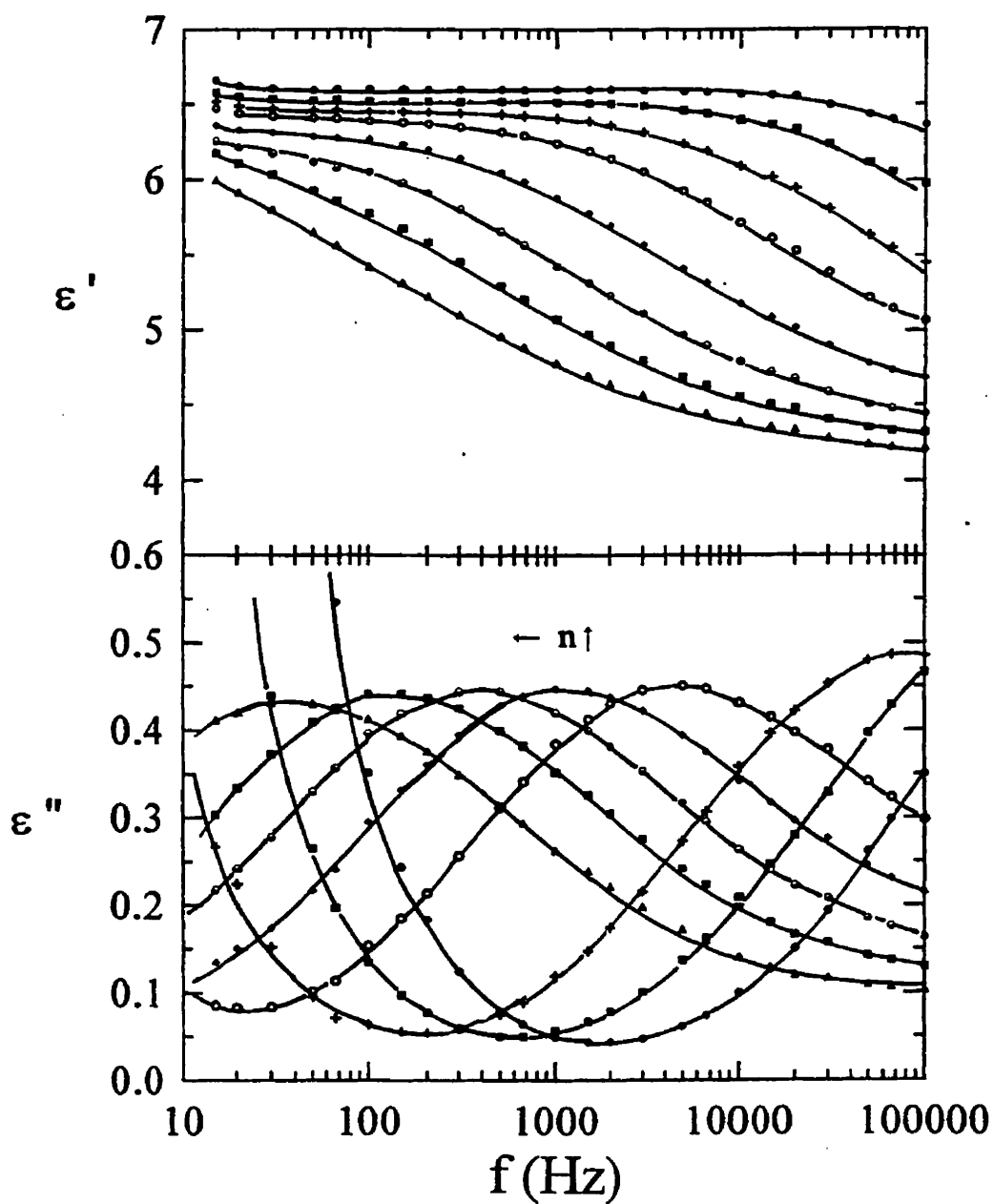
Figure 4.14: ε' and ε'', determined from Fig. 4.10 at fixed values of n is plotted against the frequency for the HMA:DGEBA mixture isothermally polymerized at 300.1K. Curves from right to left correspond to the following values of $n/10^{23}$: 2.89, 3.01, 3.12, 3.22, 3.31, 3.39, 3.47, 3.55, 3.61.

4.11, 4.12, 4.13 and 4.14 are shown in Figures 4.15, 4.16, 4.17 and 4.18, respectively. The shape of these plots is a skewed arc.

These complex plane plots are analyzed in the same manner as the ε' and ε'' spectra of the unreacted mixtures, as outlined in Section 4.1.3. While the analysis is the same, the data represent two different phenomena. In the unreacted mixtures, there was an increase in τ_0 as the temperature was increased and the structure remained the same. In the polymerizing mixtures, there is an increase in τ_0 at a fixed temperature as the number of bonds increased, and hence the structure changes. The resulting fits according to the stretched exponential function are shown as full lines in Figures 4.15, 4.16, 4.17 and 4.18, and the parameters used for the fits, ε_s, ε_∞, β and τ_0 listed in Table 4.5, for the ANIL:DGEBA mixture at 333.4 and 343.4K, and Table 4.6, for the CHMA:DGEBA mixture at 313.4K and the HMA:DGEBA mixture at 300.1K.

From the data in Tables 4.5 and 4.6, ε_s decreases as n increases, while β and ε_∞ remain essentially constant. The decrease in ε_s is about 5-7% for all mixtures. τ_0 increases by several orders of magnitude, from a value near 1 μs at low values of n, to a value of ~3000 μs at higher n values. Since the frequency range was limited, these parameters could not be easily measured for higher values of n, however, it is expected that τ_0 would continue to increase and ε_s decrease.
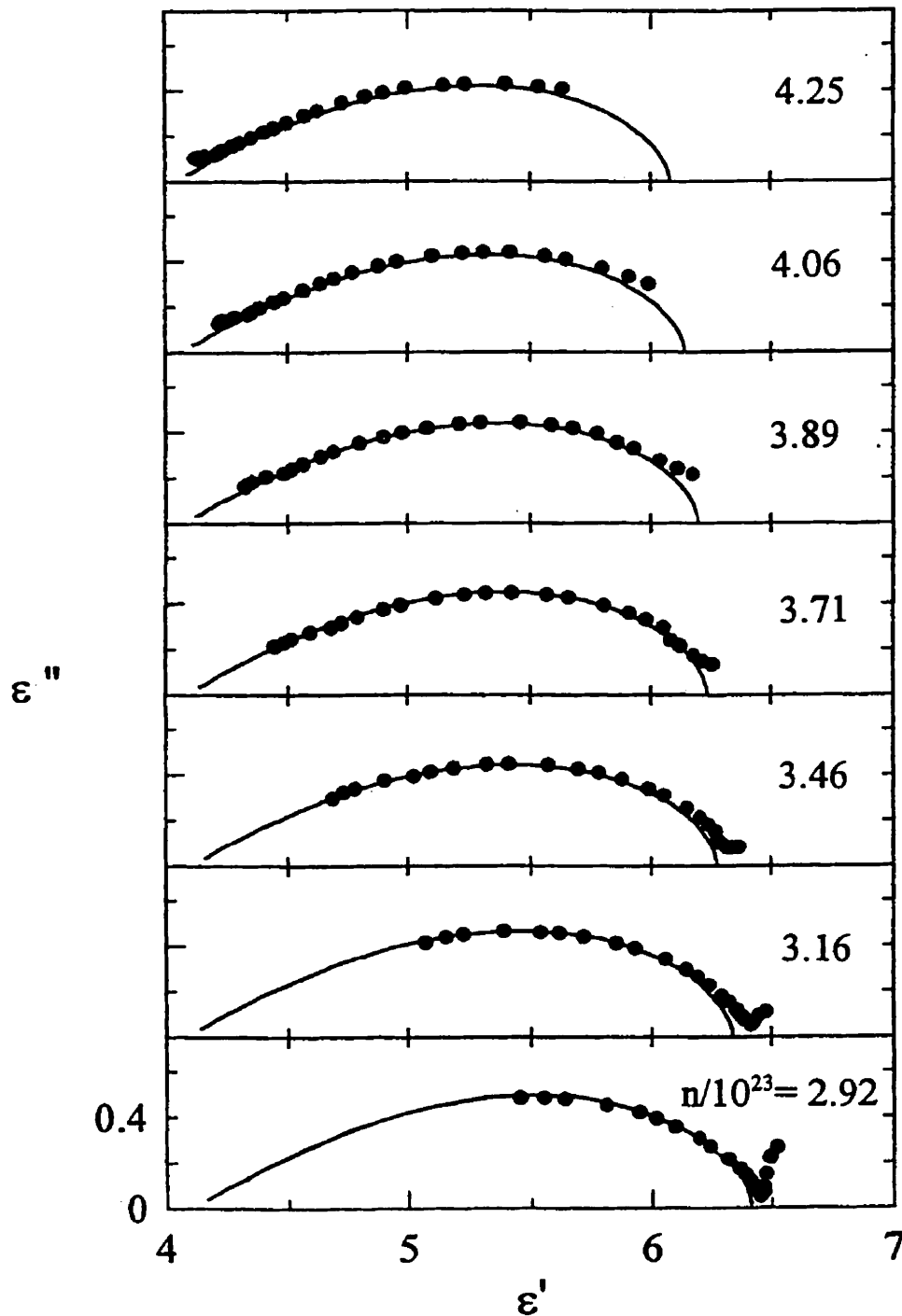
Figure 4.15: Cole-Cole plots of ε'' against ε' corresponding to the data from Fig. 4.11 for the ANIL:DGEBA mixture isothermally polymerized at 333.4K, at the values of n as indicated. The fit to the stretched exponential function according to the parameters listed in Table 4.5, is shown as the solid line.
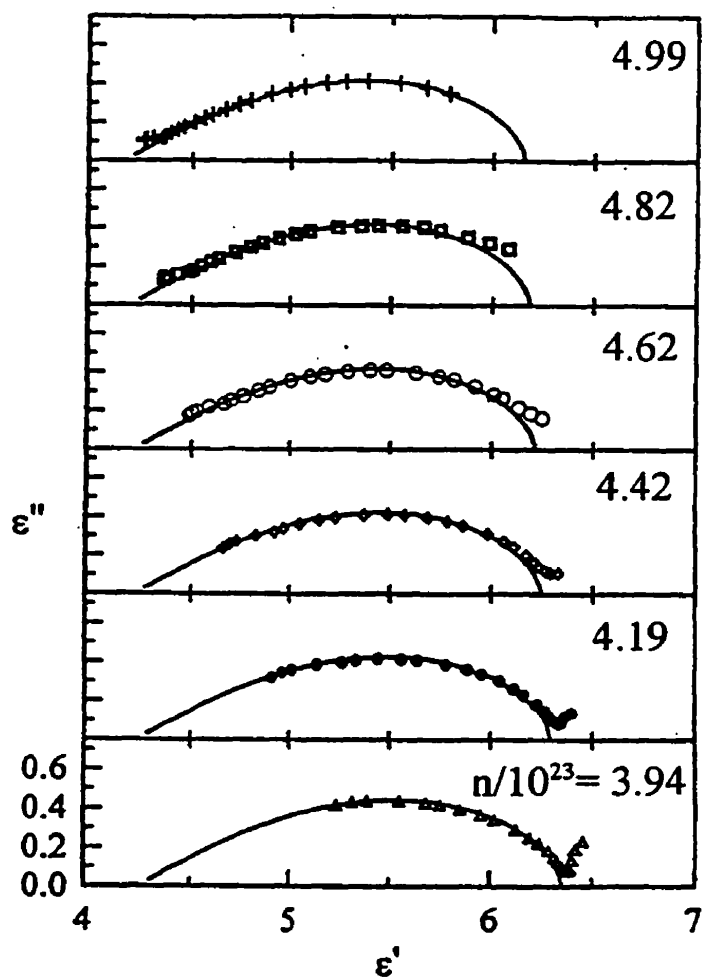
Figure 4.16: Cole-Cole plots of ε'' against ε' corresponding to the data from Fig. 4.12 for the ANIL:DGEBA mixture isothermally polymerized at 343.4K, at the values of n as indicated. The fit to the stretched exponential function according to the parameters listed in Table 4.5, is shown as the solid line.
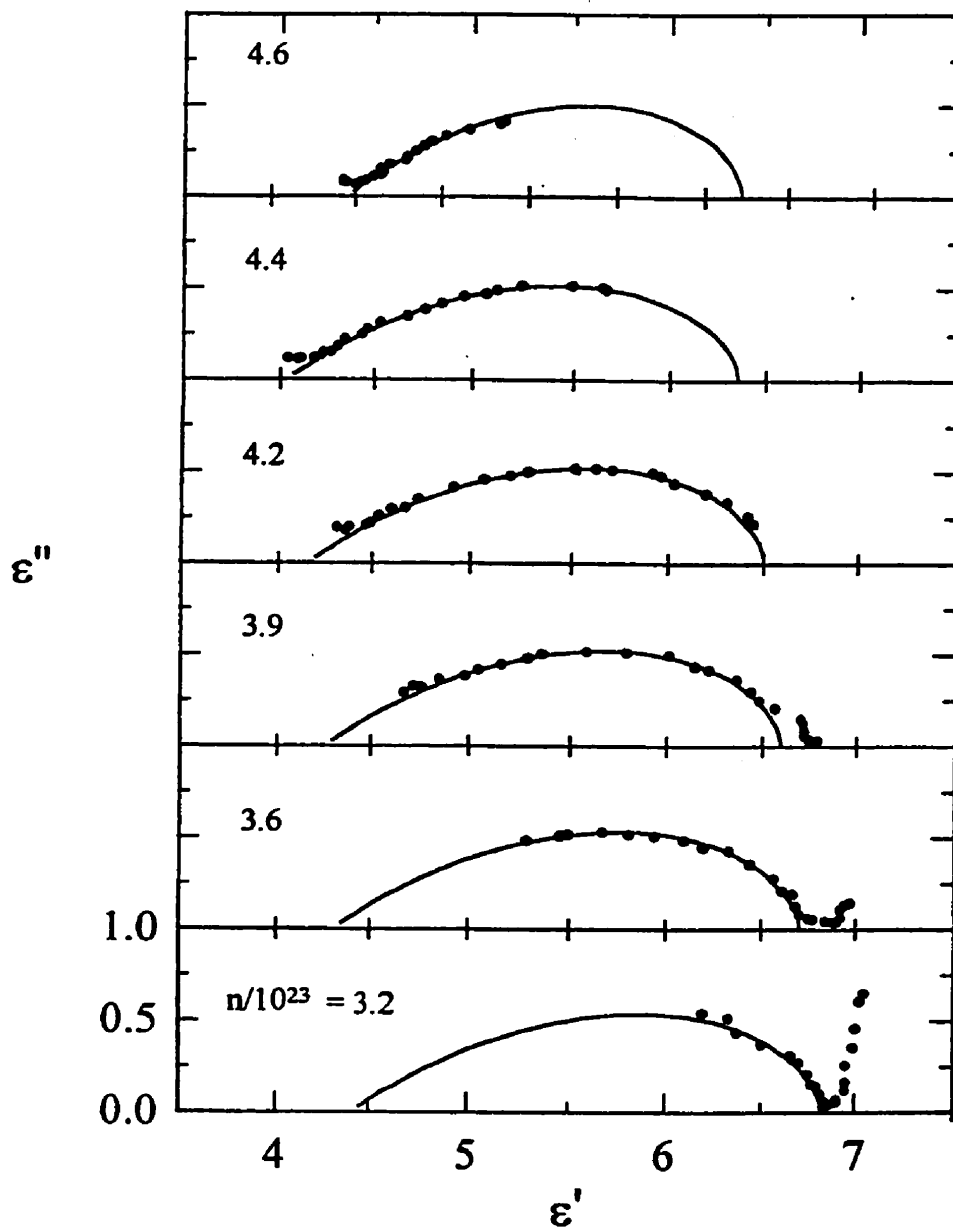
Figure 4.17: Cole-Cole plots of ε'' against ε' corresponding to the data from Fig. 4.13 for the CHMA:DGEBA mixture isothermally polymerized at 313.4K, at the values of n as indicated. The fit to the stretched exponential function according to the parameters listed in Table 4.6, is shown as the solid line.
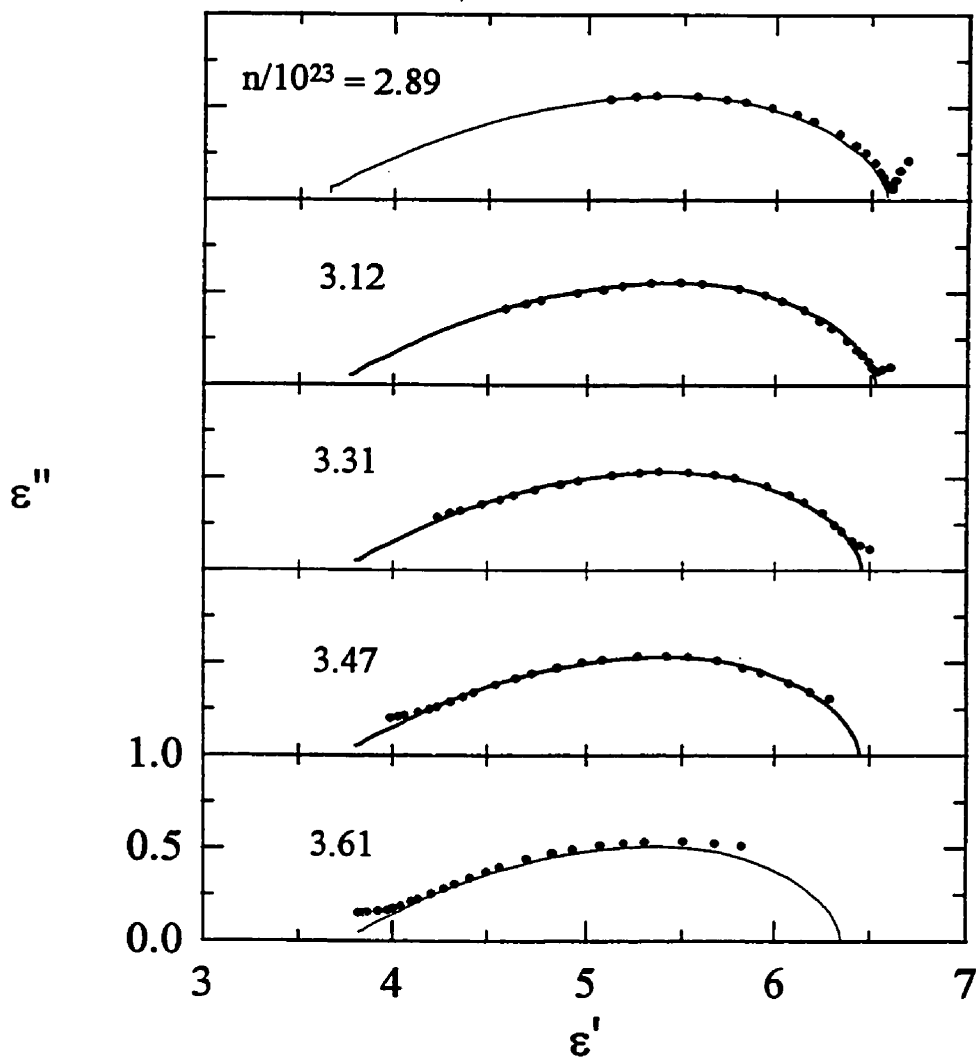
Figure 4.18: Cole-Cole plots of ε'' against ε' corresponding to the data from Fig. 4.14 for the HMA:DGEBA mixture isothermally polymerized at 300.1K, at the values of n as indicated. The fit to the stretched exponential function according to the parameters listed in Table 4.6, is shown as the solid line.

Table 4.5   Parameters for the stretched exponential fit to the frequency spectra of the ANIL:DGEBA mixture at 333.4 and 343.4K for different values of n.

T/K	$n\,/10^{23}$	ε_s	ε_∞	β	$\tau_o\,/\mu s$
333.4	2.92	6.42	4.1	0.37	1.5
	3.16	6.32	4.06	0.37	4.5
	3.46	6.27	4.1	0.37	23
	3.71	6.26	4.08	0.37	100
	3.89	6.2	4.07	0.38	300
	4.06	6.14	4.06	0.38	850
	4.25	6.08	4.04	0.38	2500
343.4	3.94	6.31	4.24	0.37	3
	4.19	6.27	4.23	0.37	12.5
	4.42	6.24	4.22	0.37	50
	4.62	6.21	4.21	0.37	200
	4.82	6.19	4.19	0.37	700
	4.99	6.16	4.16	0.37	2250

Table 4.6   Parameters used for stretched exponential fit to the dielectric spectra of the CHMA:DGEBA mixture at 313.4K and the HMA:DGEBA mixture at 300.1K, at different values of n.

Mixture	$n / 10^{23}$	ε_s	ε_∞	β	$\tau_0/\mu s$
CHMA:DGEBA	3.2	6.82	4.4	0.40	.5
	3.6	6.7	4.3	0.40	4.0
	3.9	6.6	4.25	0.40	40
	4.2	6.5	4.15	0.40	400
	4.4	6.35	4.03	0.40	3500
	4.6	6.22	3.95	0.40	30000
HMA:DGEBA	2.89	6.59	3.55	0.33	2.40
	3.01	6.56	3.72	0.35	6.40
	3.12	6.53	3.69	0.35	14.0
	3.22	6.50	3.71	0.35	33.0
	3.31	6.46	3.73	0.35	79.0
	3.39	6.45	3.73	0.35	190.0
	3.47	6.45	3.73	0.35	490.0
	3.55	6.37	3.75	0.37	1100
	3.61	6.34	3.75	0.36	2900

4.3.3 Changes in the Dielectric Properties with Increasing n at Constant Frequency

A method for analyzing the dielectric relaxation data during the curing of thermoset polymers under isothermal conditions has been developed by Mangion and Johari(1990) and extended to analyze non-isothermal curing of thermosets by Parthun and Johari (1992(c)). This method will be used to determine if it is applicable for the study of linear chain polymer formation.

In section 4.2.1, the stretched exponential form of the relaxation function $\phi=\exp[-(t/\tau_0)^\beta]$ was used to analyze the data obtained at different temperatures as a function of increasing frequency. The normalized complex function $N^*(\omega\tau_0)= N'(\omega\tau_0)-iN''(\omega\tau_0)$, representing the Laplace transform of the relaxation function ϕ, is then a function of both frequency ω and τ_0. For measurements at a single frequency, the observed changes in the measured ε' and ε'' occur because of a changing τ_0. For the analysis, β in the stretched exponential function is assumed to be independent of the degree of chemical conversion, or n. Then ε^* is given as,

$$\varepsilon^*(n,T,\omega) = \varepsilon_\infty(n,T) + [\varepsilon_s(n,T) - \varepsilon_\infty(n,T)]N^*(\omega\tau_o) \qquad (4.12)$$

where the measured properties are dependent on the extent of chemical reaction, given by n, the temperature and the frequency of measurement. For the isothermal polymerization, both T and ω were constant. From the data in Tables 4.5 and 4.6, it was found that ε_s changed by ~7% and ε_∞ by less than 10% during the isothermal polymerization of all three mixtures. For this analysis, this change is considered to be negligible in comparison to the several orders of magnitude increase in τ_0 and thus ε_s

and ε_∞ are assumed to remain constant during polymerization. Eqn. (4.12) then may be written as,

$$\varepsilon^*(n) = \varepsilon_\infty + \Delta\varepsilon\, NHx[\omega\tau_o(n)],\qquad(4.13)$$

where $\Delta\varepsilon=(\varepsilon_s - \varepsilon_\infty)$, and τ_o is a function of increasing n.

The stretched exponential form of the relaxation function is modified (Johari and Mangion, 1990; Parthun and Johari, 1992(a),(b)) as,

$$\phi(t) = \exp\left[-(t/\tau_o)^\gamma\right],\qquad(4.14)$$

where γ is a new distribution parameter applicable only for the behaviour of a mixture undergoing changes due to chemical reaction. It is distinguished fundamentally from the parameter β in the stretched exponential function in that the latter is only applicable for the dielectric characterization of chemically and physically stable materials.

In order to analyze the experimental data in terms of Eqn.(4.13), it is necessary first to evaluate both ε_s and ε_∞. The complex plane plots of ε'' against ε' measured at constant frequencies during polymerization are shown in Figures 4.19, 4.20, 4.21 and 4.22 for the ANIL:DGEBA mixture at 333.4K and 343.3K, the CHMA:DGEBA mixtures at 313.4K and the HMA:DGEBA mixture at 300.1K respectively. These plots are distinguished from those in Figures 4.15-4.18 in that each data for the latter corresponds to a unique value of frequency at constant n. ε_s and ε_∞ were determined by extrapolating the complex plane plots of the experimental ε'' against ε' to the horizontal axis and obtaining the low and high n value intercepts. The curing
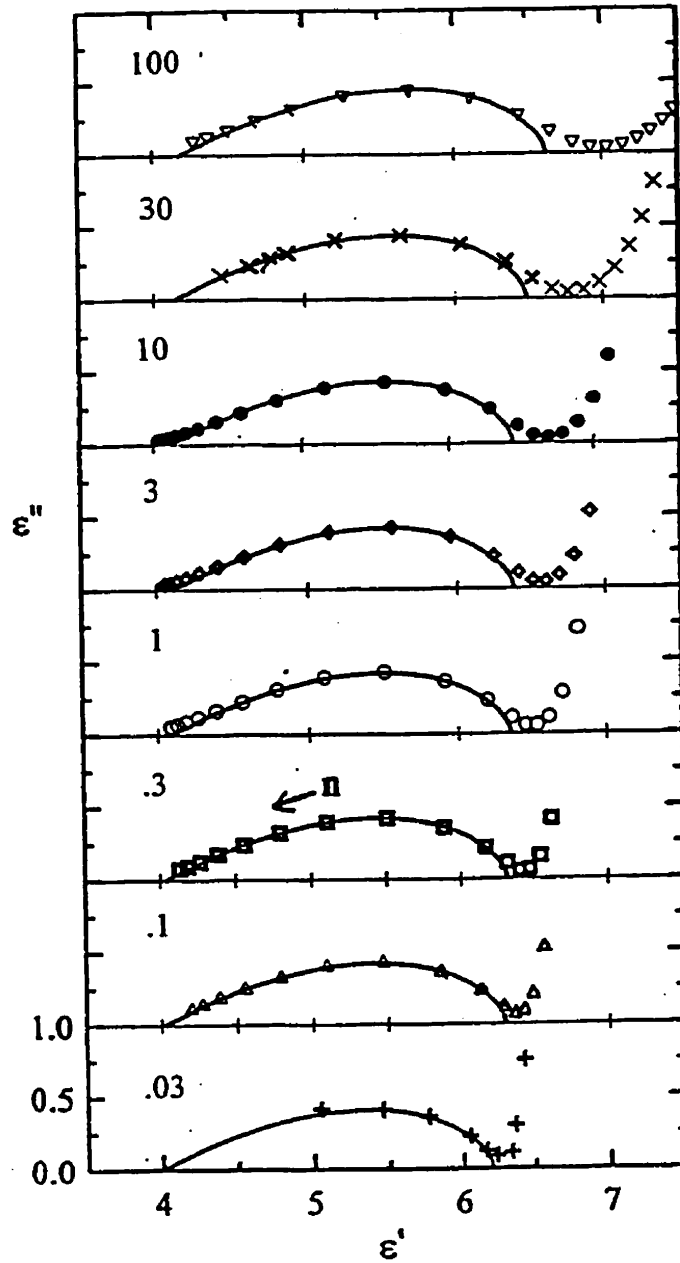
Figure 4.19: Cole-Cole plots of ε'' against ε' corresponding to the data from Fig. 3.6 for the ANIL:DGEBA mixture isothermally polymerized at 333.4K, at frequencies as indicated. The fit to the stretched exponential function according to the parameters listed in Table 4.7, is shown as the solid line.
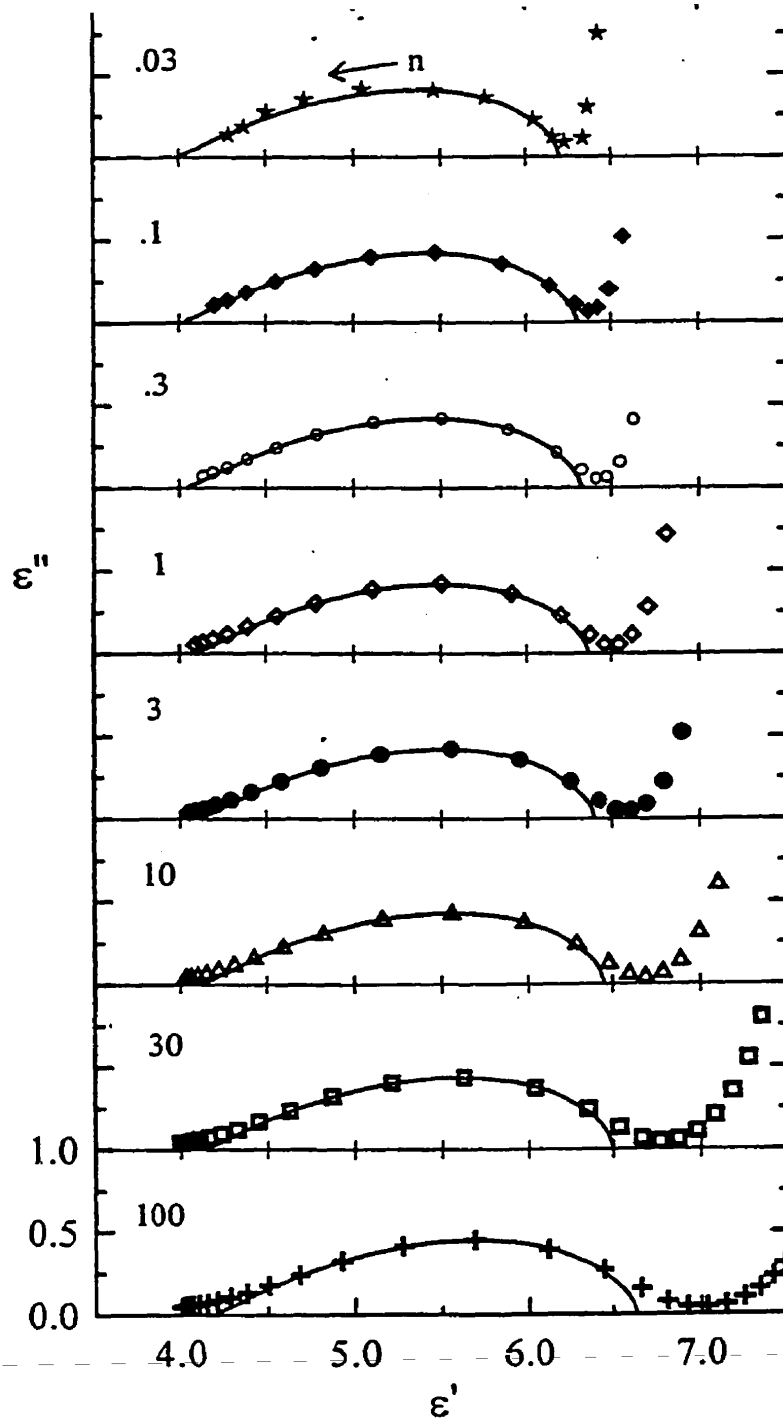
Figure 4.20: Cole-Cole plots of ε'' against ε' corresponding to the data from Fig. 3.7 for the ANIL:DGEBA mixture isothermally polymerized at 343.4K, at frequencies as indicated. The fit to the stretched exponential function according to the parameters listed in Table 4.7, is shown as the solid line.
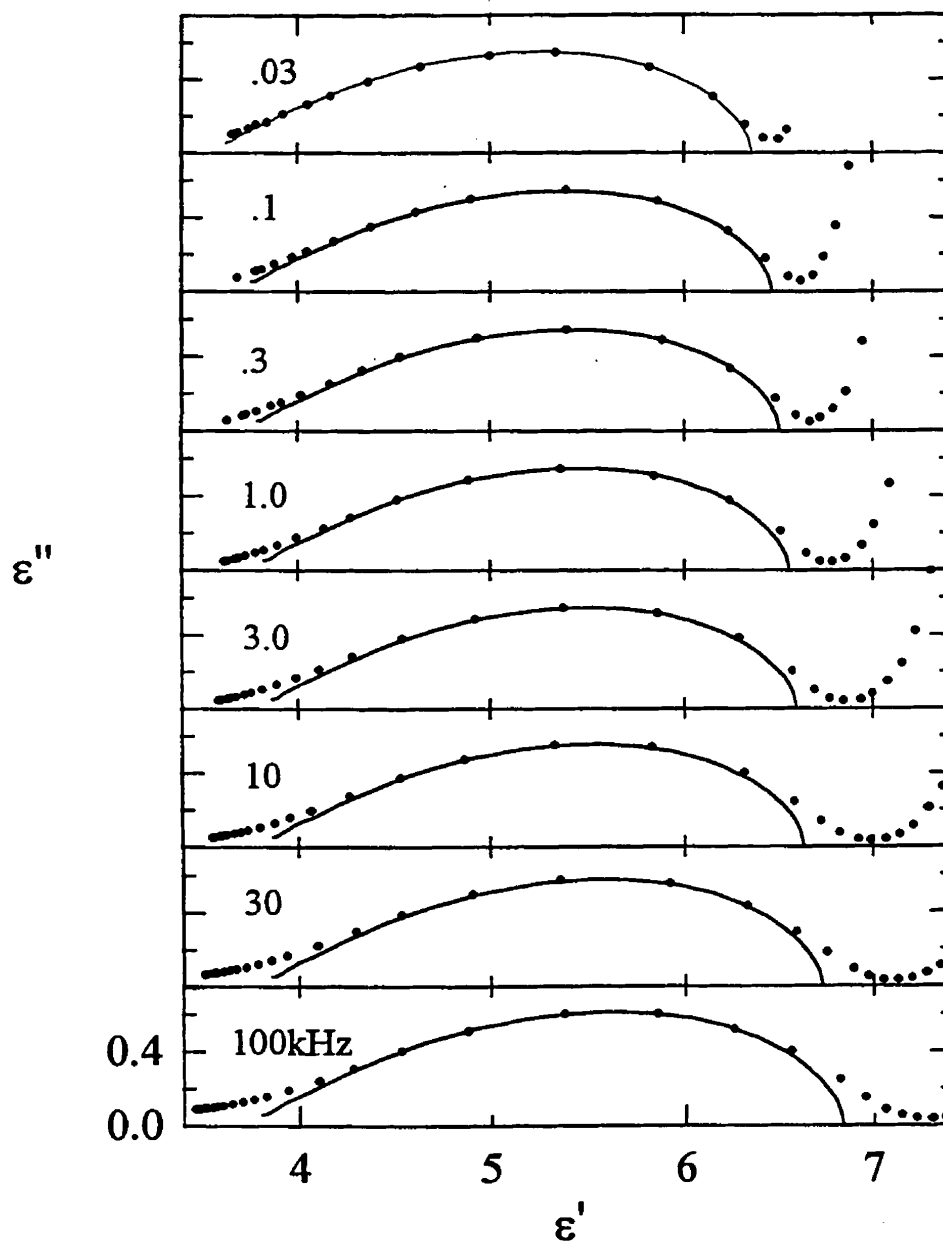
Figure 4.21: Cole-Cole plots of ε'' against ε' corresponding to the data from Fig. 3.8 for the CHMA:DGEBA mixture isothermally polymerized at 313.4K, at frequencies as indicated. The fit to the stretched exponential function according to the parameters listed in Table 4.8, is shown as the solid line.
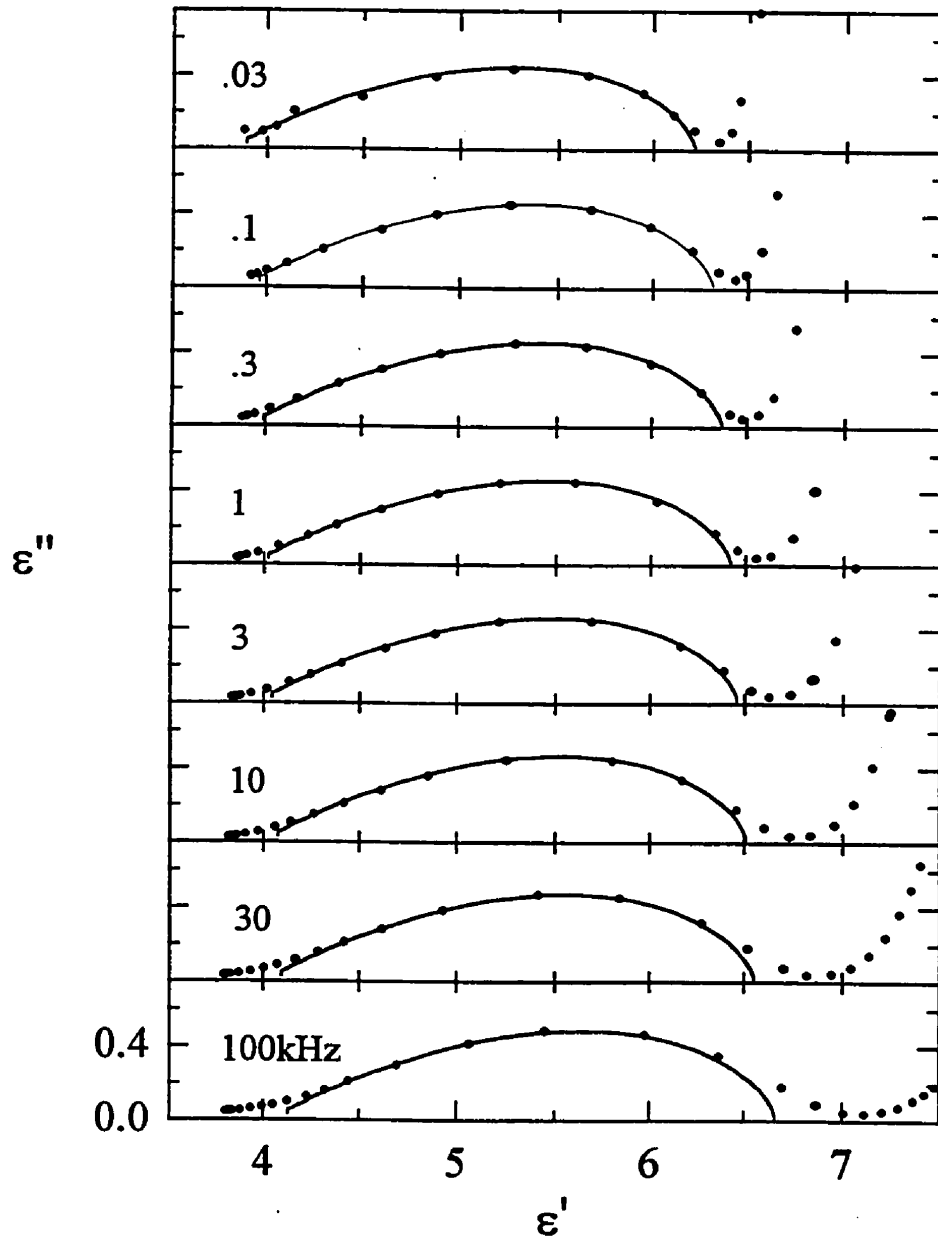
Figure 4.22: Cole-Cole plots of ε'' against ε' corresponding to the data from Fig. 3.9 for the HMA:DGEBA mixture isothermally polymerized at 300.1K, at frequencies as indicated. The fit to the stretched exponential function according to the parameters listed in Table 4.8, is shown as the solid line.

parameter, γ, was then evaluated from the values of N'_m and N''_m, which are the values of the real and imaginary components of the normalized complex function N^* at the maximum value of N'', according to the equations (Moynihan et al, 1973),

$$N'_m = \frac{\varepsilon'_m - \varepsilon_\infty}{\Delta \varepsilon} \quad ; \quad N''_m = \frac{\varepsilon''_m}{\Delta \varepsilon}, \tag{4.15}$$

where ε''_m is the value of the maximum in the plots against increasing n and ε'_m is the value of the permittivity at n corresponding to ε''_m. The curves calculating from this fitting are shown as the full lines in Figures 4.19-4.22 for measurements made at 8 different frequencies for the ANIL:DGEBA, CHMA:DGEBA and HMA:DGEBA mixtures respectively. In all cases the fits are adequate, with deviation occurring in the high frequency data at high values of n, when the dielectric loss, ε'', does not approach a near zero value. The values of the parameters ε_s, ε_∞ and γ used for the fits for eight of the frequencies are listed in Tables 4.7 and 4.8, for the DGEBA:ANIL polymer at the two isothermal temperatures, and Table 4.9 and 4.10 for the DGEBA:CHMA and DGEBA:HMA polymers respectively.

A method for obtaining the value of the relaxation time, τ_0, at any time, or equivalently n, has been outlined by Johari and Mangion (1990) and tested for isothermal (Parthun and Johari, 1992(a) (b); Deng and Martin, 1994) and non-isothermal (Parthun and Johari, 1992(c)) polymerization. The complex plane plots of ε'' against ε' were shown above to be well described by the stretched exponential relaxation function. Since each fitted data corresponds to a unique value of $\omega\tau_0$, at fixed frequencies, each point describes a unique value of τ_0. The relaxation time can

then be evaluated by matching the values of ε'' and ε' obtained from the fit to those obtained experimentally at any n. If the calculated data points did not match the measured data points, but did lie on the curve, they were linearly interpolated. The relaxation time thus calculated are shown as plots of log τ_0 against n in Figure 4.23 for the ANIL:DGEBA mixture at 333.4 and 343.4K and in Figure 4.24 for the CHMA:DGEBA and HMA:DGEBA mixtures at 313.4K and 300.1K, respectively, for measurements at 0.03, 1 and 100 kHz. Other frequencies have been omitted for clarity. Also included are the τ_0 values obtained form the analysis of the spectra at fixed values of n. For all three mixtures the plots are qualitatively similar. The relaxation time increases from a low value at small n towards a limiting value at high values of n with the range of data extending over eight decades from $\sim 10^{-8}$ to ~ 1 s. The data obtained from all frequencies superpose, as do the data obtained from the analysis of the spectra at fixed values of n. This agreement of values from the two procedures confirms that the analysis of the single frequency data is correct, and is in agreement with the results obtained by others employing the same method for the analysis of thermoset formation (Tombari and Johari, 1992; Deng and Martin, 1994). The approximation that ε_s, ε_∞ and γ remain constant with increasing n does not significantly affect the calculated values (Parthun et al, 1995(d)). This has also been shown in recent work by Wasylyshyn and Johari (1996), where simulated data was calculated assuming changing ε_s and ε_∞ values and constant β over 4 decades of frequency. In this analysis, the generated data were analyzed for one frequency according to the method outlined at the beginning of this section, and it was found that
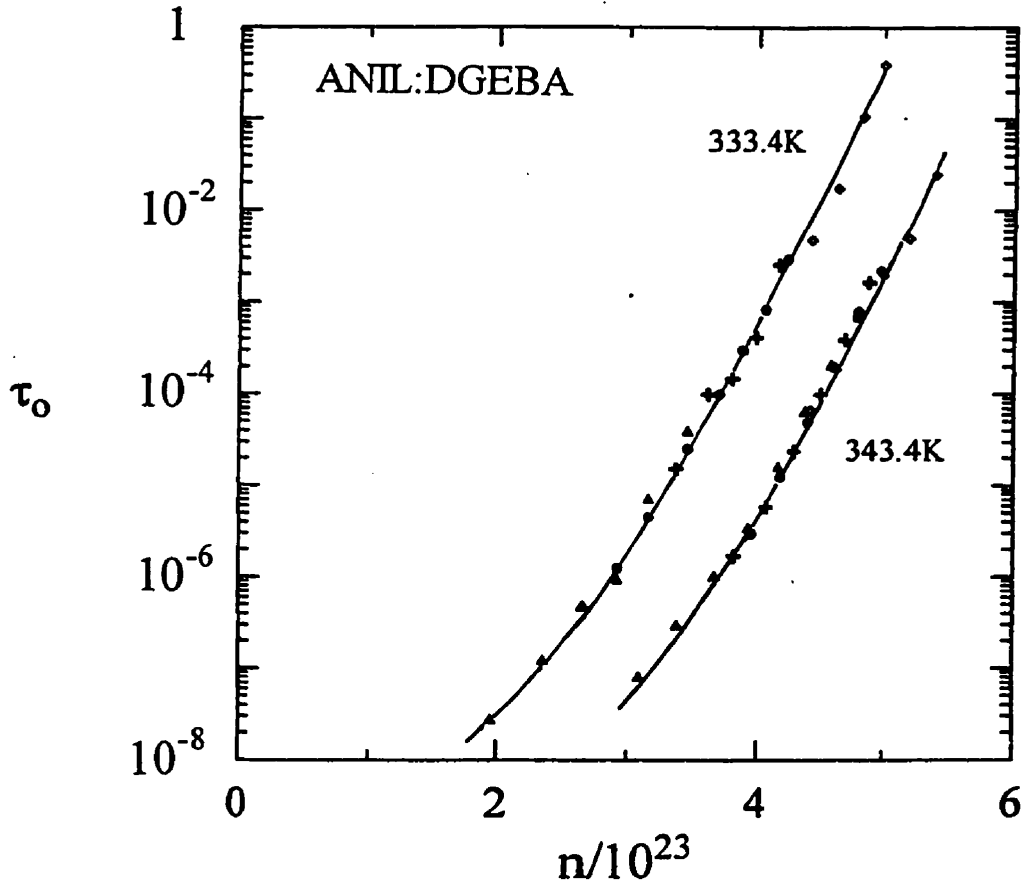
Figure 4.23: The relaxation time, τ_o, calculated from the stretched exponential formalism for the ANIL:DGEBA system during isothermal polymerization at the temperatures indicated is plotted against the number of bonds formed. The values of τ_o superpose for all frequencies, as well as for data from the spectra at constant n.
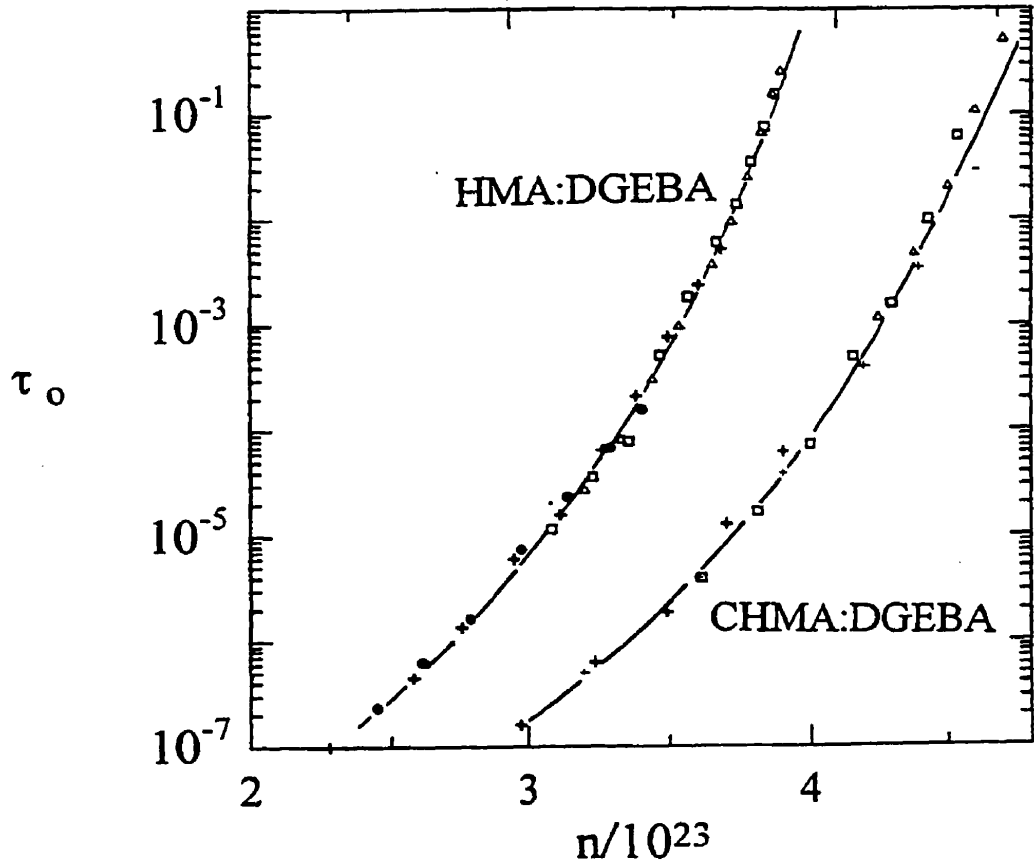
Figure 4.24: The relaxation time, τ_0, calculated from the stretched exponential formalism for the CHMA:DGEBA and HMA:DGEBA mixtures during isothermal polymerization 313.4 and 300.1K respectively is plotted against the number of bonds formed. The values of τ_0 superpose for all frequencies, as well as for data obtained from the spectra at constant n.

the parameter γ was in close agreement with the parameter β and further that the assumption of constant ε_s and ε_∞ did not lead to significant errors in the value of relaxation time determined.

Table 4.7   Parameters used for the fits to the constant frequency data for the

ANIL:DGEBA mixture during polymerization at 333.4 and 343.4K

ANIL:DGEBA	333.4K			343.4K		
f/kHz	ε_s	ε_∞	γ	ε_s	ε_∞	γ
0.03	6.22	3.80	0.33	6.20	4.00	0.33
0.10	6.32	3.87	0.33	6.30	4.03	0.33
0.30	6.37	3.90	0.33	6.32	4.05	0.33
1.0	6.42	3.93	0.33	6.36	4.10	0.33
3.0	6.46	3.95	0.33	6.39	4.12	0.33
10.0	6.51	3.98	0.33	6.45	4.13	0.33
30.0	6.55	4.00	0.33	6.50	4.15	0.33
100.0	6.66	4.03	0.33	6.63	4.19	0.33

Table 4.8   Parameters used for the fits to the constant frequency data for the

CHMA:DGEBA and HMA:DGEBA mixtures (Johari and Pascheto

1995) during polymerization at 313.4 and 300.1K, respectively.

	CHMA:DGEBA 313.4K			HMA:DGEBA 300.1K		
f/kHz	ε_s	ε_∞	γ	ε_s	ε_∞	γ
0.03	6.60	3.8	0.34	6.35	3.54	0.33
0.10	6.68	3.83	0.34	6.46	3.68	0.33
0.30	6.71	3.84	0.34	6.32	4.05	0.33
1.0	6.74	3.87	0.34	6.36	4.10	0.33
3.0	6.79	3.94	0.34	6.39	4.12	0.33
10.0	6.81	3.97	0.34	6.45	4.13	0.33
30.0	6.84	4.00	0.34	6.50	4.15	0.33
100.0	6.98	4.07	0.34	6.63	4.9	0.33

4.3.4   Changes in the dc Conductivity During Macromolecular Growth.

Prior to the appearance of the peak in the plots of ε'' against n in Figures 4.7 -
4.10, the dielectric features are dominated by dc conductivity (Sheppard and Senturia,
1986; Mangion and Johari, 1990, Parthun and Johari, 1992(a); Johari, 1994). There
are several sources for the dc conductivity of the liquid mixtures whose contributions
change during the macromolecular growth. The mixtures in this study contained
impurity ions, namely Na^+ and Cl^- formed during the commercial preparation of the

DGEBA and H⁺ and OH⁻ ions from the moisture present and the partial dissociation of the amine. It is also inferred that Zwitter ions are formed in the reaction mixture (Alig and Johari 1992). The amine, OH⁻ and H⁺ ions and a diamine by itself, can also form a partially connected network structure through H-bonds in the mixture, allowing then a charge transfer via the proton migration. As the macromolecule grows, the viscosity increases and the mobility, μ, of the ions decrease according to the Stokes-Einstein relation $\mu \propto \eta^{-1}$. Thus σ_0, the dc conductivity, decreases since $\sigma_0 \propto c\mu$, where c, the concentration of the ions, remains constant. There are also other effects that are related to the removal of ions themselves. First, there is an increase in the association constant, K_A, when ε_s decreases with an increase in n according to,

$$K_A = \frac{4\pi N_A^3}{3000} \exp\left[\frac{Z_1 Z_2 e^2}{a \varepsilon_s k_B T}\right], \tag{4.16}$$

where Z_1 and Z_2 are the ionic charges, N_A is the Avogadro number, e the electronic charge, a the ion-size parameter, and $k_B T$ the thermal energy, all of which remain constant here. Because ε_s appears in the exponential term, it has a large effect in reducing the population of mobile ions and increasing those of ion pairs. Second, the number of Zwitter ions also rapidly decreases as the molecules combine, approaching a near zero value as $n \to N_A$ (Alig and Johari 1993). Third, as the amine chemically reacts, its protons are removed to form OH groups (see Chapter 1), which would disrupt the motion of protons in an existing H-bond network. This disruption also reduces the contribution to σ_0, but this decrease is expected to occur in a manner different from that given by the classical equations, because, within the assumption of H-bond connectivity, one broken H-bond between two amine molecules leads to one covalent bond formed between the N and C atoms.

The growth of the macromolecule here does not produce an infinitely connected network of covalent bonds, so that in the strict sense gelation should not occur. The solid product after the reaction for all mixtures became a viscous liquid at high temperatures and subsequently vitrified on cooling, in the same manner as linear chain polymers (McCrum et al. 1967). Entanglements could have occurred, but clearly the product was not crosslinked.

Neither are the aniline molecules expected to form an H-bonded network structure extended enough to provide a long-range proton conduction, unless a substantial amount of H_2O was present. Thus, σ_0 was expected to decrease with increasing n, but not to show an approach towards a singularity similar to that observed in diamine:epoxy thermoset formation (Mangion and Johari, 1990(a); Parthun and Johari, 1992(a), 1992(b)). To examine this, the change of σ_0 with time was analyzed in terms of the two equations,

$$\sigma_o(t_r) - \sigma_o(t \to 0)\left[\frac{t_{crit} - t_r}{t_{crit}}\right]^X, \qquad (4.16)$$

$$\sigma_o(t_r) - A_\sigma exp\left[\frac{B_\sigma}{t_r - t_o}\right], \qquad (4.17)$$

where t_r is the time of reaction, σ_0 ($t_r \to 0$) is the dc conductivity when n $\to$ 0, t_{crit} is the time to approach a critical point according to percolation theory (Djarbourov, 1986), x is the critical exponent, and A_σ, B_σ and t_0 are empirical constants for the equation describing the approach to a singularity. The values of all parameters have been found to vary with temperature (Parthun and Johari, 1992(a); 1992(b)). The data of σ from Figure 3.13 for the ANIL:DGEBA mixture at 333.4 and 343.4K are replotted against t_r in Figure 4.25 on an enlarged scale. The points for all frequencies
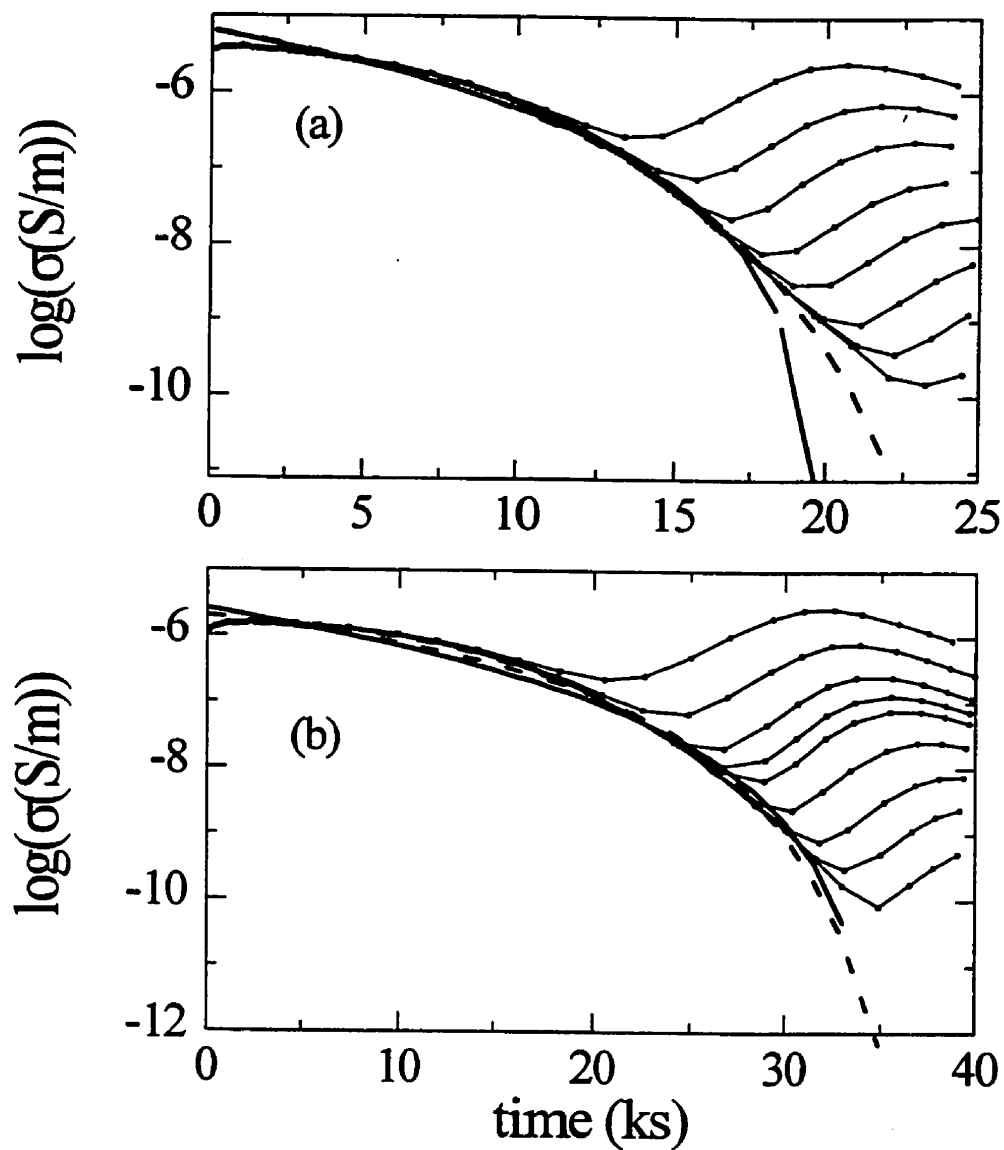
Figure 4.25:   Plots of σ against time for the ANIL:DGEBA mixture during isothermal
polymerization at 333.4 and 343.4K. Fits are drawn for the power law
expression (Eqn. 4.16) as full lines and for the singularity equation (Eqn. 4.17)
as dashed lines. Parameters used for the fits are listed in the text.

lie on the same curve at short times, and it is these data that are used for fitting Eqns. (4.16) and (4.17). The best-fit curves according to Eqn. (4.16) and calculated from the parameters $\sigma_0(t_r \rightarrow 0)$ = 6.36 and 2.55 μS/m, t_{crit} = 20 and 35 ks, and x = 3.373 and 3.799 for the 343.4 and 333.4K data respectively, are shown as full lines in Figure 4.25(a). The best-fit curves according to Eqn. (4.17) and calculated from the parameters A_σ = 772 and 42.5 μS/m , B_σ = -143.4 and -128.0 ks and t_0= 30 and 42 ks for the 343.4 and 333.4K data, respectively, are shown as dashed lines in Figure 4.25(b). Neither fit is adequate, with substantial deviations occurring at the short and intermediate time range. The fits to the CHMA:DGEBA and HMA:DGEBA data, not shown here, were equally poor. It is concluded then that the observed decrease in conductivity is not due to the approach to a singularity or critical point, as is seen in the formation of network structures, but rather is a reflection of the decrease in the ionic mobility as the viscosity increases during macromolecular growth.

4.3.5 α-Relaxation in the Fully Reacted State

The dielectric spectra for the fully reacted ANIL:DGEBA and HMA:DGEBA polymers, shown in Figures 3.15-3.17 were analyzed in the same manner as the spectra for the unreacted mixtures, as discussed in Section 4.3.1. For the CHMA:DGEBA mixture it was necessary to first subtract the effect of dc conductivity, as outlined in section 4.1. The fits to the resolved dipolar relaxation data are shown as complex plane plots of ε'' against ε' in Figures 4.26, 4.27 and 4.28 for the ANIL:DGEBA, CHMA:DGEBA and HMA:DGEBA mixtures respectively. In all cases the fit is adequate, with deviations appearing at high frequencies. The parameters used for the
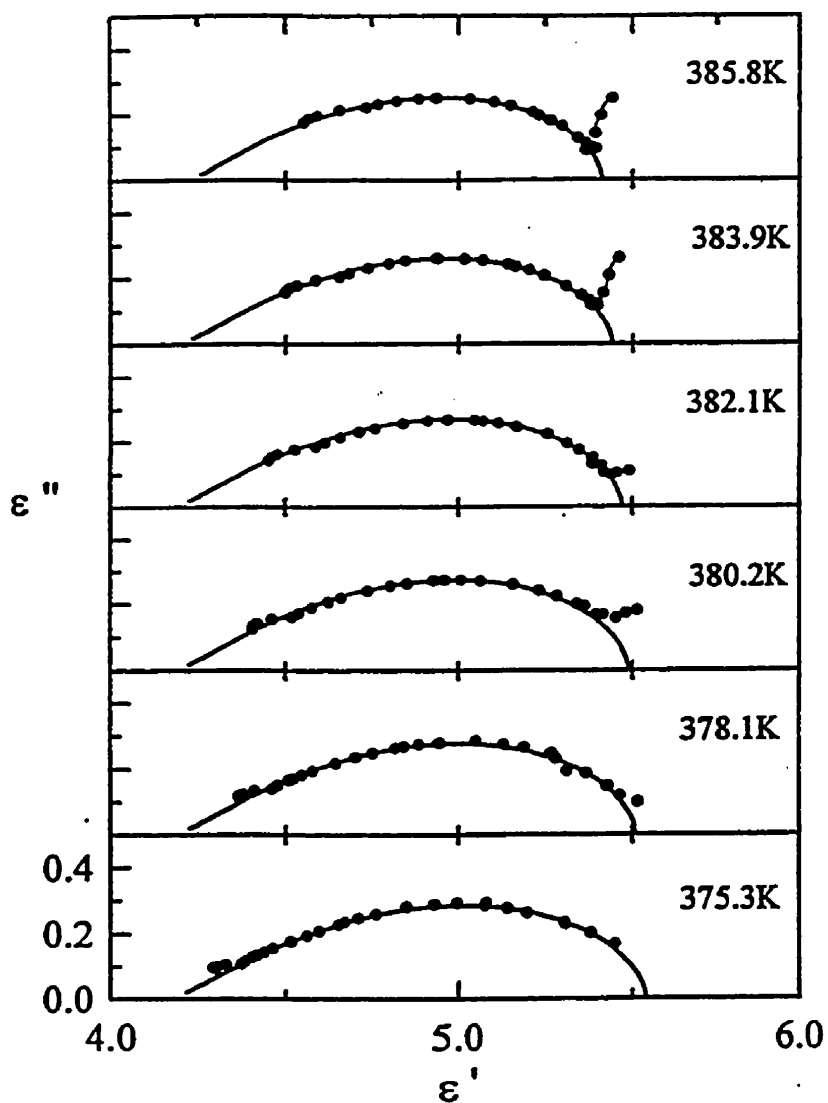
Figure 4.26: Complex plane plots of ε'' against ε' for the ANIL:DGEBA mixture in the fully polymerized state for isothermal measurements made at 375.3, 378.1, 380.2, 382.1, 383.9 and 385.8K, as indicated. The best-fit curves according to the stretched exponential relaxation function, shown as full lines, were calculated from the parameters in Table 4.9
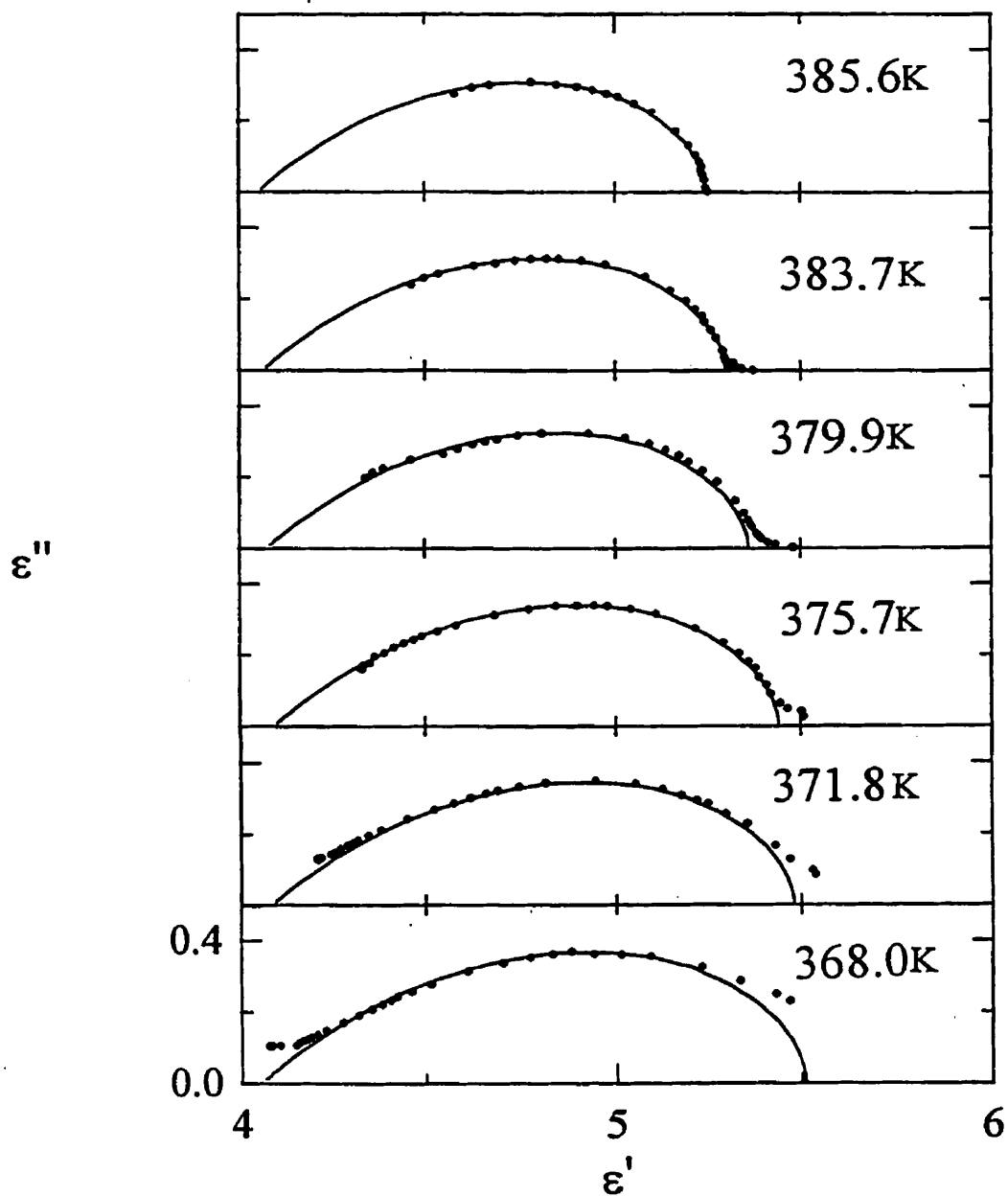
Figure 4.27: Complex plane plots of ε'' against ε' for the CHMA:DGEBA mixture in the fully polymerized state for isothermal measurements made at 366.8, 368.0, 370.0, 371.8, 373.9, 375.7, 378.1, 379.9, 381.9, 383.7, 385.6, 387.6 and 390.4K, as indicated. The best-fit curves according to the stretched exponential relaxation function, shown as full lines, were calculated from the parameters in Table 4.10
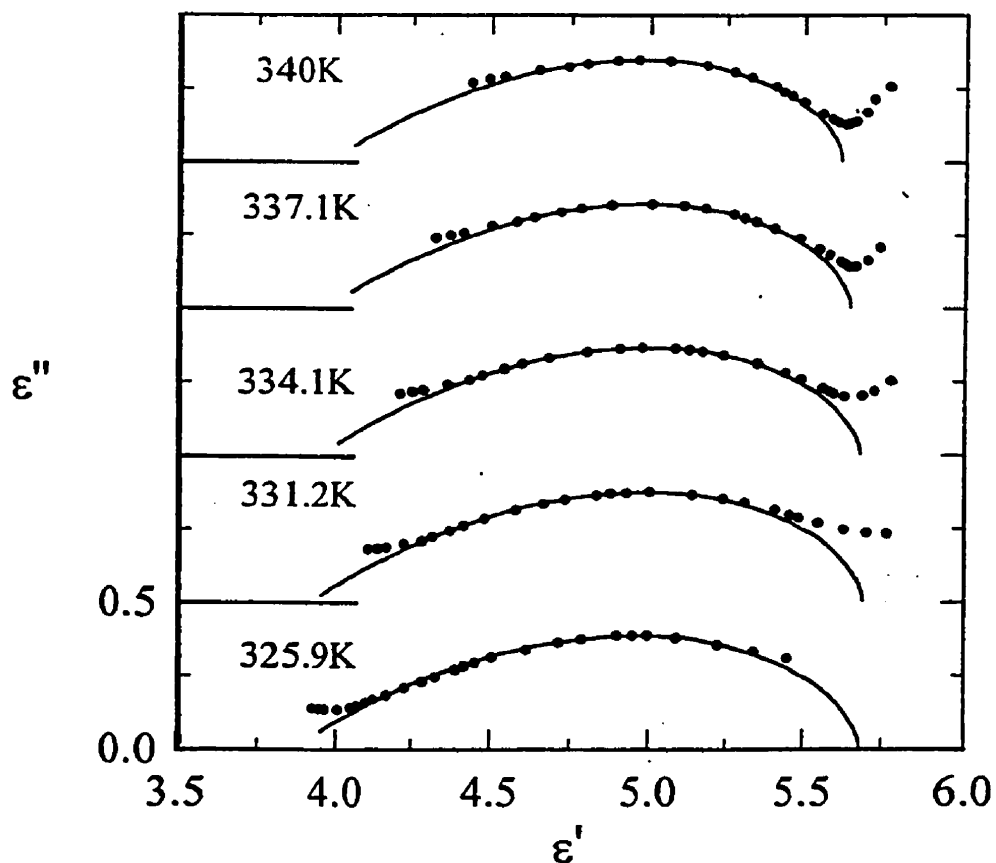
Figure 4.28: Complex plane plots of ε'' against ε' for the HMA:DGEBA mixture in the
fully polymerized state for isothermal measurements made at 325.9, 331.2,
334.1, 337.1 and 340.0K, as indicated. The best-fit curves according to the
stretched exponential relaxation function, shown as full lines, were calculated
from the parameters in Table 4.11.

fits are summarized in Tables 4.9, 4.10 and 4.11 for the three mixtures, and they are shown in plots against the reciprocal of temperature in Figure. 4.29.

Table 4.9 Parameters used for the stretched exponential fits to the fully reacted ANIL:DGEBA polymer for spectra measured at constant temperatures.

Temp/K	$\Delta\varepsilon$	ε_s	ε_∞	β	$\tau_o/\mu s$
372.5	1.35	5.55	4.19	0.39	2500
375.3	1.34	5.54	4.19	0.39	770
378.1	1.31	5.51	4.20	0.39	300
380.2	1.29	5.49	4.20	0.38	150
382.1	1.27	5.47	4.20	0.38	80
383.9	1.24	5.44	4.21	0.38	40
385.8	1.21	5.41	4.21	0.38	23
387.7	1.18	5.38	4.21	0.38	12
389.5	1.16	5.36	4.22	0.38	6.5

Table 4.10   Parameters used for the fit to the stretched exponential function for the dielectric spectra of the CHMA:DGEBA mixture at constant temperatures as indicated.

Temp(K)	$\Delta\varepsilon$	ε_s	ε_∞	β	τ_o (μs)	σ_{dc} (nS/m)
366.8	1.47	5.55	4.08	0.45	3000	0.06
368.0	1.46	5.51	4.05	0.46	1400	0.09
370.0	1.43	5.5	4.07	0.46	750	0.14
371.8	1.40	5.48	4.08	0.45	350	0.31
373.9	1.38	5.46	4.08	0.45	180	0.45
375.7	1.35	5.44	4.09	0.46	100	0.52
378.1	1.31	5.40	4.09	0.46	48	0.94
379.9	1.29	5.38	4.09	0.46	30	1.16
381.9	1.26	5.33	4.07	0.46	18	1.58
383.7	1.24	5.30	4.06	0.46	10.5	2.06
385.6	1.22	5.27	4.05	0.46	7	2.60
387.6	1.20	5.25	4.05	0.47	4.3	3.60
390.4	1.18	5.22	4.04	0.48	2.5	4.71

Table 4.11   Parameters used for the stretched exponential fit to the dielectric spectra of the fully reacted HMA:DGEBA polymer at temperatures as indicated (Johari and Pascheto 1995).

Temp (K)	$\Delta\varepsilon$	ε_s	ε_∞	β	$\tau_0/\mu s$
323.0	1.83	5.61	3.78	0.37	4000
325.9	1.83	5.68	3.85	0.38	1330
328.2	1.82	5.72	3.90	0.38	670
331.2	1.78	5.69	3.91	0.38	205
334.1	1.76	5.68	3.94	0.38	80
337.1	1.69	5.65	3.96	0.38	34
340.0	1.67	5.62	3.97	0.38	15

The relaxation time, τ_0, is plotted against 1/T in Figure 4.30. The curves are not linear, rather there is curvature, similar to the curve for the unreacted liquid mixture, with deviation from the Arrhenius equation $\tau_0 = \tau_\infty \exp(E_a/RT)$.

An alternative method for the analysis of such spectra has been proposed by Jonscher (1983). He considered that all dielectric data may be analyzed in terms of an empirical "universal" equation for the conductivity, such that,

$$\sigma(\omega) = A + B\omega^n, \tag{4.18}$$
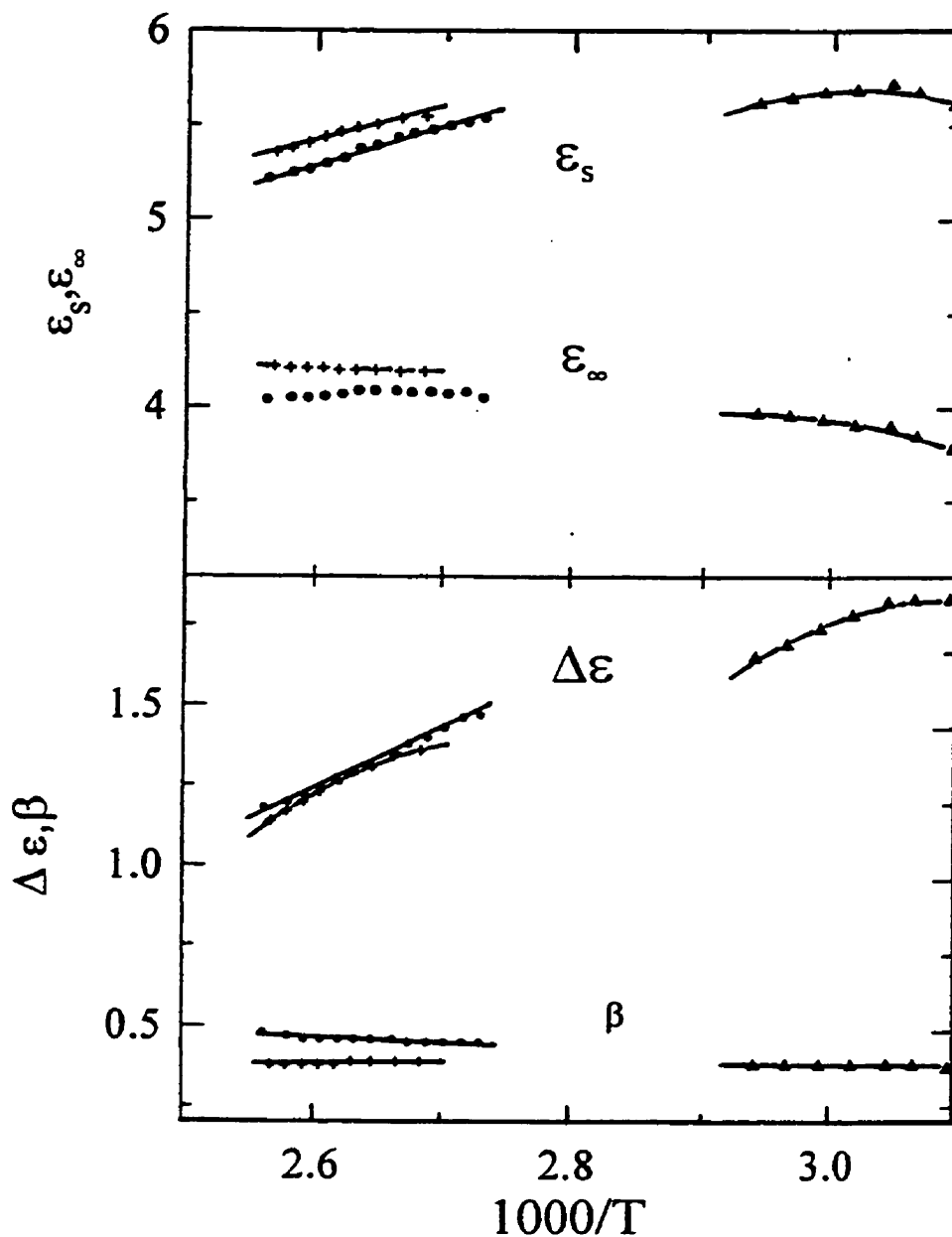
Figure 4.29:   The parameters ε_s, ε_∞, β and $\Delta\varepsilon$ determined from the stretched exponential fits to the spectra of the three mixtures in the fully reacted state, are plotted against the reciprocal of temperature. Notations areas follows: ANIL:DGEBA (+), CHMA:DGEBA (•) and HMA:DGEBA (Δ).
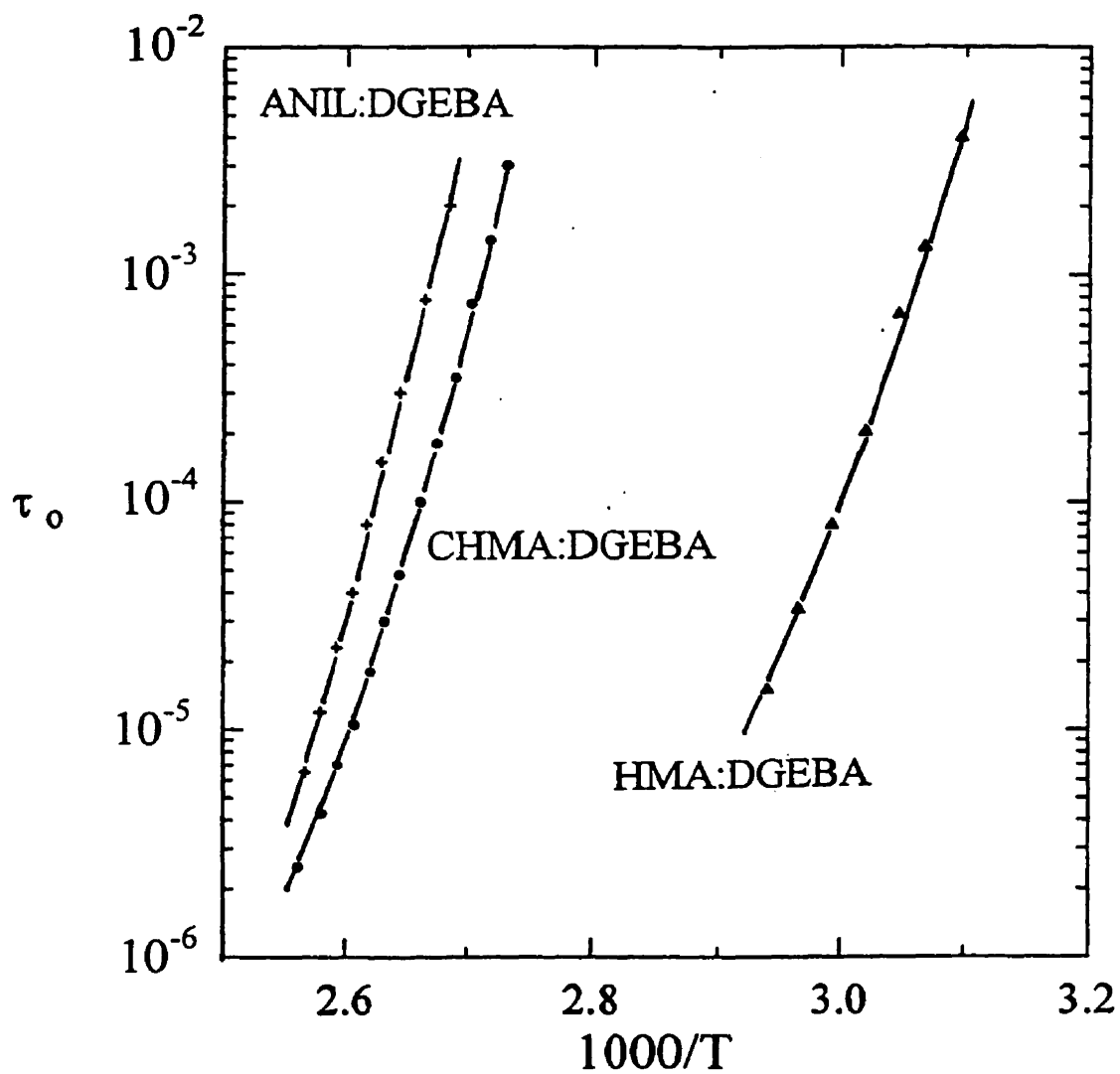
Figure 4.30: The relaxation time, τ_0, determined from the stretched exponential fits to the spectra of the three mixtures, as indicated, in the fully polymerized state, is plotted against the reciprocal of temperature.

where A, B and n̈ are frequency independent, empirical parameters. According to Eqn. (4.18), at low frequencies σ approaches a constant value, and at high frequencies increases according to a power law equation. The advantage of Eqn. (4.18) is that it predicts a "universal" scaling relation for the dielectric response of all materials. The theory has provided the starting point for a wide range of power law descriptions of the dielectric response, particularly for highly conducting mixtures (Sidebottom et al, 1994), but in itself provides little physical insight into the contributions to the observed dielectric response.

It is useful to examine the applicability of Eqn. (4.18) for the CHMA:DGEBA mixture previously discussed above, which was analyzed according to the method outlined in Section 4.1. The ε'' spectra data from Figure 3.13 were used to calculate σ, and the results are shown as logarithmic plots of σ against frequency in Figure 4.31 for the CHMA:DGEBA mixture in the fully reacted state. The plots show an approach towards a limiting plateau value at low frequencies. As the temperature is increased, the plateau region extends towards higher frequencies and its magnitude increased. At high frequencies, there does not appear to be an approach to a power law type behaviour, as would be indicated by a linear curve. It does not then seem reasonable to consider the observed response to be described in terms of Eqn. (4.18), rather, the analysis presented in Section 4.1 seems a more physically reasonable description. It is likely that the power law behaviour described by Jonscher is due to the high frequency tail of the dielectric relaxation process, though more work is required to show this in detail.
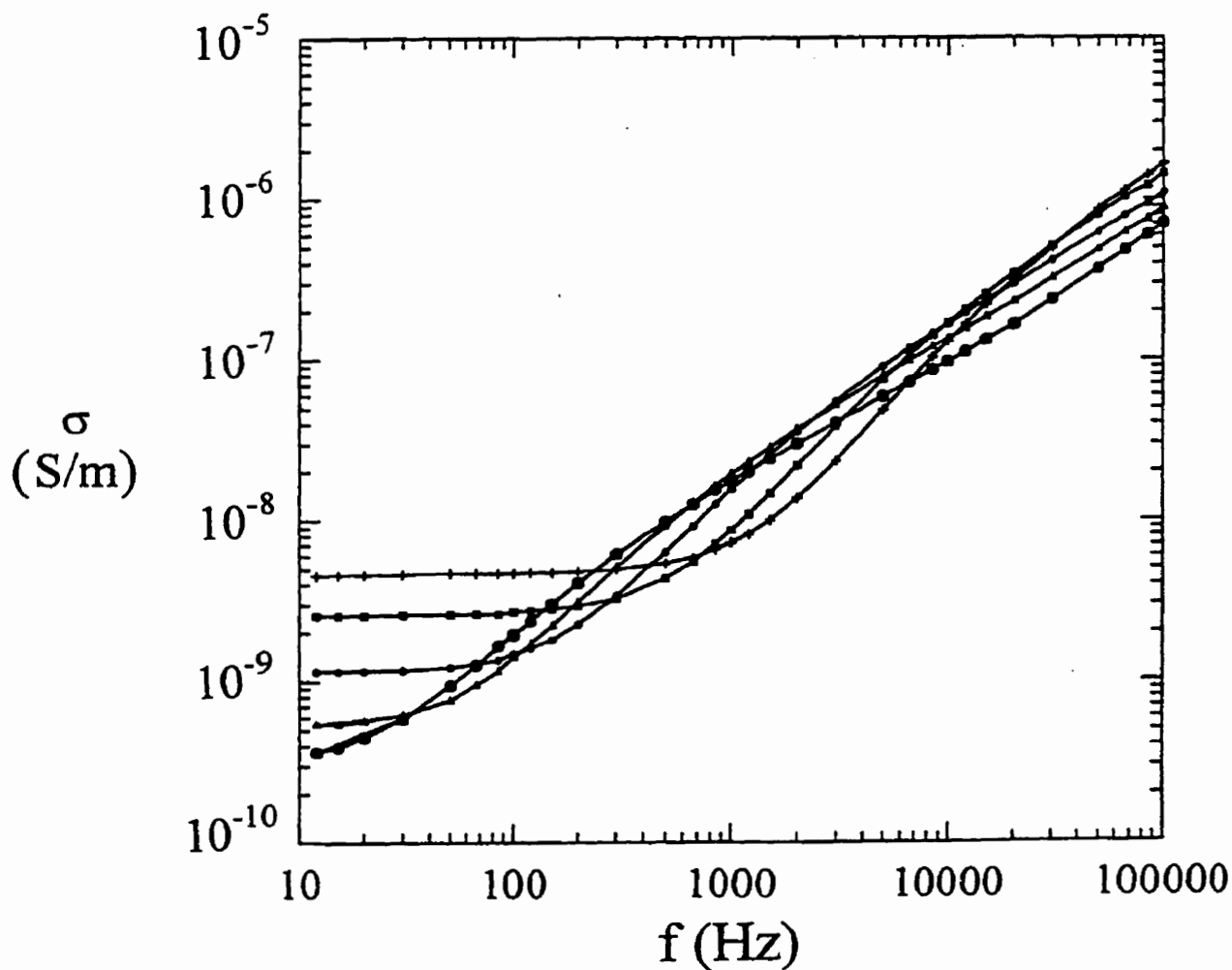
Figure 4.31: The conductivity, σ, of the CHMA:DGEBA mixture, corresponding to the data shown in Fig. 3.13, is plotted against the frequency. Plots shift towards lower frequencies as the temperature is lowered. No linearity is seen in the curves at high frequency, suggesting that a power law relation, as given by Eqn. 4.18, is not followed.

4.3.6 The Changes in the Parameters ε_s, ε_∞ and β During Polymerization.

The change in ε_s with increasing temperature and n for all three mixtures is shown as a plot of ε_s against temperature in Figure 4.32. The vertical decrease is that occurring during polymerization. For both the molecular liquid and fully reacted states, ε_s decreased for all three mixtures with increasing temperature. During isothermal reaction, ε_s decreased by 0.5 -0.8 for the three mixtures. This decrease is a combined effect of a change in the dipole moment, its orientational correlation, an increase in the number density of the dipole and a decrease in ε_∞, according to the Kirkwood-Fröhlich relation (Fröhlich, 1949),

$$\varepsilon_s - \varepsilon_\infty + \left(\frac{3\varepsilon_s}{2\varepsilon_s + \varepsilon_\infty}\right)\frac{4\pi N_d}{3k_B T} g \mu_o^2 , \qquad (4.19)$$

where N_d is the number of dipoles per unit molar volume, k_B the Boltzmann constant, μ_o the vapour phase dipole moment and g the orientation correlation factor, which is a measure of the short-range order of the structure.

When the reaction produces a macromolecule, the density of the liquid increases by 5-10% (Choy and Plazek, 1986). This increase alone will increase ε_s, according to Eqn.(4.19), by an almost equivalent amount, which is between 0.7 and 0.8 (10% of $\varepsilon_s(t_r \to 0)$ for the three mixtures). If the density alone is taken into account, ε_s should increase rather then decrease. Then according to Eqn. (4.19), the observed decrease must be attributed to a decrease in $g\mu_o^2$. To resolve the term $g\mu_o^2$, the change in μ_o must be known. However, this could not be measured. Nevertheless, qualitative resolution of the changes in g and μ_o is possible. When a covalent bond
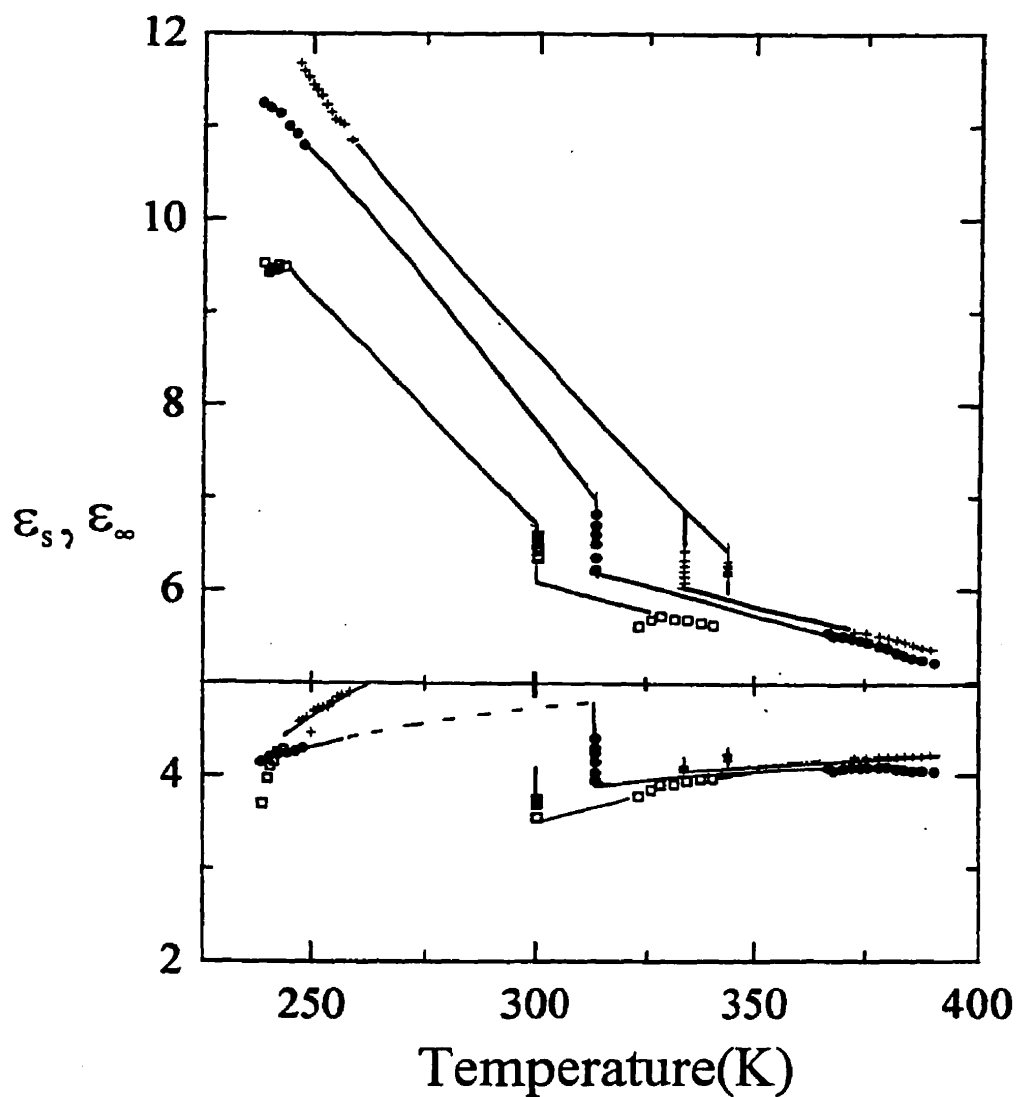
Figure 4.32: The change in ε_s and ε_∞ with increasing temperature and during polymerization for the three mixtures as indicated are plotted against temperature. The changes at low temperatures are for the molecular liquid state and at high temperatures the fully polymerized state. The vertical changes are those seen with increasing reaction during isothermal polymerization. Notations are ANIL:DGEBA (+), CHMA:DGEBA (•) and HMA:DGEBA (□). The lower temperature vertical decrease for the ANIL:DGEBA mixture is for the 333.4K polymerization and the higher temperature for the 343.4K polymerization.

forms on chemical reaction in the liquid, one -OH group is produced, one cyclic ether group is removed and the dipolar contribution by rotational diffusion of the aniline molecule as it attaches itself to the growing chain by its nitrogen atom and NH_2 groups are removed. The effect is then more likely to be due to a decrease in g, i.e. that the dipole moments become less correlated or are even ferroelectrically correlated in the fully reacted state.

The change in ε_∞ with increasing T and n is also shown in Figure 4.32 for all three mixtures. ε_∞ increased slightly with increasing temperature in both the molecular liquid and fully reacted states. ε_∞ also decreased by 0.4-0.6 with increasing n as shown by the vertical decrease at the polymerization temperature for all mixtures. Since $\varepsilon_\infty = n_D^2 + \Delta\varepsilon_{vib}$, this decrease is numerically equal to the sum of the change in n_D^2, the square of the optical refractive index, and in the contributions from the vibrational polarization, $\Delta\varepsilon_{vib}$. Increase in density is expected to increase n_D^2, but it also increases the frequency of the phonon modes, thereby decreasing $\Delta\varepsilon_{vib}$ according to the Kramers-Krönig relation,

$$\Delta\,\varepsilon_{vib} = \frac{1}{2\pi}\int_0^\infty \frac{K(\nu)}{\nu^2}\,d\nu\,, \qquad (4.20)$$

where K is the absorptivity of the band of frequency ν. Hence, our conclusion should be that the decrease in ε_∞ during polymerization is predominantly a reflection of the increase in the phonon frequency on chemical reaction.

The breadth of the spectrum of relaxation times, related to β in the stretched exponential fits, remains unchanged with increasing temperature for the molecular

liquid states of the ANIL:DGEBA and CHMA:DGEBA mixtures and for the fully polymerized states of all three mixtures. For the HMA:DGEBA mixture in the molecular liquid state, the breadth decreases with increasing temperature. Such changes with temperature are not unusual (McCrum 1967) as the distribution of relaxation times, and hence the activation energies is greater at lower temperatures while approaching Debye like behaviour at high temperatures.

During polymerization, the breadth of the spectra remains essentially constant for all mixtures, with the value of β ranging from 0.33-0.40. However, since the measurements upper frequency limit was 100 kHz, no information of the changes in the spectra at short times of reaction, or equivalently low values of n, could be determined. In a detailed study of the polymerization of an epoxy resin and a diamine using high frequency (10kHz-10GHz) dielectric techniques, Tombari and Johari (1992) showed that β decreased during the initial stages of reaction towards a limiting value at long times. That is inferred as well from the finding that β for the molecular liquid, which is expected to increase with temperature, was higher than β during reaction for the CHMA:DGEBA and ANIL:DGEBA mixtures, and was expected to be higher at 300K for the HMA:DGEBA mixture. Thus for the ANIL:DGEBA and CHMA:DGEBA mixtures, the distribution of relaxation times broadens during the reaction when the van der Waals' interaction are replaced by covalent bonds in the fully polymerized state. For the HMA:DGEBA mixtures, it is unclear whether the distribution broadens or narrows, since the value of β for the molecular liquid at 300K could not be determined. How much the increase in β for the fully reacted state is due

to increased thermal energy (340K for the polymerized state as contrasted with 240K for the molecular liquid) is yet to be investigated (Johari and Pascheto, 1995).

4.3.5 Evolution of a Bimodal Distribution

Figures 3.6-3.9 reveal a second feature in addition to the α-relaxation during the growth of the macromolecules. At times after the appearance of the α-relaxation, ε'' begins to increase with increasing frequency. The result is that at long times, the value of ε'' at 10 kHz is less than that at 100 kHz. Strictly interpreted, this means that after a certain period of time, or equivalently after conversion beyond a certain value of n, molecular entities with a relaxation rate comparable to the measurement frequency begin to from again, and an effect similar to the first ε'' peak may appear again. This is an incorrect interpretation, since further reactions would only increase the size of the existing entities which already have relaxation rates that are lower than the measurement frequency. On careful scrutiny of the Figures 3.6-3.9, it can be seen that the slope $(\partial \varepsilon''/\partial t_r)_\omega$ for $\omega > 10$ kHz decreased with increasing time of reaction, and also decreased with increasing ω when measured for the same time of reaction. The plots for different frequencies crossed over at certain values of the time of reaction, t_r, or n, and ε'' increased with increase in ω for a given t_r or n after this cross-over. This may be expressed in terms of n as,

$$\left(\frac{\partial \varepsilon''}{\partial \ln(\omega)} \right)_n = \left(\frac{\partial \varepsilon''_\alpha}{\partial \ln(\omega)} \right)_n + \left(\frac{\partial \varepsilon''_\beta}{\partial \ln(\omega)} \right)_n , \qquad (4.21)$$

where the subscripts refer to the contributions from the α- and sub-T_g or β-relaxation processes. For n beyond the ε'' peak, the first term on the right hand side of Eqn(4.21) is negative, and the second term positive, because the condition $\omega\tau_0$ for the β-process has not been reached. If only the first term on the right hand side of Eqn(4.21) contributes, then as the relaxation time increases with increasing n, the magnitude of ε'' should be higher for progressively decreasing frequencies. The initial opposite trend observed for highest n values in Figures 4.7-4.10 must therefore be seen as evidence for a secondary β-process for which $\omega\tau_0$ is less than 1.

Figure 4.33 shows this more clearly. Here typical results for the ANIL:DGEBA mixture polymerized at 343.4K are shown as plots of ε'' against frequency for several higher values of n. The rapid increase in ε'' beginning at about 15 kHz demonstrates that a high frequency process is present in the macromolecular product and is discernable in the high frequency region only for high values of n. All results for the other systems show qualitatively similar behaviour, with the magnitudes of the features differing. While it may seem that these spectra indicate that the high frequency process is a new molecular dynamics since it seems to emerge and separate from the main α-process, GHz frequency range measurements by Tombari and Johari (1992) suggest the converse. If the spectra could be normalized with respect to the high frequency relaxation-peak, not observed here, they would show that it is the α-relaxation peak that emerges and progressively separates from the high frequency process. Thus it appears that during the growth of the macromolecule, there is a transition from a unimodal to a bimodal distribution of molecular dynamics, and that this transition is observable in dielectric measurements. Such changes from unimodal
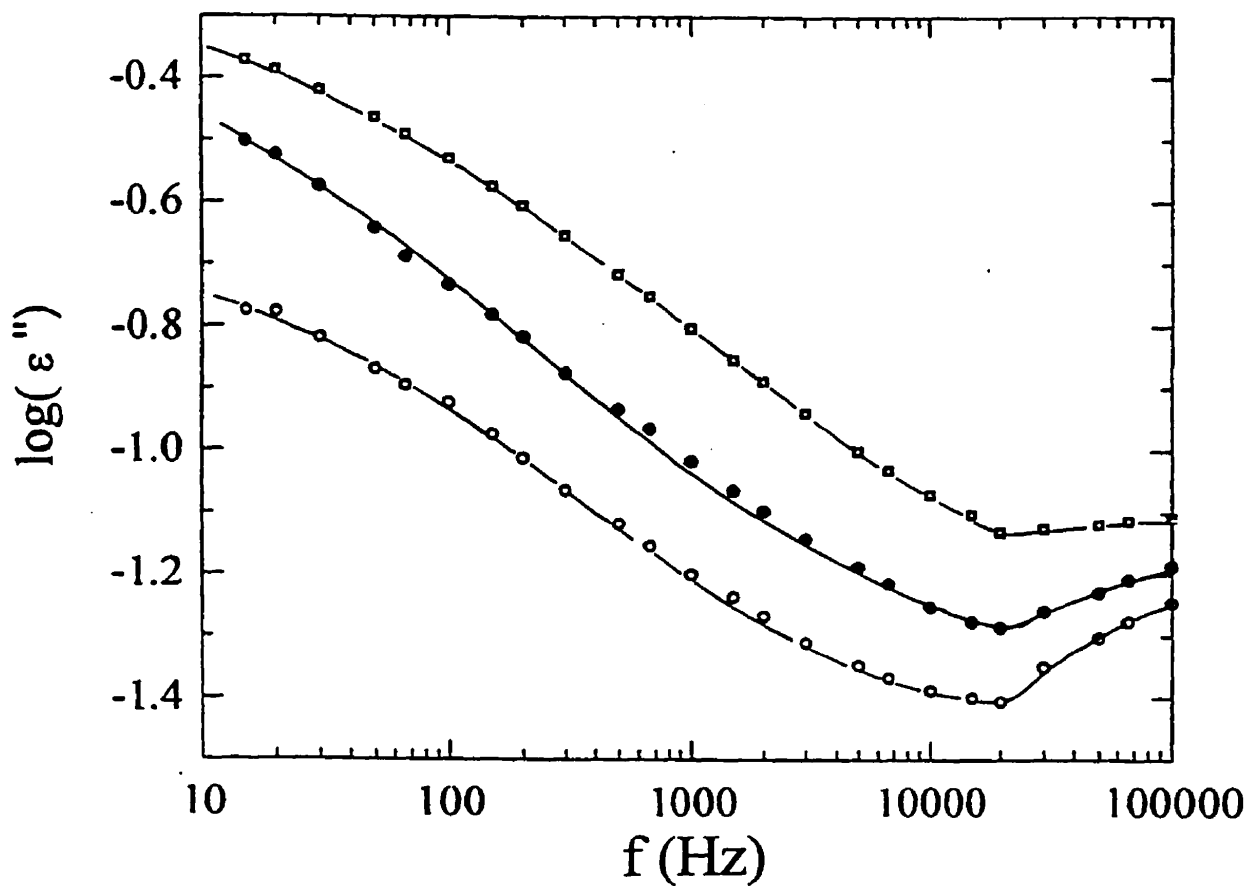
Figure 4.33: ε'' is plotted against frequency the ANIL:DGEBA mixture at 343.4K at high values of constant $n/10^{23}$: 5.2 (□), 5.38 (•), 5.49 (O). Note the increase at high frequencies (>10kHz).

to bimodal distributions have also been seen in both molecular (Johari 1973) and polymeric liquids (Johari 1985) on their supercooling, and on their compression under isothermal conditions (Johari and Whalley 1972). The evolution of these dynamics will be discussed in Chapter VI.

CHAPTER V

Ultrasonic Studies During the Growth of a Macromolecule

5.1 Longitudinal Modulus Changes During Growth.

The velocity of sound waves and their attenuation with increasing time of reaction were shown in Figures 3.15 and 3.16 for the three systems. To summarize; the velocity increased in a step-wise manner and the attenuation increased to a peak value, and thereafter decrease towards a lower value with increasing time of reaction.

It is useful to begin the analysis by describing the data, as outlined in Chapter IV for the dielectric data, in terms of the number of chemical bonds formed. The calorimetric data for the three systems at the temperatures corresponding to those in the ultrasonic studies, were used to calculate the number of chemical bonds formed, and the results are shown as plots of n against time in Figures 5.1 and 5.2, for the CHMA:DGEBA and the ANIL and HMA:DGEBA systems respectively. Typically, the plots are sigmoidal in shape with the magnitude of the sigmoidal step increasing and shifting to shorter times of reaction, as the temperature increased. This is expected for two reasons. As the temperature of reaction increased, the temperature dependent kinetics of the reaction are increased, resulting in faster conversion. The decrease in the long-time limiting number of bonds formed with decreasing temperature results from the effects of the changing glass transition temperature, T_g during formation. As outlined in Chapter IV, as chemical reaction occurs, the T_g of the resulting structure increases sharply. If measurements are made isothermally at
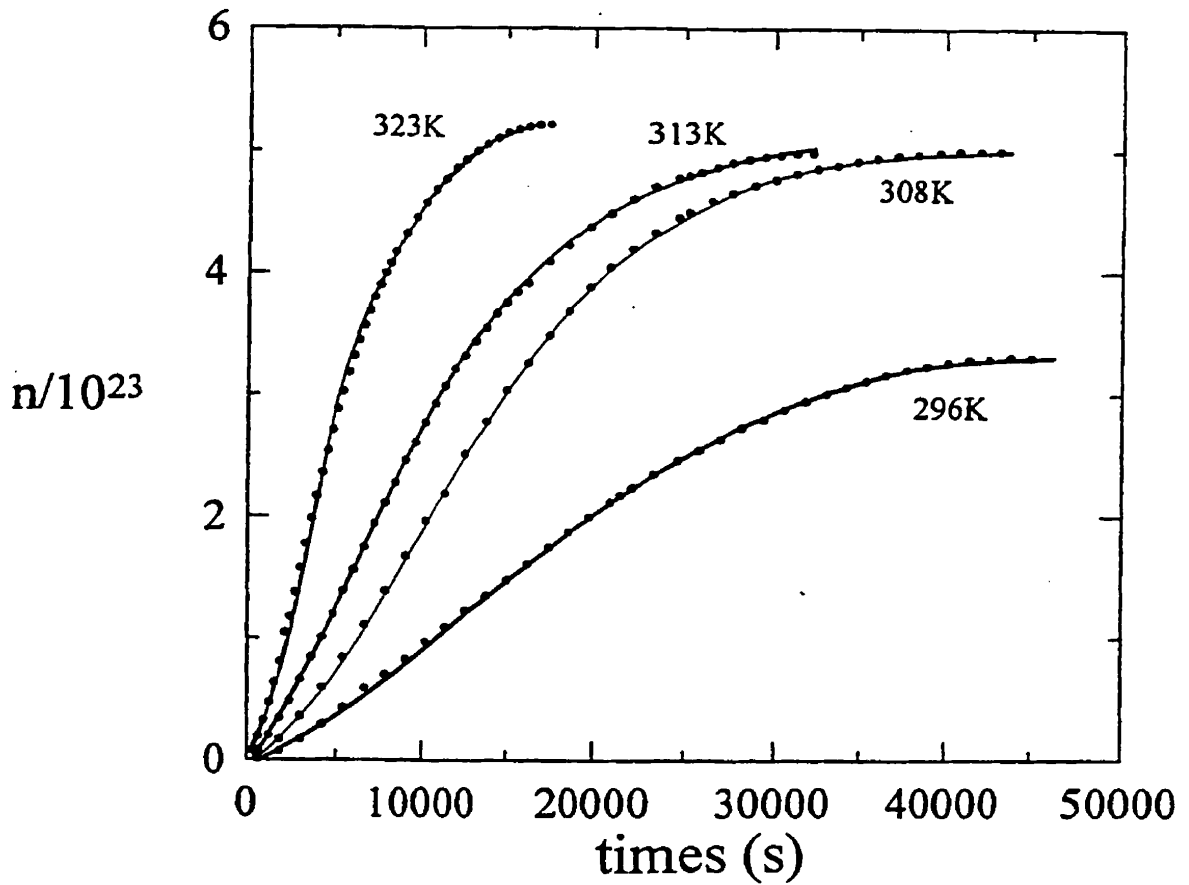
Figure 5.1:   The number of chemical bonds formed during the isothermal polymerization of the CHMA:DGEBA mixture is plotted against the time of chemical reaction for polymerizations at the temperatures as indicated.
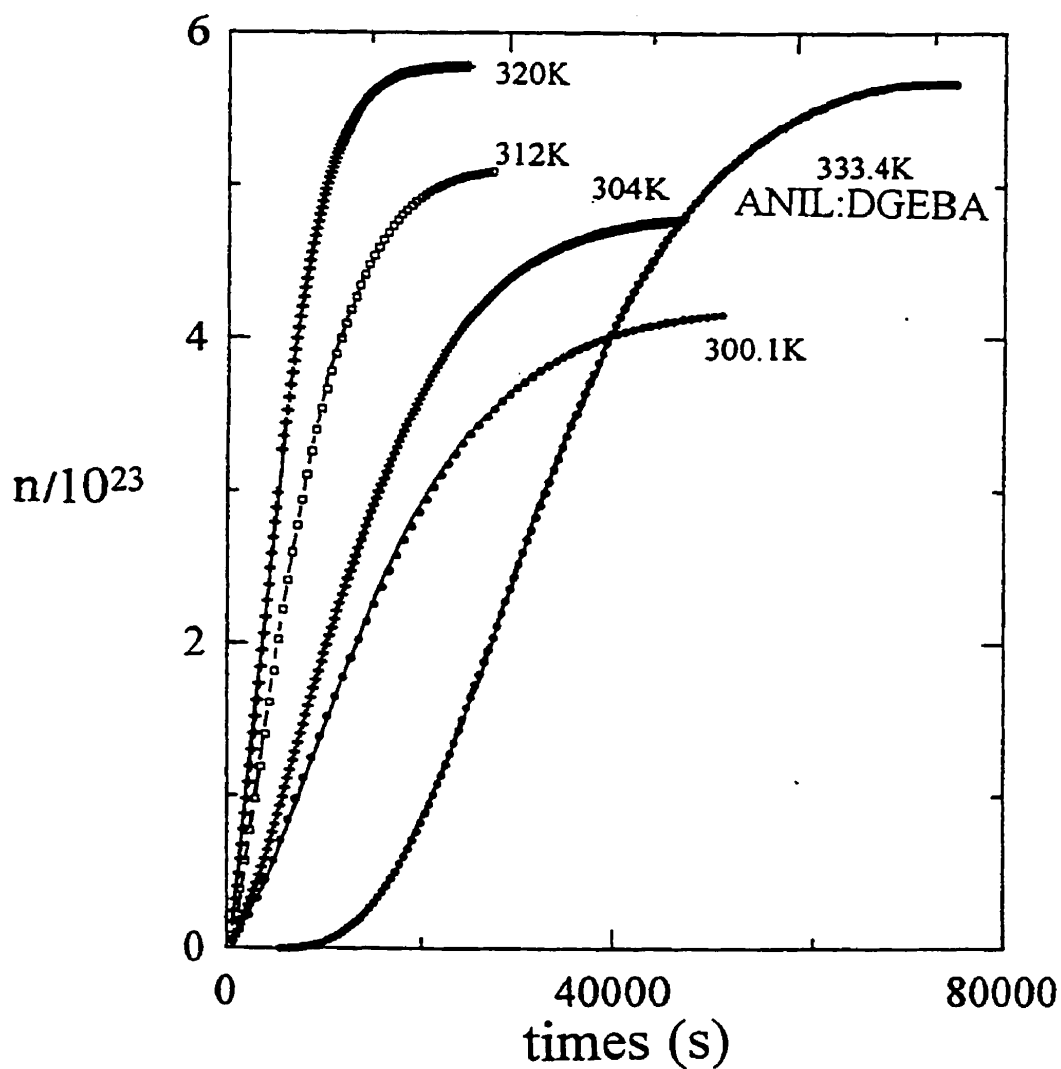
Figure 5.2: The number of chemical bonds formed during the isothermal polymerization of the HMA:DGEBA mixture is plotted against the time of chemical reaction for polymerizations at the temperatures as indicated. Also plotted is the number of chemical bonds formed during isothermal polymerization of the ANIL:DGEBA mixture at 333.4K.

temperatures below the glass transition temperature of the fully reacted systems, vitrification will occur at some point during the chemical reaction, which in turn effectively ceases the reaction. At lower temperatures this point occurs at a lower extent of chemical reaction. If the sample is then heated above this temperature, then reaction can again proceed.

The longitudinal modulus, L^* (= L' - iL''), is related to v and α according to,

$$L' - \rho v^2, \tag{5.1}$$

$$L'' - \frac{2\rho\alpha v^3}{\omega}, \tag{5.2}$$

where ρ is the density and ω (=$2\pi f$) is the angular frequency. The density of the amine:epoxy mixtures as calculated from their respective densities is ~ 1 kg/m^3. Since the changes in the density on polymerization are small (~ 5%) (Choy and Plazek, 1986), it is assumed that the density remains constant during reaction. Using this assumption, L' and L'' were calculated using the experimental v and α, and are plotted against n in Figures 5.3 and 5.4. L' increased slowly with increasing n at low values of n. Following this, there was an increase towards a limiting value, with the curves shifting towards lower values of n as the temperature decreased. L'' increased towards a peak whose magnitude increased and shifted to higher values of n as the temperature increased. Following this peak, L'' decreased towards a limiting value higher than the original starting value, with the limiting value decreasing with decreasing temperature.

Figure 5.3: The real and imaginary components, L' and L", of the complex longitudinal modulus during isothermal polymerization of the CHMA:DGEBA mixture, is plotted against the number of bonds formed. Notations are: 296K($\triangle$), 308K($\square$), 313K(+) and 323K($\bigcirc$).

Figure 5.4:   The real and imaginary components, L' and L", of the complex longitudinal modulus during polymerization of the HMA:DGEBA mixture, is plotted against the number of bonds formed. Notations are: 300.1K(•), 304K(+), 312K(□) and 320K(x). Also plotted is the data for the isothermal polymerization of the ANIL:DGEBA mixture at 333.4K

By analogy to the dielectric behaviour, the increase in L' and the corresponding peak in L" correspond to a relaxation process in which there is an increase in relaxation time with increasing chemical reaction. The changes that occur during reaction may be written as (Alig and Johari, 1992, Parthun and Johari, 1995(c)),

$$L^{*}(n) = L_{o}(n) + [L_{\infty}(n) - L_{o}(n)] \int_{0}^{\infty} e^{i\omega t} \left(\frac{\partial \Phi(n)}{\partial t} \right) dt, \qquad (5.3)$$

where L_{0} and L_{∞} are the limiting low and high frequency values of L^{*} and Φ is the stretched exponential form of the relaxation function. The values of L_{0} and L_{∞} are expected to increase by ~5% during polymerization owing to the increase in the density of the mixture (Alig and Johari, 1992). The change in the relaxation time over the chemical reaction leading from a liquid mixture to a glassy polymer is ~13 orders of magnitude, corresponding to a change in viscosity from ~ 10 to 10^{14} poise, according to the Stokes-Einstein relation. Thus, the changes in relaxation time were assumed to dominate the relaxation behaviour, and L_{0} and L_{∞} were assumed to be constant with changing n. Eqn. (5.3) is then rewritten as,

$$L^{*}(n) = L_{o} + [L_{\infty} - L_{o}] N^{*}[\omega \tau(n)], \qquad (5.4)$$

where $N^{*} = N' - iN''$ is the complex relaxation function, discussed in Section 4.3.2.

The analysis of the L^{*} data is carried out in an manner analogous to that of the complex permittivity data described earlier. Complex plane plots of L" against L' corresponding to the data in Figures 5.3 and 5.4 are shown in Figures 5.5 and 5.6. The shapes of these plots is a broad, highly skewed arc. The stretched exponential function was fitted to the experimental data, and the results are shown as solid lines in
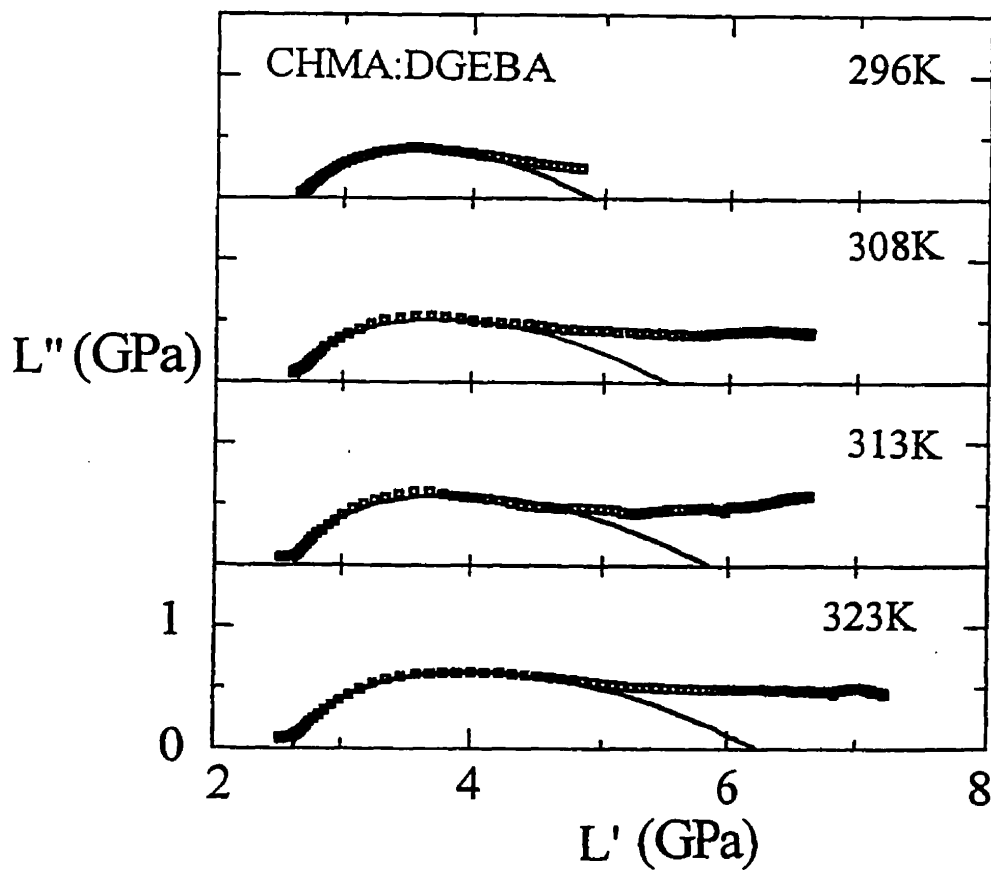
Figure 5.5:   Complex plane plots of L" against L' for measurements during the isothermal polymerization of the CHMA:DGEBA mixture at temperatures as indicated. Full lines are the fits to the stretched exponential functional form according to the parameters given in Table 5.1.
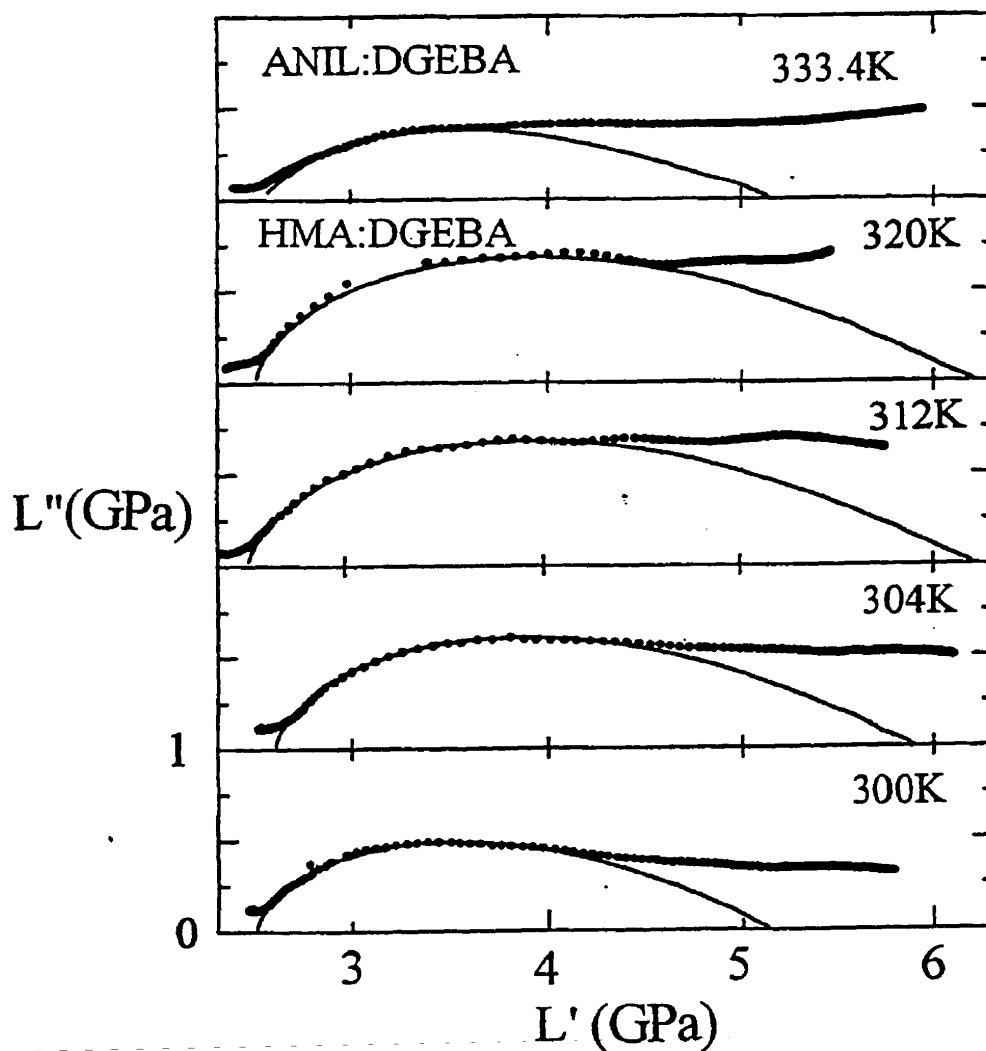
Figure 5.6: Complex plane plots of L" against L' for measurements during the isothermal polymerization of the HMA:DGEBA mixture at temperatures as indicated. Full lines are the fits to the stretched exponential functional form according to the parameters given in Table 5.1. Also plotted is the data for the isothermal polymerization of the ANIL:DGEBA mixture at 333.4K.

Figures 5.5 and 5.6. The fit is adequate at low values of n, but becomes poor at higher values of n. The values of L_o, L_∞ and γ used for the fits are listed in Table 5.1.

Table 5.1   Parameters used in stretched exponential fits to the ultrasonic data measured at 2.25 MHz, for the CHMA:DGEBA, HMA:DGEBA and ANIL:DGEBA systems at the temperatures as indicated.

System	Temp/K	L_o (GPa)	L_∞ (GPa)	γ
CHMA:DGEBA	296	2.70	4.90	0.33
	308	2.65	5.50	0.32
	316	2.63	5.83	0.32
	323	2.63	6.23	0.31
HMA:DGEBA	300	2.50	5.15	0.33
	304	2.60	5.90	0.33
	312	2.50	6.20	0.33
	320	2.50	6.20	0.34
ANIL:DGEBA	333.4	2.55	5.15	0.26

The temperature dependence of the parameters used for the fitting differs for the three systems. L_0 decreases with increasing temperature for the CHMA and HMA systems. L_∞ increases with increasing temperature for the CHMA system and decreases for the HMA system. γ remains essentially constant ~0.33, for the CHMA:DGEBA and HMA:DGEBA mixtures at all temperatures. It is much lower for the ANIL:DGEBA mixture.

Since each data in the fit corresponded to a unique value of $\omega\tau_0$, τ_0 can be calculated for the region over which the fit is acceptable. This was done, and are shown as plots of the logarithm of τ_0 against n in Figure 5.7 and 5.8 for the three systems as listed on the plots. τ_0 increased by ~4 orders of magnitude over the range of n where the fit was acceptable, with the values at constant values of n increasing with decreasing temperature. This increase with decreasing temperature is expected since for fixed values of n, the relaxation time should follow an Arrhenius temperature dependence $\tau_0 \propto \exp(E_a/RT)$, where E_a is an activation energy for structural relaxation.

5.2   Longitudinal Compliance Changes During Macromolecular Growth.

An alternate representation of the ultrasonic data is in terms of the complex longitudinal compliance, C^* (= $C' + iC''$), which is related to the longitudinal modulus by,

$$C^* = \frac{1}{L^*} = C' + iC'' = \frac{L'}{L'^2 + L''^2} - i\frac{L''}{L'^2 + L''^2}, \tag{5.5}$$
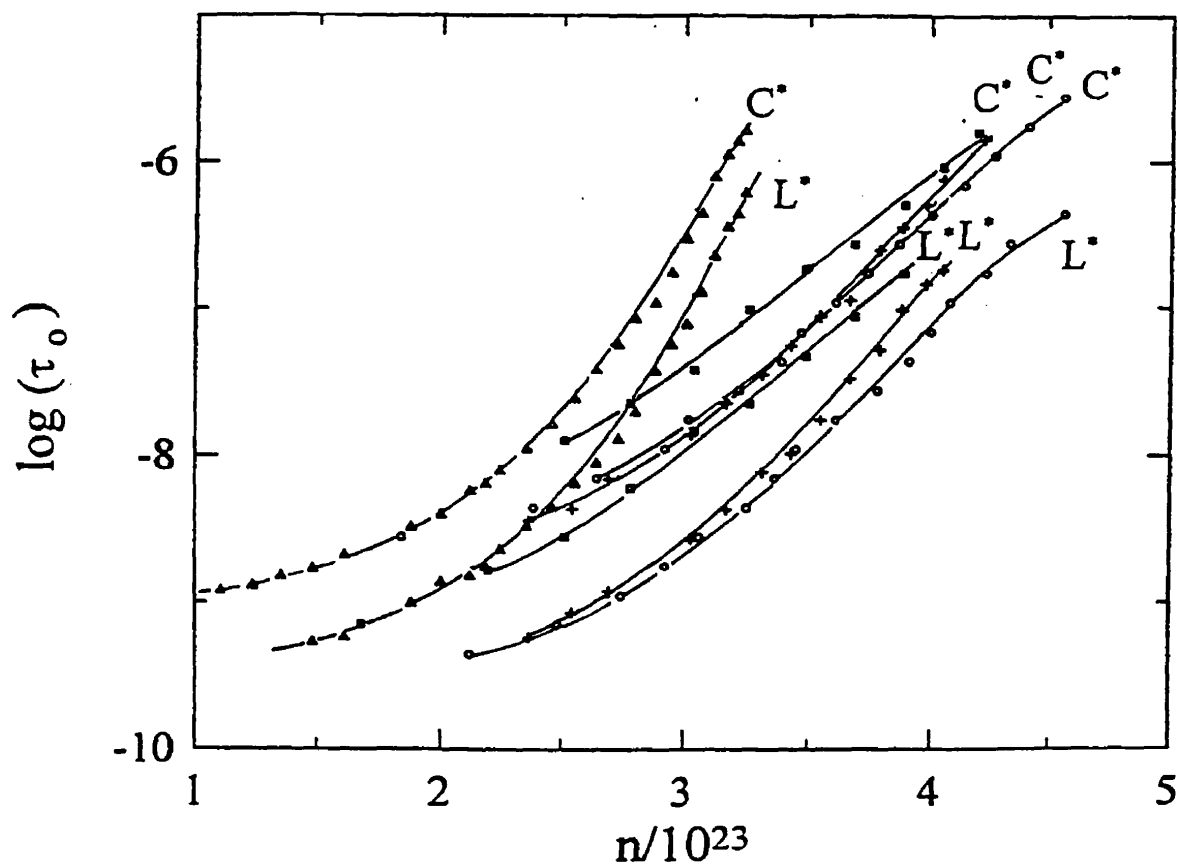
Figure 5.7: The relaxation time, τ_o, as determined from the fits to the complex plane plots of the longitudinal modulus and compliance data, is plotted against the number of bonds formed for the isothermal polymerization of the CHMA:DGEBA mixture at temperatures corresponding to those in Fig. 5.3. L^* denotes the longitudinal modulus data and C^* the longitudinal compliance data.
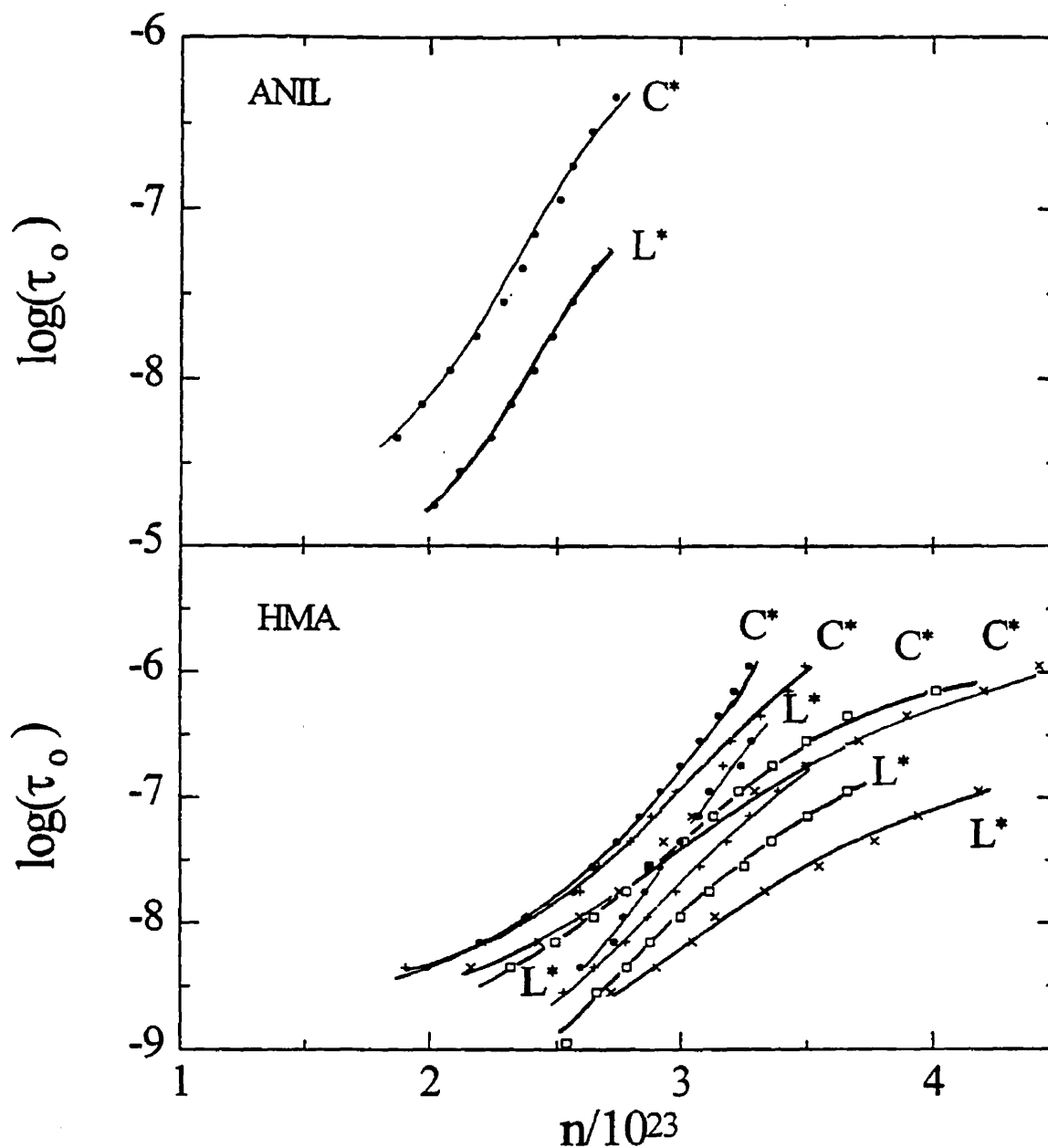
Figure 5.8: The relaxation time, τ_o, as determined from the fits to the complex plane plots of the longitudinal modulus and compliance data, is plotted against the number of bonds formed for the isothermal polymerization of the HMA:DGEBA mixture at temperatures and notations corresponding to those in Fig. 5.4. L^* denotes the longitudinal modulus data and C^* the longitudinal compliance data. Also plotted is the data for the isothermal polymerization of the ANIL:DGEBA mixture at 333.4K.

where C' and C" are the real and imaginary components of C*. While the use of the shear compliance, $J^* = (1/G^*)$, is widespread in the study of the mechanical behaviour of viscoelastic and anelastic materials (Ferry, 1980), the use of the longitudinal compliance is more recent (Alig et al, 1988, Parthun and Johari, 1995(b)). Its chief advantage lies in the resolution of small features in the corresponding modulus data.

The longitudinal modulus data shown in Figures 5.3 and 5.4 were used to calculate the corresponding compliance data, and these are shown as plots of C' and C" against n in Figures 5.9 and 5.10, and as plots of C" against C' in Figures 5.11 and 5.12. In contrast to L', C' decreased with increasing n towards a limiting value. C" increased through a peak towards a low value with increasing n.

The complex plane plots of C" against C' have the shape of a skewed arc, with less broadened features than those seen in the corresponding plots of L*. At high values of n, the plots tend towards a low limiting value of C". The data may be described by a form analogous to Eqn.(5.3) as,

$$C^*(n) = C_\infty + [C_o - C_\infty)] \int_0^\infty e^{i\omega t} \left(\frac{\partial \Phi(n)}{\partial t} \right) dt, \qquad (5.6)$$

where again it is assumed that both C_0 (=1/L_0) and C_∞ (= C_0- ΔC =1/L_∞) are constant with increasing n. The fits to the curves are shown as solid lines in Figures 5.11 and 5.12. The agreement is adequate with deviations occurring at both the low and high limiting values of n. The fitting parameters C_0, C_∞ and γ are summarized in Table 5.2.
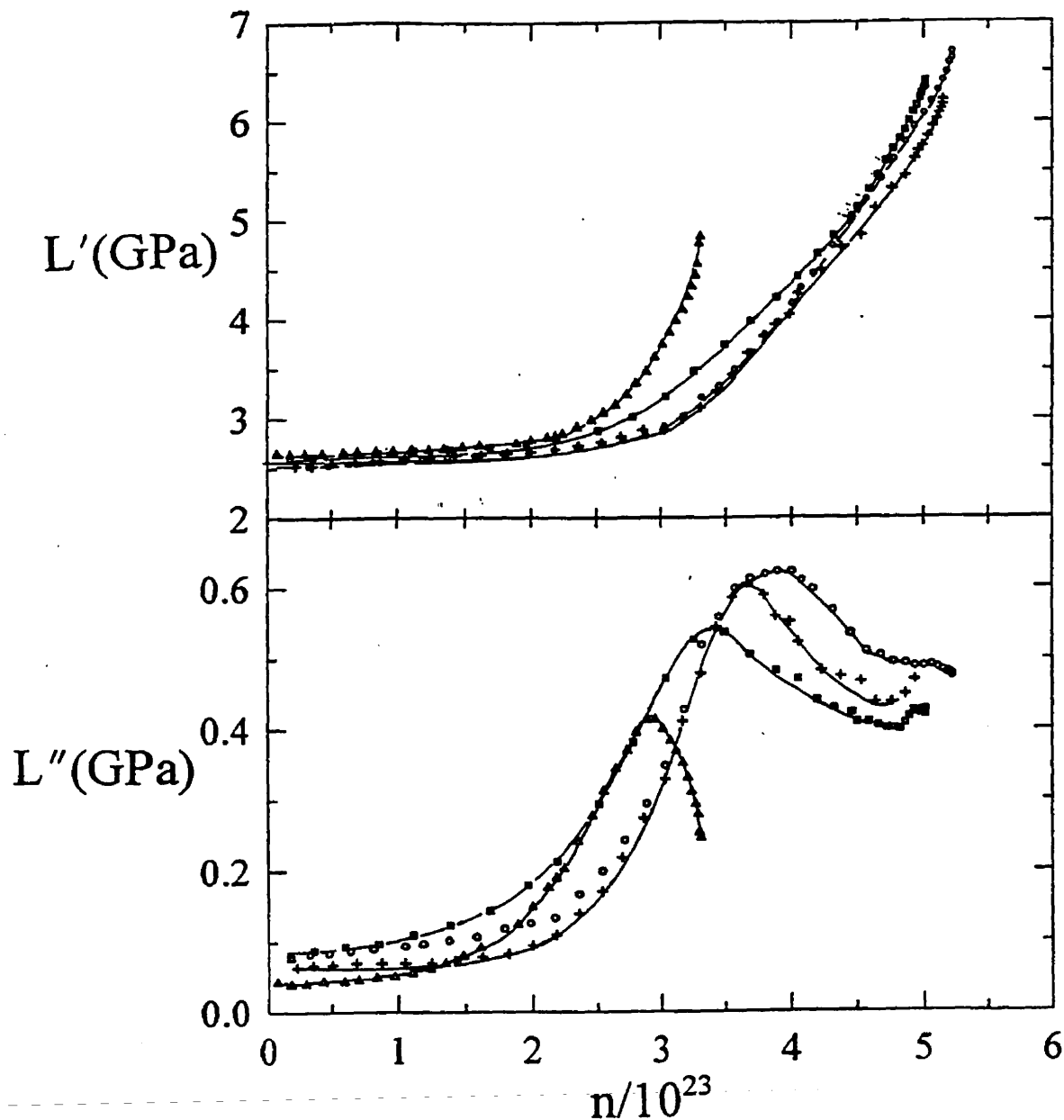
Figure 5.9: The real and imaginary components, C' and C'', of the complex longitudinal compliance measured during isothermal polymerization of the CHMA:DGEBA mixture, is plotted against the number of bonds formed. Notations are: 296K(△), 308K(□), 313K(+) and 323K(○).
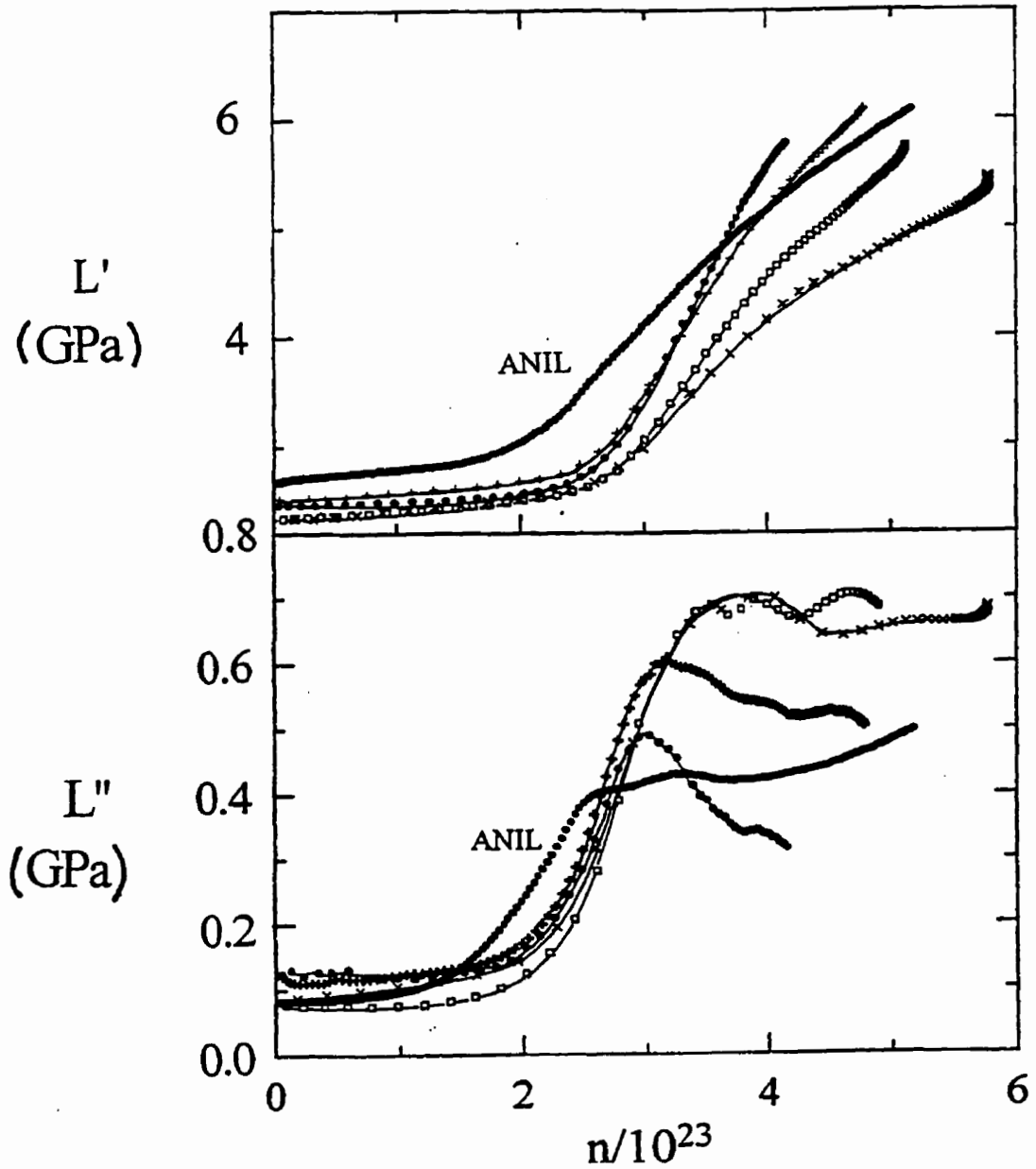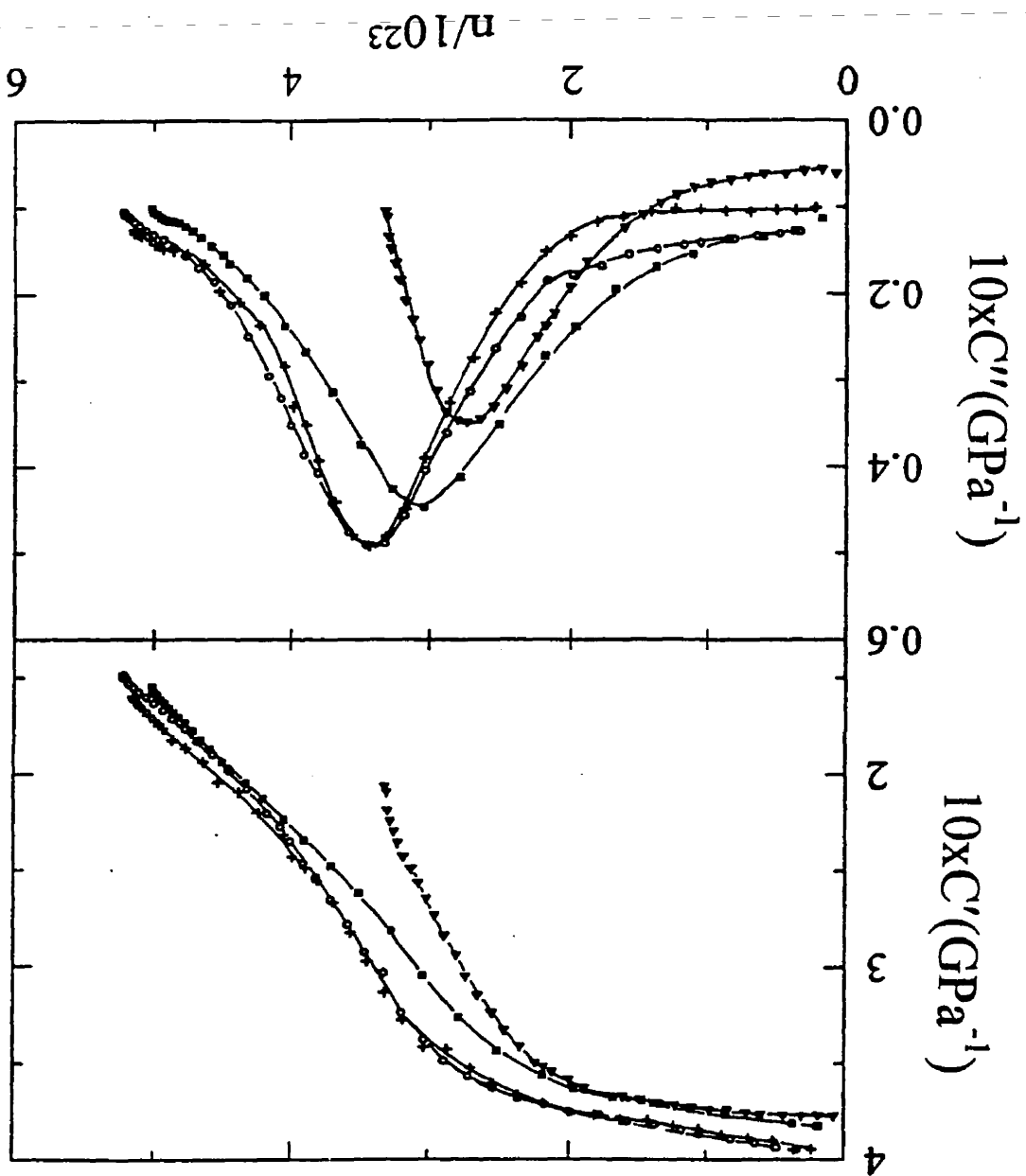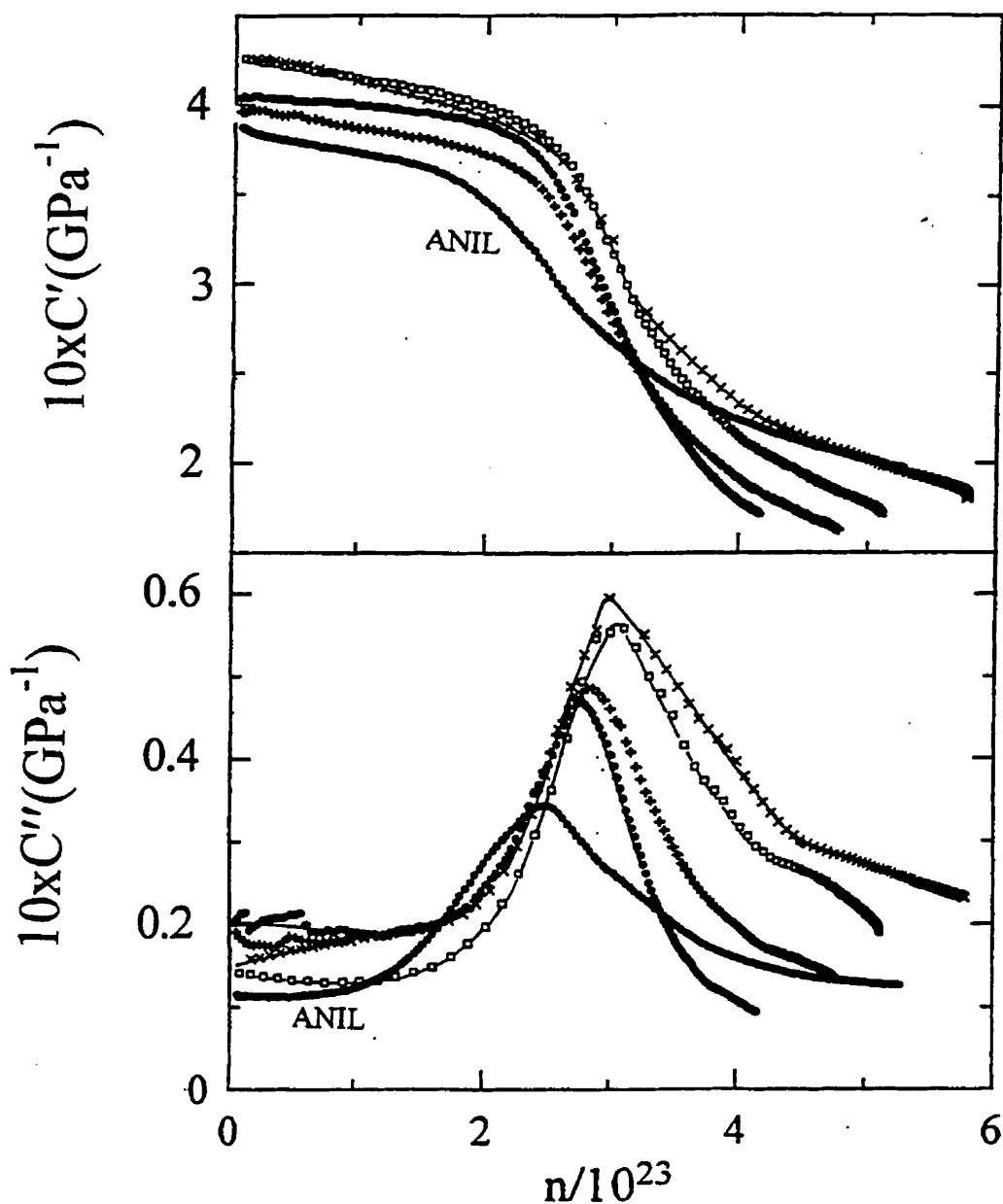
Figure 5.10: The real and imaginary components, C' and C", of the complex longitudinal compliance measured during isothermal polymerization of the HMA:DGEBA mixture, is plotted against the number of bonds formed. Notations are: 300.1K(•), 304K(+), 312K(□) and 320K(x). Also plotted is the data for the isothermal polymerization of the ANIL:DGEBA mixture at 333.4K
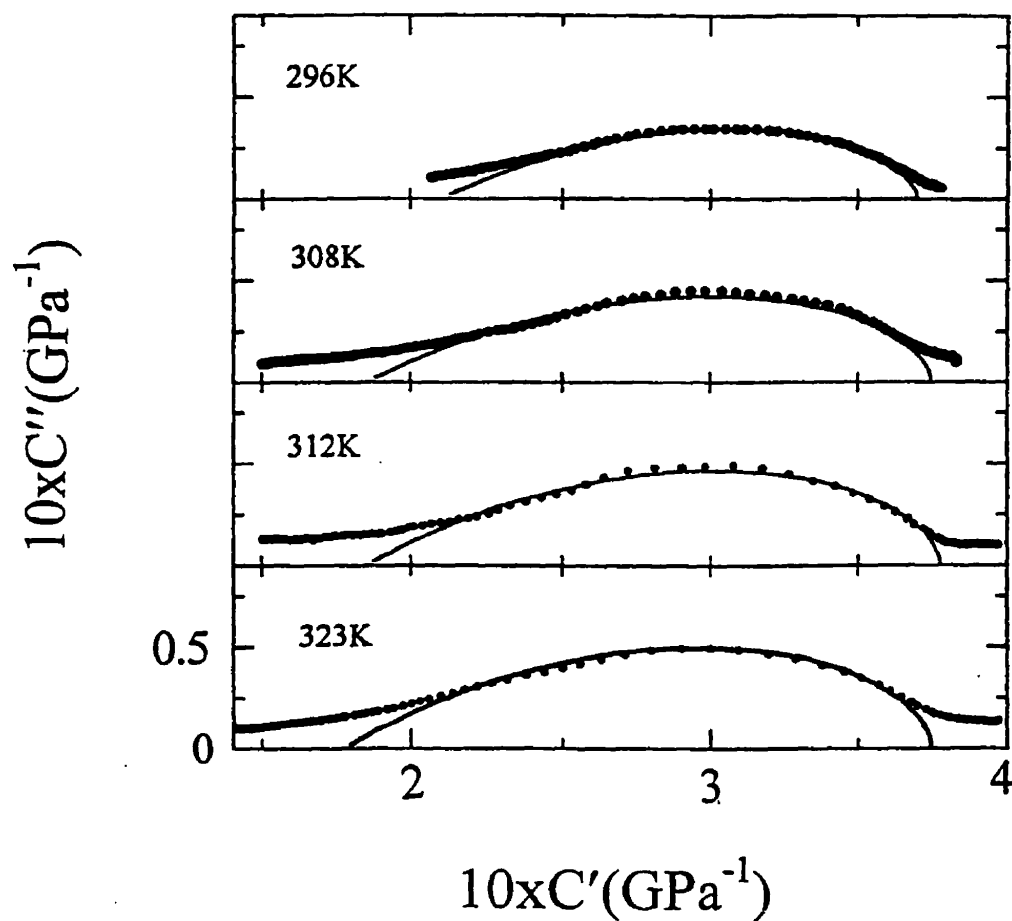
Figure 5.11: Complex plane plots of C'' against C' for measurements during the isothermal polymerization of the CHMA:DGEBA mixture at temperatures as indicated. Full lines are the fits to the stretched exponential functional form according to the parameters given in Table 5.2.
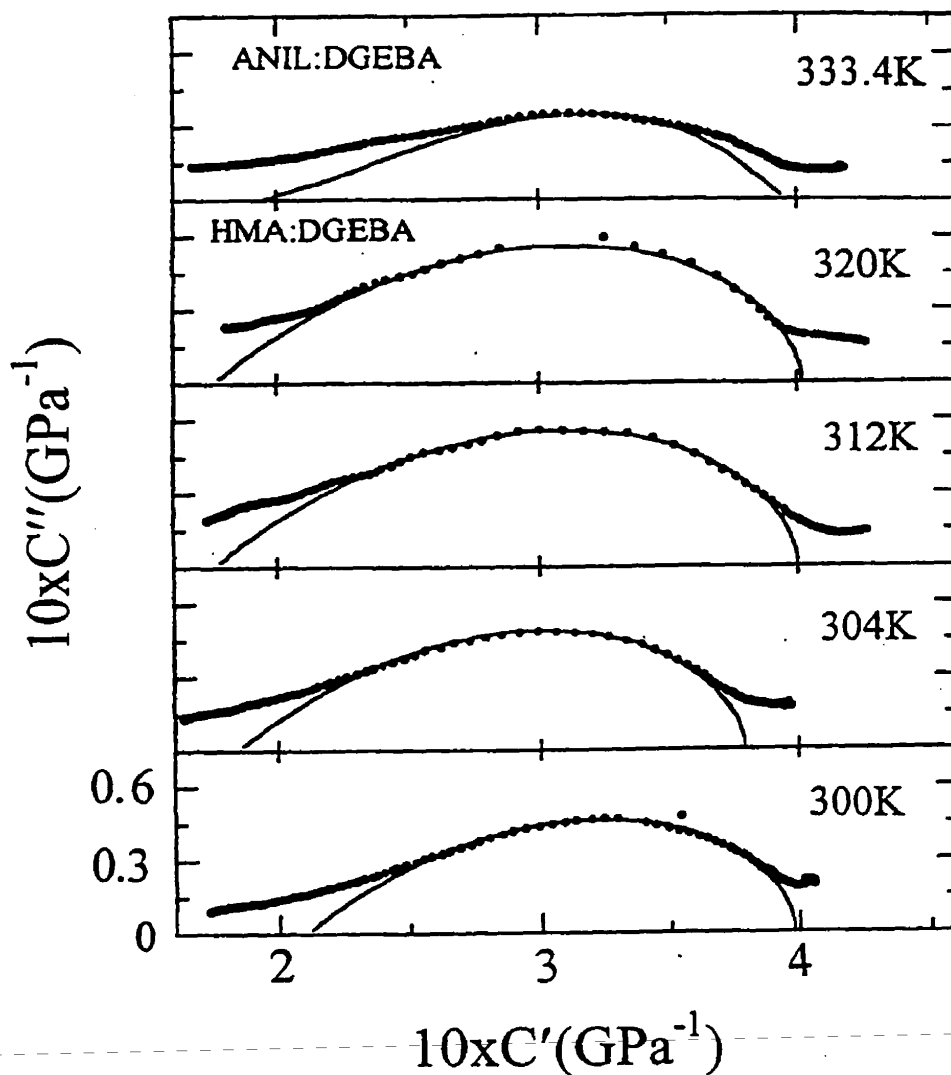
Figure 5.12: Complex plane plots of C″ against C′ for measurements during the isothermal polymerization of the HMA:DGEBA mixture at temperatures as indicated. Full lines are the fits to the stretched exponential functional form according to the parameters given in Table 5.2. Also plotted is the data for the isothermal polymerization of the ANIL:DGEBA mixture at 333.4K.

Table 5.2 Value of the parameters C_o, C_∞ and γ used for the stretched exponential fits to the compliance data for the three systems at temperatures as indicated.

System	Temp/K	$10 \times C_o(1/GPa)$	$10 \times C_\infty(1/GPa)$	γ
DGEBA:CHMA	296	3.71	2.10	0.39
	308	3.75	1.85	0.41
	312	3.78	1.85	0.44
	323	3.80	1.80	0.45
DGEBA:HMA	296	3.98	2.1	0.45
	304	3.86	1.84	0.44
	312	4.00	1.75	0.45
	320	4.02	1.75	0.45
DGEBA:ANIL	333.4	3.95	1.95	0.31

As with the longitudinal modulus data, it was possible to calculate τ_o as a function of n from the fits to the compliance data. These are also shown as plots of $\log(\tau_o)$ against n in Figures 5.7 and 5.8.

The magnitude of τ_o obtained from the compliance data is typically 5-10 times that obtained from the modulus data, with the difference becoming less as n increases.

γ also differs in the two formalisms. It is less for L^* than for C^*. Differences for both are a consequence of the formalisms themselves, and indicate that for the same molecular structure, the relaxation parameters differ when the manner of representation differs. This presents a difficulty in distinguishing the merits of the two formalisms Such variations have been seen also for polymer systems for the reciprocal quantities G^* and J^* ($=1/G^*$) obtained from low frequency dynamic mechanical measurements (McCrum et al 1967), and a corresponding situation also appears in the dielectric permittivity, ε^* and its reciprocal quantity, the electrical modulus, M^*.

5.3   The β- or Sub T_g-Relaxation and Molecule's Growth.

The dielectric studies outlined in Chapter IV, and earlier studies (Tombari and Johari, 1992), of these and similar crosslinked systems show that when n (in earlier studies, the description was given in terms of the time after the initiation of reaction) spontaneously increases, a new relaxation process, namely the α-relaxation process emerges and shifts to lower frequencies at a much greater rate with increase in n than the original β-, or sub T_g- relaxation process. At high values of n (or t_r), both then can contribute to the molecular dynamics. Qualitatively similar occurrences on decreasing the temperature of a structurally stable material are of course well known, and the analogy is seen between n and the reciprocal of temperature.

Although the β-relaxation process has not been clearly discerned in the results shown in Figures 5.3, 5.4, 5.9 and 5.10, there is certainly evidence for it, particularly at high values of n when the attenuation, L'' and C'' do not reach a zero value as n →

N_A. However, it the spectra of either L^* or C^* were measured for fixed values of n, the β-process would come into clear evidence as a relaxation peak. Such measurements of the ultrasonic spectra are unfortunately prohibitively expensive owing to the large number of different assemblies needed, i.e. one for each frequency. Nevertheless, it is possible to demonstrate by suitable simulation of data the shapes of the L′ and L″ plots against n when the relaxation times for the α- and β-relaxation processes diverge as n spontaneously increases.

The simulation will be based on the τ_0 data for the polymerization of the CHMA:DGEBA mixture at 323K. This data can be well described by an empirical equation of the form,

$$\tau_\alpha(n) = \tau_{oo} \exp\left[P_\alpha n^x\right], \qquad (5.7)$$

where τ_{oo}, the limiting value as n → 0, is equal to 15 ns, $P_\alpha = 2\times10^{-55}$ and x =2.5. For the β-relaxation process, τ_β is assumed to follow,

$$\tau_\beta(n) = \tau_{oo} \exp\left[P_\beta n\right], \qquad (5.8)$$

so that as n → 0, $\tau_\alpha = \tau_\beta$= 15 ns and for higher values of n the processes split. P_β was chosen as 1.45×10^{-23}. The simulated data, shown as plots of the logarithm of τ_α and τ_β against n in Figure 5.13, clearly show how the splitting of the two processes might occur.

To simulate L^* it is necessary to choose a form of the relaxation time distribution. For simplicity of calculations, a Cole-Davidson form (Davidson and Cole, 1951) and given by,
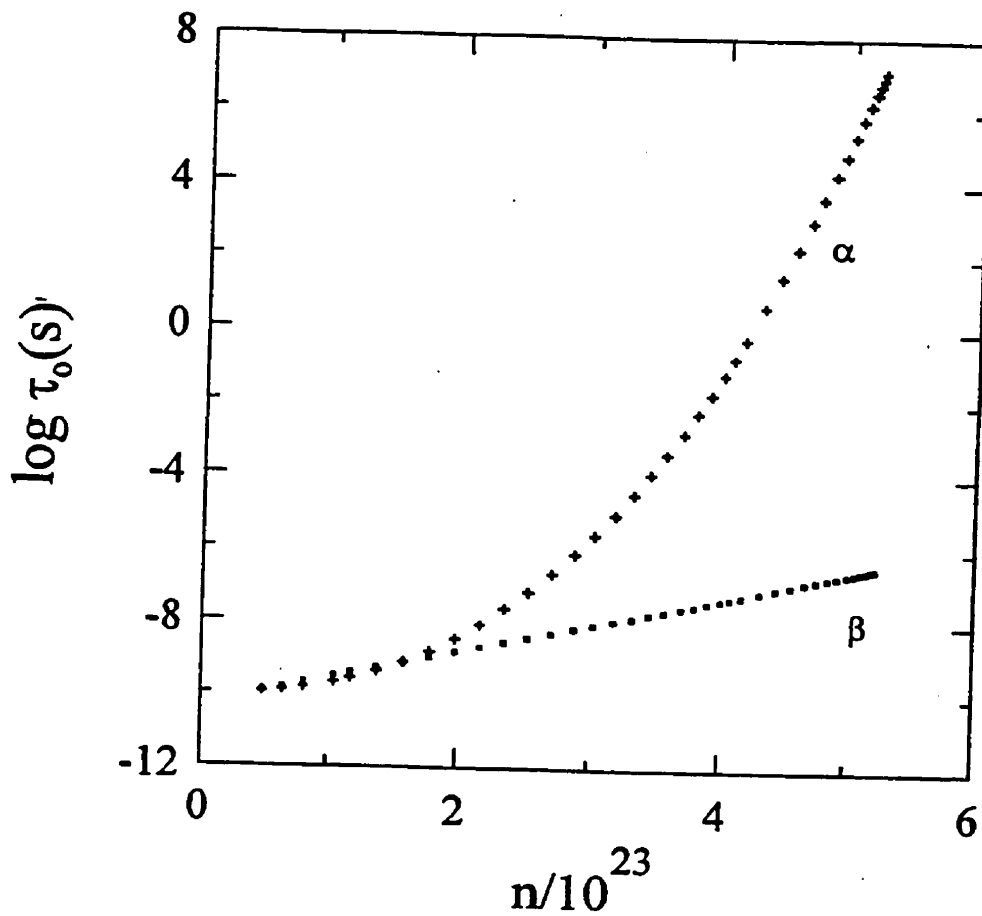
Figure 5.13: Simulated data showing the increase in the relaxation time for the α-relaxation process, $\tau_\alpha(n)$, and the sub-T_g, or β-relaxation process, $\tau_\beta(n)$, with increasing number of bonds formed. The parameters used in the simulation are listed in section 5.3.

$$L^{*}(n) = L_{\infty} + \frac{1}{1+(i\omega\tau_{o}(n))^{\beta_{cd}}} , \qquad (5.9)$$

was used for both relaxation processes. The real and imaginary components were calculated from,

$$L'(n) = L_{\infty} + \Delta L[cos(\Phi)]^{\beta_{DC}}cos(\Phi\beta_{DC})$$
$$L''(n) = \Delta L [cos(\Phi)]^{\beta_{DC}}sin(\Phi\beta_{DC}), \qquad (5.10)$$

where,

$$\Phi = tan^{-1}[\omega\tau_{o}(n)] . \qquad (5.11)$$

The parameters L_{o} = 2.6 GPa, and $L_{o} + \Delta L_{\alpha} + \Delta L_{\beta}$ = 6.8 GPa were taken from the data for the 323K polymerization of CHMA:DGEBA. The following values were assumed for the remaining parameters: $\beta_{cd,\alpha} = \beta_{cd,\beta} = 0.2$ (which is equivalent to 0.34 for the stretched exponential form (Lindsey and Patterson, 1980)), $\Delta L_{\alpha} = 2.7$ GPa and $\Delta L_{\beta} = 1.5$ GPa. L' and L" were calculated using Eqns. (5.10) and (5.11) and the above parameters, and the results shown as plots of L' and L" against n in Figure 5.14(a) and in the plot of L" against L' in Figure 5.14(b), with the contributions from the α- and β-relaxation processes delineated. This type of analysis in admittedly subjective; however its value lies in recognizing that changes in n as observed here are a consequence of the splitting of the α-process from the β-process as n increases, and that for high values of n, the β-process makes a dominant contribution to L^{*}, particularly at high frequencies.
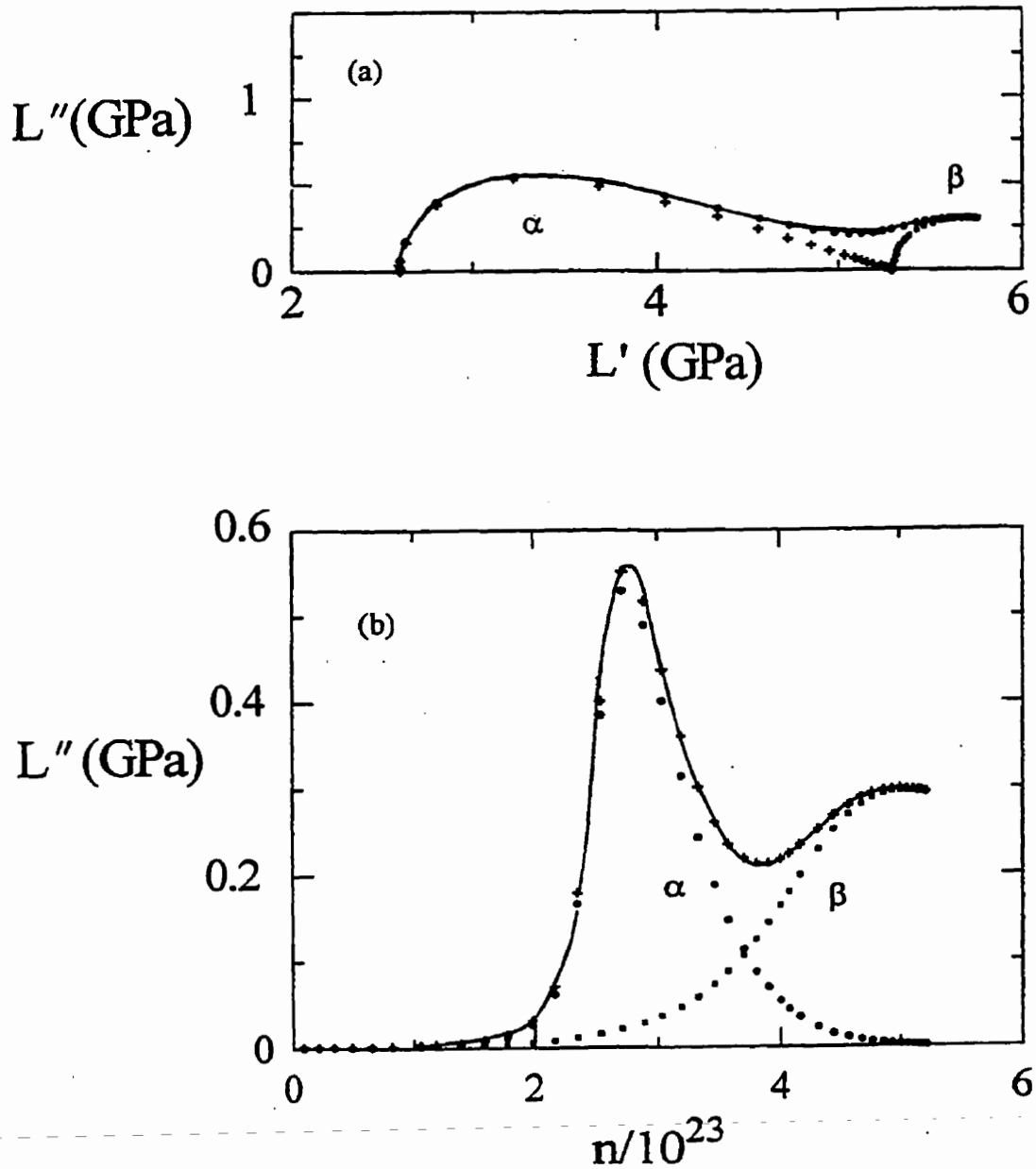
Figure 5.14: (a) Complex plane plot of L" against L' for the simulation based on contributions from both α-relaxation and β-relaxation processes, as discussed in section 5.3. α here refers to the α-process, and β, the sub T_g- or β-process. The solid line denotes the sum of the two contributions. (b) Plot of L" against n based on contributions from both relaxation processes as discussed in section 5.3. The labels are as those in plot (a).

5.4   The Bulk and Shear Contributions to Relaxation

As outlined in Chapter II, the ultrasonic relaxation observed in the modulus or compliance measurements of liquids can also be discussed as a combination of bulk modulus, K^*, and shear modulus, G^*, components. This is done when the velocity and attenuation of shear waves are known, and K^* is determined from the difference, $K^* = L^* - 4/3G^*$. K^* can also be determined from the bulk compressibility of the liquid, B^*, since $K^* = 1/G^*$, particularly in the high and low frequency limits. However, the imaginary component, iK'', is not easily deduced from such measurements. It is instructive to discuss the relative contributions of K^* and G^* in determining L^* here, particularly in view of the fact that the shear contribution is often assumed to be the dominant contribution to L^*.

In Chapter II, the contributions from K^* and G^* to the velocity, v, and the attenuation for a single relaxation time process were given as,

$$v^2 = \frac{1}{\rho}\left(K_o + \frac{\Delta K \omega^2 \tau_v^2}{1 + \omega^2 \tau_v^2} + \frac{4}{3}\frac{G_\infty \omega^2 \tau_s^2}{1 + \omega^2 \tau_s^2}\right) \tag{5.12}$$

and,

$$\alpha \lambda = \pi \left[\frac{\dfrac{\Delta K \omega \tau_v}{1 + \tau_v^2} + \dfrac{4}{3} \dfrac{G_\infty \omega t_s}{1 + \omega^2 \tau_s^2}}{K_o + \dfrac{\Delta K \omega^2 \tau_v^2}{1 + \omega^2 \tau_v^2} + \dfrac{4}{3} \dfrac{G_\infty \omega^2 \tau_s^2}{1 + \omega^2 \tau_s^2}} \right] \qquad (5.13)$$

where all parameters are as described in Chapter II.

Litovitz and Davies (1960) discussed the physics of ultrasonic relaxation in liquids and showed that the contributions from K^* and G^* were additive when molecular diffusion involved both volume and shear relaxations. For a single relaxation time, Eqns.(5.12) and (5.13) can be written in terms of the real and imaginary components of L^* as,

$$L' = L_o + \frac{\Delta L \omega^2 \tau_v^2}{1 + \omega^2 \tau_v^2} \left[\frac{1 + \left(\dfrac{\omega \tau_v}{\alpha} \right)^2 - \dfrac{4}{3} \dfrac{G_\infty}{\Delta L} (1 - \alpha^2)}{1 + \left(\dfrac{\omega \tau_v}{\alpha} \right)^2} \right] \qquad (5.14)$$

and,

$$L'' = \frac{\Delta \omega \tau_v}{1 + \omega^2 \tau_v^2} \left[\frac{\omega^2 \tau_v^2 \left(\dfrac{4}{3} \dfrac{G_\infty}{\Delta L} - \dfrac{4}{3} \dfrac{G_\infty}{\Delta L} \alpha + \dfrac{1}{\alpha} \right) + \alpha + \dfrac{4}{3} \dfrac{G_\infty}{\Delta L} (1 - \alpha^2)}{\alpha \left(1 + \left(\dfrac{\omega \tau_v}{\alpha} \right)^2 \right)} \right] \qquad (5.15)$$

where $\alpha = \tau_v / \tau_s$. It should be noted here that Eqn(5.15) differs from the corresponding Eqn(113) given by Litovitz and Davies(1960) in two ways; first it is written in terms of τ_v and not τ_s, and second, the term $\omega\tau$ outside the parentheses and other terms inside the parentheses are quite different then theirs. Perhaps there is a transcription error in their Eqn(113), since it does not yield M_∞ in the limit as $\omega\tau \to \infty$ (here L' is the same as their L', and ΔL as their M_2).

Before describing the results in terms of a suitable modification of Eqns(5.14) and (5.15), it is noted that as $\omega\tau \to 0$, L' $\to K_o$, and that the contribution from the shear modulus is essentially zero. Thus the plots of L' against n, shown in Figures (5.14) and (5.15), begin from a floor value of K_o with no contributions from G'. L' then increases towards its limiting value (7.2 GPa for the CHMA:DGEBA at 323K) with the difference, 4.6 GPa being the sum of ΔK ($= K_\infty - K_o$) and $4/3G_\infty$. A list of G_∞/K_∞ values summarized by Litovitz and Davies (1960) in Table XI, p.320, shows that it varies from 0.17 for polyisobutylene to 0.65 for a molecular liquid, isobutyl bromide, but the values for most liquids is less than 0.36. Thus the magnitude of K_∞ is 2-6 times that of G_∞. Evidently then, the increase in L' from a liquid-like value of 2.6 GPa to a solid-like value of 7.2 GPa observed here for the CHMA:DGEBA at 323K, is predominantly associated with the increase in K'. G' does contribute, but its magnitude is much less, though it no doubt increases by many orders of magnitude from virtually 0 to 1 GPa as n increases.

Marvin and McKinney's (1960) summary of the thorough studies of poly-isobutylene carried out by several groups, clearly showed that K' and not G' makes the

largest contribution to L', when L' and G' are measured over a wide $\omega\tau$ range at 298K. They also reported that, at least at this temperature, τ_v/τ_s is close to one. This has also been confirmed by Litovitz and Davies (Table III, p. 335, 1960), where τ_v/τ_s varied from 0.46 to 4.6 for different liquids, with long chain molecules showing the highest values. For the purpose of the analysis here, Eqns(5.14) and (5.15) are written for an asymmetric distribution of relaxation times, as given by Davidson and Cole (1951),

$$L' = L_o + \Delta L \cos(\phi_v)^{\beta_v} \cos(\phi_v \beta_v) +$$
$$\frac{4}{3} G_\infty \left[\cos(\phi_s)^{\beta_s} \cos(\phi_s \beta_s) - \cos(\phi_v)^{\beta_v} \cos(\phi_v \beta_v) \right] \tag{5.16}$$

and

$$L'' = \Delta L \cos(\phi_v)^{\beta_v} \sin(\phi_v \beta_v) +$$
$$\frac{4}{3} G_\infty \left[\cos(\phi_s)^{\beta_s} \sin(\phi_s \beta_s) - \cos(\phi_v)^{\beta_v} \sin(\phi_s \beta_s) \right] \tag{5.17}$$

where,

$$\phi_v = \tan^{-1}(\omega\tau_v) \quad ; \quad \phi_s = \tan^{-1}\left(\frac{\omega\tau_v}{\alpha} \right), \tag{5.18}$$

and β_v and β_s are the distribution parameters for the volume and shear relaxations respectively.

To illustrate how K^* and G^* can be deconvoluted from the measured L^* values, the real and imaginary components of L^* measured for the CHMA:DGEBA system at 323K were analyzed by a reiterative procedure using various values of β_v, β_s, α and G_∞ and the measured values $\Delta L = 4.2$ GPa, $K_o = L_o = 2.8$ GPa. The values that fitted

the data in the complex plane plot of L″ against L′ were $\beta_v = \beta_s = 0.15$, $\tau_v/\tau_s = 8$ and $G_\infty = 1$ GPa. The calculated and measured L′ and L″ from the resolved K′, G′, K″ and G″ are shown as plots of L′ and L″ against n in Figure 5.15. Such deconvolution could also be done in terms of the stretched exponential decay function, outlined in Chapter II, and discussed in Section 5.3, for which β_v and β_s are equal to 0.29, but the complexity of such an analysis did not warrant further examination of the merit of the two descriptions for distribution of relaxation times. Furthermore, this analysis should be seen as instructive of the roles of K* and G* in determining L*, and not as a unique analysis of the data. Marvin and McKinney (1960) have shown a similar analysis of the L* spectra, but theirs was based on experimentally measurement of G* and L*. Nevertheless, Figures 5.15 (a) and (b) show a remarkable resemblance to their Figures 1 and 2.

For future work it would be useful to obtain data for L* and G* as a function of temperature both in the molecular liquid and fully polymerized states, as well as during isothermal reaction under isothermal conditions. This would allow for the contributions from both the bulk and shear components to be distinguished, while also providing insight and qualitative information about their relative contributions to the magnitude of the sub-T_g or β-relaxation process.

5.5 Relation Between the Dielectric and Ultrasonic Data.

Since the dielectric and ultrasonic polymerizations were carried out at the same temperatures for three of the measurements, it is possible to compare the results in
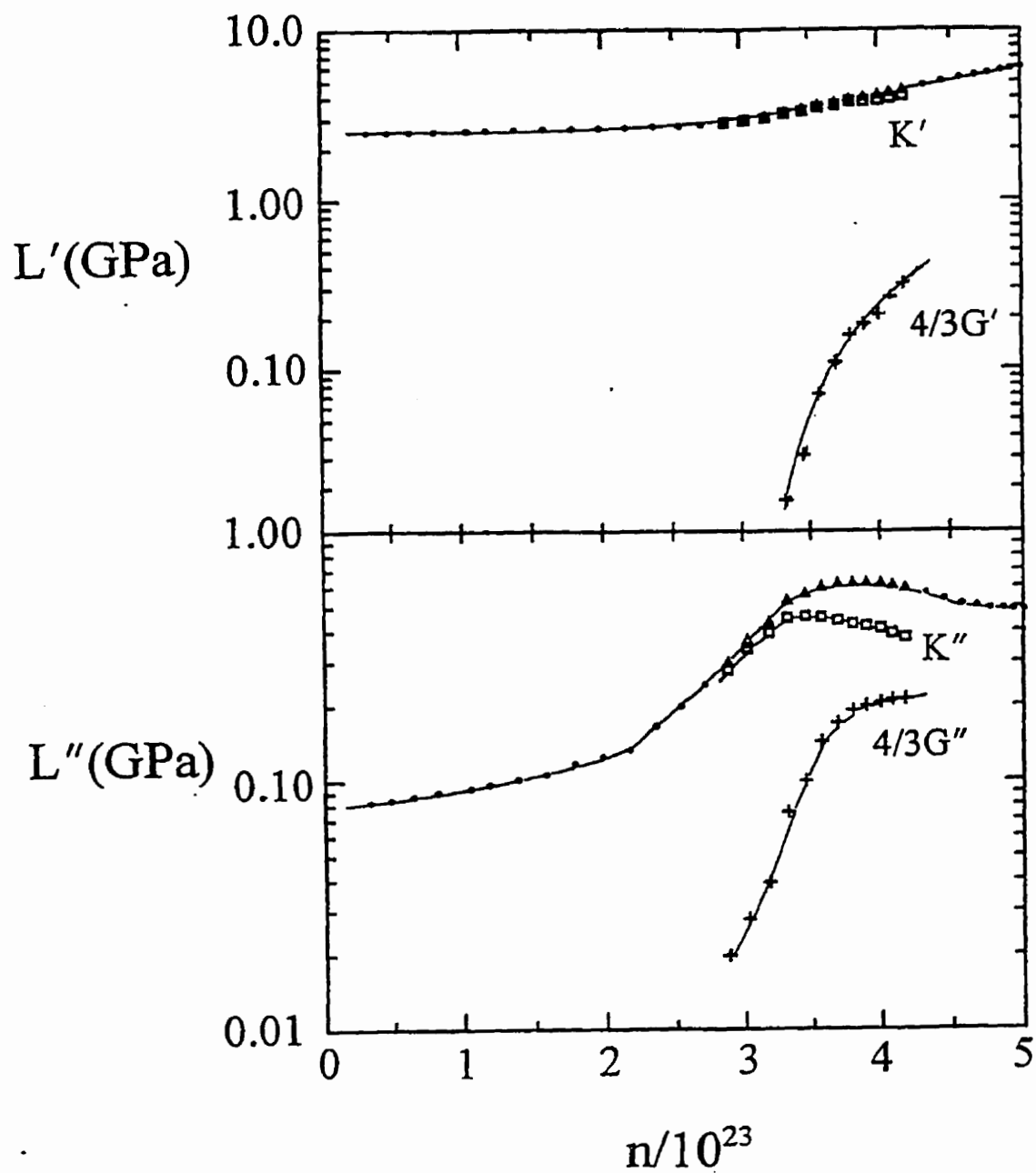
Figure 5.15: Plots of L′ and L″ against n based on contributions from both bulk and shear contributions, as discussed in section 5.4. K here refers to the contributions from the bulk modulus, and G, the contributions from the shear modulus. The solid line shows the sum of the two contributions.

terms of the relaxation times. To do this, the data for $<\tau>$ $(=\tau_0/\beta)\Gamma(1/\beta))$ obtained from the analyses of the dielectric and ultrasonic data, are replotted against the time of chemical reaction in Figures 5.16, 5.17 and 5.18 for the ANIL:DGEBA, CHMA:DGEBA and HMA:DGEBA mixtures, respectively, at the temperatures as listed on the plots. $<\tau>$ determined from both the longitudinal modulus and compliance data are included on the plots. These plots show that the values of $<\tau>$ from the longitudinal compliance formalism match closely with those from the dielectric analysis, where as those obtained from the longitudinal modulus data . While such agreement has been noted before in the literature (McCrum et al, 1967), it has previously only been seen for measurements of physically stable systems. The agreement between the $<\tau>$ is likely fortuitous rather than physical, since the relaxation mechanisms for mechanical and dielectric phenomena are not related (McCrum et al, 1967). However, from the perspective of materials processing, such a relation could allow for process control systems to be designed incorporating both measurement techniques.
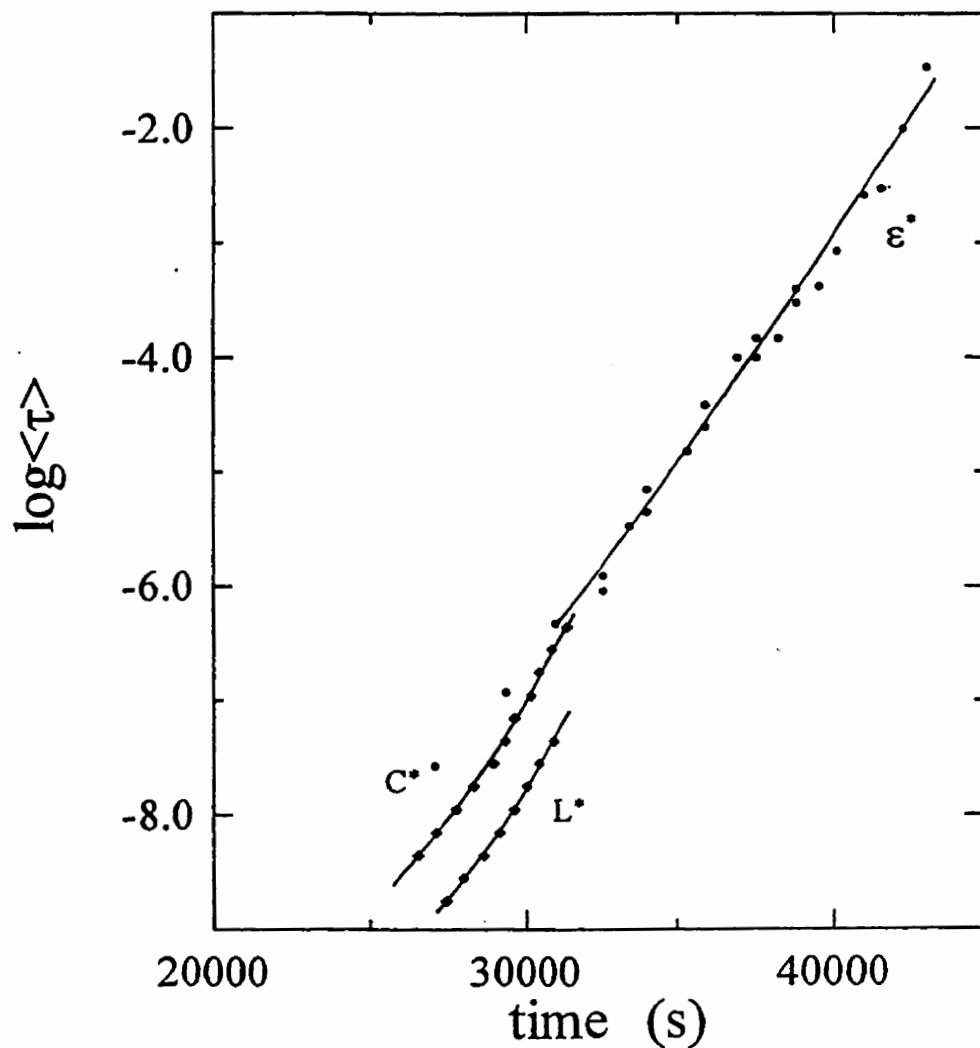
Figure 5.16: The relaxation time <τ> determined from the analysis of both the ultrasonic and dielectric measurements during the isothermal polymerization of the ANIL:DGEBA mixture at 333.4K is plotted against the time of chemical reaction. ε* refers to the dielectric data, L* the complex modulus data and C* the complex compliance data.

Figure 5.17: The relaxation time <τ> determined from the analysis of both the ultrasonic and dielectric measurements during the isothermal polymerization of the CHMA:DGEBA mixture at 313.4K is plotted against the time of chemical reaction. ε* refers to the dielectric data, L* the complex modulus data and C* the complex compliance data.
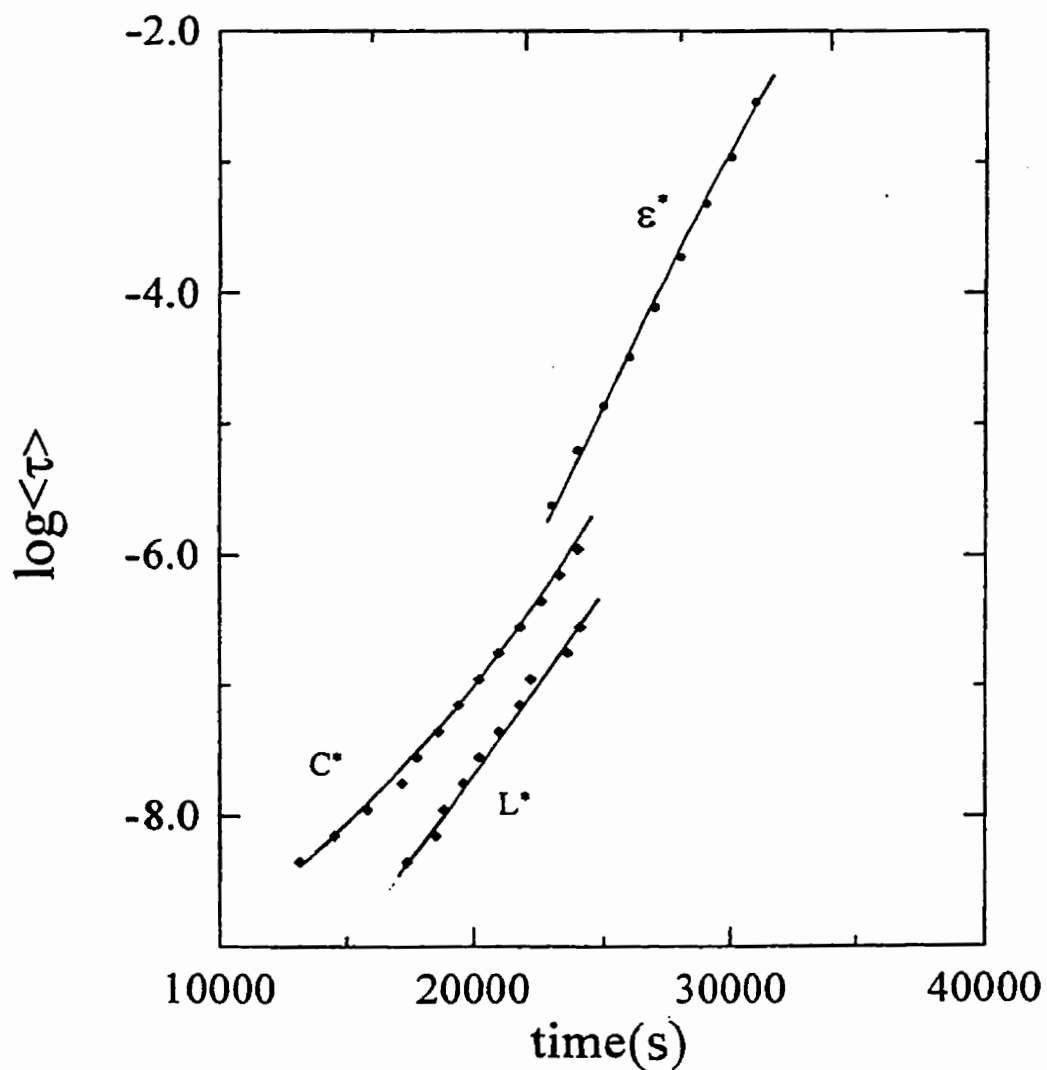
Figure 5.18: The relaxation time $\langle\tau\rangle$ determined from the analysis of both the ultrasonic and dielectric measurements during the isothermal polymerization of the HMA:DGEBA mixture at 300.1K is plotted against the time of chemical reaction. ε^* refers to the dielectric data, L^* the complex modulus data and C^* the complex compliance data.

CHAPTER VI: EVOLUTION OF LOCALIZED RELAXATION PROCESSES DURING A MACROMOLECULE'S GROWTH

6.1   Introduction.

It is generally known that all solid amorphous materials show dielectric and mechanical relaxations which are attributed to localized diffusion in an otherwise rigid matrix, or Johari-Goldstein relaxation. (This term is used to maintain a distinction between this relaxation process and the must faster relaxation process which is used in the development of mode-coupling theory and in its subsequent experimental tests, as for example done in recent reviews in Science by Angell (1995) and by Frick and Richter (1995)). The Johari-Goldstein relaxation is the faster atomic or molecular diffusion process by which a material partially relaxes the mechanical or electrical stress applied to it, without permanent deformation or charge transport.

In a recent theory for the rheology of molecular glasses and polymers developed by Cavaille et al (1989), low and high energy sites in the disordered structure are seen as structural defects where molecular motion is most probable, and therefore faster, because of the non-cooperative nature of the rotational-translational diffusion of atoms (Johari 1973; 1982), molecules or molecular segments at the defect sites. In this theory (Cavaille et al, 1989), the Johari-Goldstein relaxation is the zeroth order (n=0) motion of the hierarchy of motions beginning from the time corresponding to the localized diffusion at a certain temperature and extending to longer cooperative

diffusion of a large number of atoms or molecules in that structure at that temperature. Thus, the localized atomic or molecular diffusion acts as a precursor for the long-range diffusion that is manifested as the α-relaxation and leads ultimately to the large scale deformation or polarization of the amorphous solid.

Glassy states of rigid molecules as well as those of macromolecular materials of all types of structures show this relaxation with qualitatively similar features (Johari, 1973, McCrum et al, 1967). Nevertheless, their qualitative features in terms of the diffusion time, and temperature differ. So, as a macromolecule grows via addition reactions of its molecular components, the features of the Johari-Goldstein relaxation evolve from those of a vitrified molecular state to those of a vitrified macromolecular state, as the reaction progresses with time. The characteristics of this evolution, the details of the experiments done to observe them, the data analysis and conclusions of the study are described in this chapter, where a number of misconceptions on the subject, which have recently appeared in the literature, have been clarified. The text of this chapter is presented in terms of a paper published in the Journal of Chemical Physics, vol 103, pp 7611-7617 (1995), which follows:

before and after their polymerization

M. G. Parthun and G. P. Johari

Department of Materials Science and Engineering, McMaster University, Hamilton, Ontario L8S 4L7, Canada

Dipolar diffusion in the glassy and supercooled liquid states of 12 molecular substances and of their linear chain or network polymerized states formed by condensation polymerization at different temperatures and times have been studied by measuring the dielectric absorption for a fixed ac frequency of 1 kHz. The study showed that as the extent of polymerization increased with increasing isothermal temperature of polymerization, the sub-T_g relaxation peak due to localized molecular motions in the molecular state became gradually extinct, and a corresponding peak at a higher temperature evolved and reached its maximum height. The temperature of the sub-T_g relaxation peak in the polymerized state differed from that of the α-relaxation peak of the supercooled molecular liquid by as much as 70 K, but, in several cases, the two temperatures were similar. Reasons for the latter occurrence are given in phenomenological terms. It is concluded that the localized relaxation modes of the polar segments of the macromolecule are not related to the modes of molecular diffusion in the monomeric liquid state above its T_g. The localized relaxation characteristic of the glassy molecular state persists in the incompletely polymerized state, where it is seen as a γ-relaxation. © *1995 American Institute of Physics.*

I. INTRODUCTION

When a mechanical stress, or an electric field, is applied to an amorphous solid, it undergoes recoverable deformations, or electrical polarizations, of two types: The first is due to localized atomic diffusion within the otherwise rigid disordered structure, and the second is due to long-range atomic diffusion; the latter leads to a macroscopic deformation or viscous flow when the mechanical stress is sustained for an overly long duration.[1] The kinetics of both types of diffusion are time and temperature dependent. In the mechanical and dielectric spectrometry, the two effects are revealed as separate peaks in the energy absorption or relaxation spectrum, at a high frequency for the first and a low frequency for the second.[2–4]

The first, or faster process has been called the β-relaxation. (It is now often referred to as the Johari–Goldstein relaxation, as for example in Refs. 5 and 6, so that it can be distinguished from other relaxation processes deduced from neutron scattering measurements.[6]) The second, or slower process is generally referred to as the α-relaxation. In dielectric measurements of polymers or monomeric liquids made for a fixed sinusoidal frequency at different temperatures, their relaxation peaks are observed usually at a temperature below the calorimetric glass transition temperature, T_g, for localized atomic diffusion, and above T_g for the long-range atomic diffusion. In their absorption, or loss spectrum, the two peaks are separated in the frequency plane, but this separation is lessened as the temperature is increased.[2] In several cases,[3] the two peaks remain distinctly resolved even when the temperature is several degrees above T_g. A similar terminology is used for dielectric relaxations in orientationally disordered crystals,[7] in which molecules confined to lattice sites do not diffuse in a manner similar to that in liquids.

The two relaxations are observed generally when a liquid or orientationally disordered crystal is cooled, and, as observed for glycerol,[8] when a liquid is compressed at a fixed temperature. Both cooling and compression cause a decrease in the configurational contributions to the volume, enthalpy and entropy when the radial distribution function of the liquid, a measure of the packing density of atoms, reversibly changes. Our recent studies on a macromolecule's growth have shown that manifestly similar changes occur in both the thermodynamics and the relaxation kinetics when the number of covalent bonds formed is irreversibly and spontaneously increased by condensation reactions at a fixed temperature.[9] That is, as a macromolecule grows, the volume, enthalpy and entropy decrease continuously, the heat capacity decreases abruptly at the vitrification time, and a localized relaxation process, which is different from that observed in the original molecular liquid, comes into evidence as the slower relaxation becomes progressively more slow under isothermal conditions. Thus the plots of the two relaxation rates against the number of bonds formed (or the reaction time) obtained from measurements made during the course of the macromolecule's growth mimic the Arrhenius plots of the corresponding relaxation rates of the structurally invariant, unreacted molecular liquid.[10] This has led to an inference that the localized relaxation of the macromolecule is in some manner similar to the α-relaxation of the molecular liquid from which the macromolecule was formed,[11] particularly, when the temperatures of the two relaxation peaks measured for 1 kHz frequency are found to be closely similar, as in our recent studies.[12,13] This inference seems to put into question the validity of the proposed mechanism for sub-T_g relaxation in terms of a defect theory[14] according to which, the localized relaxation at defect sites in a disordered structure is considered as the zeroth order ($n=0$) motion of a hierarchy of motions, and thus the localized relaxation acts as a precursor of the α-relaxation or viscous flow of a

whether such an inference is meaningful. We do this here and conclude that the currently available data do not support the inference that the α-relaxation of the molecular liquid is the same as the sub-T_g relaxation of its polymerized state. The temperatures of the α-relaxation peak of the molecular liquid, and of the sub-T_g relaxation peak of its polymerized state, become similar when certain conditions cause the Arrhenius plots of the α and the sub-T_g relaxations in the two chemically distinct states of the same chemical constituents to cross each other.

II. EXPERIMENT

Ethylene diamine, propylene diamine, hexamethylene diamine, aniline, n-hexylamine, cyclohexylamine, n-octylamine, 4,4' diaminodiphenyl methane, 4,4' diamino-diphenyl sulfone and triethylene tetramine of >99% purity were purchased from Aldrich Chemicals. N,N'-dimethyl-benzylamine was a sample from a previous study by Alig et al.[15] Diglycidyl ether of bisphenol-A (DGEBA), Mw=380 and functionality (epoxy groups per molecule)=2, was donated by Shell Chemicals as EPONs 828 and 815. 4-4' diphenylcyanate dimethylmethane (DPDM), a difunctional cyanate, was donated by Rhone Poulenc, Kentucky. DGEBA used for polymerization with N,N' dimethylbenzylamine was a sample also from a previous study by Alig et al.[15] All chemicals were used without further purification. Accurately weighed amounts were mechanically mixed for 2 min in a glass container and then transferred to a 10 mm diameter glass container for all samples except the DPDM, which required no mixing and was melted at 373 K. An 18-plate miniature tunable capacitor, which acted as dielectric cell, was immersed in the liquid in the glass container, and the absence of bubbles between the capacitor plates ensured. A copper-constantan thermocouple junction was immersed in the liquid at a depth about 1 mm below the ceramic part of the miniature capacitor, and held at a fixed position in the vial by means of a cork stopper. In several of the studies, whose results are included here, the dielectric cell was a concentric electrode assembly which was hermetically sealed as described by Mangion and Johari.[16(a),(b)] The details of the dielectric measurements assembly, the thermostat, temperature controls and source of errors are given in earlier papers.[16(a),(b)]

Experiments were needed for obtaining information on how the kinetics of the localized motions changes when the temperature of polymerization is changed. Therefore, the dielectric properties of the unreacted DGEBA:ethylene diamine, DGEBA:propylene diamine and DGEBA:hexamethylene diamine (molar ratio 2:1) molecular liquids were first studied. Separate samples of the same molecular liquid were then polymerized by holding them isothermally for a certain time period. After this isothermal polymerization, each sample was rapidly cooled to 77 K, and its dielectric properties measured again from 77 K to about 320 K. The procedure was repeated with a new sample now kept at a different temperature, but for about the same time period as

FIG. 1. The dielectric loss, ϵ'', of the DGEBA:ethylene diamine mixture measured for 1 kHz frequency is plotted against temperature. Curve (a) is for the unreacted mixture, others are for the incompletely polymerized states obtained after reaction at a certain temperature (for a certain duration). (b) 296.2 K (41.9 ks), (c) 305.3 K (47.6 ks), (d) 313.7 K (36.5 ks), (e) 324.2 K (8.7 ks), (f) 335.3 K (10.0 ks), (g) 343.3 K (17.6 ks). Inset shows simulated data with $\tau_\alpha = 3.2 \times 10^{-60} \exp(270\,000/RT)$, $\tau_{sub-T} = 1 \times 10^{-13} \exp(28\,000/RT)$, $\Delta\epsilon_\alpha = 9 - 0.003T$, $\Delta\epsilon_{sub-T} = 0.3 + 0.0005T$, $\beta_\alpha = 0.4$, $\beta_{sub-T} = 0.2$, $(T > T_g)$ $\sigma_0 = 5 \exp(-41\,600/RT)$, $(T < T_g)$ $\sigma_0 = 1 \times 10^{-7} \exp(-8400/RT)$. Parameters are as discussed in the text. The solid line is the combined effects of dipolar relaxation and dc conductivity, and the dots are the respective low temperature sub-T_g relaxation and high temperature α relaxation.

before. Thus each molecular liquid was polymerized at six or more temperatures and in each case the dielectric relaxation of the product studied.

III. RESULTS

As the purpose here was to examine the features of localized relaxation in the glassy-molecular and -polymeric states, the results expressed in terms of the dielectric loss, ϵ'', against the temperature plots would seem to be sufficient. The ϵ'' peak height for a fixed frequency measurement at 1 kHz here is a measure of the strength of the relaxation, and its temperature a measure of its kinetics. The logarithmic scale plots of ϵ'' against the temperature for the molecular and partly polymerized states of the DGEBA mixtures with ethylene diamine, propylene diamine and hexamethylene diamine are shown in Figs. 1–3. The temperature and time conditions of polymerization, after which the properties were measured, are given in the figure captions.
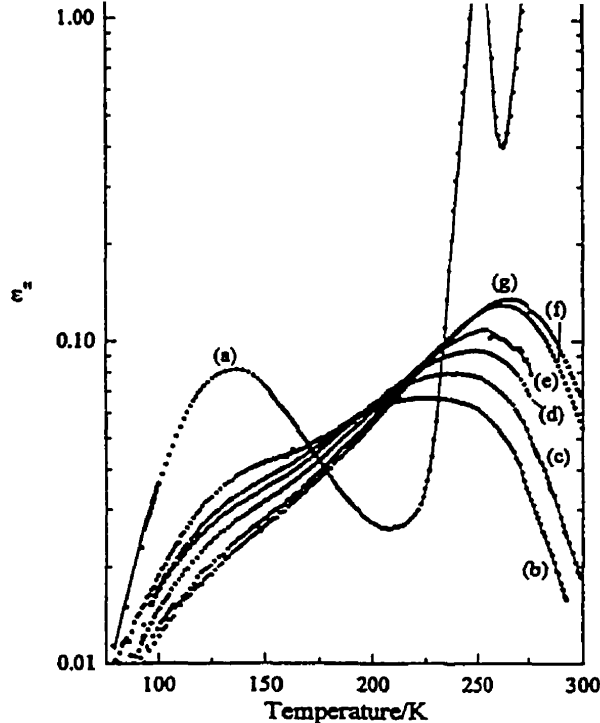
FIG. 2. The dielectric loss, ϵ'', of the DGEBA:propylene diamine mixture measured for 1 kHz frequency is plotted against temperature. Curve (a) is for the unreacted mixture, others are for the incompletely polymerized states obtained after reaction at a certain temperature (for a certain duration). (b) 294.9 K (65.0 ks), (c) 303.8 K (67.9 ks), (d) 315.5 K (70.9 ks), (e) 323.7 K (57.7 ks), (f) 335.0 K (57.9 ks), (g) 346.0 K (57.9 ks).
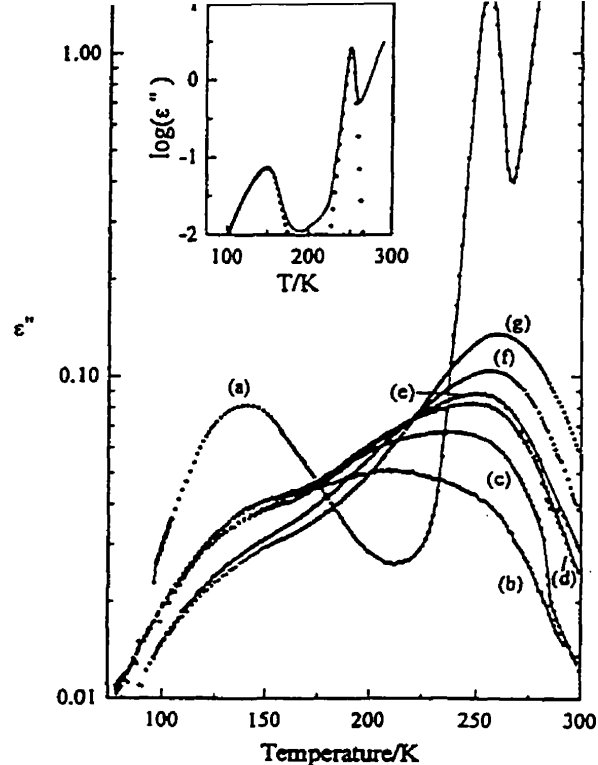
FIG. 3. The dielectric loss, ϵ'', of the DGEBA:hexamethylene diamine mixture measured for 1 kHz frequency is plotted against temperature. Curve (a) is for the unreacted mixture, others are for the incompletely polymerized states obtained after reaction at a certain temperature (for a certain duration). (b) 284.3 K (74.8 ks), (c) 296.5 K (59.0 ks), (d) 304.2 K (70.0 ks), (e) 312.3 K (41.6 ks), (f) 324.2 K (37.9 ks), (g) 336.5 K (33.0 ks).

The corresponding plots for the DGEBA mixture with N,N' dimethylbenzylamine, in which the amine acted as a catalyst and did not become part of the polymer network, are shown in Fig. 4. The ϵ'' plots for the stoichiometric (1:1 molar) DGEBA mixtures with aniline, cyclohexylamine, n-hexylamine and n-octylamine, both in their molecular [labeled (a)] and polymerized [labeled (b)] states, are shown in Fig. 5. The corresponding plots of the molecular and polymerized states of DPDM are shown in Fig. 6. All the plots for the molecular states show two ϵ'' relaxation peaks, one due to the low temperature localized relaxation and the second due to the long-range diffusion and relaxation in the vicinity of 250 K. The upswing of ϵ'' with increasing temperature, after the α- or high temperature-relaxation peak has appeared, is due to a rapid increase in the dc conductivity with temperature. ϵ'' plots of the partially polymerized states in Figs. 1–4 and 6 show two sub-T_g relaxation peaks, and in Fig. 5 show one localized or sub-T_g relaxation peak, and one α-relaxation peak at temperatures above 325 K. Here also the upswing of ϵ'' after the α-relaxation peak has appeared is due to the increase in dc conductivity with increase in temperature.

The essential information deduced from these plots is summarized in Table I. It contains values of the ϵ''-peak height and its temperature for the sub-T_g relaxation of the

molecular and polymerized states, and that of the α relaxation of the molecular liquid state. Reference is given when the data are taken from our previous or unpublished work, and the structural form of the polymer, network or linear chain (nw or lc), is indicated.

It must be noted that polymerization did not reach, nor is it expected to reach, (100%) completion in any of the studies but, as concluded before,[16(a),(b),17] the temperature of the sub-T_g relaxation peak reached a limiting high value. The ϵ''-peak height has been found to increase when chemical reactions predominate and to decrease when physical aging effects predominate,[18] thus producing a maximum in the plots of ϵ''-peak height against the combined reaction and aging time. The ϵ''-peak height given in Table I is therefore close to the value corresponding to this maximum. In several cases,[16(a),(b),17] a negligibly small amount of polymerization occurred during the mixing of the liquid when mixing was done at a high temperature so that the solid component could melt and facilitate mixing. The sub-T_g relaxation peak in such cases was smaller in magnitude than that for the unreacted molecular glass, and an additional plateaulike feature was seen at temperatures between the α- and sub-T_g relaxation peaks.
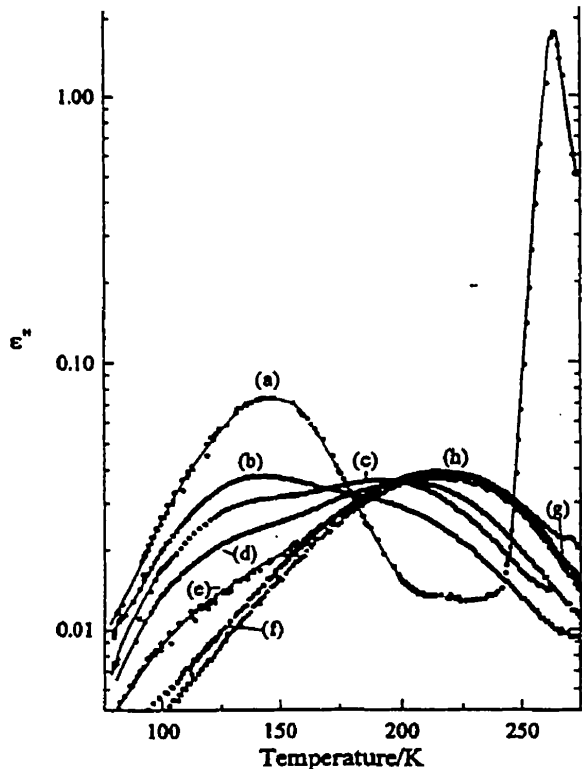
FIG. 4. The dielectric loss, ϵ'', of the DGEBA:N-N' dimethylbenzylamine mixture measured for 1 kHz frequency is plotted against temperature. Note that in this case the amine does not become part of the network structure; it merely acts as a catalyst. Curve (a) is for the unreacted mixture, others are for the incompletely polymerized states obtained after reaction at a certain temperature (for a certain duration). (b) 323.2 K (29.0 ks), (c) 332.2 K (17.7 ks), (d) 342.1 K (12.3 ks), (e) 355.5 K (8.2 ks), (f) 367.8 K (5.6 ks), (g) 380.2 K (5.45 ks), and (h) 391.8 K (6.20 ks). Data are replotted from Alig and Johari, Ref. 24.

FIG. 5. The dielectric loss, ϵ'', of the (i) DGEBA:aniline, (ii) DGEBA:cyclohexylamine, (iii) DGEBA:n-hexylamine, and (iv) DGEBA:n-octylamine mixtures measured for 1 kHz frequency is plotted against temperature. (a) the plots for the unreacted mixtures and (b) the mixtures after polymerization. The time and temperatures of polymerization for the fully reacted polymers were (i) 120 ks at 343.4 K, (ii) 120 ks at 313.4 K, (iii) 36 ks at 300.1 K + 86 ks at 400 K, and (iv) 36 ks at 300 K + 86 ks at 400 K. Curves for (i) have been shifted upwards by 6 decades, for (ii) by 4 decades and for (iii) by 2 decades, and their corresponding baselines drawn at $\epsilon''=0.01$. Data for the DGEBA:aniline polymer are replotted from Parthun and Johari, Ref. 12; those for the DGEBA:n-hexylamine from Johari and Pascheto, Ref. 13.

IV. DISCUSSION

We first discuss the relaxation features of the molecular states of the various liquids. Data in Table I and Figs. 1–5 show that there is a prominent relaxation peak in the temperature range 120–160 K and that there is an α-relaxation peak in the range 240–290 K for the various compositions, but no clear third peak, except for the plots of DGEBA:n-hexylamine in Fig. 5(iii)(a) (also see note to Ref. 13). Nevertheless, a small plateaulike feature appeared in the temperature range 200–225 K in Figs. 4(a) and 5(i)(a). This plateaulike feature seems to be associated with the distribution of α-relaxation times, and has been denoted by Colmenero et $al.$[19] as the α' process when observed in the thermally stimulated depolarization current measurements. Muzeau et $al.$[20] found similar plateaulike features in the mechanical loss measurements at 1 Hz frequency on rate heating poly(methyl methacrylate), which was rapidly cooled from above its T_g to 77 K before the dynamic mechanical measurements. The Muzeau et $al.$[20] studies and further studies[21] have shown that such peak- or plateaulike features

are spurious, as they are absent in slowly cooled or annealed samples, and therefore are not indicative of a separate relaxation process.

Additionally, since the magnitude of the plateau in Figs. 4(a)–5(i)(a) is small, it is likely a manifestation of the contribution from the dc conductivity, σ_0, and hence to ϵ'' ($=\sigma/\omega\epsilon_0$, where ϵ_0 is the permittivity in vacuum). To illustrate this, ϵ'' data was simulated assuming three contributions: a sub-T_g relaxation, an α relaxation and a dc conductivity. The relaxation time, τ, was assumed to follow an Arrhenius relation for both relaxation processes, as was σ_0. Since the relaxation spectrum for such systems is typically non-Debye, a Davidson–Cole[22] type distribution of the form,

$$\epsilon^* = \epsilon_\infty + \frac{\Delta\epsilon}{(1+i\omega\tau)^\beta},$$ (1)

was used, where ϵ_∞ is the high-frequency limit of the permittivity, $\Delta\epsilon$ the dielectric dispersion and ω the angular fre-
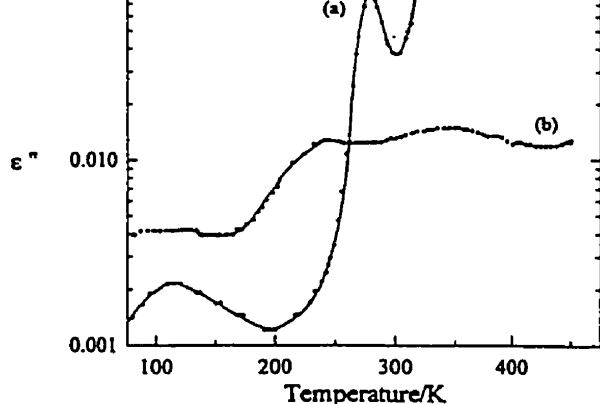
FIG. 6. The dielectric loss, ϵ'', of the DPDM measured for 1 kHz frequency is plotted against temperature. Curve (a) is for the unreacted mixture and (b) after polymerization at 450 K for 108 ks. The magnitude of the feature for the molecular state is lower than expected, possibly due to partial crystallinity. DPDM melts at 363 K.

quency, with the parameter β, denoting the skew of the distribution, which we assume to be independent of temperature. ϵ'' was calculated from,[22]

$$\epsilon'' = \Delta\epsilon[\cos\Phi]^\beta \sin(\Phi\beta); \quad \Phi = \arctan(\omega\tau). \quad (2)$$

To illustrate the effect of dc conductivity on the dielectric features such as those in Figs. 1–5, we calculate an ϵ'' curve with increasing temperature for a fixed frequency of 1 kHz. For this purpose, $\Delta\epsilon$ was assumed to increase linearly with increasing temperature for the sub-T_g-relaxation pro-

temperature dependence; one above T_g and a second below. The calculated plot of the logarithm of ϵ'' against temperature is shown in the inset of Fig. 1, with the parameters used for the simulation listed in the figure caption. The combined effects of both dc and dielectric relaxation show a plateau, similar to that seen in Figs. 4 and 5(i)(a). Therefore, we conclude that, as for other molecular liquids,[2,3] all liquids studied here have only one sub-T_g relaxation peak which is attributed to the localized motions in the otherwise rigid matrix of a glass (see also note to Ref. 13 regarding the spurious effect of a second peak below T_g in Fig. 5(iii)(a). This peak appears at different temperatures for different mixtures, but remains in the 120–160 K range.

We now discuss how the features of the sub-T_g relaxations change on increasing the isothermal temperature of polymerization. Figures 1–4 show that the features of the localized relaxation in the glassy state of the molecular liquid change in several ways as it is polymerized at different temperatures. The prominent peak at 120–160 K, which is characteristic of the molecular liquid, becomes gradually extinct. Concurrently, a new sub-T_g relaxation peak emerges at a higher temperature, grows, and shifts to a higher temperature still as the reaction temperature is increased. To help understand this effect of temperature, we consider how polymerization itself is affected by an increase in the temperature. It is generally recognized that increasing the reaction temperature has two effects on the polymerization kinetics: First the rate of reaction increases according to the Arrhenius rate constant equation ($k\propto\exp[-E/RT]$) and second, the viscosity of the liquid of a certain polymerized chemical structure

TABLE I. The temperature of the ϵ'' relaxation peak and its height (ϵ''_{max}) for the molecular and nearly fully polymerized states. References are given to those data taken from literature.

Substance	Temperature/K			ϵ''_{max}			Structure (nw/lc)
	α-peak (molec)	sub-T_g peak (molec)	sub-T_g peak (polym)	α-peak (molec)	sub-T_g peak (molec)	sub-T_g peak (polym)	
DGEBA:ethylene diamine	256	141	260	1.55	0.086	0.135	nw
DGEBA:propylene diamine	252	139	266	1.54	0.085	0.135	nw
DGEBA:hexamethylene diamine	249	140	262	1.64	0.081	0.142	nw
DGEBA:4,4' diaminodiphenyl methane [Ref. 16(b)]	272	142	265	1.57	0.046	0.097	nw
DGEBA:4,4' diaminodiphenyl sulfone [Ref. 16(b)]	290	148	250	4.81	0.053	0.051	nw
DGEBA:triethylene tetramine (Ref. 25)	269	157	296	1.24	0.066	0.253	nw
DPDM (Ref. 25)	279	124	352	0.078	0.002	0.014	nw
DGEBA:aniline (Ref. 12)	250	134	250	1.72	0.07	0.075	lc
DGEBA: cyclohexylamine (Ref. 25)	244	145	257	1.48	0.092	0.088	lc
DGEBA:n-hexylamine (Ref. 13)	241	120	242	1.41	0.032	0.056	lc
DGEBA:n-octylamine (Ref. 25)	256	137	229	0.94	0.041	0.040	lc
1.0 DGEBA:0.1 N-N' dimethylbenzylamine (Ref. 24)	264	149	214	1.75	0.074	0.039	nw

tion occurs after a greater extent of reaction at a higher temperature than at a lower temperature. These effects are different from those noted in the time-temperature-transformation diagrams, where the various phases' states are drawn schematically.[23] Thus the effects of a temperature increase, when the time allowed for the reaction is predetermined or limited, and the effects of increasing the time of reaction when the temperature is fixed are manifestly similar. Both underscore the importance of the extent of reaction or the number of covalent bonds formed in the chemical structure on the sub-T_g relaxations.

An increase in the number of covalent bonds formed not only decreases the height of the low temperature peak but also produces a new, higher temperature relaxation peak. The similarity of the observations in Figs. 1–6 against that in Fig. 5 in Ref. 16(b), confirms that the evolution of the sub-T_g-relaxation features in the structure formed after reaction at different temperatures of increasing magnitude is similar to that observed when the reaction time is increased and the temperature is kept fixed. The effect observed seems to transcend the details of the molecular nature of the liquid. As several of the polymers formed have network structures and others linear-chain structures, as indicated in Table I, it is also evident that the effect does not depend upon the nature of the polymeric structure formed, but depends only on the number of covalent bonds and the hindrance to dipolar reorientation.

In our earlier studies,[16(a),(b),17,18] it was shown that an increase in the reaction time at a constant temperature tends to increase the height of the sub-T_g-relaxation peak, and that physical ageing tends to decrease it. Thus after a certain time of reaction followed by annealing, the latter of the two effects dominates and the peak height decreases with the annealing time. References 16(a),(b), 17, and 18 may be consulted for a detailed discussion of the effect. Here, it seems sufficient to compare the peak heights measured before and after the polymerization, even though the extent of polymerization is unknown in several cases, and it is not certain whether or not annealing or physical aging of the polymer has decreased the peak height.

The data in Table I clearly show that the temperature of the α-relaxation peak of the molecular liquid mixture, which varies from one type to another, is significantly different from the temperature of the sub-T_g-relaxation peak in all cases, being as much as 50 K higher for DGEBA:N,N' dimethylbenzylamine and 73 K lower for DPDM, and that no relation seems to exist between this difference and the chemical nature of the substance. This alone indicates that molecular diffusion in the supercooled molecular liquid does not become the local mode of segmental motion in the glassy polymer formed on condensation reaction. Despite that, there may be conditions for which the α-relaxation peak of some molecular liquids can appear at a temperature closer to that of the sub-T_g-relaxation peak of its polymerized state. We discuss these conditions in the following.

Figure 7 is an illustration of how the rates of the α-relaxation and sub-T_g-relaxation may be compared. Here
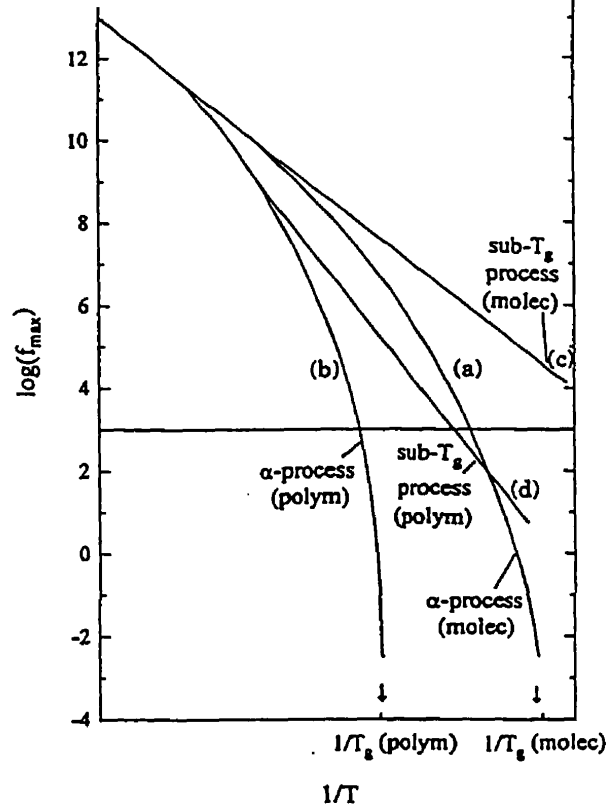
FIG. 7. An illustration for the variation of the α- and sub-T_g-relaxation rates with the reciprocal of temperature. Curve (a) is the rate of the α relaxation of the unreacted molecular liquid, curve (b), that of its fully polymerized state. Curve (c) is the rate of the sub-T_g relaxation of the molecular liquid state and curve (d) that of its fully reacted state. Note that the prominent sub-T_g relaxation of the molecular liquid becomes what is known as the γ-relaxation in the polymer. The horizontal line is drawn for 1 kHz frequency.

the rates of both processes, as given by the peak frequency of ϵ'', in the molecular and the polymer states are plotted against the reciprocal temperature. Curve (a) illustrates the change of the α-relaxation rate of the molecular liquid and curve (b) that of its polymerized state. Curve (c) illustrates the change of the sub-T_g-relaxation rate of the molecular liquid and curve (d) of that of its polymerized state. The temperature where curve (a) and curve (d) cross over is one at which the relaxation rates of the two different processes in two different states would be the same. The horizontal line in Fig. 7, is drawn for a fixed frequency of 1 kHz and is shown so as to lie above the crossover point of curve (a) and curve (d), but it may lie below the crossover point. In this illustration, the temperature of the relaxation peak for the α process of the molecular liquid is lower than that of the sub-T_g process of the glassy polymer. But, depending on the frequency used, the temperature of the sub-T_g-relaxation peak of the polymerized state may be the same, higher or lower than the temperature of the α-relaxation peak of the unreacted molecular liquid. Furthermore, the relaxation rate at which the two curves cross over may itself vary from one substance to another. As is seen in Table I, the temperature of the

molecular liquid from which the polymer is formed, and for one it is the same. For the remaining seven cases the former is higher than the latter. So, the crossover occurs at a lower relaxation rate than 10^3 Hz as illustrated in Fig. 7 for four of the systems, at 10^3 Hz for one and higher than 10^3 for the remainder. For several cases, particularly, DGEBA-$N.N'$ dimethylbenzylamine mixture and the DPDM, the crossover occurs at a much larger difference between the temperatures of the α relaxation of the supercooled liquid and of the sub-T_g-relaxation peak of its polymerized state. Thus the mere coincidence of the two such temperatures measured only for a single frequency does not indicate that the underlying processes have a single origin.

As demonstrated before (e.g., in Figs. 2 and 5, Tables I and II in Ref. 16(b), and Fig. 8 in Ref. 24), the sub-T_g-relaxation peak of the molecular liquid does not significantly shift in the temperature plane as the liquid is polymerized, only its height decreases. This has been confirmed by Cassettari et al.,[10] who did dielectric studies at microwave frequencies. So, the sub-T_g-relaxation peak observed for the polymerized state neither involves the same modes of motion, albeit more restricted, as the α-relaxation of its unreacted molecular liquid, nor does it correspond to the sub-T_g-relaxation observed for the molecular glass. We also view the sub-T_g-relaxation originally of the glassy molecular liquid as the γ-relaxation that persists in its incompletely polymerized state, as has been noted in several earlier papers,[16(a),(b),17] and hope to improve on this picture in the future.

[1] For a review, see G. P. Johari, in *Plastic Deformation of Amorphous and Semi-Crystalline Materials*, 1982, Les Houches Lectures, edited by C. G'sell and J. Perez (Les Editions de Physique, Paris, 1982), pp. 109-141.

[2] G. P. Johari and M. Goldstein, J. Chem. Phys. 53, 2372 (1970).

[3] G. P. Johari, Faraday Symp. Chem. Soc. 6, 42 (1972); J. Chem. Phys. 58, 1766 (1973); Polymer 27, 866 (1986).

[4] Richert and A. Blumen (Springer-Verlag, Berlin, 1994), pp. 309-330.

[5] C. A. Angel, Science 267, 1924 (1995).

[6] B. Frick and D. Richter, Science 267, 1939 (1995).

[7] G. P. Johari, Ann. N.Y. Acad. Sci. 279, 117 (1976).

[8] G. P. Johari and E. Whalley, Faraday Symp. Chem. Soc. 6, 23 (1972).

[9] For a review see G. P. Johari, in *Disorder Effects on Relaxation Processes*, edited by R. Richert and A. Blumen (Springer-Verlag, Berlin, 1994), pp. 627-656.

[10] M. Cassettari, G. Salvetti, E. Tombari, S. Veronesi, and G. P. Johari, J. Mol. Liq. 56, 141 (1993); J. Noncryst. Solids 172-174, 554 (1994).

[11] Discussion at the Dielectric Society Meeting on, "Impedance Spectroscopy at Electrodes and Interfaces" held at the University of Kent, U.K., 10-12, April (1995); see also the abstract entitled, "Dielectric Relaxation Spectroscopy of Polymerizing Systems," by G. Williams, C. Duch, J. Fournier, S. Andrews, and I. Smith in the book of abstracts of the papers presented at that meeting.

[12] M. G. Parthun and G. P. Johari, J. Chem. Phys. 103, 440 (1995).

[13] G. P. Johari and W. Pascheto, J. Chem. Soc. Faraday Trans. 91, 343 (1995). Recent calorimetric studies of a 1:1 mixture of DGEBA:n-hexylamine have shown that the mixture partly crystallizes on cooling, and that the ϵ' peak and ϵ' rise at ca. 175 K is, as suspected before, due to partial melting of the sample on heating (Ref. 25). This peak, which appears in Fig. 1(a) in Ref. 13 and Fig. 5iii(a) here, is spurious.

[14] J. Y. Cavaille, J. Perez, and G. P. Johari, Phys. Rev. B 39, 2411 (1989).

[15] I. Alig, K. G. Häusler, K. Nanke, E. Domaritius, and M. Fedke, Acta. Polym. 40, 590 (1989).

[16] (a) M. B. M. Mangion and G. P. Johari, Macromolecules, 23, 3687 (1990); (b) J. Polym. Sci. B, Polym. Phys. 29, 437 (1991).

[17] M. B. M. Mangion, M. Wang, and G. P. Johari, J. Polym. Sci. B, Polym. Phys. 30, 445 (1992).

[18] D. Sidebottom and G. P. Johari, Chem. Phys. 147, 205 (1990).

[19] J. Colmenero, A. Alegria, J. M. Alberdi, J. J. del Val, and J. Ucar, Phys. Rev. B 35, 3995 (1987).

[20] E. Muzeau, J. Y. Cavaille, R. Vassoille, J. Perez, and G. P. Johari, Macromolecules 25, 5108 (1992).

[21] E. Muzeau, G. Vigier, and R. Vassoile, J. Noncryst. Solids 172-174, 575 (1994).

[22] D. W. Davidson and R. H. Cole, J. Chem. Phys. 19, 1484 (1951).

[23] M. T. Aronhime and J. K. Gillham, Adv. Polym. Sci. 78, 83 (1986).

[24] I. Alig and G. P. Johari, J. Polym. Sci. B, Polym. Phys. 31, 299 (1993).

[25] Unpublished data from Johari and co-workers.

CHAPTER VII

CONCLUSIONS

The experiments, data analysis and the discussion on the calorimetric, dielectric and ultrasonic studies presented here have led to the following conclusions:

Irreversible changes in the complex permittivity that occur with increase in the number of covalent bonds are phenomenologically similar to the reversible changes in the complex permittivity observed generally on supercooling of the liquid. There is an equivalence in terms of the relaxation time and its distribution when either covalent bonds are formed during polymerization or the liquid is cooled. The static permittivity changes differently in the two cases, decreasing in the former and increasing in the latter.

The distribution of relaxation times of the unreacted molecular liquid was less than that of the polymerized product, and remained constant over a relatively narrow range of temperature. For the ANIL:DGEBA, CHMA;DGEBA and HMA:DGEBA mixtures studied, the breadth of the distribution remained essentially constant during polymerization.

The relaxation time increased in a sigmoidal manner, and the static permittivity decreased towards a limiting value as n increased. As n increased, a second relaxation process, named here the α-relaxation process, separated from the main or sub T_g-

relaxation process, and shifted to the lower frequency side of the spectra. This behaviour is remarkably similar to that observed on supercooling molecular and polymeric liquids.

Measurement of velocity and attenuation of the ultrasonic waves in a liquid in which molecules grow in size irreversibly with time, yielded revealing information on the molecular dynamics of liquid as it approached vitrification at a fixed temperature. In particular, the real and imaginary components of the complex longitudinal moduli and compliance changed from liquid-like to solid-like values as the relaxation time increased irreversibly with increasing molecular size. The phenomenology of this process is analogous to that of a relaxation process measured for a structurally invariant liquid either by increasing the frequency at fixed temperatures or alternately by decreasing its temperature and measuring at a fixed frequency, and is analogous to the behaviour observed in the dielectric studies.

The study revealed that the unimodal, asymmetric distribution of relaxation times splits into a bimodal distribution of α- and sub T_g-processes, each contributing to the change in the elastic or mechanical properties of the liquid as the size of its molecules grows. The predominant contribution to the modulus was associated with bulk rather than shear deformability.

A comparison of the dielectric relaxation features of 12 polymerizing liquids, of differing chemistry and physical structure in the polymerized state as they underwent isothermal polymerization at different isothermal temperatures showed that the effects of

a temperature increase, when the time allowed for the reaction is predetermined or limited, and the effects of increasing the time of reaction when the temperature is fixed, were manifestly similar.

An increase in the number of covalent bonds formed not only decreased the height of the low temperature peak but also produced a new, higher-temperature relaxation peak. This confirmed that the evolution of the sub-T_g relaxation features in the structure formed after reaction at different temperatures of increasing magnitude was similar to that observed with increase in the reaction time when the temperature is kept fixed. The effect observed seems to transcend the details of the molecular nature of the liquid. As several of the polymers formed had network structures and others linear-chain structures it was also evident that the effect does not depend upon the nature of the polymeric structure formed, but depended only on the number of covalent bonds and the hinderance to dipolar reorientation. The sub-T_g relaxation peak observed for the polymerized state neither involved the same modes of motion, albeit more restricted, as the α-relaxation of its unreacted molecular liquid, nor did it correspond to the sub-T_g relaxation observed for the molecular glass.

REFERENCES

Alig, I, Steiber, F., Wartewig S., Polymer, 1988, 29, 975.

Alig, I., Lellinger, D., Nanke, K., Rizos, A. and Fytas, G., J. Appl. Polym. Sci., 1992, 44, 829.

Alig. I., Lellinger, D. and Johari, G.P., J. Polym. Sci. Part B: Poly. Phys, 1992, 30, 791.

Alig, I. Nanke, K. and Johari, G.P., 1994, J. Polym. Sci. Part B: Polym. Phys., 32, 835.

Alig, I. and Johari, G.P., 1993, J. Polym. Sci. B, Polym. Phys., 31, 299.

Alig, I., Junker, M., Jenninger, W. and Frisch, H.F., 1995, Europhys. Conf. Abstr. 19D.

Angell, C.A., Science, 1995, 267, 1924.

Barlow, A.J. and Erginsav, A., 1972, Proc. R. Soc. Lond. A., 327, 175.

Barlow, A.J. and Erginsav, A., 1975, Polymer, 16, 110.

Barton, J.M., 1985, Adv. Polym. Sci., 72, 111.

Bidstrup, S.A., Sheppard, N.F. and Senturia, S.D., 1989, Polym. Eng. Sci., 29, 325.

Cassettari, M., Salvetti, G., Tombari, E. and Johari, G.P., 1993, J. Polym. Sci., B, Polym. Phys., 31, 199; 1994, Physica A, 201, 95.

Cavaille, J.Y., Perez, J. and Johari, G.P., 1989, Phys. Rev. B, 39, 4411.

Charlesworth, J.M., Polym. Eng. and Sci., 1988, 28, 221, and references therein.

Chern, C-S. and Poehlein, G.W., 1987, Polym. Eng. and Sci., 27, 788.

Choy, I.-C. and Plazek, D.J., 1986, J. Polym. Sci. Part B: Polym. Phys., 24, 1303.

Cole, K.S. and Cole, R.H., 1941, J. Chem. Phys., 9, 341.

Cole, R.H. and Tombari, E., 1991, J. Noncrystall. Solids, 131-133, 969.

Colemenero, J., Alegria, A., Alberdi, J.M., del Val, J.J. and Ucar, J., 1987, Phys. Rev. B, 35, 3995.

Cracknell, A.P., Ultrasonics, Wykeham Publication Ltd., London, 1980.

Daniel, V.V., Dielectric Relaxation, Academic Press, London and New York, 1967.

Davidson D. W. and Cole, R. H., 1950, J. Chem. Phys. 18, 1417.

Davidson D. W. and Cole, R. H., 1951, J. Chem. Phys. 19, 1484.

Debye, P., 1929, Polar Molecules, Chem. Catalogue, N.Y.

Deng, Y. and Martin, G.C., 1994, J. Polym. Sci.: Part B: Polym. Phys., 32, 2115.

Dishon, M., Weiss, G.H. and Bendler, J.T., 1985, J. Res. Natl. Bur. Stand., 90, 27.

Djarbourov, M., 1988, Contemp. Phys., 29, 273.

Dusek, K., 1986, Adv. Polym. Sci. 78, 1.

Ellis, B. in Chemistry and Technology of Epoxy Resins, (Chapman and Hall, London, 1993) p. 1.

Fuoss, R.M. and Kirkwood, J.G., 1941, J. Amer. Chem. Soc., 63, 369.

Frohlich, H., Theory of Dielectrics, (Clarendon Press, Oxford, 1949).

Gillham, J.K., 1986, Adv. Polym. Sci., 78, 83.

Gupta, A., Macromolecules, 1991, 24, 3459.

Hamon, B.V., 1952, Proc. IEEE, 99, pt II, 291.

Havriliak, S. and Negami, S., 1966, J. Polym. Sci.: Part C, 14, 99.

Horie, K., Hiura, H., Sawada, M., Mita, I. and Kambe, H., 1970, J. Polym. Sci.: Part A1, 8, 1357.

Hopkinson, J., 1877. Phil. Trans. Royal Soc., 167, 599.

Hureaux, C. and Sellaima, E., 1973, C.R. Acad. Sci. Paris, Part B, 227, 691.

Johari, G.P., 1973, J. Chem. Phys., 58, 1744.

Johari, G.P. in Plastic Deformation of Amorphous and Semi-crystalline Materials, eds. C. G'sell and J. Perez (Les Editions de Physique, PAris, 1982) p. 109.

Johari, G.P. in Chemistry and Technology of Epoxy Resins, ed. B. Ellis, (Chapman and Hall, London, 1993) p. 175.

Johari, G.P., *Dynamics of Irreversibly Forming Macromolecules*, in Disorder Effects in Relaxation Processes, ed. A. Blumen and R. Richert (Springer-Verlag, 1994(a)) p. 627.

Johari, G.P., J. Chem. Soc. Faraday Trans., 1994(b), 90, 883.

Johari, G.P. and Goldstein, M., 1970, J. Chem. Phys., 53, 2372.

Johari, G.P. and Smyth, C.P., 1972, J. Chem. Phys., 56, 4411.

Johari, G.P. and Pathmanathan, K., 1988, Phys. Chem. Glasses, 29, 219.

Johari, G.P. and Mangion, M.B.M., 1991, J. Noncryst. Solids, 131, 921.

Johari, G.P., Wasylyshyn, D.A., and Jain, S.K., 1994, J. Chem. Soc. Faraday Trans., .

Johari, G.P. and Pascheto, W., 1995, J. Chem. Soc. Faraday Trans., 91, 343.

Johnson, J.F. and Cole, R.H., 1951, J. Amer. Chem. Soc., 73, 4536.

Khanna, U. and Chanda, M., 1993, J. Appl. Polym. Sci., 49, 319.

Kohlrausch, R., 1854, Ann. Phyz. (Leipzig), 91, 179.

Kranbuehl, D.E., Delos, S., Hoff, M. and Haverty, P., 1989, Polym. Eng. Sci., <u>29</u>, 285.

Kranbuehl, D.E., 1991, J. Noncrystal. Solids, <u>131-134</u>, 930.

Lairez, D., Emery, J.R., Durand, D. and Pethrick, R.A., 1992, Macromolecules, <u>25</u>, 7208.

Lindsey, C.P. and Patterson, G.D., 1980, J. Chem. Phys., <u>73</u>, 3348.

Litovitz, T.A., Lyon, T. and Peselnick, L., 1954, J. Chem. Phys., <u>26</u>, 566.

Litovitz, T.A. and Davis, C.M., in <u>Physical Acoustics</u>, editor W.P. Mason, Academic Press, 1965, p. 281.

McCrum, N.G., Read, B.E. and Williams, G., 1967, <u>Anelastic and Dielectric Effects in Polymeric Solids</u>, Wiley, New York.

Macdonald, J.R. (editor), <u>Impedence Spectroscopy-Emphasizing Solid Materials and Systems</u>, Wiley-Interscience, New York, 1987.

Macedo, P.B., Moynihan, C.T. and Bose, R., 1972, Phys. Chem. Glasses, <u>13</u>, 171.

Mangion, M.B.M. and Johari, G.P., 1990(a), J. Polym. Sci. **B**, Polym. Phys., <u>28</u>, 1621.

Mangion, M.B.M. and Johari, G.P., 1990(b), Macromolecules, <u>27</u>, 3687.

Mangion, M.B.M. and Johari, G.P., 1991(a), Polymer, <u>32</u>, 2747.

Mangion, M.B.M. and Johari, G.P.,1991(b), J. Polym. Sci. **B**, Polym. Phys., <u>29</u>, 1117.

Mangion, M.B.M. and Johari, G.P.,1991(c), J. Polym. Sci. **B**, Polym. Phys., <u>29</u>, 1127.

Mangion, M.B.M. and Johari, G.P., 1991(d), J. Polym. Sci. **B**, Polym. Phys., <u>29</u>, 437.

Mangion, M.B.M. Wang, M. and Johari, G.P., 1992, J. Polym. Sci. **B**, Polym. Phys., **30**, 445.

May, C.A. and Tanaka, Y. eds., <u>Epoxy Resins. Chemistry and Technology</u>, Marcel Dekker, New York, 1973.

Meier, G., Hagenah, J.U., Wang, C.H., Fytas, G. and Fischer, E.W., 1987, Polymer.

Meister, R., Marhoeffer, C.J., Sciamand, R., Cotter, L., and Litovitz, T., 1960, J. Appl. Phys., <u>31</u>, 854.

Miexner, J., Ann. Physik, 1934, <u>43</u>, 470; Acustica, 1952, <u>2</u>, 101; Kolloid-Zt, 1953, <u>134</u>, 47; Z. Naturforsch, 1954, <u>9a</u>, 654.

Muzeau, E., Cavaille, J.Y., Perez, J., and Johari, G.P., 1992, Macromolecules, <u>25</u>, 5108.

Muzeau, E., Vigier, G. and Vassoille, R., 1994, J. Noncryst. Solids, <u>172-174</u>, 575.

Mikolajzak, G., Cavaille, J.Y. and Johari, G.P., Polymer, 1987, <u>28</u>, 2023.

Moynihan, C.T., Boesch, L.P. and Laberge, N.L., 1973, Phys. Chem. Glasses, <u>14</u>, 122.

Osei-Owusu, A., Martin, G.C. and Gotro, J.T., 1992, Polym. Eng. Sci., <u>32</u>, 535.

Papidakis, E.R., 1974, J. Appl. Phys., <u>45</u>, 1218.

Parthun, M.G. and Johari, G.P., 1992(a) J. Polym. Sci. <u>B</u>, Polym. Phys., <u>30</u>, 655.

Parthun, M.G. and Johari, G.P., 1992(b), Macromolecules, <u>25</u>, 3149; 1992(c), <u>25</u>, 3254.

Parthun, M.G. and Johari, G.P., 1995(a), J. Chem. Soc. Faraday Trans. <u>91</u>, 329. Eqn(16) for the definition of K should not have the hyphen sign.

Parthun, M.G. and Johari, G.P., 1995(b), J. Chem. Phys, <u>102</u>, 6301.

Parthun, M.G. and Johari, G.P., 1995(c), J. Chem. Phys., 103, 440. On p. 448, $TS_{conf}=0$ should be read as $TS_{conf}=\infty$

Parthun, M.G. and Johari, G.P., 1995(d), J. Chem. Phys., 103, 7611.

Parthun, M.G., Wasylyshyn, D.A. and Johari, G.P., J. Mol. Liq., 1996, 69, 219.

Pascheto, W., Parthun, M.G., Hallbrucker, A. and Johari, G.P., 1994, J. Noncrystal. Solids, 171, 183.

Perkin-Elmer Corporation, 1970, Thermal Analysis Newsletter, 9.

Pethrick, R.A., 1973, J. Macromol. Sci. - Revs. Macromol. Chem., C9, 91.

Senturia, S. and Sheppard, N.F., Adv. Polym. Sci., 1986, 80, 1, and references therein.

Sheppard, N.F. and Senturia, S.D, 1986, Polym. Eng. Sci., 26, 354.

Sidebottom, D.L. and Johari, G.P., 1990, Chem. Phys., 147, 205.

Sidebottom, D.L., 1994, Phys. Rev. E, 48, 391.

Sofer, G.A. and Hauser, E.A., 1952, J. Polym. Sci., 8, 611.

Stern, F., 1963, Solid St. Phys., 15, 299.

Taskoprulu, N.S., Barlow, A.J. and Lamb, J., 1961, J. Acoust. Soc. Amer, 33, 278.

Tombari, E. and Cole, R.H., 1991, J. Noncryst. Solids, 131-133, 969.

Tombari, E. and Johari, G.P., 1992, J. Chem. Pys., 97, 6677.

Tombari, E. and Johari, G.P., 1993, J. Chem.Soc., Faraday Trans., 89, 2477.

Wagner, K.W., 1913, Ann der Physik, 40, 817.

Wasylyshyn, D.A., Parthun, M.G. and Johari, G.P., 1996, J. Mol. Liq., 69, 283.

Wasylyshyn, D.A. and Johari, G.P., 1996, J. Chem. Phys., submitted.

Weiss, G.H., Bendler, J.T. and Dishon, M., 1985, J. Chem. Phys., 83, 1424.

Whitehead, J.B. and Banos, A., 1932, Trans. AIEE, 51, 392.

Williams, G. and Watts, D.C., 1970, Trans. Faraday Soc., 66, 80.

Williams, G., Chem. Rev., 1972, 72, 56.

Williamson, R.C., 1969, J. Acoust. Soc. Amer., 45, 1251.

Yeager, W.A., 1936, Physica, 7, 434.

APPENDIX I: LIST OF SYMBOLS

Constants

ε_o: permittivity in vacuum (8.8514 pF/m)

N_A: Avogadro Number (6.023×10^{23} atoms/mol)

R: gas constant (8.31433 J/K/mol)

i: $\sqrt{-1}$

π: pi = (3.1415927..)

Symbols

δ: phase angle lag (rad)

$\underline{E}$:   magnitude of applied sinusoidal electric field

$\underline{D}$:   charge displacement of applied sinusoidal electric field

f: frequency (Hz)

ω: angular frequency ($2\pi f$)

P(t):   time dependent electrical polarization

P_∞:   instantaneous electrical polarization

P_o: limiting electrical polarization

$\Phi(t)$:   time-dependent relaxation function for polarization

ε_s: static permittivity

ε_∞:   high frequency limiting permittivity

$\Delta\varepsilon$:   dielectric dispersion = $(\varepsilon_s - \varepsilon_\infty)$

τ: relaxation time (s)

τ_o: characteristic relaxation time (s)

$\langle\tau\rangle$:   average relaxation time (s)

β_{cd}:   Davidson-Cole distribution parameter

β:	stretched exponential distribution parameter
I_σ:	current due to ionic motion
G:	bulk conductance (S/m, or $Ohm^{-1}m^{-1}$)
V:	applied voltage
σ:	conductivity (S/m, or $Ohm^{-1}m^{-1}$)
σ_o:	direct current (dc) conductivity (S/m, or $Ohm^{-1}m^{-1}$)
C_o:	capacitance in vacuum (F)
C:	capacitance of sample (F)
Cp:	capacitance of a capacitor in parallel configuration (F)
Rp:	resistance of a resistor in parallel configuration (Ohm)
Z_x:	resistance of unknown in digibridge
e_1, e_2:	voltages measured in digibridge
C_p:	heat capacity (J/mol)
H:	enthalpy (J)
v:	velocity of sound pulse (m/s)
I:	intensity of sound pulse
α:	attenuation of sound pulse (Nep/m)
η:	viscosity (Poise)
ρ:	density (kg/m^3)
P:	compressional pressure stress (Pa)
S:	compressional pressure strain
K:	compressional modulus (Pa)
K_o:	limiting low frequency compressional modulus (Pa)
K_∞:	limiting high frequency compressional modulus (Pa)

G:	shear modulus (Pa)
G_∞:	limiting high frequency shear modulus (Pa)
L:	longitudinal modulus (Pa)
C:	longitudinal compliance (1/Pa)
λ:	wavelength (m^{-1})

Functions

| $\Gamma(x)$: | gamma function of x |
| L(x): | Laplace Transform of x |

APPENDIX II: METHOD FOR FITTING DATA

An important component of the work involved the fitting of the dielectric and ultrasonic data according to equations based upon a stretched exponential form of the relaxation function given by,

$$\Phi(t) = \exp\left[-(t/\tau_o)^{\gamma}\right],$$

(A.1)

where τ_o is the characteristic relaxation time, and γ a parameter that characterizes the breadth of the relaxation. Eqn. (A.1) is used in describing the fit to the data obtained for one frequency of measurement as a function of increasing time of reaction.

To describe the method, dielectric data will be considered, but it should be noted that the analysis of ultrasonic data is identical in method.

In Chapter II, the Boltzmann superposition principle was used to show that the complex permittivity, ε^*, can be written as,

$$\varepsilon^*(\omega\tau_o) = \varepsilon_\infty + (\varepsilon_S - \varepsilon_\infty) \int_0^\infty e^{-i\omega t}\left[-\frac{\partial\Phi}{\partial t}\right]dt,$$

(A.2)

where the parameters are as described in detail in the text. Eqn.(A.2) is rewritten as,

$$\varepsilon^*(\omega\tau_o) = \varepsilon_\infty + (\varepsilon_S - \varepsilon_\infty)N^*(\omega\tau_o),$$

(A.3)

where $N^*(\omega\tau_o)=N'(\omega\tau_o)+iN''(\omega\tau_o)$ is the normalized relaxation function, which by definition is the LaPlace transformation of the integral term in Eqn.(A.2). As outlined in Chapter IV, the real and imaginary components of the complex permittivity are given in terms of the real and imaginary components of the normalized relaxation function as,

$$\frac{\varepsilon''(\omega\tau_o)}{\Delta\varepsilon} = N''(\omega\tau_o) \quad ; \quad \frac{\varepsilon'(\omega\tau_o) - \varepsilon_\infty}{\Delta\varepsilon} = 1 - N'(\omega\tau_o), \tag{A.4}$$

where the parameters are as described earlier. The values of both $N'(\omega\tau_o)$ and $N''(\omega\tau_o)$ are given in tables by Dishon et al (1987) for discreet values of the product $\omega\tau_o$. For the dielectric data measured as a function of increasing time of reaction at fixed frequency, the tabulated values are used to determine the changing relaxation time.

To fit the data, values of ε_S and ε_∞ were taken from the complex plane plots of ε'' against ε'. This normalized data was then plotted in the complex plane on a computer. If the short and long time limits for the normalized plot on the x-axis (i.e. the normalized $(\varepsilon'-\varepsilon_\infty)/\Delta\varepsilon$ axis) did not tend towards 0 and 1, the parameters ε_S and ε_∞ were changed. When the data fit the limits adequately, the parameter γ was adjusted so that the tabulated values of for N'' and $(1-N')$ would fit the normalized permittivity data according to Eqn.(A.4). The tabulated values of N'' and $(1-N')$ are provided for different values of γ and $\omega\tau_o$. These tables are for limited values of γ, with a wide interval between subsequent γ values in some cases. Thus, when the normalized experimental values of ε'' and ε' did not correspond to the available values in the tables, the data in the tables were

interpolated for intermediate values of γ and $\omega\tau_0$ to correspond to the experimental

values. This gave the value of γ, and since ω was fixed, τ_0 could be determined.

It would be useful to fit such data by computation alone, but the computation time

necessary for calculating a set of N" and (1-N') for different $\omega\tau_0$ for a fixed γ value is

prohibitively long when $\gamma < 0.4$

150mm

6"
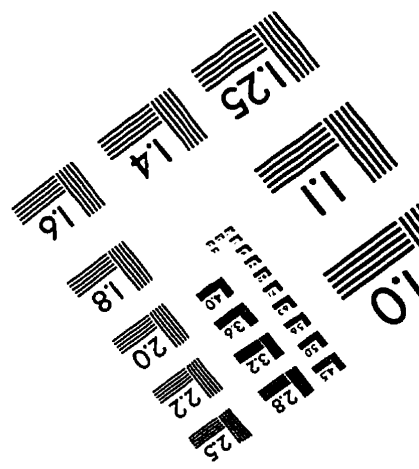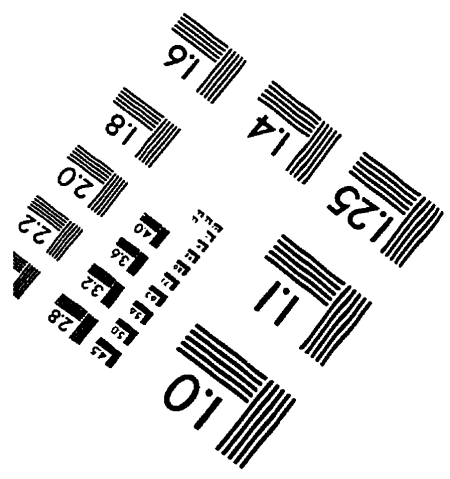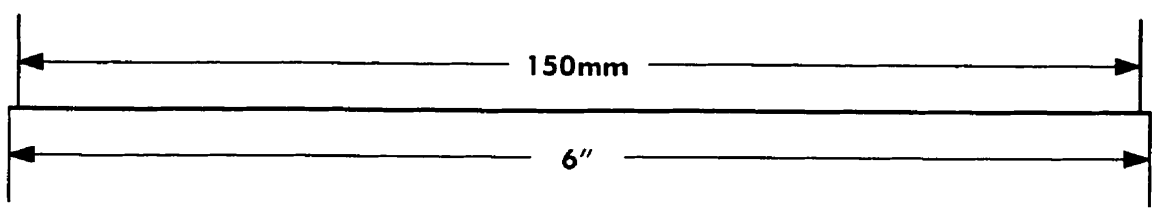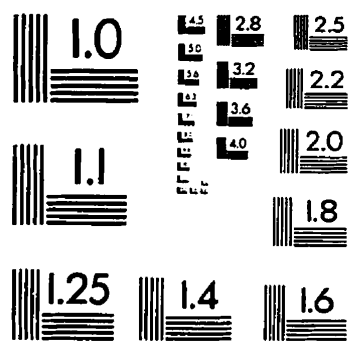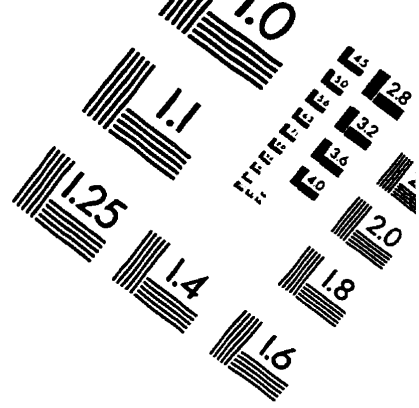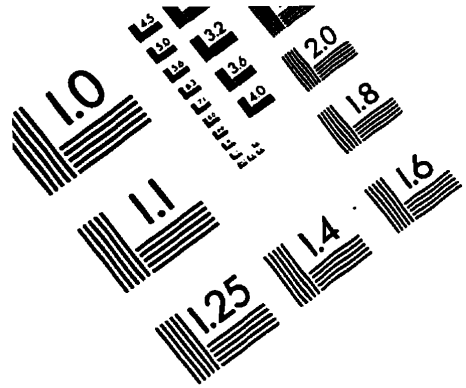
APPLIED IMAGE . Inc
1653 East Main Street
Rochester, NY 14609 USA
Phone: 716/482-0300
Fax: 716/288-5989